Studies of Copper Trafficking Proteins from *Bacillus subtilis* by Native Mass Spectrometry

A thesis submitted in partial fulfilment of the requirements
for the degree of Doctor of Philosophy in Chemistry

January 2017

Kristine L. Kay
University of East Anglia
Department of Chemistry

Kristine L. Kay

January 2017

Studies of Copper Trafficking Proteins from *Bacillus subtilis* by Native Mass Spectrometry

Abstract

Copper is essential for life, but potentially toxic due to its ability to redox cycle and displace metal cofactors. Therefore, ubiquitous protein networks exist to safely handle and deliver copper. Copper is removed from the cell via an integral membrane P_{1B}-ATPase, characterised by its soluble metal-binding domains (MBDs) which receive copper from Atx1-like copper chaperones in the cytoplasm. The mechanism of copper removal is unknown. Low molecular weight thiol species (LMWT) may play a role in cellular copper trafficking. The metallochaperone (CopZ) and soluble domains of the ATPase (CopAab) from *Bacillus subtilis* each bind Cu(I) with high affinity/specificity and form higher-order assemblies. Native electrospray ionisation mass spectrometry (ESI-MS) revealed formation of multiple copper-bound species with increasing Cu(I) level; cooperative formation of $Cu_4(CopZ)_2$ and $Cu_6(CopAab)_2$ was observed. The affinity for Cu(I) of bacillithiol (BSH), the primary LMWT in the *B.subtilis* cytoplasm, was determined to be β_2 = 4.1 x 10^{17} M^{-2}. ESI-MS revealed reduced intensity of dimeric forms of CopZ and CopAab in the presence of BSH (and other LMWT) due to copper competition; bacillithiolation of CopZ was observed. Higher order copper-bound complexes were observed for metallochaperones from *Streptomyces lividans* and *Saccharomyces cerevisiae*, and their decrease in the presence of LMWT. Rapid and reversible copper transfer between CopZ and CopAab was observed with similar rate constants at 25 °C for forward (247 $\pm$ 2.2 s^{-1}) and reverse (258 $\pm$ 2.6 s^{-1}) directions of transfer. The rate constant was independent of concentration, suggesting the rate-limiting step is first-order, and likely to be protein complex formation. Kinetic studies demonstrated that protein complex formation resulted in a 7-fold increase in the rate of copper transfer; a copper-bound CopZ:CopAab complex was observed via ESI-MS. Bidirectional copper transfer between CopZ and CopAab consistent with a regulatory role for the MBDs.

Declaration

Acknowledgements

I would like to extend a huge thanks and my sincerest gratitude to my supervisor, Prof Nick Le Brun, who provided opportunity and support throughout my PhD. I am grateful that you pushed me along when I needed it, but were always positive and encouraging, even when things were not exactly going to plan!

I am very grateful to both Dr Fixit Jason Crack and Dr Make-worky Justin Bradley who earned these nicknames through their invaluable day-to-day guidance around the lab. Jason, learning to operate and extract data from the mass spec would have been quite the daunting struggle without your input. Your wealth of experience enabled you to provide matter-of-fact explanations and advice, which sometimes conveniently doubled as entertaining storytelling. Justin, you have been a never-ending source of insightful suggestions —not once did I ask for help and not receive more than I asked for, and more than I even knew I needed. And of course your fitting wisecracks were always entertaining, but actually helped put things into perspective too.

Thank you to the other members of the Le Brun group, Sophie Bennett, Dr Erin Dodd, and Maite Pellicer-Martinez for being such a pleasure to work with, and create a supportive, convivial work atmosphere. Thank you to my supervisory committee member Dr Myles Cheesman, who genuinely always was enthusiastic and willing to help. Thanks to my examiners Dr Claudia Blindauer and Dr Tharin Blumenschein for taking the time to evaluate my thesis, and provide me with valuable, constructive feedback. Thank you to Prof Julea Butt for serving as the independent chair of my viva, and to the members of the Butt group who have been lovely to share a workspace with: almost Dr Emma Ainsworth, Dr Colin Lockwood, Dr Tony Blake, Dr Jess van Wonderen and Sam Rowe. Thank you to Prof Chris Dennison and Kerrie Brusby for providing copper chaperone samples, and thanks to Dr Jonathan Worrall and Dr Amanda Chaplin for providing copper chaperone samples and related figures found herein. Thank you to Dr Nick Watmough for access to stopped flow instrumentation, and to Dr Andrew Hemmings for allowing me to give crystallography a try.

And finally, thank you to Colin Kay, my favourite scientist, who has always supported me in every way he knows how.

Contents

List of Figures

List of Tables

List Of Abbreviations	
ATP-BD	ATP-binding domain
AUC	Analytical ultracentrifugation
BCS	Bathocuproine sulfonate
BSH	Bacillithiol
CcO	Cytochrome c oxidase
CCS	Copper chaperone for superoxide dismutase
CD	Circular dichroism
CMC	Critical micelle condition
CopA-FL	Full-length CopA
CRF	Collision radiofrequency
CRM	Charge residue model
CV	Column volumes
DDM	n-dodecyl-β-D-maltoside
DEAE	Diethyl-aminoethyL
DTT	Dithiothreitol
ESI	Electrospray ionisation
GSH	Glutathione
HIC	Hydrophobic interaction chromatography
HPLC	High performance liquid chromatography
ICP-AES	Inductively coupled plasma atomic emission spectroscopy
IEM	Ion evaporation model
IMAC	Immobilised metal affinity chromatography
IPTG	Isopropyl β-D-1-thiogalactopyranoside
isCID	In-source collision induced dissociation
ITC	Isothermal titration calorimetry
LB	Lysogeny broth
LBA	Lysogeny broth + agar
LC-MS	Liquid chromatography mass spectrometry
LMWT	Low molecular weight thiol species
M/z	Mass-to-charge
MBD	Metal-binding domains
Mr	Parent mass
MS	Mass spectrometry
MT	Metallothionein
NMR	Nuclear magnetic resonance
NTA	Nitrilotriacetic acid
OG	Octaethylene glycol
pI	Isoelectric point
Pi	Inorganic phosphate
Q	Quaternary amine
SDS-PAGE	Sodium dodecyl sulfate polyacrylamide gel electrophoresis
SEC	Size exclusion chromatography
TM	Tetrathiomolybdate
TMBS	Transmembrane metal-binding site
TOF	Time-of-flight
V0	Void volume (SEC)
Ve	Elution volume (SEC)
Vpp	Volts per plate
Vt	Total volume (SEC)

Chapter 1

Introduction

1.1 Copper as a Bioelement

Copper is the 29th element in the periodic table and its biochemical effects have been long exploited by human society as it was used by the ancient Greeks, Aztecs and Egyptians for medicinal purposes, such as sterilising wounds and drinking water [1]. Its other uses include metallurgy, on its own and alloyed in bronze, and more recently its ductility and conductivity have made it useful in wiring [2]. Copper has been identified as an essential nutrient in the human diet [3], and copper deficiency is associated with anaemia through its adverse effects on iron uptake in animals [4].

The bioavailability of copper can be traced back to the rise of photosynthetic cyanobacteria 2.5 billion years ago which oxygenated the Earth's oceans and atmosphere, and drastically altered the solubility and bioavailability of metals [5]. Prior to this, copper existed in insoluble sulfides as Cu(I) and was not bioavailable; early biological processes on earth requiring redox function primarily used water soluble ferrous iron [2]. Oxygenation of the atmosphere led to the mass precipitation of iron in the oceans as it oxidised from Fe(II) to Fe(III), making it largely unavailable for biological utilisation [6]. Conversely, other metal ions including copper became more bioavailable as they were released from their sulfide forms.

Newly soluble copper was initially dangerous to early life, but the altered chemistry caused by oxygenation eventually forced organisms to adapt to what metals were available [5]. Oxidative metabolism required a metal that could function at higher potentials than those used for anaerobic metabolism [7]. Most copper enzymes work between +0.25 and +0.75 V, which is higher than the Fe(III)/Fe(II) potential [2]. The changes in metal utilisation are evident in the relationship between copper usage and metabolism; though few anaerobic organisms utilise copper, many aerobic organisms utilise copper because they evolved ways to harness copper redox chemistry for metabolism without suffering any of its deleterious effects [6].

Copper has two stable, naturally occurring isotopes, ^{63}Cu and ^{65}Cu, with 69% and 31% abundance, respectively. Cu(II) has a $3d^9$ valence electron configuration and usually exists in coordination number 4 (square planar), 5 (trigonal bipyramidal or square pyramidal) or 6. Cu(I) has a full valence shell $3d^{10}$ and prefers coordination numbers 2, 3, or 4 (tetrahedral) though coordination 5 does exist [8]. Cu(I) is a soft Lewis acid and has a tendency to bind soft bases such as thiols, hydrides, alkyl groups, cyanide and phosphines. Cu(II) will bind these ligands as well but, as an intermediate acid, it will form complexes with other ligands such as sulfate and nitrate. Therefore, protein binding sites for copper dominated by amino acids with side chains that are soft ligands containing nitrogen and sulfur donor atoms: histidine, cysteine and methionine [6] (**Figure 1.1.1**).

This ligand set affords cuproproteins a variety of properties in terms of binding strength, hydrophobicity and charge state. Deprotonation of the first nitrogen on the histidine imidazole ring generates a neutral nitrogen donor, and the second generates an anionic imida-

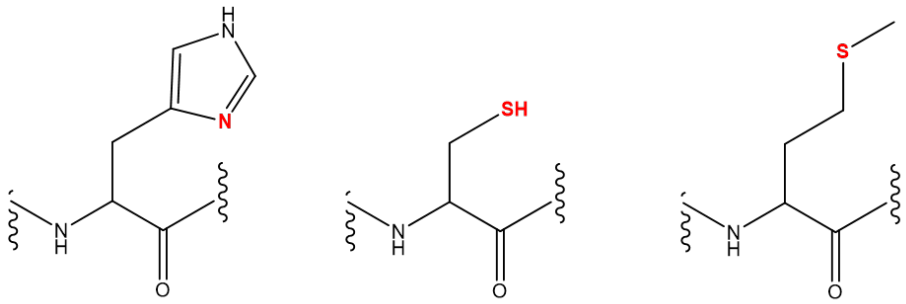

Figure 1.1.1: Typical Cu(I) ligands. Based upon the coordination preferences of Cu(I) as a soft Lewis acid, protein binding sites for Cu(I) usually feature ligands from Cys, Met and/or His.

zolate that is able to bridge two metal ions. Cysteine can also bridge two metal centres via an anionic thiolate that forms upon deprotonation, and can also oxidise to form disulfide bonded cystine. The neutral sulfur donor on the thioether of methionine serves as the active metal-binding site, which is not pH-dependent like histidine and cysteine. Methionine is also more hydrophobic than histidine or cysteine which affects solvent accessibility [6].

The metal centre formed by these ligands can take on varied geometry and composition, determining its redox potential, which enables cuproproteins to keep copper in the appropriate oxidation state. A larger reduction potential of the metal centre will favour keeping copper in its Cu(I) state and a lower reduction potential will favour copper in its Cu(II) state.The cytoplasm has a reduction potential of -0.29 V and is rich in thiolates [9] which, as soft donors, can bind Cu(I) very tightly, ensuring that copper is only present in the cytoplasm safely as Cu(I) complexes and not as a free cation. The less toxic Cu(II) is more abundant in aerobic environments such as the extracellular milieu [10].

Because redox-active copper is more reactive in its reduced state, it is potentially very

toxic [5]. If ions were freely available in the cytoplasm, copper could undergo the production of dangerous hydroxyl radicals via Fenton chemistry [1]:

$$Cu(I) + H_2O_2 \quad \longrightarrow \quad Cu(II) + OH^- + OH^\bullet \tag{1.1}$$

$$Cu(II) + O_2^- \quad \longrightarrow \quad Cu(I) + O_2 \tag{1.2}$$

Thus redox cycling of copper leads to the net equation:

$$O_2^- + H_2O_2 \quad \longrightarrow \quad O_2 + OH^\bullet + OH^- \tag{1.3}$$

Hydroxyl radicals are very reactive and can damage many cellular molecules including proteins, nucleic acids, and lipids. Copper toxicity can also occur through disruption of protein structure through interactions with the polypeptide backbone, and can displace other metal cofactors, interrupting enzyme function. Displacement of iron from iron-sulfur clusters has been demonstrated in *Escherichia coli* for proteins in the branched-chain amino acid synthesis pathway [11].

The copper ion's reduction potentials enable its proteins to engage in a wide variety of functions which are roughly grouped into broad classes: those that transport copper and those that use copper as a cofactor [6]. Proteins involved in copper trafficking generally are Cu(I)-binding proteins involved in maintenance of copper homeostasis within cells. These proteins transfer copper to enzymatic or catalytic proteins as Cu(I), where copper is utilised as a cofactor and cycled between the Cu(I) and Cu(II) oxidation states [12].

1.2 Copper Homeostasis Across Biology

Cuproenzymes exploit the ability of copper to cycle between the oxidised Cu(II) and reduced Cu(I) forms, which serves a wide range of catalytic functions [8]. Copper has been classed as a cofactor for several dozen enzymes in higher organisms and microbes [7], which function in electron transfer, catalysis and oxygen transport.

In order to safely supply copper to metabolic enzymes, networks of copper trafficking proteins carry out management of this essential yet potentially toxic metal [13]. It is believed that half of a given cuproproteome is involved in copper trafficking [12] but mechanisms and regulation of uptake, distribution and efflux are not fully characterised.

Though metabolic utilisation of copper in enzymes is more common in higher order organisms, few organisms have been found which lack copper detoxification machinery [7]. Below is an overview of copper proteins across biology: common cuproenzymes, the proteins which comprise a typical copper trafficking network, and some of their structural and functional features in eukaryotic and prokaryotic organisms.

Cuproenzymes

Cytochrome c oxidase

The most commonly occurring cuproprotein in biology is cytochrome c oxidase (CcO) [14]. CcO plays a central role in aerobic respiration as the terminal electron acceptor in the

electron transport chain. CcO sits within the inner mitochondrial membrane and contains four redox active metal sites, two heme sites (hemes a and a3) and two copper sites (Cu_A and Cu_B) [12]. CcO translocates four protons across the mitochondrial membrane and reduces molecular oxygen. The delivery of copper to cytochrome c oxidase is carried out through the cooperative efforts of four proteins in humans and yeast. Cox17 is a cysteine-rich protein which delivers copper to Sco1 and Sco2 and Cox11, all of which are anchored to the inner mitochondrial membrane. These proteins then insert copper into the Cox1 and Cox2 domains of CcO [15].

Copper/zinc superoxide dismutase

Copper/zinc superoxide dismutase (Cu/Zn-SOD) has become one of the best-characterised copper-containing enzymes, as it has been linked with angiogenesis, cancer, and neurodegenerative disease [16]. Cu/Zn-SOD disproportionates superoxide to dioxygen and hydrogen peroxide, thus providing protection from oxidants which arise from the environment or as a side effect of aerobic metabolism. Cu/Zn-SOD plays diverse roles in cell signaling and serve as a virulence factor of pathogens, and carries out catalysis at a rate close to the diffusion limit ($\sim 10^9$ M^{-1} s^{-1} [17]) and over quite a wide pH range (pH = 5 – 10). Homodimeric Cu/Zn-SOD acquires copper in the cytosol and contains one copper and one zinc ion per subunit. Copper is the enzymatically active metal, found at the end of a funnel-shaped cavity formed by residues in loop VII [18]. Zinc interacts with this loop and with the copper site (via a bridging histidine) to secure the redox active cofactor and stabilise the protein fold.

Copper trafficking proteins

Management and distribution of copper is largely handled by a few groups of proteins: importers, chaperones, metallothioneins, and exporters. In addition, the copper trafficking function of these proteins may be complemented by low molecular weight thiol (LMWT) containing species in the cytoplasm, which play a complex role *in vivo* including modulation of redox status [19] [20] [21]. LMWT thiol ligands have high affinity for soft metals including Cu(I), and evidence suggests they may influence cytoplasmic copper levels [22] [23] [24]. Examples of LMWT are glutathione (GSH) in humans [25], mycothiol (MSH) in actinomycetes [26], and bacillithiol (BSH) in *B.subtilis* [27] (see Section 4.2.3).

Import proteins

Active uptake mechanisms are essential for importing copper in organisms which actively utilise copper in their metabolic pathways. The use of cuproenzymes is rarer among prokaryotes, and therefore in this domain fewer copper uptake proteins have been defined [7]. The primary known mechanism of copper import into cells involves the eukaryotoic Ctr family of plasma membrane-associated high-affinity copper transport proteins. The Ctr proteins were first identified in yeast (Ctr1), and their deletion results in defective mitochondrial oxidative phosphorylation [28]. Ctr proteins use a concentration gradient to drive copper into the cell by way of a pore at the interface [6].

In other eukaryotes, Ctr1 analogs have been identified (hCtr1 in humans and mCtr1 in mouse); in lower-order organisms, other copper import proteins have been identified, YcnJ

in *B. subtilis* [29], HmtA in *Pseudomonas aeruginosa* [30]). In addition, other mechanisms for copper uptake have been proposed including divalent metal transporter DMT1 (human) [31] and methanobactins (bacteria) [32].

Copper chaperones

After being taken up into the cell, copper is transported as cargo by high-affinity chaperones which deliver copper to the correct destination [33]. These proteins are often referred to as the Atx1-like copper chaperones, after the first metallochaperone to be identified [34]. In addition to escorting cellular copper to its required target, it has been demonstrated that Atx1-like chaperones may play a role in cellular copper storage [35] and gene regulation [36].

Atx1-like chaperones are usually approximately 70 residues long comprising a conserved $\beta\alpha\beta\beta\alpha\beta$ motif, connected by loop regions with a MXCXXC binding motif [37]. Coordination to the Cu(I) is digonal or trigonal [38] [39] with flexibility in the loop containing the copper-binding site; this low-coordinate, flexible geometry helps facilitate transfer of copper to another protein [6]. The copper-binding motif is surface-exposed with the two cysteines located in the first loop and the beginning of the first α-helix. NMR data have demonstrated a distorted linear coordination, with S-Cu-S bond angles of 115 – 120° [40] [41].

Metallothioneins

Metallothioneins (MTs) are small, intracellular metal-binding proteins found in bacteria, plants, invertebrates and vertebrates, which display considerate diversity across biology.

In vertebrates, MTs are frequently considered a binding reservoir for divalent metals, and are $\sim$ 60 – 70 amino acids in length and contain up to 20 cysteines. The bacterial MTs contain proteins which are neither homologous in sequence nor related by evolution to the animal MTs [10]; these proteins are cysteine-rich but also contain aromatic residues including His [42]. One bacterial copper-specific MT has been identified, MymT, from the Gram-positive *Mycobacterium tuberculosis* [43], which has little homology to other MTs and features a unique motif (CHCXXGXXYRCTC). Other prokaryotic MTs, in species from the cyanobacterial genus *Synechococcus*, seem primarily to function in Zn^{2+} homeostasis, whereas MT from other organisms may function in stress response and detoxification of divalent metals. Though gene deletion has confirmed MymT functions in protection against copper toxicity, overexpression of other MTs in bacteria has led to metal buildup rather than detoxification. This, coupled with the fact that they are relatively rare in bacterial sequences, makes their role in nature unclear [42].

Typically, MTs are investigated *in vitro* for their capacity to bind multiple divalent metal ions. It has been demonstrated MT can provide essential metals Zn^{2+} and Cu^{+} to apo-enzymes [44]. Their ability to bind multiple metals makes their potential role *in vivo* complex. For example, MT may serve to sequester and donate zinc to metalloproteins for which zinc is a cofactor, giving MT the potential to influence numerous cellular processes including gene regulation, cell proliferation, differentation and apoptosis. In addition, zinc is a regulator of glutathione (GSH) synthesis which links MT further with metal trafficking *in vivo* [45]. The thiol ligands of GSH have a high affinity for Cu(I), making this one of several ways that metallothionein could be linked to copper homeostasis.

Membrane exporters

The P_{1B}-type ATPases function with specificity towards soft Lewis acids including copper (see Figure 8.1.1). P_{1B}-type ATPases couple the energy released by dephosphorylation of ATP with active transport of a Cu(I) ion across a transmembrane channel, which follows the Albers-Post catalytic cycle. A crystal structure was solved of CopA from *Legionella pneumophilla* [46], which provided the first complete atomic structure of a P_{1B}-type ATPase. From this, a three-step pathway for transmembrane copper transport was proposed, but the full mechanism for copper transfer and efflux is not fully understood.

A distinct feature of P_{1B}-type ATPases are soluble, cytoplasmic metal-binding domains (MBDs) located at the N-terminal end. In addition, at the mouth of the transmembrane channel is a metal-binding site (MBS), which in P_{1B}-type ATPases is a CPC motif [47]. It has been demonstrated that Cu(I) can be transferred from Atx1-like chaperones directly to this MBS [48], suggesting that MBDs may not facilitate entrance of copper to the transmembrane channel.

Though the role of MBDs in cellular copper removal is unclear, copper transfer from the Atx1-like copper chaperones to the MBDs has been demonstrated [49] [50] [51] [52]. Like the copper chaperones, each MBD typically contains a ferredoxin-like fold with a conserved CXXC motif [12] (see Chapter 5), and their interaction is facilitated by complementary structural elements (see Chapter 6). Both display an extremely high affinity for Cu(I), creating a shallow thermodynamic gradient for copper transfer.

Copper trafficking in eukaryotes

Copper trafficking networks vary across biology depending upon the complexity of the organism and the extent to which it utilises copper ions in its metabolism. For example, active transport uptake mechanisms are crucial for species which actively utilise copper as an enzymatic cofactor.

Homo sapiens

In humans, copper is a necessary cofactor for embryonic development and respiration and, thus, is an essential component of the diet. Copper is absorbed by diffusion across the mucosal membrane in the stomach and small intestine and excreted primarily via the bile at a rate of $\sim$ 1 mg / day. Under normal circumstances, up to 75% is recycled among the digestive tract and bodily fluids/tissues, especially the liver [15].

Copper uptake occurs via the hCtr1 transporter [53], from which it is bound to intracellular copper chaperones, Atox1, CCS or Cox17. It is not clear how cytoplasmic copper chaperones acquire Cu(I) from hCtr1 [54]. Atox1 delivers Cu(I) to ATP7A/B (see below), CCS delivers Cu(I) in the cytoplasm to SOD1 and Cox 17 delivers Cu(I) to the mitrochondria for insertion into cytochrome c oxidase (with the assistance of additional proteins) [55]. High-affinity copper binding by intracellular molecules such as albumin, ceruloplasmin and transcuprein, GSH and metallothioneins have also been demonstrated [15].

Atox1 is a 68-residue Atx1-like copper chaperone in humans, featuring a surface-exposed MXCXXC copper binding site in a ferredoxin-like fold. Atox1 has been shown

to dimerise *in vitro* [56], with the Lys60 involved in hydrogen bonding at the dimer interface [57]. Lys60 and Thr11 were found to participate in electrostatic networks that stabilize the Cu-bound form and, in the apoform, determine the solvent exposure of the two Cys [58].

The copper chaperone Atox1 delivers copper to the secretory pathway and docks with the P_{1B}-type ATPases, ATP7B in the liver, or ATP7A in other cells [59]. Most enzymes acquire copper from ATP7A/B in the Golgi. Deficient functioning of ATP7A and ATP7B are associated with Menkes and Wilson disease, respectively. Menkes disease [60] results in copper deficiency due to limited absorption of dietary copper; Wilson disease [61] is a copper-overload disorder resulting in accumulation of copper in the liver and brain [13].

Saccharomyces cerevisiae

Copper uptake in yeast occurs primarily by way of Ctr1, which features three transmembrane helices which form a pore across which copper is transported [62] and is regulated by Fre1/Fre2. A second Ctr protein, Ctr3, and low affinity Smf1 and Fet4 permeases also participate in copper uptake [63]. The Ctr proteins act on reduced copper Cu(I) which means a metalloreduction event takes place at or near the membrane before Cu import.

Copper then is delivered to one of three cytoplamic chaperones, Ccs1, Atx1 or Cox17 [64]. Ccs inserts copper into SOD in the cytoplasm, and Cox17 delivers copper at the mitochondrial membrane to Sco1 and Cox11 for donation to the Cu_A and Cu_B sites, respectively, of CcO. Atx1 delivers copper to the P-type ATPase Ccc2 at the Golgi apparatus for incorporation into the iron transport protein Fet3. In addition, a varying quantity of cellular copper exists bound to MTs, Cup1 and Crs5, whose expression are regulated by a

copper-responsive transcription factor Ace1 [65].

Atx1 is a 73 amino acid, namesake protein of the cytosolic copper chaperone group [34]. *S. cerevisiae* Atx1 was the first metallochaperone to be discovered [34] and solution structures of Cu(I)-bound and apo forms of Atx1 [41]. Yeast mutants deficient in Atx1 suffer from impaired iron uptake due to impaired copper supply to Fet3, whose activity is required for iron importer Ftr1 [14]. Copper transfer and complex formation have been observed *in vitro* for Atx1/Ccc2 [66] [67]. Ccc2 is an integral membrane copper ATPase, with two cytoplasmic metal-binding domains that in typical fashion are structurally similar to Atx1, each with a fold and MXCXXC copper binding motif [68]. Surface lysine residues provide complementary electrostatic charge to the negative surface of Ccc2a [14], with Lys65 important for Cu delivery to Ccc2. During copper transfer it seems that Atx1 undergoes structural changes, where the cysteines move to become more solvent-exposed, while Ccc2 structure changes very little [37].

Copper trafficking in prokaryotes

Prokaryotic copper-trafficking systems have been characterised in several species such as *Escherichia coli*, *Pseudomonas aeruginosa*, and *Enterococcus hirae*. A distinction can be made between prokaryotes which utilise copper for metabolism and those who simply possess copper defense mechanisms. Though copper trafficking networks can be smaller in some prokaryotes, these systems must meet metabolic and structural requirements. For example, cyanobacteria utilise copper within the photosynthetic electron transport chain

as a cofactor for plastocyanin, which is found in the thylakoid. In order for copper to be transported across the thylakoid membrane, in cyanobacteria copper is available in the cytoplasm [33].

In Gram-positive bacteria such as *B. subtilis*, ATPase membrane transporters are sufficient to remove excess copper from the cytosol. But Gram-negative bacteria require membrane transporters to remove copper from the cytoplasm, but also need a way to remove excess copper from the periplasm. One example the CusCFBA operon in *E. coli*, which encodes a protein system to export copper from the periplasm and is comprised of inner membrane pump Cus A, periplasmic proteins CusB and CusF, and the outer membrane pump CusC [69]. [70]

Streptomyces lividans

Recently, Atx1-like copper chaperones have been characterised from the species *Streptomyces lividans*. Streptomycetes are Gram-positive, aerobic, soil dwelling-bacteria [71]. The life cycle of Streptomyces involes germination of spores which form a network of mycelium that grows into aerial hyphae. From there, cell division takes place and the hyphae mature into new spores. Copper is esssential for the development of spores into aerial mycelium [72]. The twin-arginine translocation (Tat) pathway secretes a large number of proteins with a metal cofactor. When this pathway is deleted, limited if any aerial mycelium are produced, but can be restored by copper supplementation, suggesting this pathway secretes cuproproteins necessary for development [71].

S. lividans possesses multiple CopZ and P_{IB}-type ATPase genes [73]. As is typical

for copper efflux systems, they are upregulated through Cu(I) binding of copper sensitive operon repressor (CsoR). In *S. lividans*, CsoR regulates a 3-loci regulon comprising two copZA-like operons and its own csoR gene. Cu stress increases the transcript levels of the copZ and copA genes, and eventually the csoR gene. Under the transcriptional control of CsoR are CopZ-3079 and CopZ-1317, two Atx1-like proteins. Though copper transfer from these CopZ proteins to the ATPase has not yet been demonstrated *in vitro*, unidirectional Cu(I) transfer to CsoR has been demonstrated [74]. Transcription levels suggested that CopZ-1317 contributes much less to Cu(I) resistance than does CopZ-3079, as during copper stress, CopZ-1317 is less than 2% of transcription.

1.3 Copper trafficking in *Bacillus subtilis*

Bacillus subtilis is a non-pathogenic, soil-dwelling bacterium capable of sporulation and formation of biofilms, the genome sequence of which was published in 1997 [75]. It is one of the best-characterised bacteria, with the transcriptome, proteome, secretome and metabolome all available [76]. It has been important to humans for over 1000 years, dating back its use in fermentation of soybeans in Japan [76]. Today *B. subtilis* is primarily used as an enzyme factory in biotechnology. As a member of the Bacillales, the only order of phylum Firmicutes which use copper as a cofactor in metabolism [7], *B. subtilis* requires the machinery to prevent copper toxicity and regulate copper homeostasis.

B. subtilis imports copper ions across the membrane by way of an uptake pump YcnJ, encoded by the *ycnJ* gene. In copper-limiting conditions, the *ycnJ* gene has been shown to be upregulated, and $\triangle$ycnJ mutants have shown reduced growth. The *ycnK* gene encodes for a transcriptional regulator YcnK, which forms a dimer and acts in response to elevated copper as a repressor for the ycnJ gene [77].

The copper efflux system in *B. subtilis* is encoded by the copZA operon, and comprises an Atx1-like chaperone CopZ and P_{1B}-type ATPase CopA to shuttle excess copper out of the cell [78]. The copZA operon is transcriptionally regulated by a CsoR-like regulator [79] encoded upstream of the copZA operon. In the presence of elevated copper levels (but not other metals), the operon is derepressed [29], and mutation of this operon has been demonstrated to increase copper sensitivity [78].

CopZ binds copper with high affinity to keep cytosolic levels of copper at extremely

low concentrations [77]. The CopZ protein is 69 amino acid residues long and contains a typical $\beta\alpha\beta\beta\alpha\beta$ fold; its solution structure was published in 2001 [40]. CopA, predicted to possess eight transmembrane domains, transports copper across the cell membrane using energy generated by ATP hydrolysis. CopA contains two soluble MBDs (CopAa and CopAb), that are similar in structure to CopZ, containing two $\beta\alpha\beta\beta\alpha\beta$ domains connected by a short dipeptide linker [80].

Copper binding to CopZ and to a soluble protein containing the CopA N-terminal domains (denoted CopAab) has been studied. CopZ dimerises upon binding Cu(I) to form $Cu(CopZ)_2$ complex which binds up to 3 additional Cu(I) ions to form $Cu_4(CopZ)_2$ [35]. The high-resolution crystal structure of $Cu_4(CopZ)_2$ indicates a tetranuclear Cu(I) cluster at the interface of the two CopZ monomers [81]. CopAab has been shown to bind multiple Cu(I) ions, likely leading to the formation of $Cu_4(CopAab)_2$ [80]. This dimeric species is luminescent and loss of signal above 2 Cu / protein suggests this dimeric species may bind additional Cu(I) ions.

Binding of Cu(I) has also been characterised to the individual soluble MBDs (CopAa and CopAb). CopAb binds Cu(I) with high affinity, and dimerises above a level of 1 Cu/protein, generating a weakly luminescent Cu(I) cluster [82]. CopAa too binds with high affinity and was demonstrated by analytical ultracentrifugation to form a tetramer upon binding of copper [83]. However, CopAa could not accommodate high copper loadings and demonstrated instability upon addition of copper >1 / protein; this instability was not observed in a mixture of CopAa/CopAb.

1.3.1 Aims of the project

B. subtilis CopZ and CopAab have been demonstrated to interact *in vivo*, with copper transfer rapid and reversible [84]. CopZ and CopAab, as well as proteins from other organisms, have been shown to bind multiple Cu(I) ions, but spectroscopic studies have been unable to resolve the mixture of species which forms with changing Cu(I) levels. Among other functions, LMWT may play a role in cellular metal trafficking and have been shown to affect association state of CopZ [52]. Therefore, the aims of the project are:

- Employ native electrospray ionisation mass spectrometry (ESI-MS) to analyse the *Bacillus subtilis* copper trafficking system.
- Compare the copper-binding behaviour of a mixture of CopAa and CopAb to the protein containing both domains CopAab.
- Explore the influence of BSH upon copper-binding behaviour of copper trafficking proteins, via spectroscopy and native ESI-MS.
- Examine the formation of higher order complexes by chaperones from from *S. lividans* and *S. cerevisiae*.
- Examine the mechanism and kinetics of copper transfer between CopZ and CopAab via stopped flow and UV-visible absorbance.
- Purify integral membrane protein CopA.

Chapter 2

Materials and Methods

2.1 Molecular Biology

Escherichia coli strains JM109 and BL21(DE3) were used for protein expression and grown at 37 °C in Lysogeny Broth (LB) broth [85] or on LB plates supplemented with 1% (w/v) agar (LBA). Ampicillin was used at a concentration of 100 μg/mL where appropriate. Plasmid DNA was isolated from 5 mL or 40 mL cultures of *E. coli* using a plasmid prep kit (Qiagen) which follows the alkaline lysis method [86]. *E. coli* cells were made competent by the $CaCl_2$ method [87], and stored at -80 °C. Transformation of *E. coli* cells with plasmid DNA was carried out using the heat shock method [88]. Here, 1 μg of plasmid DNA was added to 0.2 mL aliquots of competent cells and incubated on ice for 30 min. The cells were heat shocked at 42 °C for 90 s and returned to ice for 10 min. Then 0.8 mL LB broth at 37 °C was added and cells were incubated at 37 °C for 45 min. Cells were pelleted by centrifugation for 10 min at 5000 × g. Finally, 0.8 mL of the supernatant was removed and the pellets resuspended in the remaining 0.2 mL before plating on LBA plates with ampicillin and overnight incubation at 37 °C.

2.2 Expression Constructs and Protein Purification

2.2.1 CopZ

The CopZ expression vector was constructed previously by Dr Margaret Kihlken by inserting the *copZ* (*yvgY*) gene into a pAlterEx-1 expression vector creating plasmid **pMKNC6** for the overproduction under control of the T7 promotor, of wild-type CopZ [89] with the sequence as listed in **Figure 2.2.1**.

```
MEQKTLQVEG MSCQHCVKAV ETSVGELDGV SAVHVNLEAG KVDVSFDADK
VSVKDIADAI EDQGYDVAK
Isotopically Averaged Molecular Mass = 7338.166 Da
```

Figure 2.2.1: Sequence encoded by pMKNC6 Primary sequence of CopZ, as produced using pMKNC6 and the isotopically averaged molecular mass of the sequence

WT-CopZ was produced by inoculating 2.5 L (5 $\times$ 500 mL) of LB with ampicillin at 100 μg/mL, with 5 mL of overnight culture of *E. coli* JM109 containing pMKNC6. These cultures were incubated at 37 °C, 200 rev/min until the OD_{600nm} reached 0.4 – 0.6, at which point IPTG (Formedium) was added to a final concentration of 0.5 mM and the cultures incubated at at 37 °C, 200 rev/min, for a further 4.5 hr. Cells were harvested by centrifugation at 5000 $\times$ g for 20 min at 4°C and resuspended in 100 mL of 100 mM HEPES, pH 7.0. Lysozyme (Sigma) was added to a final concentration of 0.1 mg/mL and the cells incubated at 30 °C for 15 min at 100 rev/min. DNAse I and RNAse A (Sigma) were each added to a final concentration of 6 μg/mL. The cells were sonicated while on ice for 2 $\times$ 8 min 20 s using a Status US200 ultrasonicator (Novara) in pulse mode (0.2 s per s) set at 50%

power. The lysate was centrifuged at 39,000 $\times$ g for 20 min at 4 °C. The supernatant was taken slowly to 75 °C with gentle stirring, held for 15 min and placed on ice for a further 15 min. The suspension was centrifuged at 39,000 $\times$ g for 20 min at 4°C. DTT (dithiothreitol) (Formedium) was added to the supernatant to a final concentration of 15 mM, and the solution passed through a 0.45 μm filter (Sartorius). The protein solution was then applied to 2 $\times$ 5 mL HiTrap DEAE anion exchange column (GE Healthcare) previously equilibrated with 10 column volumes (CV) Buffer A (100 mM HEPES, 15 mM DTT, pH 7.0). The column was subsequently washed with a further 10 CV Buffer A before eluting with a 10 CV gradient of 0 to 1 M NaCl in the same buffer, with CopZ eluting at a concentration of $\sim$ 300 mM NaCl. To remove contaminating nucleic acids, $(NH_4)_2SO_4$ was added to fractions containing CopZ (determined by SDS-PAGE analysis), to a final concentration of 3 M. The protein solution was then loaded onto a 15 mL phenyl-sepharose hydrophobic interaction chromatography (HIC) column (GE Healthcare), previously equilibrated with 5 CV 100 mM HEPES, 100 mM NaCl, 3 M $(NH_4)_2SO_4$, 15 mM DTT, pH 7.0. The column was washed with 20 CV binding buffer before applying a 100 mL gradient of 3 – 0 M $(NH_4)_2SO_4$, with CopZ eluting at approximately 2.4 M $(NH_4)_2SO_4$. Fractions containing CopZ (as determined by SDS-PAGE analysis) were buffer exchanged into 100 mM HEPES, 100 mM NaCl, pH 7.0 and concentrated to $<$2.5 mL, using an centrifugal ultrafiltration unit (Vivaspin; Millipore) at 8000 $\times$ g and 4°C. The protein solution was passed through a 0.45 μm filter (Sartorius) and DTT added to a final concentration of 15 mM before applying to the Sephacryl S-100 gel filtration column, equilibrated in 100 mM HEPES, 100 mM NaCl, pH 7.0. Fractions containing CopZ (as determined by SDS-PAGE analysis) were concentrated to $<$10 mL

using centrifugal ultrafiltration unit as above, before aliquoting and flash freezing.

2.2.2 His_6CopZ

The His_6-tagged CopZ plasmid was constructed previously by Dr Margaret Kihlken, where the *copZ* (*yvgY*) gene was inserted into a pET21a (Promega) expression vector, generating plasmid **pMKNC3**, which produces a protein fused to a C-terminal His_6tag. Overexpression of this plasmid in *E. coli* produces a protein with the sequence in **Figure 2.2.2**.

```
MEQKTLQVEG MSCQHCVKAV ETSVGELDGV SAVHVNLEAG KVDVSFDADK
VSVKDIADAI EDQGYDVAKL EHHHHHH

Isotopically Averaged Molecular Mass = 8403.285 Da
```

Figure 2.2.2: Sequence encoded by pMKNC3 Primary sequence of His_6CopZ, as produced using pMKNC3 and the isotopically averaged molecular mass of the sequence

His_6-CopZ was produced by inoculating 2.5 L (5 $\times$ 500 mL) of LB with ampicillin at 100 μg/mL with 5 $\times$ 5 mL of overnight culture of *E. coli* BL21(DE3) containing pMKNC3. The cultures were then incubated at 37 °C, 200 rev/min until the OD_{600nm} reached 0.4 – 0.6, when IPTG (Formedium) was added to a final concentration of 0.5 mM and the cultures were incubated with shaking for a further 4.5 hr. Cells were harvested by centrifugation at 5000 $\times$ g for 20 min at 4°C and resuspended in 100 mL Buffer A (20 mM Tris-HCl, 0.5 M NaCl, 5 mM imidazole, pH 7.5). Lysozyme (Sigma) was added to a final concentration of 0.1 mg/mL and the cells incubated at 30 °C for 15 min at 100 rev/min. DNAse I and RNAse A (Sigma) were added to a final concentration of 6 μg/mL. The cells were sonicated while on ice, for 2 $\times$ 8 min 20 s using a Status US200 ultrasonicator (Novara) in pulse mode

(0.2 s per s) set at 50% power. The lysate was centrifuged at 39,000 $\times$ g for 20 min at 4°C. DTT (Formedium) was added to the supernatant to a final concentration of 15 mM and the solution passed through a 0.45 μm filter (Sartorius) before loading onto 2 $\times$ 5 mL HiTrap affinity column (GE Healthcare) charged with Ni^{2+}, according to the manufacurer's instructions. The column was subsequently washed with 10 column volumes (CV) Buffer A, and then 25 CV Buffer B (20 mM Tris-HCl, 3 M NaCl, 50 mM imidazole, pH 7.5) to remove nucleic acid contamination. After reequilibrating in Buffer A, a 10 CV gradient from 0.05 to 1 M imidazole was applied, with His_6-tagged CopZ eluting at a concentration of $\sim$ 300 mM imidazole. Fractions containing CopZ (determined by SDS-PAGE) were buffer exchanged into 100 mM HEPES, 100 mM NaCl, pH 7.5 using an centrifugal ultrafiltration unit (Vivaspin; Millipore), and concentrated to a final volume $<$10 mL before aliquoting and flash freezing.

2.2.3 CopAab

Construction of the CopAab expression vector was carried out by Dr Margaret Kihlken and Dr Chloe Singleton. The 473 bp fragment of the *copA* encoding the two soluble domains of CopA was isolated and inserted into pET21a (Promega) expression vector, creating plasmid **pCSNC1** [80]. Overexpression of this plasmid in *E. coli* produces the protein with sequence in **Figure 2.2.3**.

CopAab was produced by inoculating 2.5 L (5 $\times$ 500 mL) of LB with ampicillin at 100 μg/mL with 5 mL of overnight culture of *E. coli* BL21(DE3) containing pCSNC1. These cultures were incubated at 37 °C, 200 rev/min until the OD_{600nm} reached 0.4 – 0.6, at which

```
MLSEQKEIAM QVSGMTCAAC AARIEKGLKR MPGVTDANVN LATETSNVIY
DPAETGTAAI QEKIEKLGYH VVTEKAEFDI EGMTCAACAN RIEKRLNKIE
GVANAPVNFA LETVTVEYNP KEASVSDLKE AVDKLGYKLK LKGEQDS

Isotopically Averaged Molecular Mass = 15913.134 Da
```

Figure 2.2.3: Sequence encoded by pCSNC1 Primary sequence of CopAab, as produced using pCSNC1 and the isotopically averaged molecular mass of the sequence.

point IPTG (Formedium) was added to a final concentration of 0.5 mM and the cultures incubated at at 37 °C, 200 rev/min, for a further 4 hr. Cells were harvested by centrifugation at 5000 × g for 20 min at 4°C and resuspended in 100 mL of 100 mM HEPES, pH 7.0. Lysozyme (Sigma) was added to a final concentration of 0.1 mg/mL and the cells incubated at 30 °C for 15 min at 100 rev/min. DNAse I and RNAse A (Sigma) were each added to a final concentration of 6 μg/mL. The cells were sonicated while on ice for 2 × 8 min 20 s using a Status US200 ultrasonicator (Novara) in pulse mode (0.2 s per s) set at 50% power. The lysate was centrifuged at 39,000 × g for 20 min at 4°C. The supernatant was taken slowly to 75 °C with gentle stirring, held for 15 min and placed on ice for a further 15 min. The suspension was centrifuged at 39,000 × g for 20 min at 4°C. DTT (Formedium) was added to the supernatant to a final concentration of 15 mM, and the solution passed through a 0.45 μm filter (Sartorius). The protein solution was then applied to 2 × 5 mL HiTrap DEAE anion exchange column (GE Healthcare) previously equilibrated with 10 column volumes (CV) Buffer A (100 mM HEPES, 15 mM DTT, pH 7.0). The column was then washed with a further 10 CV Buffer A before eluting with a 10 CV gradient of 0 to 1 M NaCl in the same buffer, with CopAab eluting at a concentration of ∼170 mM NaCl. To re-

move contaminating nucleic acids, $(NH_4)_2SO_4$ was added to fractions containing CopAab (determined by SDS-PAGE analysis), to a final concentration of 3 M. The protein solution was then loaded onto a 15 mL phenyl-sepharose hydrophobic interaction chromatography (HIC) column (GE Healthcare), previously equilibrated with 5 CV 100 mM HEPES, 100 mM NaCl, 3 M $(NH_4)_2SO_4$, 15 mM DTT, pH 7.0. The column was washed with 20 CV binding buffer before applying a 100 mL gradient of 3 – 0 M $(NH_4)_2SO_4$. Fractions containing CopAab (as determined by SDS-PAGE analysis) were buffer exchanged into 100 mM HEPES, 100 mM NaCl, pH 7.0 and concentrated to $<$2.5 mL, using an centrifugal ultrafiltration unit (Vivaspin; Millipore) at 8000 $\times$ g and 4°C. The protein solution was passed through a 0.45 μm filter (Sartorius) and DTT added to a final concentration of 15 mM before applying to the Sephacryl S-100 gel filtration column, equilibrated in 100 mM HEPES, 100 mM NaCl, pH 7.0. Fractions containing CopAab (as determined by SDS-PAGE analysis) were combined and dialysed against 100 mM HEPES 1 mM EDTA, pH 7.0 to remove any traces of bound metal ions. CopAab was then dialysed against EDTA-free buffer concentrated to $<$10 mL using an centrifugal ultrafiltration unit as above, before aliquoting and flash freezing.

2.2.4 CopAa

Cloning of the CopAa expression vector was carried out by Dr Chloe Singleton, where the fragment of the *copA* gene encoding the first soluble domain of CopA was cloned into pET21a (Promega), generating **pCSNC2** [83]. Overexpression of this plasmid in *E. coli* produces a 72-residue protein with the sequence in **Figure 2.2.4**.

E. coli BL21(DE3) containing pCSNC2 cultures were used to inoculate, typically, 5 $\times$

```
MLSEQKEIAM QVSGMTCAAC AARIEKGLKR MPGVTDANVN LATETSNVIY
DPAETGTAAI QEKIEKLGYH VV

Isotopically Averaged Molecular Mass = 7697.846 Da
```

Figure 2.2.4: Sequence encoded by pCSNC2. Primary sequence of CopAa, as produced using pCSNC2 and the isotopically averaged molecular mass of the sequence.

500 mL of Lysogeny Broth media with ampicillin at 100 μg/mL in 2 L flasks, followed by incubation at 37 °C 200 rev/min until OD_{600nm} reached 0.6. IPTG was added to a final concentration of 0.4 mM and the cultures were incubated for a further 3 h. Cells were harvested by centrifuging at 5,000 × g at 4°C for 20 min. Cell pellets were resuspended in 100 mM HEPES, pH 7.0 containing lysozyme (Sigma) at a concentration of 0.1 mg/mL, and incubated at 30 °C for 15 min with gentle shaking. RNase A (Sigma) and DNAse I (Sigma) were added to a final concentration of 6 μg/mL, before sonicating cells for 2 × 8 min 20 s using a Status US200 ultrasonicator (Novara) in pulse mode (0.2 s per s) set at 50% power. The lysate was centrifuged at 39,000 × g for 20 min at 4°C and the supernatant heated slowly to 50 °C, stirred continuously for 15 min, and placed on ice for a further 15 min. The suspension was centrifuged at 39,000 × g for 20 min at 4°C. Dithiothreitol (Formedium) was added at a final concentration 5 mM to the supernatant, which was filtered at 0.45 μM (Satorius) before applying to 2 × 5 mL HiTrap Q anion-exchange column (GE Healthcare), where the protein was eluted using a 0 –1 M NaCl gradient, with CopAa eluting at approximately 550 mM NaCl. To fractions containing CopAa (determined by SDS-PAGE analysis), bulk precipitation was carried out to separate protein from contaminating nucleic acid, by adding $(NH_4)_2SO_4$ to a particular concentration (% w:v), incubating 1 hour at 4°C

with gentle stirring, then centrifuging at 39,000 $\times$ g for 20 min at 4°C. The first cut at 60% w:v led to precipitation of contaminating proteins, with the majority of CopAa located in the supernatant. The second and third cuts at 80% w:v and 90% w:v $(NH_4)_2SO_4$ resulted in the majority of protein including CopAa in the pellet, with contaminating nucleic acid washed away in the supernatant. Semi-pure CopAa was concentrated to $<$2.5 mL, using an centrifugal ultrafiltration unit (Vivaspin; Millipore) at 8000 $\times$ g and 4°C. The protein solution was passed through a 0.45 μm filter (Sartorius) and DTT added to a final concentration of 15 mM before applying to a Sephacryl S-100 gel filtration column, equilibrated in 100 mM HEPES, 100 mM NaCl, pH 7.0. Fractions containing CopAa (as determined by SDS-PAGE analysis) were combined, aliquoted and flash frozen.

2.2.5 CopAb

Cloning of the CopAb expression vector was carried out by Dr Chloe Singleton, where the fragment of the *copA* gene encoding the second soluble domain of CopA was cloned into pET21a (Promega), generating **pCSNC3** [82]. Overexpression of this plasmid in *E. coli* BL21(DE3) produces a 74-residue protein with the sequence in **Figure 2.2.5**.

```
TEKAEFDIEG MTCAACANRI EKRLNKIEGV ANAPVNFALE TVTVEYNPKE
ASVSDLKEAV DKLGYKLKLK GEQDS

Isotopically Averaged Molecular Mass = 8233.305 Da
```

Figure 2.2.5: Sequence encoded by pCSNC3. Primary sequence of CopAb, as produced using pCSNC3 and the isotopically averaged molecular mass of the sequence.

E. coli BL21(DE3) cultures containing pCSNC3 cultures containing ampicillin at 100

μg/mL, were used to inoculate 5 × 500 mL of Lysogeny Broth media in 2 L flasks, followed by incubation at 37 °C and 200 rpm until OD_{600nm} reached 0.4 – 0.6, when IPTG was added to a final concentration of 0.4 mM and the cultures were incubated for a further 3 hr. Cells were harvested by centrifuging at 5,000 × g at 4°C for 20 min. Cell pellets were resuspended in 100 mM HEPES, pH 7.0 containing lysozyme (Sigma) at a concentration of 0.1 mg/mL, and incubated at 30 °C for 15 min with gentle shaking. RNase A (Sigma) and DNAse I (Sigma) were added to a final concentration of 6 μg/mL, before sonicating cells for 2 × 8 min 20 s using a Status US200 ultrasonicator (Novara) in pulse mode (0.2 s per s) set at 50% power. The lysate was centrifuged at 39,000 × g for 20 min at 4°C and the supernatant heated slowly to 75 °C, stirred continuously for 15 min, and placed on ice for a further 15 min. The suspension was centrifuged at 39,000 × g for 20 min at 4°C. Dithiothreitol (Formedium) was added at a final concentration 15 mM to the supernatant, and filtered at 0.45 μM (Satorius) before applying to 2 × 5 mL HiTrap Q anion-exchange column (GE Healthcare), where the protein was eluted using a 0 –1 M NaCl gradient, with CopAb eluting at approximately 500 mM NaCl. To remove contaminating nucleic acids, $(NH_4)_2SO_4$ was added to fractions containing CopAab (determined by SDS-PAGE analysis), to a final concentration of 3 M, and centrifuged at 39,000 × g for 20 min at 4°C. The protein solution was then loaded onto a 15 mL phenyl-sepharose hydrophobic interaction chromatography (HIC) column (GE Healthcare), previously equilibrated with 5 CV 100 mM HEPES, 100 mM NaCl, 3 M $(NH_4)_2SO_4$, 15 mM DTT, pH 7.0. The column was washed with 20 CV binding buffer before applying a 100 mL gradient of 3 – 0 M $(NH_4)_2SO_4$. Fractions containing CopAb (as determined by SDS-PAGE analysis) were buffer exchanged into 100

mM HEPES, 100 mM NaCl, pH 7.0 and concentrated to $<$ 2.5 mL, using an centrifugal ultrafiltration unit (Vivaspin; Millipore) at 8000 $\times$ g and 4°C. The protein solution was passed through a 0.45 μm filter (Sartorius) and DTT added to a final concentration of 15 mM before applying to the Sephacryl S-100 gel filtration column, equilibrated in 100 mM HEPES, 100 mM NaCl, 15 mM DTT, pH 7.0. Fractions containing CopAb (as determined by SDS-PAGE analysis) were buffer exchanged and concentrated, as above, to $<$ 10 mL, before aliquoting and flash freezing.

2.3 Protein Isolation and Chromatography

2.3.1 Anion Exchange Chromatography

Ion exchange chromatography separates proteins based upon their charge, which is controlled by selecting the appropriate buffer pH. The pH at which a protein has no net charge is its isoelectric point (pI), dictated by the number of charged functional groups. In order to facilitate good recovery, it is desirable to operate $>$1.0 pH units away from the protein's pI to ensure it has sufficiently strong interaction with the ion exchange resin.

Anion exchange resins are coated in positively charged functional groups to bind negatively charged proteins, with varied functional groups available for varied tightness of the binding. The stationary phases used here consisted of cross-linked agarose bound to either the weak exchanger, diethyl-aminoethyl (DEAE), or the strong exchanger quaternary amonnium (Q), the structures of which are shown in **Figure 2.3.1**.

After passing a protein solution through an anion exchange column to bind negatively

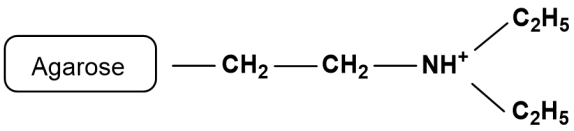

Structure of DEAE Anion Exchange Resin

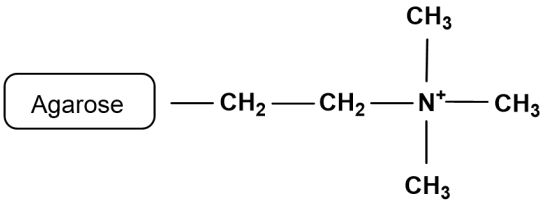

Structure of Q Anion Exchange Resin

Figure 2.3.1: Anion exchange chromatography resin. Structures of the anion exchange chromatography resins used in purification of *B. subtilis* copper trafficking proteins.

charged proteins, a salt gradient is applied to elute the proteins gradually. As the ionic charge of the mobile phase in increased, the salt ions compete with bound proteins for the positively charged resin functional groups, and proteins will elute in order of the strength of their interaction with the resin (i.e., the most weakly bound proteins elute first).

2.3.2 Immobilised Metal Affinity Chromatography

IMAC was developed [90] based upon the affinity observed between divalent metal ions and histidine residues in solution, but immobilised to allow protein fractionation. Nitrilotriacetic acid (NTA) is the chelating ligand used to affix the Ni^{2+} to agarose [91]. Modern microbiology and recombinant protein purification enabled the addition of oligohistidine extensions to known protein sequences, allowing their selective binding to the IMAC resin. NTA is a tetradentate ligand for the Ni^{2+}, leaving two valencies available for histidine im-

idazole. This ratio has been demonstrated to be optimal for higher protein recovery with minimal metal ion leaching [91].

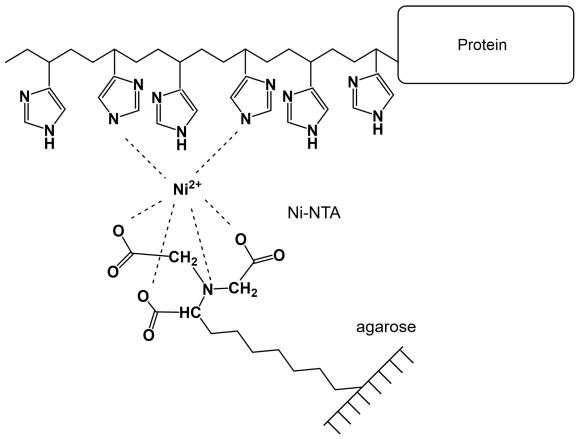

Figure 2.3.2: Ni^{2+}-NTA IMAC resin. Structural representation of a hypothetical His_6-tagged protein bound to Ni^{2+}-NTA IMAC resin, used in purification of recombinant proteins such as His_6-CopZ.

Clarified protein solution is passed through an Ni^{2+} IMAC column to selectively bind hexa-histidine tagged proteins, with a small amount of imidazole in the mobile phase to prevent non-specific binding with the aim of only the hexahistidine protein being immobilised. Then a gradient of imidazole is applied to elute the proteins gradually as the imidazole molecules compete for the NTA chelating ligand, hopefully eluting only the hexa-histidine tagged protein.

2.3.3 Size Exclusion Chromatography

Size exclusion chromatography separates proteins based upon size, by filtering them through a stationary phase that has a porosity defined to separate a particular size range. These porous beads are packed into a column, which will have two parameters to define its use: the volume excluding the matrix pores (void volume, V_0) and the combined volume inside

and outside the pores (total volume, V_t). The matrix should be selected with a fractionation range such that it elutes after the V_0 but within V_t [92].

Proteins elute in order of decreasing size, as larger molecules can only access the void volume and thus take less time to traverse the column, whereas smaller molecules diffuse into the matrix pores, causing them to elute later. For a particular protein or molecule, its elution volume, V_e, will be affected by its shape (hydrodynamic volume) and molecular weight. Overall, the V_e will be determined by its partition coefficient, K_{av}, the portion of stationary phase it can access. This can be defined as [93]:

$$V_e = V_0 + K_{av}(V_t - V_0) \tag{2.1}$$

which can be rearranged to give

$$K_{av} = (V_e - V_0)/(V_t - V_0) \tag{2.2}$$

To maximise resolution, gel filtration is carried out with a small sample volume, usually 1 – 5 % of the total bed volume. Typically, SEC is carried out at moderate ionic strength (0.1 – 0.2 M) to disrupt weak electrostatic protein-matrix interactions [92].

2.4 Nucleic acid removal

Purification of *B. subtilis* copper trafficking proteins typically involved a step involving a high salt wash devoted to removal of contaminating nucleic acid fragments. For His-tagged

proteins, this was carried out with the protein bound to the Ni^{2+} IMAC column, but proteins lacking a His-tag required a different approach to allow separation of nucleic acid from protein: hydrophobic interaction chromatography (HIC) for proteins soluble at high ionic strength; ammonium sulfate bulk precipitation for proteins insoluble at high ionic strength.

2.4.1 Hydrophobic Interaction Chromatography

Hydrophobic interaction chromatography (HIC) separates proteins based upon their hydrophobicity. Liquid water molecules form ordered clusters arising from intramolecular hydrophobic interactions. The order of this structure is disrupted at the interface with another phase or hydrophobic molecule, where water orients itself to form a sharp interface with the hydrophobic portion. For a water-soluble protein, hydrophobic side chains are typically driven to the protein interior upon folding, but the minimal energy state typically will be a thermodynamic compromise based upon the solution, relaxing the fold in some regions to expose hydrophobic patches. HIC capitalises upon this, using a high ionic strength buffer to enhance the interaction between the hydrophobic protein surfaces and the hydrophobic resin. Water molecules are attracted away from the protein, enhancing protein interaction with the hydrophobic resin.

HIC is useful after ion exchange chromatography when the sample is already in high salt buffer. The Phenyl-Sepharose HP contains a hydrophobic aryl group attached to a Sepharose matrix, comprised of crosslinked agarose. The solution containing the isolated protein of interest is passed through a 15 mL Phenyl-Sepharose HP column to bind the protein. After washing with high salt binding buffer to separate protein from contaminating

nucleic acid, the ionic strength is decreased to elute the purified protein.

2.4.2 Bulk precipitation

Protein precipitation techniques involve altering the ionic strength of solution containing protein(s) of interest, to decrease its solubility and separate it from the other solution components. The ability of a particular salt to salt out is described by the Hofmeister series, which arranges ions in order of chaotropic nature, the ability to disrupt the hydrogen bonding network in solution. This type of precipitation is reversible as the protein is not precipitated through denaturation but, rather, is dehydrated due to salt ions competing for the solvating water molecules. Though ammonium sulfate produces relatively higher precipitation effects, it also promotes protein-protein interactions. Several rounds of precipitation enabled separation of the dehydrated protein from soluble nucleic acid. A protein's solubility curve is defined by Equation 2.3.

$$\log S = \beta - K_s(I/2) \tag{2.3}$$

Here, because the constants β and K_s are characteristic of the protein, the solubility (S) of the protein in mg/mL of solvent is controlled through alteration of $\Gamma/2$, the ionic strength [94].

2.5 SDS-PAGE

Sodium dodecyl sulphate polyacrylamide gel electrophoresis (SDS-PAGE) utilises an electric field to separate macromolecules in order to estimate their relative molecular mass,

by moving them through a polyacrlyamide gel containing sodium dodecyl sulfate (SDS). The anionic SDS will unfold protein, creating an unstructured linear chain, and imparts a negative charge based upon protein size. Therefore all proteins in a mixture will contain a roughly uniform charge-to-mass ratio, and are thus resolved by size as they migrate through the polyacrylamide, by way of attraction to the positively charged electrode.

SDS-PAGE gels were prepared using a Hoefer SE-250 gel electrophoresis assembly. Typically 8 $\times$ 7 cm gels were prepared at 20% acrylamide for proteins of interest $<$10 kDa; otherwise 15% polyacrylamide gels were used. Cell suspensions or purified protein samples were mixed 50:50 with concentrated sample buffer (4% SDS, 20% glycerol, 100 mM Tris/HCl pH 6.8, 0.2% bromophenol blue in deionised water). DTT was added to a final concentration of 300 mM immediately before heating cells at 100 °C for 10 min. Between 12 μL and 15 μL of each sample was then loaded, along with PageRuler^{TM} Unstained Low Range Protein Ladder (3.4 to 100 kDa), and gels run for $\sim$45 min at 180 V, using a Consort E844 power source. Gels were then soaked in staining solution (40% v/v methanol, 10% v/v acetic acid, 0.1% Coomassie Brilliant Blue^{TM}) for 30 min, then soaked in destaining solution (40% v/v methanol, 10% v/v acetic acid) for 2 $\times$ 1 hour, or until bands were clearly visible.

2.6 Metal Ion Additions

Prior to the addition of Cu^{+}, proteins were treated with 15 mM DTT in an anaerobic glove box (Faircrest, O_2 $<$2ppm), after which DTT was removed by buffer exchange using a PD-

10 desalting column (GE Healthcare). Copper was added as a solution of Cu(I) prepared from Cu(I)Cl, in 1 M NaCl, 100 mM HCl under anaerobic conditions. Additions of metal ions during titrations were made using a microsyringe (Hamilton) into a septum-sealed quartz cuvette. Control experiments where Cu(I) was titrated into buffer alone resulted in no change of the spectroscopic properties of the buffer, therefore observed changes were due to Cu(I)-binding to the protein or copper chelator.

2.7 UV-Visible Spectroscopy

UV-visible spectroscopy is carried out by measuring the energy absorbed by a sample from light in the UV (240 – 400 nm) and visible (400 – 800 nm) wavelength range. Wavelength and energy are related by the equation:

$$E = h(c/\lambda) \tag{2.4}$$

where h is Planck's constant and c is the velocity of light in vacuum. Photon energy between 200 and 780 nm allows excitation of outer valence electrons and selected inner shell d-d transitions. Typically, bonding orbitals are fully populated and transitions between ground and excited states are accommodated by electrons jumping to anti-bonding orbitals [95]. For proteins, these $\pi \rightarrow \pi^*$ transitions are observed in the aromatic sidechains of Tyr, Trp and Phe which absorb light in the near-UV region (240 – 300 nm) [96].

Absorbance is a dimensionless quantity representing the proportion of incident light

intensity (I_o) that is transmitted through the sample (I), and is defined by the equation:

$$A = log(I_o/I) \tag{2.5}$$

The absorbance measured by a UV-vis spectrometer is used to determine protein concentration according to the Beer-Lambert Law:

$$A = \varepsilon cL \tag{2.6}$$

where A is absorbance, ε is molar extinction coefficient (units M^{-1} cm^{-1}), c is protein concentration (units M), L is cell path length (units cm). Each chromophoric residue contributes to the molar extinction coefficient of a protein, but this value is dependent on the protein fold and must be determined experimentally. Here, the molar extinction coefficients reported for each protein have been determined experimentally previously [97]. In order to ensure accuracy of this value, it is essential that the protein is effectively purified as contaminants or other proteins would contribute to the absorbance. Removal of nucleic acid contamination with high-salt wash steps during purification was essential, as pyrimidine and purine ring systems experience their own $\pi \rightarrow \pi^*$ transitions that create overlapping absorbance at 260 nm [95]. Also, disulfide bonds formed between two cysteine residues also give rise to an absorbance band near 260 nm and, so, protein concentrations were calculated after reduction of disulfide bonds using dithiothreitol.

2.8 Circular Dichroism

Circular dichroism spectroscopy is a technique that measures the difference in absorption by chiral molecules of left- and right-handed circularly polarised light (L-CPL and R-CPL, respectively). Chiral molecules exist as isomers which form non super-imposable mirror images, called enantiomers. Most amino acids, and thus proteins, are chiral.

CD occurs at wavelengths absorbed by a chiral molecule, using a polarimeter to measure the rotation of the linearly polarised wave upon travelling through the sample. Light is passed through two monochromators, whose optics ensure light is monochromated and linearised, before passing through a modulator.

When the resultant, circularly polarised light is passed through an optically active sample, the L-CPL and R-CPL will be absorbed to different degrees. Thus, the light becomes elliptically polarised and thus magnitude of circular dichroism is expressed as molar ellipticity [ϑ] (angle whose tangent is ratio of minor and major ellipse axes) or (here) as the absorption difference, $\Delta\epsilon$:

$$\Delta\epsilon(\lambda) = \epsilon_L(\lambda) - \epsilon_R(\lambda) \tag{2.7}$$

where ϵ_R and ϵ_L are extinction coefficients of right- and left-handed components of light of wavelength λ, and the units of $\Delta\epsilon$ are $M^{-1}cm^{-1}$ [98].

CD spectra of proteins are not the sum of the individual residues but depend upon the overall protein structure, with individual elements displaying their own CD behaviour. The far-UV spectra ($<$250 nm) are dominated by amide chromophores and denote ele-

ments of secondary structure. The near-UV spectra (250 –350 nm) are dominated by $\pi \rightarrow \pi^*$ transitions of aromatic residues and denote ligand-binding, tertiary structure and protein folding [99]. Here, CD spectra have been recorded to establish the range of ligand concentration over which protein conformational changes have taken place. Previous CD spectroscopical studies have established the near-UV fingerprint of CopZ over a range of Cu(I) / protein ratios, establishing the signal changes at (+) 265 nm and (-) 335 nm to arise from ligand-metal charge transfer bands.

2.9 Stopped Flow UV-Visible Spectroscopy

Stopped flow rapid reaction kinetics enables rapid sample mixing and monitoring of spectral changes with time. The stopped flow design comprises two sample syringes from which the flow is controlled by a drive ram. When a shot is fired, a predetermined volume of each sample is combined in a mixing chamber and driven through to an observation cell. Filling of the subsequent stop syringe determines when flow is stopped, which simultaneously triggers data acquisition. This enables reactions to be monitored at a controlled temperature with an extremely short dead time (< 2 ms). In order to monitor absorbance changes associated with bidirectional copper transfer between CopZ and CopAab, samples of apoprotein and its copper-loaded partner were loaded into the sample syringes and several shots fired to establish a baseline before spectral acquisition. For data collection, the temperature of the syringe chamber was controlled and equilibrated, and three individual shots were averaged for each experiment.

2.10 Layout and Function of ESI-TOF Mass Spectrometer

The ESI mass spectrometer comprises the stages: ion source, transfer, mass analyser, and TOF/detector. A schematic of the Bruker microToF Q III ESI-MS instrument used in this work is presented in **Figure 2.11.1** [100]. After the sample is introduced to the ESI source, by way of a continuous flow system into the spray chamber, charged analyte ions are generated. The ion cloud is focused into a stable trajectory and guided by applied voltages at progressively decreasing pressure through the subsequent stages. The transfer stage (funnels/hexapole) focuses the ion beam and mass analysers (quadrupole/collision cell) sort and separate ions according to their m/z ratio, with selected ions passed to the TOF/detector where their abundance is measured as an electric signal, from which a mass spectrum is generated.

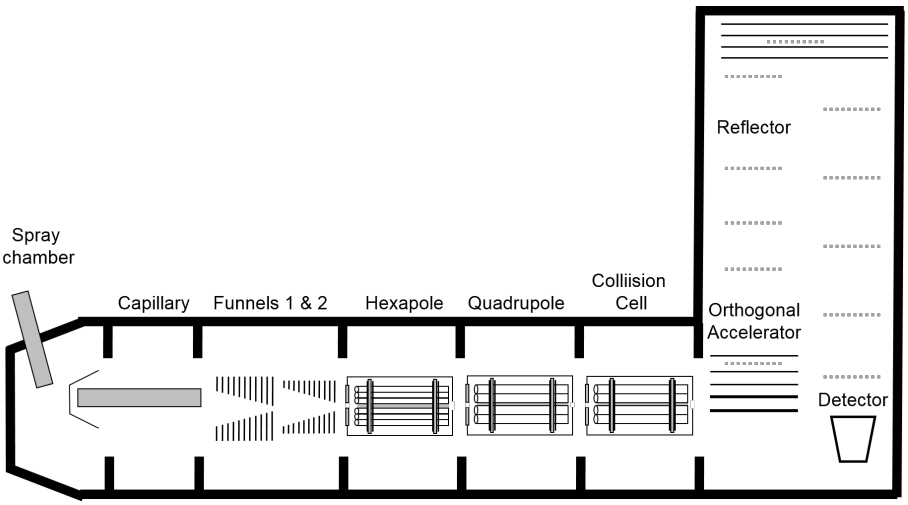

Figure 2.10.1: ESIMS schematic Representation of the stages comprising the Bruker micrOTOF Q III ESI-MS. The sample is introduced through the spray chamber, with resulting gas-phase analytes focused in the funnels and hexapole, and guided through the mass analysers, then to the TOF/detector which generates a mass spectrum. Figure adapted from [100].

2.10.1 The Ion Source and Electrospray Ionisation

Electrospray ionisation requires the generation of small charged droplets due to the presence of an electric field. The process of electrospray ionisation is depicted in **Figure 2.11.2** and can be described in terms of three steps: production of charged droplets, solvent evaporation and final droplet ionisation, whereby the gas phase ion is formed.

The ESI process takes place when a dilute ($\sim$ 1 – 15 μM) liquid sample passes at low flow rate ($\sim$ 1 – 5 μL / min) through a nebulizer needle into the spray chamber. Volatilisation of the sample is aided by a sheath of nebuliser gas (N_2) that flows around the tip of the needle. Ionisation takes place in one of two modes, defined by the polarity applied which creates electron flow, either to or from the capillary. Though it is common for charge to be applied to the needle, the Bruker microToFQ III generates an electric field by applying a high voltage to the capillary and spray shield. In positive mode, solvent oxidation occurs and positively charged ions are selected due to the charge differential applied between the needle and capillary; in negative mode, the opposite occurs, selecting for negatively charged ions. Polar solvents are amenable to these redox processes; when water is used, for example, the reactions in Equations 2.8 – 2.10 will take place [101].

$$2H_2O \quad \longrightarrow \quad O_2 + 4H^+ + 4e^- \tag{2.8}$$

$$2H_2O \quad \longrightarrow \quad H_2O_2 + 2H^+ + 2e^- \tag{2.9}$$

$$H_2O \quad \longrightarrow \quad HO^* + H^+ + e^- \tag{2.10}$$

The process of charged droplet formation in positive mode, for example, would begin when accumulation of positive charges would cause the solution to be repelled from the capillary needle and drift toward the outlet (also influenced by flow). As the fluid meniscus is drawn outward from the capillary tip a cone shape, called the Taylor cone [102], is formed and the high field strength and turbulence in this region causes a fine stream of liquid to be ejected. This stream easily breaks up into droplets of approximately 3 μm in diameter which are subjected to further evaporation by the stream of nebulisation gas flown coaxially around the spray needle.

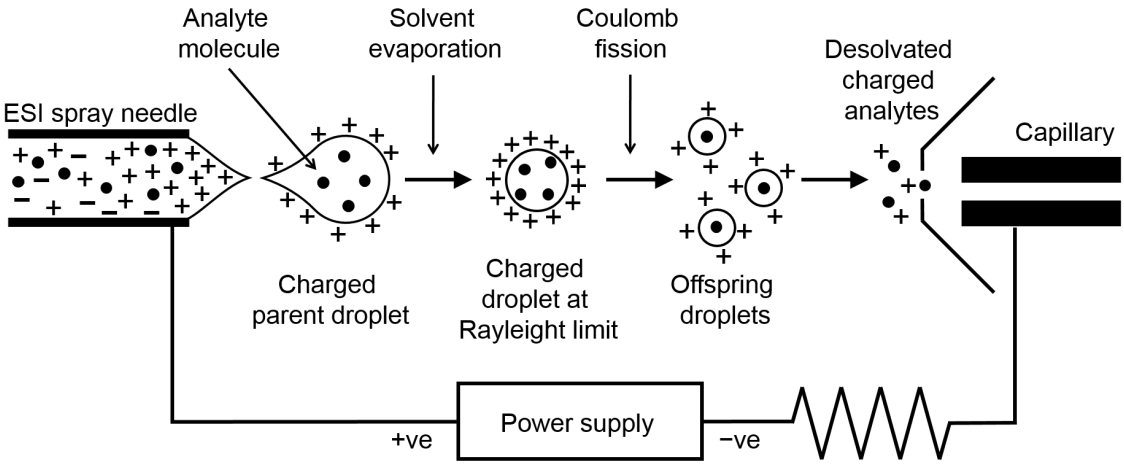

Figure 2.10.2: Mechanism of electrospray ionisation. Representation of the ESI process that takes place upon introduction of liquid sample into the spray needle. Applied voltage between the spray needle and capillary assists with ionisation and draws the gas-phase analyte ions into instrument. Drying gas (N_2) that flows countercurrent to the ion path prevents entry of uncharged components.

The potential energy is minimised within these charged droplets by arrangement of positive charges on the droplet surface. These positive charges also help drive the flow

of ions toward the counterelectrode i.e., the heated, charged capillary at the entrance to the mass analyser. Opposing forces in the droplet are surface tension which tries to retain spherical shape and Coulomb repulsion between like charges which tries to break down spherical shape. Solvent evaporation occurs rapidly between the spray needle and capillary, decreasing the droplets' size. As the droplet shrinks, the surface charges encroach upon each other until the Rayleigh limit is reached, beyond which further expansion is facilitated by Coulombic repulsion and the droplets disburse into smaller droplets. The offspring droplets typically hold about 2% of the mass and 15% of the charge of the parent droplet [101] so, in addition to being smaller, the offspring droplets also feature a decreased ratio of mass-to-charge. Successive cycles of evaporation and expansion result in formation of a nanodroplets with high charge, which undergoes a final step of desolvation to form the charged analyte. The typical lifetime of a droplet is < 10 ms, dependent upon factors including ion spray voltage, solvent, nebuliser gas flow and temperature.

The ions generated via ESI-MS are produced by addition (or removal) of a charged atom/molecule (such as H^+ or $NH_4{}^+$) and are therefore termed quasi-molecular ions; a true molecular ion would occur through removal or addition of an electron [103]. The mechanism by which charged gas-phase analytes form from the evaporated nanodroplets is under debate, with two proposed models: the charge residue model (CRM) and the ion evaporation model (IEM). In the charged residue model (CRM) [104], the final product of repeated solvent evaporation and Coulomb fission is a final droplet sufficiently small to contain only one analyte molecule which, upon complete desolvation, is coated with surface charges to become the gas phase charged analyte. The ion evaporation model (IEM) [105] states that,

as the droplet radius shrinks, the condensing surface charge generates an electric field, which eventually is large enough to eject solvated analytes which then acquire charge as they are emitted through the droplet surface. Generally speaking, evidence supports CRM for larger biomolecules and IEM for small inorganic and organic ions [101].

Next the ion beam enters the ion transfer stage, where transmission is maximised via separation of analyte ions from drying gas and solvent before transfer to the mass analyser stage. The gas-phase charged ions are drawn into the ion transfer stages through a charged orifice plate (spray shield) mounted in front of a metal coated glass capillary. Heated drying gas (N_2) flows from behind the spray shield, countercurrent to the ion beam, to assist with drying (and thus generation of gas-phase analyte) and removal of uncharged material. Curtain gas is used in the opposite direction to the ion beam flow path to ensure only charged gas-phase ions enter the capillary [106]. A charge differential of 400 – 500 V between the spray shield and capillary helps to focus the beam through the capillary which exits into the tandem funnel section.

The funnels are at low pressure ($\sim$4 mbar) and comprised of successive, spaced rings with progressively decreasing inner diameters that generate the funnel-shaped void through which the ions are transmitted. Beam scattering is reduced through decreased pressure and an applied RF potential to overcome space-charge effects (repulsive force of a dense, like-charged ion beam) [107]. A DC potential applied to the first and last rings guides the beam toward the funnel exit. Altering the DC potential of funnel 1 affects the acceleration of ions into funnel 2, which is manipulated to carry out in-source collision induced dissociation (isCID) [100].

The gas-phase charged analytes then enter a hexapole, where the pressure is lowered to $\sim 10^{-4}$ mbar. The purpose of this stage is to effectively transport and focus the ion into the analytical quadrupole. Again, the ion beam is aligned and focused onto the hexapole axis by an applied RF voltage and a focusing lens at the end of the stage. Also at the end of the stage is a gate lens which inhibits cross-talk by ”pulsing” ions through into the mass analyser stage [100].

2.10.2 Quadrupole Mass Analysers

Prior to entering the TOF/detector stage, ions pass through the low pressure Q-q stage comprising an analytical quadrupole and a second quadrupole (collision cell) [100]. During MS operation, the analytical quadrupole acts as an ion guide which transmits a broad range of masses, with low collision cell energy to avoid fragmentation. During MS/MS operation, the analytical quadrupole acts as a mass filter to isolate a single mass, or a range of ion masses, which can be fragmented by elevated collision cell energy [101].

The analytical quadrupole contains four rods in a square configuration that generates a path in the + z-direction. An oscillating electric potential containing DC (U) and AC (V) components, equal in magnitude but opposite in sign, is applied to opposing rod pairs:

$$\phi_0 = U - V cos(\omega t) \quad and \quad -\phi_0 = -U + V cos(\omega t) \tag{2.11}$$

This oscillating field will constantly subject ions within the quadrupole to an alternating

attractive force toward the x- and y-axis. Ion motion along the z-axis is unaffected, with a separate electric potential driving acceleration through the quadrupole. The oscillating potential focuses the trajectory of the ions toward the centre of the quadrupole, with ions subjected to the net force:

$$F = [(x^2 - y^2)/r_0^2]\ [U + Vcos(\omega t)] \tag{2.12}$$

Therefore for particular values of U, V, ω, within a quadrupole of radius r_0, an ion's position, defined by x and y, will be confined within the four rods and pass through the quadrupole (stable ion trajectory). For other values, the ion strikes one of the rods and is lost (unstable trajectory) [108]. A stable ion trajectory can be defined by mathematical solutions to Equation 2.12, shown in Equations 2.13 and 2.14. These have been adapted from the Mathieu functions [109], originally derived to describe the vibrations of elliptical membranes:

$$q_u = q_x = -q_y = \frac{4zeV}{m\omega^2 r_0^2} \qquad or \qquad V = q_u(m/z)\frac{\omega^2 r_0^2}{4e} \tag{2.13}$$

$$a_u = a_x = -a_y = \frac{8zeU}{m\omega^2 r_0^2} \qquad or \qquad U = a_u(m/z)\frac{\omega^2 r_0^2}{8e} \tag{2.14}$$

Here, e is the magnitude of the electron charge, U is the DC potential, V is the RF potential; for a given quadrupole, r_0 and ω are constant.

A plot of these equations (**Figure 2.10.3**) defines regions of stability for different ions i.e., combinations of U and V which do not let x and y reach or exceed r_0. Comparing

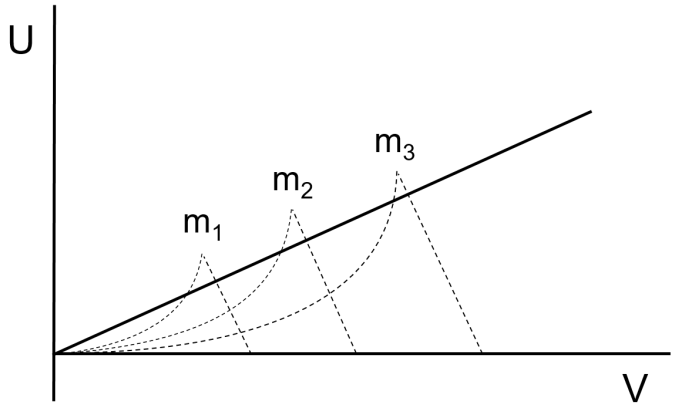

Figure 2.10.3: Regions of ion stability within a quadrupole The solutions to Eqn 2.13 and 2.14 overlap to generate triangular regions of stability for ions of different masses, as a function of U (DC voltage) and V (RF/AC voltage). The line on the plot marks the hypothetical relationship between U and V. Hypothetical masses (m) separated by 1 mass unit are labelled, where m1 $<$ m2 $<$ m3. For MS only mode, U = 0 and broad ion transmission occurs. For MS/MS mode, appropriate combinations of U and V enable particular ions to be selected and transmitted to the collision cell.

the Eqn 2.13 and 2.14 illustrates that U and V have a linear relationship. Therefore a quadrupole must be operated along this line for multiple ion detection. Due to the stability diagram shapes, increasing the slope of this line leads to greater instrumental resolution; the line drawn in Fig 2.10.3 illustrates mass detection at unit resolution. Therefore, in MS/MS mode, when both DC and AC components are present, resolution and selection of particular m/z values is possible [110].

During MS mode, the analytical quadrupole is set to RF only (U = 0) and, for low values of V, broad mass transmission is observed. Increasing V will establish a threshold mass, below which transmission through the quadrupole is not possible. For example in **Figure 2.10.3**, when U = 0, V can be selected such that all ions with masses equal or lower than

m_1 will have an unstable trajectory, and all those above m_1 will have a stable trajectory and be transmitted through the quadrupole.

After ions exit the analytical quadrupole, they enter the collision cell where pressure is elevated slightly ($\sim 10^{-4}$ vs $\sim 10^{-2}$ mbar), due to the presence of neutral N_2 collision gas [100]. Acceleration of ions into this stage at increased pressure leads to fragmentation, but also increases the risk of ion loss due to molecular collision. This is compensated by a lens at the entrance to focus the ion beam, and the RF field of the collision cell (also a quadrupole) leads to dissipation of energy, and focuses parent and fragment ions. Because arrival times to the detector are used to measure m/z values, ions must begin their journey in the TOF/detector stage simultaneously, which is controlled at the end of the collision cell. Here, during fragmentation, a transfer lens blocks transmission, while a gate lens allows transmission. This arrangement enables adjustment of the time frame for ion accumulation before transfer to the TOF/detector stage.

2.10.3 Time-of-Flight/Detector

The TOF/detector stage comprises three parts: orthogonal acceleration stage, reflector and detector. Orthogonal acceleration takes place in a region containing stacked electrodes, and occurs in two parts. First, incoming ion flow fills the pulsing region; ions which pass through are excluded from analysis. Second, voltage pulses periodically deflect the ion population upward toward the reflector. Before pulsing another ion packet upward, the previous packet would have reached the reflector.

The accelerated ions reach the deflector plate (an electrode) and are subjected to further pulsed voltage, after which they are accelerated to the TOF analyser. Due to slight variation in initial ion velocity and position within the accelerator, the final kinetic energy is variable. An advantage of orthogonal acceleration is improved resolution, as ion penetration into the reflector aids in normalising the final kinetic energy.

Detection takes place by way of a microchannel plate collector, comprising a solid core assembly with millions of microchannels, small pores 5 - 10 μm in diameter. Each of them functions as an independent electron multiplier, where the ion signal is converted and amplified into an electrical signal. This arrangement minimises saturation and occurs rapidly ($<$1 ns) to improve resolution.

The mass spectra generated feature intensity on the y-axis and mass-to-charge (m/z) ratio on the x-axis. The m/z value defines each ion measured in the detector, and is calculated by time-of-flight, acceleration voltage and length of the drift region. Determination of m/z occurs in the field-free drift region based upon the precise time it takes to impact the detector. Drift time is measured after ions are accelerated upward to a fixed kinetic energy (several thousand electron-volts), when they assume different velocities depending upon their m/z ratio.

Chapter 3

Electrospray Ionisation Mass Spectrometry for Proteins

3.1 Introduction

The development of ”soft” electrospray ionisation (ESI) [111] was a pivotal advancement for biomolecular mass spectrometry, as it allowed transfer of intact proteins to the gas phase [112], enabling investigation of biomolecular assemblies up to several hundred kilodaltons with high resolution and mass accuracy [113].

Subjecting proteins to the ESI process (Chapter 2.10) involves imparting charge via addition or removal of a proton, generating ”quasi-molecular ions” (rather than true ions generated via addition/removal of an electron). This is accomplished by nebulisation of the sample in the presence of applied voltage and, though fragmentation is unlikely due to low internal energy, molecular changes take place during the few millisecond lifetime of the charged analyte droplet [114]. Evaporating solvent causes change in forces which balance the tertiary structure of a protein: loss of hydrophobic interactions, and enhancement (typically) of electrostatic interactions [112], collapse of side chains, which alternately could form stabilising hydrogren bonds with carbonyl groups [115]. The final desolvation step is rapid (nano/picosecond range) and generates the final ”dried off” gas-phase analyte [116].

ESI-MS, like other biophysical techniques, has strengths and limitations; its interpretation requires caution and understanding of potential discrepancies between solution- and

gas-phase observations. For example, the possibility exists that distorted equilibrium would arise during ionisation due to radical concentration changes within the analyte droplet [113]. Another possibility is non-specific association between species in the ”final” droplet, which do not represent an intial association in solution [117]. Thus, ESI-MS spectra should be interpreted among a wider body of evidence. However, it has been observed that only a small percentage of gas-phase ions result from ion-molecule interactions [118] and it has been suggested that final desolvation occurs on a nanosecond timescale with no changes in protein structure [119]. Non-specific final droplet interactions are likely weak and would readily dissociate after desolvation, and can be overcome by working at low concentrations, using solutions of high purity [120]. In addition, there is strong evidence in favour of agreement between gas- and solution-phase data, for example in heat shock proteins [121], $\alpha\beta$-crystallin [122], and in myoglobin and β-lactoglobulin [123].

The versatility and high sensitivity of ESI-MS makes it a powerful approach to biochemical analysis. Experiments can be carried out on a short timescale using only picomolar amounts of protein, as opposed to the millimolar concentrations required for nuclear magnetic resonance (NMR) or isothermal titration calorimetry (ITC) [124]. Though other techniques such as surface plasmon resonance and fluorescence spectroscopy rival ESI-MS in terms of sensitivity, these techniques often require modification of analyte via immobilisation or tagging [113], whereas ESI-MS depends only upon the intrinsic property of mass.

ESI-MS also can be coupled to an high-performance liquid chromatography (HPLC). Insertion of this separation stage prior to ESI-MS allows mixtures of proteins to be resolved.

The proteins could then be subjected to a ”top-down” analysis, where the proteins are intact during ESI and subsequently fragmented in the mass spectrometer [116]. This approach could also be applied in a ”bottom-up” approach, where an enzymatically cleaved protein is separated in the HPLC, then introduced via ESI, and the fragmented peptides analysed, or potentially fragmented further, in the MS. HPLC typically involves analysis under denaturing conditions, where sample purity and protein identity can be confirmed, ionisation is encouraged (due to the increased surface area and acidified solvent), and ligand binding is inhibited due to abolition of the ”native” protein fold and related binding sites [125].

Native ESI-MS describes experiments using volatile buffer which, coupled with the gentle ionisation of the ESI process, enables weak, non-covalent interactions to be maintained. This facilitates the investigation of unfragmented analytes and their complexes, which can be investigated under near-physiological conditions. Direct infusion of the sample into the ESI source allows a mixture of analytes to be investigated simultaneously. The m/z and mass spectra enable identification of the analyte of interest, mass shifts associated with adduct formation, and ligand binding, and can also provide structural and conformational information [125].

Here, ESI-MS has been utilised in analysing unfragmented copper trafficking proteins, assessing: multimer formation, ligand binding, stoichiometry and distribution of protein species in a mixture. This chapter contains information about the steps taken to interpret these mass spectra and to optimise parameters during data acquisition.

3.2 Evaluation of Protein Mass Spectra

3.2.1 Spectrum Deconvolution

Applying the ESI process to a protein sample in volatile buffer will generate gas-phase ions which typically acquire multiple charges. In addition to varying with mass, conformation and primary sequence, there will be fluctuation in the availability of surface-exposed sites for ionisation, even within a sample. Thus the number of charges a given protein acquires will vary and the resulting m/z spectrum will contain multiple peaks.

Each protein species appears as an envelope of ion peaks in the m/z spectrum, separated by one charge, which must be resolved to obtain the neutral mass spectrum **(Figure 3.2.1)**. This is advantageous because, even for large macromolecular assemblies, the resulting range of mass-to-charge (m/z) ratios, are consolidated onto a scale typically accommodated by mass analysers.

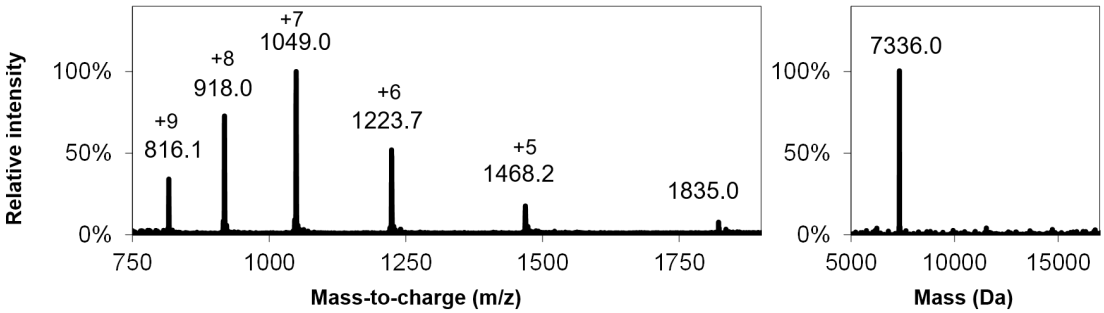

Figure 3.2.1: Mass spectrum before and after deconvolution The ESI-MS generates a mass spectrum that plots relative intensity against mass to charge ratio (**left**) where multiply charged species will appear as a grouping of peaks. The process of deconvolution converts this to a mass spectrum displaying the neutral parent mass (**right**).

This group of peaks will display a roughly Gaussian distribution, with a sequential charge state distribution i.e., there is no jump in the number of charges between peaks. Using Figure 3.2.1 as an example, acquired in positive ion mode, simple calculations can be made to resolve these peaks (deconvolution) [126]. In order to calculate the parent mass M_r, the number of charges (n_1 and n_2) on two neighboring peaks, m/z_1 (higher) and m/z_2 (lower) can be defined as:

$$n_2 = n_1 + 1 \tag{3.1}$$

Using m_H for the mass of a proton and assuming all charges *n* arise due to protonation, m/z_1 and m/z_2 can be defined by:

$$\frac{m}{z_1} = \frac{(M_r + n_1 m_H)}{n_1} \tag{3.2}$$

$$\frac{m}{z_2} = \frac{(M_r + n_2 m_H)}{n_2} \tag{3.3}$$

inserting the expression for n_2 from Eqn 3.1 into Eqn. 3.3. and using simultaneous equations to derive an expression for n_1:

$$n_1 = \frac{(m/z_2 - m_H)}{(m/z_1 - m/z_2)} \tag{3.4}$$

Subsequently, the value of M_r can be determined by rearranging Eqn 3.2 and inserting the

determined value of n for the particular value of m/z_1:

$$M_r = n_1(m/z_1 - m_H) \tag{3.5}$$

In **Figure 3.2.1**, without knowing M_r, the above method of charge deconvolution can be applied (Eqn 3.4), for example, to the neighbouring m/z values 918.0 (m/z_2) and 1049.0 (m/z_1), with charges n_2 and n_1, respectively, to determine the parent neutral mass M_r. Accordingly:

$$n_1 = (m/z_2 - m_H)/(m/z_1 - m/z_2) = (918 - 1)/(1049 - 918) = 7$$

Therefore using this value for n_1, M_r can be calculated from Eqn 3.5:

$$M_r = n_1(m/z_1 - m_H) = 7(1049 - 1) = 7336$$

This straightforward, arithmetic method works well for single compounds or mixtures where peak envelopes do not overlap. However, in many cases manual assignment would be too difficult and, therefore, an automated method is typically used, with software equipped with the capability for charge deconvolution; here, the algorithm used is Maximum Entropy Charge Deconvolution [127]. This utilises all spectral data to generate parent spectra, and was designed to overcome the noise occurring in native mass spectra, and reduce artefacts arising from overlapping peak envelopes [128]. This allows automatic generation of a neutral parent mass spectrum from charge state envelopes which appear in the mass

spectrum.

The mass spectrum before and after deconvolution is scaled in percent relative intensity, which enables spectra from different experiments to be compared on a universal scale. The raw MS data results as ions are summed as they pass the microchannel plate detector (see Chapter 2), generating absolute counts of individual ions. However, depending upon the length of experiment and number of species in solution, the total counts and maximum value of total count will be variable. Therefore these values are typically normalised to the highest absolute count, which becomes 100% relative intensity. Percentages which are normalised to the most intense peak will ”weight” species differently compared to the case where percentages represent a propotion of total molecules present.

ESI-MS charge deconvolution generates a neutral mass based upon the number of observed charges (protons in positive ion mode) on each m/z peak. Depending upon the protein's initial charge in solution, the number of additional protons acquired may not equal the observed charge state. Thus, though the mass spectrum prior to deconvolution indicates the number of protons bound in the gas phase, the neutral mass does not report on solution phase characteristics such as charge or number of protons retained by side chains [129]. Furthermore, in the case of a protein with a metal ion bound, the positively charged ion will offset the number of protons bound to achieve the observed charge state [106]. Here, it has been assumed that the charge state observed is attributable to protonation, except where mass shifts such as those due to Cu^{+} are observed.

3.2.2 Exact Mass Analysis

Confirming the exact mass of the protein of interest is essential in order to identify it and monitor mass shifts. The reported mass for a protein is usually its isotopically averaged neutral mass, with the mass contribution of each element weighted according to its natural abundance. For example, the mass of carbon is 12.011 due to the natural abundance of ^{12}C = 98.9% and ^{13}C = 1.1%, but the proportion of carbon-13 in a protein structure might vary slightly from 1 out of every 100 carbon atoms. Therefore, a protein sample will contain a mixed population of molecules that, in a mass spectrum, is displayed as a cluster of peaks (**Figure 3.2.2**), or envelope, centred upon the isotopically averaged mass.

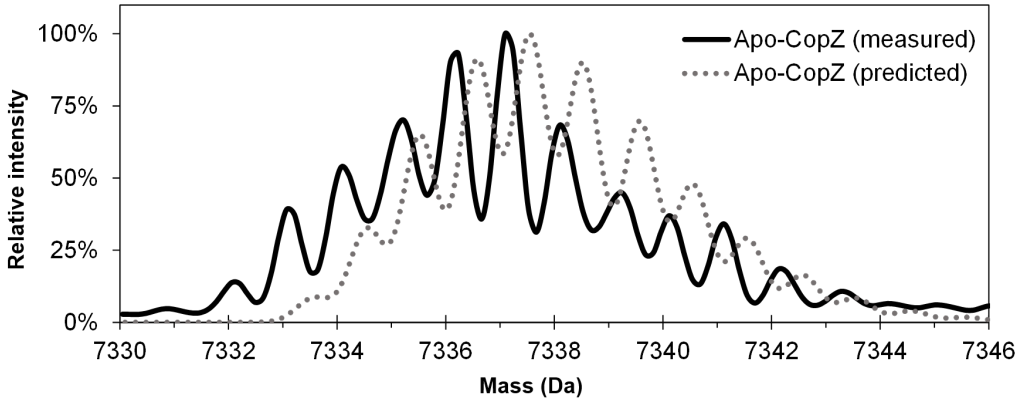

Figure 3.2.2: CopZ isotopic distribution observed by ESI-MS. Because the isotopic composition of a protein will vary from molecule to molecule, the mass of the most intense peak (most abundant isotopomer) could vary from spectrum to spectrum. Thus the species mass is taken from the peak centroid.

The most intense peak in the mass envelope is greater than the protein's monoisotopic mass, reflecting the increased likelihood of heavier isotopes being included in the molecular structure for larger molecules such as proteins. With increased protein mass,

the resolution of these isotopomers decreases as the likelihood of individual chemical formulas approaches unity, resulting in a more smoothed mass spectrum peak, centred on the averaged neutral mass. For peptides and smaller proteins, such as CopZ (M_r = 7338.1 Da), resolution of isotopic peaks is possible. **Figure 3.2.2** illustrates the overlaid mass spectra expected and acquired of CopZ, illustrating the isotopic resolution compared to that predicted based upon its sequence.

3.2.3 Charge State Distribution

The soft ionisation and high resolution of ESI-TOF-MS affords studies of intact proteins, where the identity of proteins and their complexes can be confirmed after the multiply charged mass spectrum is deconvoluted to provide the neutral mass spectrum. In addition to reporting on species' masses, interpretation of the mass spectrum prior to deconvolution provides additional insight, as the degree of protonation reports on the protein conformation. A higher charge state (greater value of z) corresponds to more sites available for protonation reflecting the higher surface area of denatured or less folded proteins [106]. In addition, a protein with many different charge states could indicate variability in surface accessibility arising if the protein has a less regular, unfolded structure. In short, more tightly folded proteins tend to have lower net charges (lower values of z) and lower distribution of charge states (fewer peaks in the m/z spectrum). **Figure 3.2.3** shows the charge state distribution arising from folded and unfolded protein in the mass spectrum of a sample of CopAab under different conditions.

The presence of denaturing solvent increases the number of peaks present and shifts

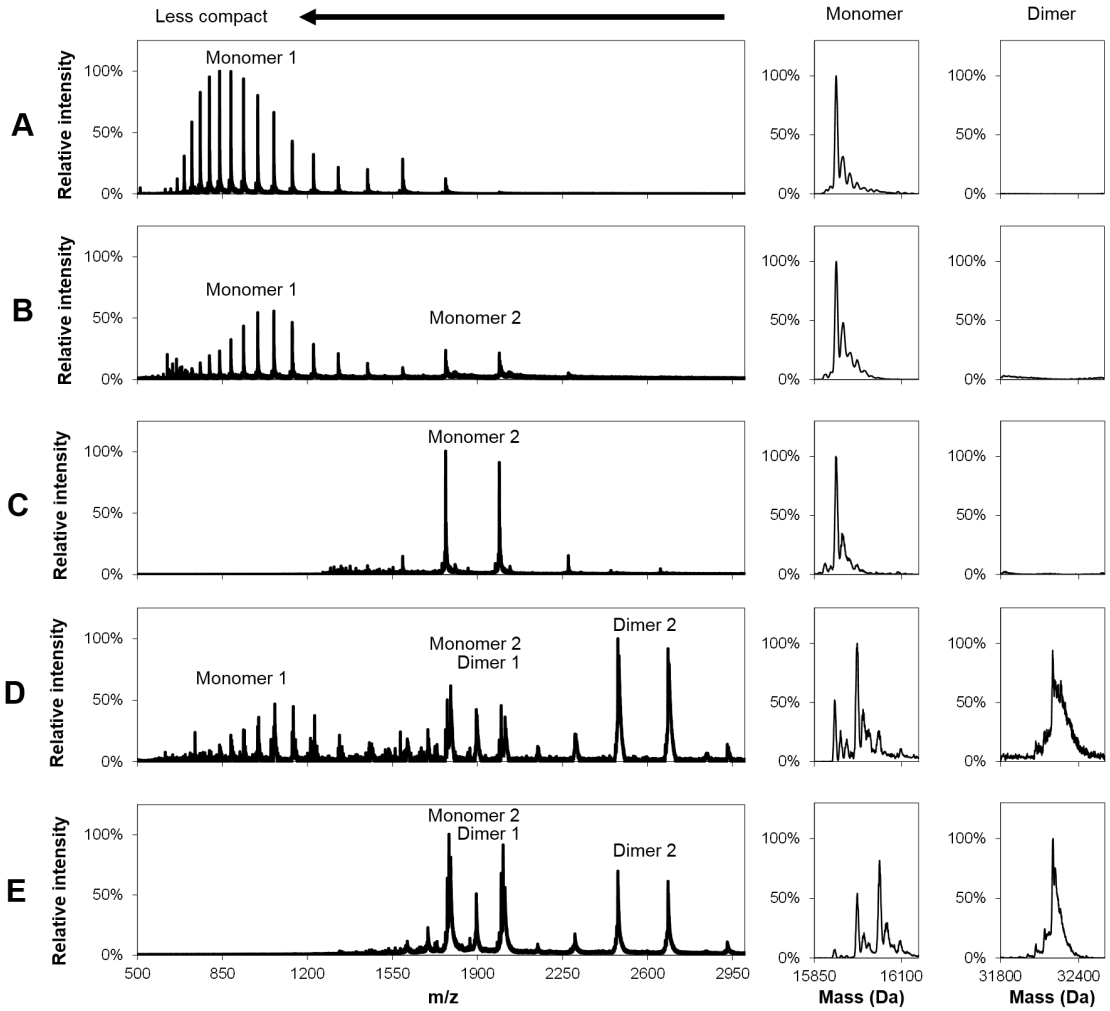

Figure 3.2.3: Mass spectra depicts folded and unfolded protein. Mass spectra recorded of CopAab: **A)** LCMS, denaturing, depicting entirely unfolded protein **B)** native, in AmmOAc + MeOH depicting partially unfolded protein **C)** native 0 Cu / protein, depicting folded protein **D)** native 4 Cu / protein + acetic acid, depicting partially folded protein, some with Cu(I) bound **E)** native 4 Cu / protein depicting folded protein with Cu(I) bound. The spectra illustrate that a single protein or mixtures of different protein species (here, monomer/dimer) in the neutral mass spectrum can be observed as multiple peak envelopes (separated or overlapping) prior to deconvolution. In addition, the monomer only spectra (A – C) illustrate that denaturing solvent leads to less folded protein, observed by a shift in m/z values. For simplicity, here, peaks not annotated.

the peak envelope, reflecting protein being in a less folded state (3.2.3A – C); this can arise from denaturation or other structural changes. Variations in solution phase conditions can partially destabilise the protein, allowing binding domain or mechanistic information

to be interpreted [122]. For example, the Cd binding behaviour of α and β domains of human metallothionein was tested at variable pH where changes in charge state distribution illustrated structural and cadmium-binding changes [130]. Shifts in charge state distribution and numbers of peaks can be used to denote multiple conformations/states of the same protein, leading to multiple peak envelopes, for example, if a protein forms multimers (see **Figure 3.2.4**).

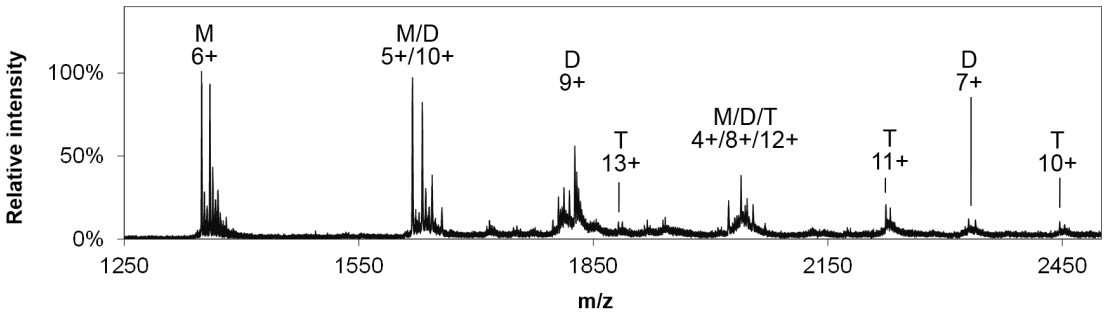

Figure 3.2.4: Multiple overlapped charge state envelopes observed for Atx1 upon Cu(I) binding. Atx1 from *S. cerevisiae* in the presence of Cu(I) forms monomer (M), dimer (D) and trimer (T), denoted by the multiple overelapping peak envelopes which appear in the mass spectrum. The charge envelope of each species has a quasi-Gaussian distribution and the charge states are sequential. Overlapped charge states are even numbered, and are grouped by multiples of the oligomeric state. Depending upon the degree of envelope shift, the odd-numbered charge states tend not to overlap.

Here, because the relative surface area to mass changes upon multimer formation, the degree of protonation will increase, but not linearly. For example, dimerisation will not lead to a doubling of the charge state [131] [132]. Because multimers do not increase their charge state directly in proportion to the number of protomers involved, the m/z ratio does not shift as a multiple of the mass increase, resulting in staggered peak envelopes.

3.3 Adapting ESI-MS method parameters

The goal of subjecting a protein to ESI under native solution conditions is to generate gas-phase analytes which are merely ”dried off”, mimicking as closely as possible the solution phase situation [119]. In order to achieve this goal, the method must be adapted to ensure thorough but gentle ionisation of a pure sample, and adjust the parameters on the ESI-MS instrument to appropriately visualise the species present in the sample.

To ensure sufficient sample quality requires high purity, removal of ion suppressants and contaminants, removal of detergents and plasticisers, and limited salt concentration to prevent ion suppression and mass shifts caused by adduct formation. In addition, a decreased amount of analyte can actually increase sensitivity, and can be achieved by either lowering sample concentration or flow rate [106].

Ultimately, optimisation of parameters in each stage of analysis must be customised for a protein's stability and gas-phase behaviour, as well as the experimental aims. When analysing the copper trafficking proteins, once pure sample was generated for ESI-MS, the proteins ionised well, with adjusting parameters to visualise the different species representing the major experimental challenge.

3.3.1 Source and Transfer Stages

Parameters in the ESI-MS source affect volatilisation and flow of ions into the transfer stage, ensuring maximal ionisation and transmission. Aerosol formation and solvent evaporation can be influenced by the nebulisation gas pressure, and the flow rate and temperature

of drying gas. Ionisation efficiency can be increased by adjusting the electrospray needle voltage and voltage gradient between needle and shield/capillary. However, here a balancing act is required where maximal ionisation takes place without thermally induced protein denaturation or “in-source decay” caused by high energy collisions [106]. For copper trafficking proteins, these parameters were adjusted slightly to minimise appearance of denatured protein with no major loss of ionisation intensity.

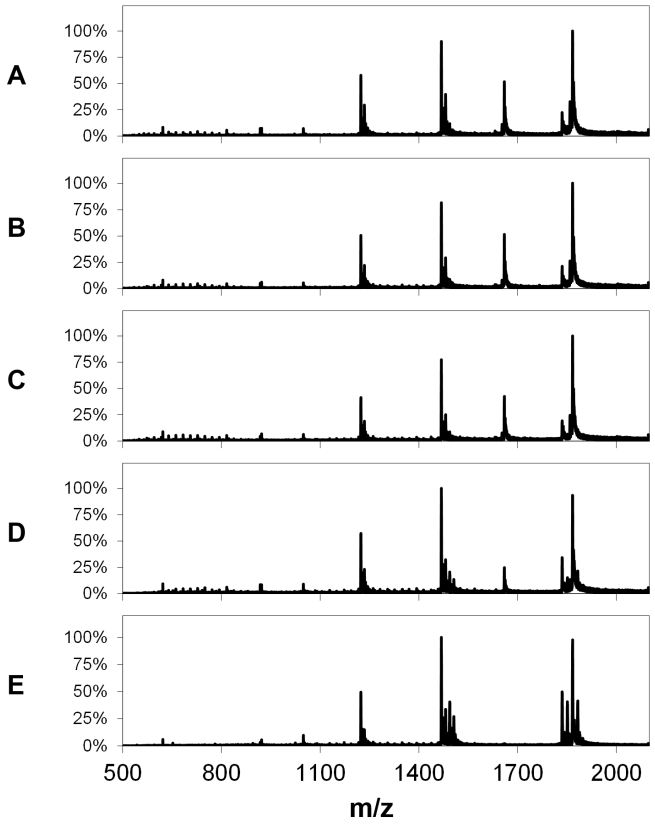

Figure 3.3.1: In-source collision induced dissociation (isCID). The process of isCID is carried out when voltages are adjusted within the transfer funnels, causing collision of analyte with neutral gas. Here, the effect of this process is shown for copper-loaded CopZ when the voltages are set at: **A)** 0 eV, **B)** 20 eV **C)** 40 eV, **D)** 60 eV, **E)** 80 eV. Spectral changes illustrate breakdown of dimeric protein species (m/z = 1675).

The first low pressure region containing the transfer funnels is the location of in-source

collision induced dissociation (isCID), where gas-phase analyte is accelerated against inert gas. This leads to increased internal energy which can be used to fragment a complex into subunits, remove salt/solvent from the analyte of interest, or potentially break covalent bonds resulting in a fragmented protein [133]. The effect of isCID upon CopZ is shown in **Figure 3.3.1**, where increasing between 0 – 80 V first led to increased overall ionisation (0 – 35 V), which is likely a result of improved focusing of the ion beam through the funnels and increased throughput into the Q-q stage. Subsequently (35 – 80 V), a decrease in intensity of the m/z = 1675 peak was observed.

In order to maximise transmission but prevent multimer breakdown, experiments using CopZ were carried with this parameter at 35 eV. For CopAab, increased ion intensity did not result from increased isCID voltage and therefore was set to zero in CopAab experiments.

3.3.2 Q-q Stage

The Q-q stage enables selection or enhancement of regions of interest of the mass spectrum, leading to improved resolution and signal intensity, and allowing changes in the analytes of interest to be visualised [134].

As described in Section 2.10.2, Collision RF (CRF) voltage is the AC component of the oscillating electric potential applied within a quadrupole which establishes the threshold for mass transmission. Increasing the CRF voltage results in an unstable trajectory for lower m/z ions. **Figure 3.3.2** illustrates the effect upon the mass spectrum of copper-loaded CopZ of CRF voltage. Optimisation was carried out at multiple copper loadings to ensure sufficient peak intensities of the overlapping monomeric/dimeric peak envelopes

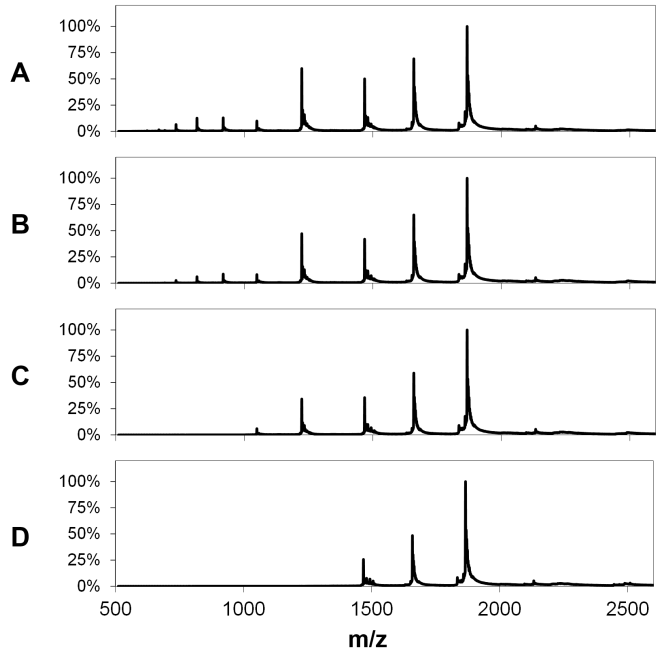

Figure 3.3.2: Effect upon mass spectrum of CRF voltage. Within the mass spectrum of CopZ (prepared at 2 Cu / protein) when all other parameters held constant, higher charge state peaks are suppressed with increased values of CRF voltage: **A)** 600 V, **B)**1600 V, **C)** 2400 V, **D)** 3200 V. The maximum possible value of CRF is 3800 V.

was attained as the copper level was changed, which established the experimental CRF voltage value of 2200 V. This also enabled exclusion of the higher charge state peaks, which represent unfolded protein that cannot bind metal, in order only to allocate intensity of folded protein to the deconvoluted mass spectra.

When a single value of CRF voltage does not enable multiple regions of the spectrum to be observed, its value can be fluctuated using the stepping function. This divides the acquisition time (weighted as %) between multiple values in order to visualise all species of interest. **Figure 3.3.3** illustrates the effect of the stepping function upon the mass spectra of copper-loaded CopAab, and shows how stepping can be used to create a combined spectrum focused on different spectral regions. In order to effectively visualise all species

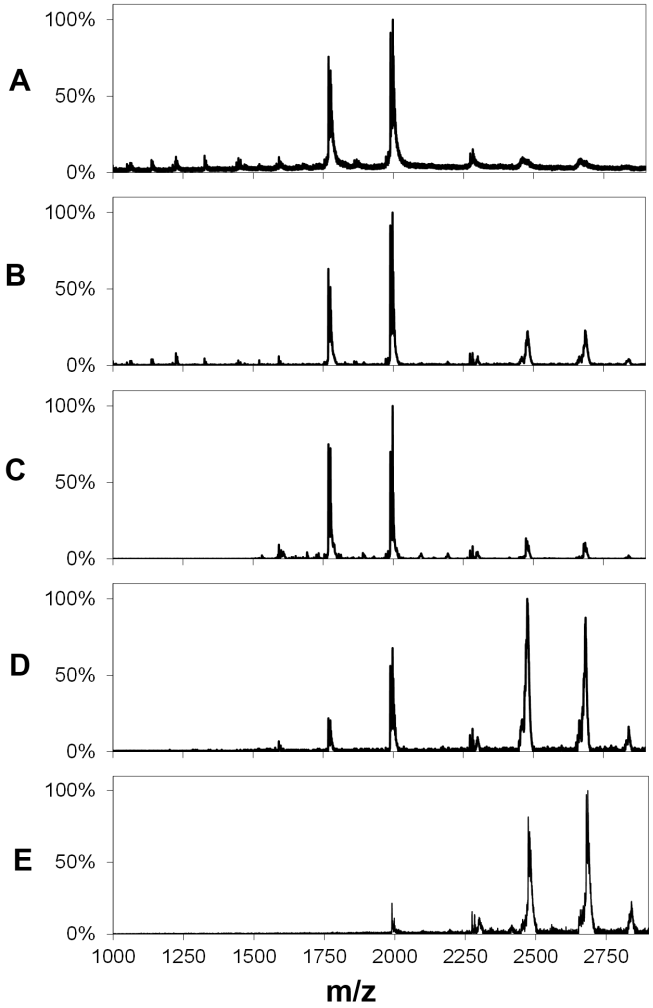

Figure 3.3.3: Stepping of CRF Voltage. During acquisition, increasing the CRF voltage leads to increased intensity of a progressively decreasing charge state. The stepping function allows this parameter to be fluctated within an experiment, and different regions of the spectrum can be observed together. **A)** 650 V monomeric peaks dominant; **B)** 2200 V, better resolution of the dimeric peaks; **C)** stepping: 90% at 2000 V, 10% at 3600 V, similar to previous; **D)** stepping: 75% at 2000 V, 25% at 3600 V, marked increase in dimer, decrease in monomer; **E)** 3600 V, near removal of monomer

together, stepping parameters were tested for multiple copper loadings of the protein, with the assistance of the automated tuning in the software.

Chapter 4

Studies Of Cu(I) Binding To CopZ

4.1 Introduction

The copper chaperone from *Bacillus subtilis*, CopZ, is a 69-amino acid residue protein containing a ferredoxin-like $\beta\alpha\beta\beta\alpha\beta$ fold in both apo- and Cu(I)-bound forms [40]. Its conserved MXCXXC Cu(I)-binding motif provides thiolate coordination to the Cu(I) at the end of loop 1, and binds Cu(I) with extraordinarily high affinity, $\beta_2 \sim 10^{22}$ M^{-2} [84]. The solution structure (see **Figure 7.1.2**) of apo- and Cu-bound CopZ indicate a monomeric species with the Cu(I) ion bound by the two cysteines and a third ligand, likely the sulfur from dithiothreitol (DTT) [40]. In addition to a CopZ monomer with a single Cu(I) ion bound, in the absence of low molecular weight thiols (LMWT) such as DTT (see below), CopZ has been demonstrated *in vitro* to dimerise upon binding Cu(I), coordinating between one and four Cu(I) ions [89]. A crystal structure of CopZ revealed a tetranuclear copper cluster coordinated at the dimer interface (**Figure 4.1.1**), with mixed trigonal and digonal Cu(I) coordination by Cys-13, Cys-16 and His-15 from each monomer [81]. Currently, the exact physiological relevance of the different forms of CopZ is unclear.

Also thought to be involved in managing cellular copper are non-proteinaceous cytoplasmic LMWT found across biology, such as glutathione (GSH) in eukaryotes [25] [135], mycothiol (MSH) in actinomycetes [26] [136], as well as coenzyme A and cysteine [137].

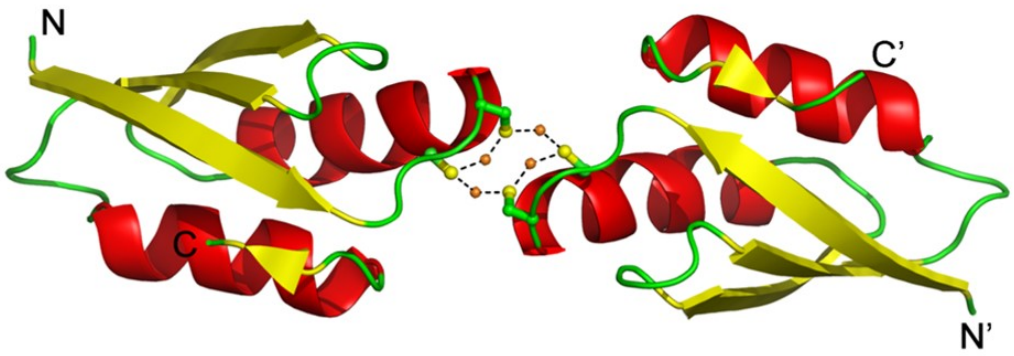

Figure 4.1.1: Crystal structure of $Cu_4(CopZ)_2$. Ribbon diagram derived from the crystal structure of CopZ solved at 1.5 Å resolution [81], depicting two CopZ monomers coordinating a tetranuclear Cu(I) cluster. Cysteine sulfurs are shown in yellow, copper ions shown in orange.

In 2009, it was discovered that low G+C Gram-positive bacteria (Firmicutes) such as *Bacillus subtilis* contains a distinct LMWT, bacillithiol (BSH), which is the α-anomeric glycoside of L-cysteinyl-D-glucosamine with L-malic acid [27]. LMWTs are known to bind Cu(I) with reasonably high affinities ($\sim 10^{-14}$ M for DTT) [138], or form heterocomplexes, as observed via NMR for CopZ, where a DTT-Cu-CopZ species was observed [40]. Through competition for Cu(I), LMWT and copper trafficking proteins may function in concert to ensure the cellular free copper concentration is virtually zero.

Previous *in vitro* studies clearly have revealed multiple Cu-bound forms of dimerised CopZ in the absence of LMWTs, while in the presence of LMWTs the copper-binding capacity of dimerised CopZ and other metallochaperone dimers [139] [52] was reduced. However, it is unknown exactly what effect this has on the CopZ speciation as spectroscopic techniques do not allow resolution of individual species within a mixture.

In order to monitor the individual species formed as CopZ responds to a fluctuation

in levels of copper in the absence and presence of LMWT, electrospray ionisation time-of-flight mass spectrometry (ESI-TOF-MS) was employed (see Chapter 3 for methods optimisation). ESI-MS has been used to characterise the metal-binding stoichiometry of other metalloproteins including metallothionein [140] and SlyD [134], along with copper chaperones CopZ *Enterococcus hirae* [141] and porcine Cox17 [142]. Knowing the relative affinities of BSH and CopZ for Cu(I), and the species which form in a mixture of CopZ, Cu(I), and BSH, provides insight into the cooperative role of BSH and CopZ in managing cytoplasmic Cu(I) in *B. subtilis*.

4.2 Materials and Methods

4.2.1 CopZ Sample Preparation For ESI-MS

CopZ was prepared as described in Section 2.2.1. Mass spectrometry samples of CopZ were prepared by first adding 15 mM DTT (Formedium) and removing reductant by passage down a G25 Sephadex column (PD10, GE Healthcare) in an anaerobic glovebox (Faircrest Engineering, O_2 concentration < 2 ppm) using 20 mM ammonium acetate, pH 7.4 (Sigma) as the elution buffer. Protein concentrations were calculated using an extinction coefficient, $\varepsilon_{276\,nm}$, of 1450 M^{-1} cm^{-1} [89]. UV-visible absorbance spectra were recorded on a Jasco V-550 spectrophotometer. To prepare Cu(I)-bound CopZ samples, a deoxygenated solution of Cu(I)Cl prepared in 100 mM HCl and 1 M NaCl was added to anaerobic, reduced CopZ using a microsyringe (Hamilton) in an anaerobic glovebox. Unbound Cu(I) was removed by passage of the sample down a G25 Sephadex column (PD10, GE Healthcare) equilibrated with 20 mM ammonium acetate pH 7.4. The protein sample was diluted with the same buffer to a working sample concentration of 15 μM.

4.2.2 Electrospray Ionisation Mass Spectrometry

Mass spectra were acquired using a Bruker micrOTOF-QIII electrospray ionisation (ESI) time-of-flight (TOF) mass spectrometer (Bruker Daltonics, Coventry, UK), in positive ion mode. The ESI-TOF was calibrated in the m/z range 300–2200 using ESI-L Low Concentration Tuning Mix (Agilent Technologies, San Diego, CA). Native protein samples were introduced to the ESI source via a syringe pump (Cole-Parmer) at 5 μL/min, and data ac-

quired for 3 min, with ion scans between 50 – 3000 m/z. MS acquisition was controlled using Bruker oTOF Control software, with parameters as follows: dry gas flow 4 L/min, nebuliser gas pressure 0.4 Bar, dry gas 130 °C, capillary voltage 4500 V, offset 500 V, isCID energy 35 eV, collision RF 2200 Vpp. LC-MS experiments were performed using an UltiMate 3000 HPLC system (Dionex, Sunnvale, CA, USA). A 1 μL injection volume of protein in 2% acetonitrile was applied to a ProSwift® reversed phase RP-1S column (4.6 × 50 mm, Dionex) at 25 °C. Gradient elution was performed at a flow rate of 200 μL/min using solvents A (0.1% formic acid) and B (acetonitrile, 0.1% formic acid), with the following chromatographic method: isocratic wash (2% B, 0–2 min), linear gradient from 2–100% B (2–12 min), followed by an isocratic wash (100% B, 12–14 min) and column re-equilibration (2% B, 14–15 min). MS acquisition parameters were as follows: dry gas flow 8 L/min, nebuliser gas pressure 0.8 Bar, dry gas 240 °C, capillary voltage 4500 V, offset 500 V, collision RF 650 Vpp. Processing and analysis of MS experimental data was carried out using Compass DataAnalysis version 4.1 (Bruker Daltonik, Bremen, Germany). The spectra were deconvoluted using the ESI Compass version 1.3 Maximum Entropy deconvolution algorithm over a mass range of 7000–16000 Da. Overlapping peak envelopes were deconvoluted manually. Exact masses were determined from peak centroids, with 3-point Gaussian smoothing applied to mass spectra of samples containing BSH and GSH.

4.2.3 Preparation Of CopZ Samples For Thiols ESI-MS

For ESI-MS experiments, CopZ was purified and prepared as described in section 2.2.1. ESI-MS experiments were carried out in 20 mM ammonium acetate, pH 7.4; CD and UV

experiments were carried out in 100 mM MOPS, 100 mM NaCl, pH 7.5. Thiol experiments were carried out using GSH (Sigma), DTT (Formedium) or BSH (synthesised as described previously [27]) (**Figure 4.2.1**), prepared anaerobically using deoxygenated LC-MS grade water (HiPerSolv, VWR)). Protein solutions were prepared using aliquots of 1.0 Cu(I) per CopZ, prepared as above, where thiol solution was added to yield ratios of 5, 10, or 25 thiol per protein.

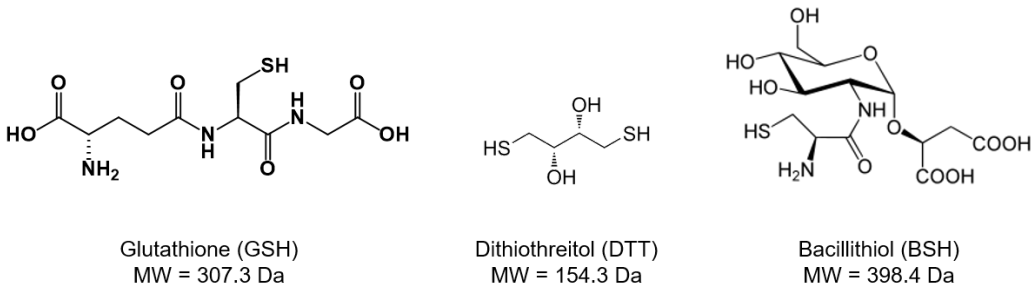

Figure 4.2.1: Structures of LMWT compounds used in ESI-MS experiments. Structures of LMWT used in ESI-MS experiments: glutathione (GSH), the eukaryotic analog of bacillithiol; dithiothreitol (DTT), a common *in vitro* reducing agent; bacillithiol (BSH), the cytoplasmic LMWT found in *B. subtilis*.

4.2.4 Determination of Cu(I)-BSH binding affinity

BSH was synthesised as described previously [143], and dissolved under anaerobic conditions using deoxygenated LC-MS grade water (HiPerSolv, VWR). The affinity of BSH for Cu(I) was determined through competition experiments with bathocuproine disulfonate (BCS), a Cu(I) chelator which forms a 2:1 complex, $[Cu(BCS)_2]^{3-}$, that exhibits an absorption band at 483 nm with ε_{483nm} = 13,300 M^{-1} cm^{-1} [144].

For the titration, 2.5 μL additions of 60 mM BSH were made in an anaerobic glove box to a 8.95 μM $Cu(BCS)_2$ solution in 100 mM MOPS, 100 mM NaCl, pH 7.5, containing 2

μM dithionite or ascorbate to scavenge trace oxygen and ensure copper existed solely as reduced Cu(I). After each BSH addition, in a septum-sealed cuvette, samples were left to equilibrate for 10 min before spectra were recorded. The A_{483nm} values were used to calculate changes in concentration of $[Cu(BCS)_2]^{-3}$ (as copper was transferred to $Cu(BSH)_2$), from which the concentrations of $Cu(BSH)_2$, free BSH and free BCS could be determined.

$$K_{ex} = \frac{\beta_2(BSH)}{\beta_2(BCS)} = \frac{[CuBSH_2][BCS^{2-}]^2}{[Cu(BCS)_2^{3-}][BSH]^2} \tag{4.1}$$

$$\beta_2(BSH) = K_{ex}\beta_2(BCS) \tag{4.2}$$

The affinity of BSH for Cu(I) was calculated using Eqn 4.1 and 4.2, [84] and assuming that BSH forms a 2:1 complex with Cu(I), as would be expected for a monothiol low molecular weight species. Here, K_{ex} is the exchange equilibrium constant for competition between BSH and BCS. The overall formation constant for $Cu(BCS)_2$, β_2, is a well-established way to define affinity of stepwise complex formation [145] (log β_2 = 19.8 [144]). The acid-base properties of BSH indicate that Cu(I)-binding is likely to be pH-dependent [143] and so the value determined here is an apparent β_2 formation constant at pH 7.5.

4.2.5 Spectroscopic Methods

UV-visible absorbance spectra were recorded on a Jasco V-550 spectrophotometer as described in Chapter 2. Near-UV CD spectra were recorded using a Jasco J-810 spectropolarimeter with a slit width of 2 nm. Intensity is expressed as $\Delta\varepsilon$ in units of M^{-1} cm^{-1}. Prior

to all Cu(I) addition experiments, CopZ was reduced with excess DTT under anaerobic conditions and buffer exchanged to remove DTT. Protein concentrations were calculated using an extinction coefficient, $\varepsilon_{276\ nm}$, of 1450 M^{-1} cm^{-1} [89], before anaerobic addition of BSH. Additions of Cu(I) to CopZ were made using a microsyringe (Hamilton) to a 1 cm pathlength septum-sealed cell.

4.3 Results: ESI-MS Studies Of Cu(I) Binding To CopZ

4.3.1 LCMS of *B. subtilis* CopZ

The mass spectra under denaturing conditions of CopZ, (apo- and at 1 Cu / protein), before and after deconvolution, are shown in **Figure 4.3.1**. Prior to deconvolution, the mass spectra displayed an envelope of multiply charged molecular ions with m/z values corresponding to $[M+nH]^{n+/n}$, where M is the molecular mass and n the number of protons carried by the protein (see Chap 3). Under denaturing conditions, the m/z spectra of apo-CopZ and 1 Cu / CopZ both displayed six peaks with charges +5, +6, +7, +8, +9 (**Figure 4.3.1**A and B).

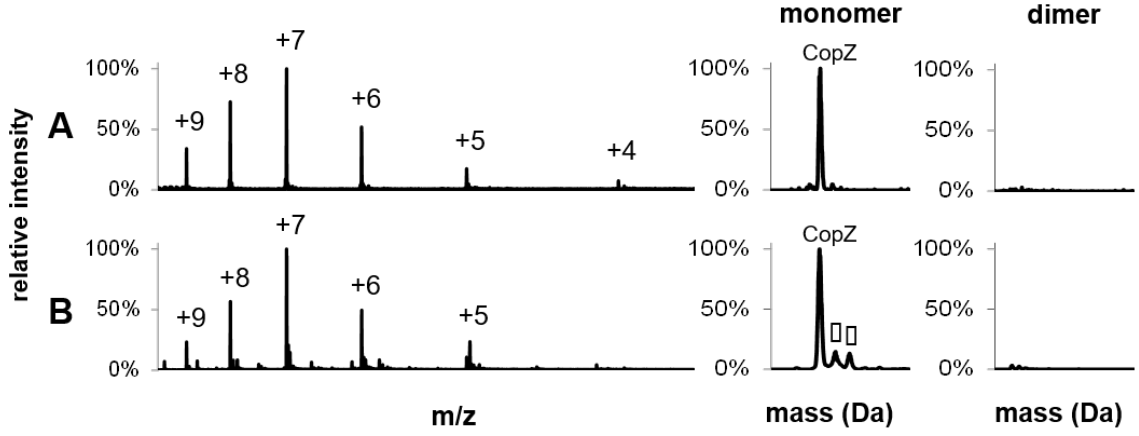

Figure 4.3.1: Charge state analysis of CopZ via LCMS The mass spectra before and after deconvolution of: **A)** apo-CopZ **B)** 1.0 Cu / CopZ, obtained under denaturing conditions of LCMS. The m/z spectra are shown on the left with the charge state of each peak labelled; monomer and dimer regions of the corresponding mass spectra are shown on the right, the protein species labelled and the symbol (□) = acetonitrile adduct.

Deconvolution of the peaks in the spectrum of apo-CopZ gave a molecular mass of 7338.1 Da, in agreement with the predicted mass of CopZ (7338.1 Da). Deconvolution of

the peaks in the spectrum of CopZ at 1 Cu / protein yielded a peak with a molecular mass of 7337.0 Da, in reasonable agreement with the predicted mass. Despite the fact that the sample was prepared with Cu(I), no peaks corresponding to copper-bound species were observed under denaturing conditions.

4.3.2 Native ESI-MS of *B. subtilis* CopZ

To investigate the Cu(I)-dependent speciation of CopZ and, in particular, the formation of dimeric CopZ, native MS spectra at 0, 0.5, 1.0, 1.5 and 2.0 Cu(I) per protein were recorded, following the approach outlined in Chapter 3. The m/z spectrum of apo-CopZ (**Figure 4.3.2A**) displayed a peak envelope containing only three major peaks with charges +4, +5 and +6. Compared to the denatured spectra, this spectrum displayed fewer major peaks with the peak envelope shifted toward higher m/z values, reflecting differences under native conditions, where the protein is folded. Fewer charges were a result of the decreased surface area of folded protein, and fewer major peaks resulted from a more tightly folded structure [146].

The mass spectra obtained with progressively increasing proportions of Cu(I) / protein (Fig 4.3.2 B – E) displayed a similar set of charged species together with an additional peak envelope with charges +8 and +9. This clearly represented a second form of the protein. The progressive changes in peak distribution in the mass spectra illustrated the changes which occurred in CopZ speciation. The monomer peak envelope displayed no change in charge state distribution upon copper binding. This suggests that CopZ was folded with no major structural rearrangements before and after copper binding occurs.

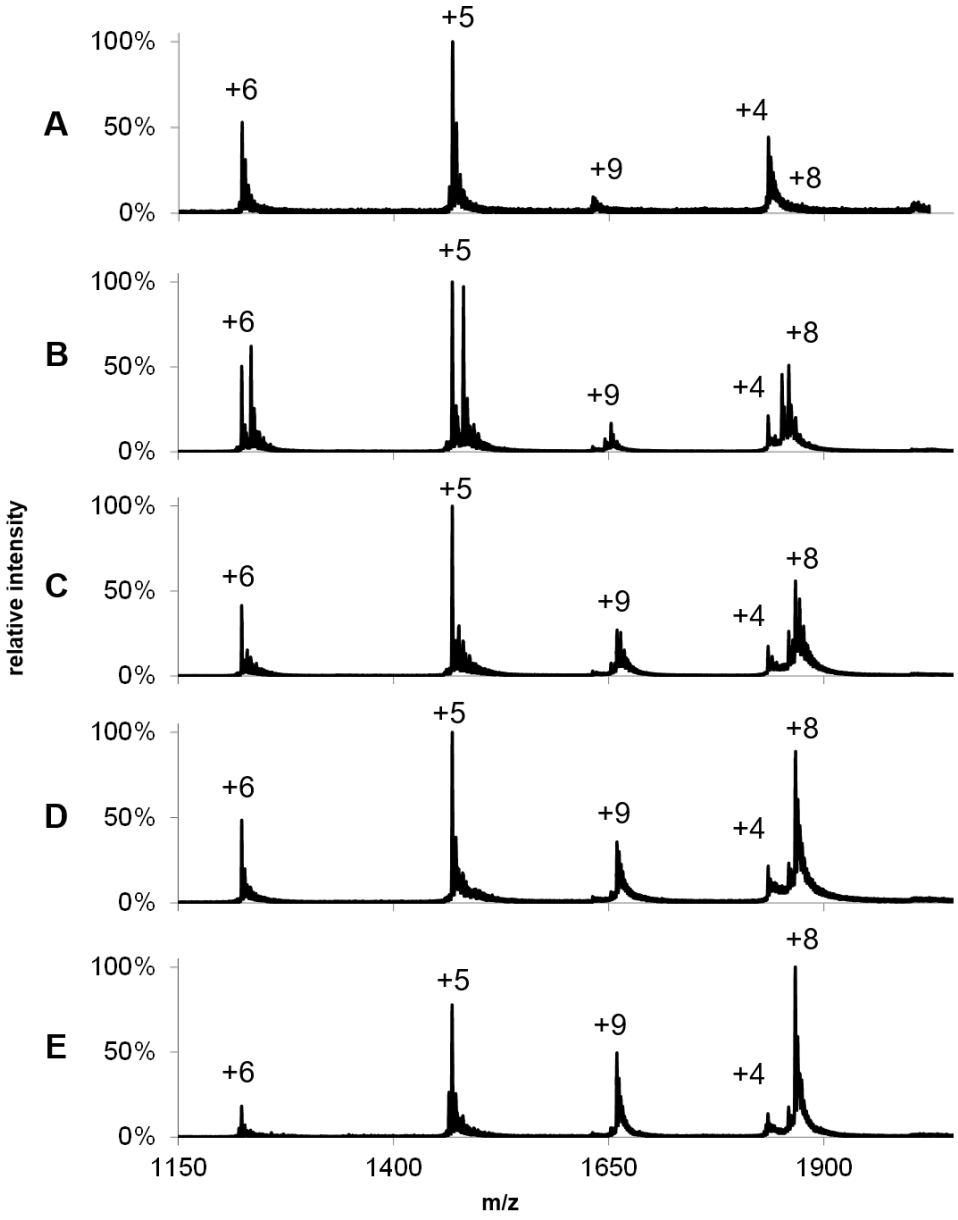

Figure 4.3.2: Mass spectra for CopZ at varied Cu(I) levels. Native m/z spectra acquired of CopZ, reconstituted with: **A)** 0 Cu/CopZ, **B)** 0.5 Cu/CopZ, **C)** 1.0 Cu/CopZ, **D)** 1.5 Cu/CopZ and **E)** 2.0 Cu/CopZ. The charge states are labelled, with +4, +5, +6 corresponding to the monomer peak envelope, and +8, +9 to the dimer peak envelope. Shifts in peak envelope intensities as Cu(I) level increased reflect the progression toward increased proportion of dimeric species.

4.3.3 Cooperative Formation Of $Cu_4(CopZ)_2$ Detected By ESI-MS

The mass spectra after deconvolution at 0, 0.5, 1.0, 1.5 and 2.0 Cu(I) per protein are presented in **Figure 4.3.3**. Under native conditions, these spectra illustrated the ability of CopZ to bind Cu(I), and revealed the metalloforms present in the samples at each copper loading. The apo-CopZ spectrum contained predominantly CopZ with a small proportion of disulfide-bonded $(CopZ)_2$. The native mass spectra also contained sodium adduct peaks of low intensity which, compared to the mass spectra generated under denaturing conditions of LCMS (**Figure 4.3.1A** and **B**), illustrated one of the issues arising when directly infusing protein samples in aqueous buffer.

At 0.5 Cu / CopZ (**Figure 4.2.3B**), the predominant species is CuCopZ, with a substantial portion of CopZ and low-intensity dimer peaks also observed. At 1.0 Cu(I) per CopZ (**Figure 4.3.3C**) a more diverse mixture of metalloforms was observed with a noteworthy increase in the dimer peak envelope, but the majority of peak intensity was still associated with the monomer peaks.

As the copper loading was increased further to 1.5 and 2.0 equivalents of Cu(I) per CopZ (**Figure 4.3.3C** and **D**), a continued progression toward increased dimer and decreased monomer peak intensities was observed, with the predominant copper-bound peak being $Cu_4(CopZ)_2$. However, at all copper loadings, a high proportion of apo-CopZ was present.

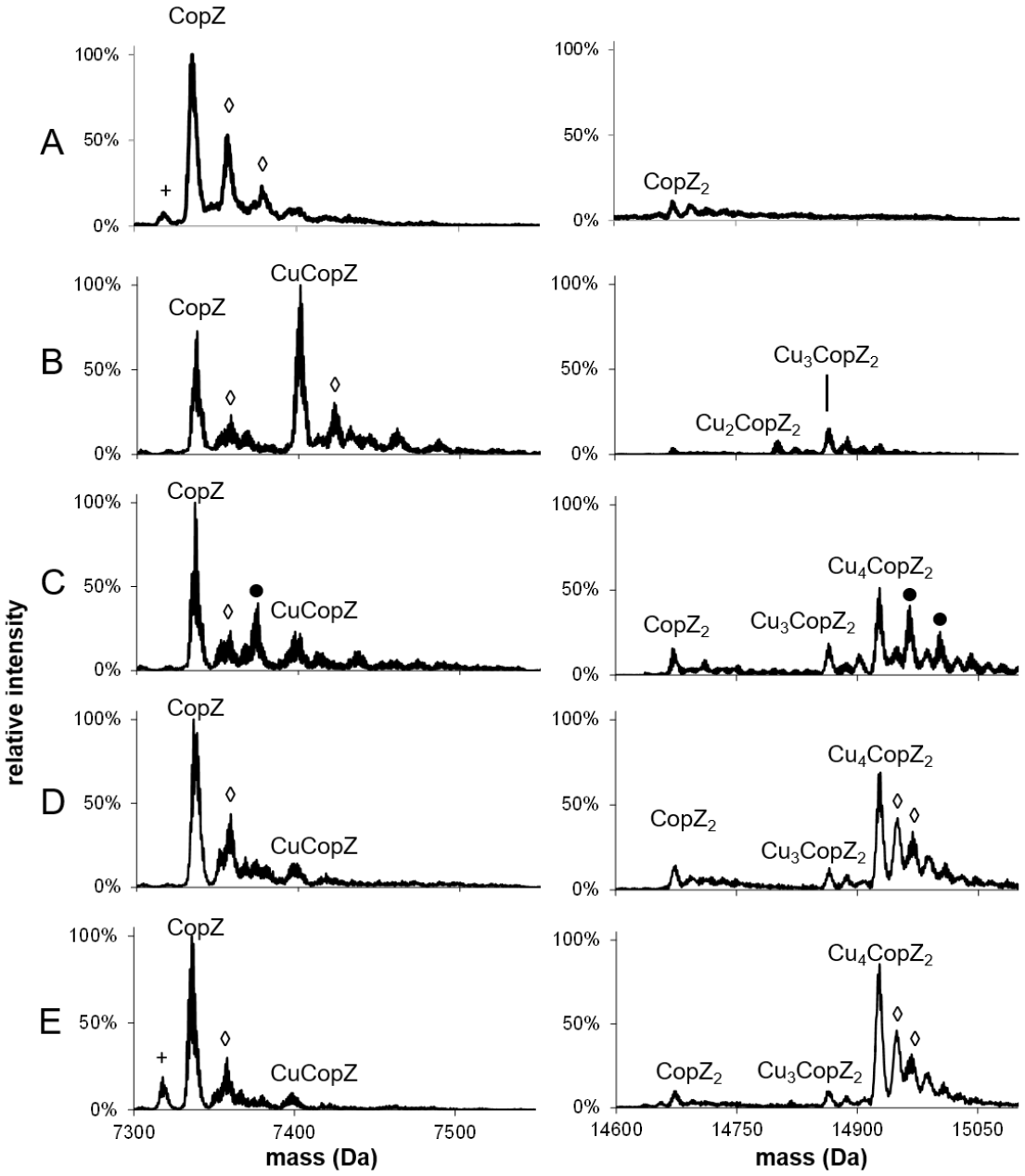

Figure 4.3.3: Deconvoluted mass spectra for CopZ at varied Cu(I) levels. Native mass spectra acquired of CopZ in 20 mM ammonium acetate, pH 7.4, reconstituted with: **A)** 0 Cu/CopZ, **B)** 0.5 Cu/CopZ, **C)** 1.0 Cu/CopZ, **D)** 1.5 Cu/CopZ and **E)** 2.0 Cu/CopZ. The protein species are labelled and symbols used as followed: (◊) = Na adduct, (+) = loss of H2O (●) = ACN adduct. Peak shifts as Cu(I) level increased reflect a progression toward dominant copper-bound species $Cu_4(CopZ)_2$.

The relative intensities and exact masses of observed species are shown in Table 4.1. The exact masses were mostly within 1 Da of the predicted mass, with the most significant departures being for low-intensity peaks, when the peak centroids were likely influenced by neighbouring sodium adducts.

Table 4.1: Species observed via ESI-MS for CopZ at varied Cu(I) levels. Observed masses and relative intensities of species in native mass spectra of CopZ prepared at 0.5, 1.0, 1.5 and 2.0 Cu / protein.

Species	Pred (Da)	0.5 Cu / CopZ		1.0 Cu / CopZ		1.5 Cu / CopZ		2.0 Cu / CopZ	
CopZ	7336.1	71.7%	7336.5	100%	7336.3	100%	7336.3	100%	7336.1
CuCopZ	7399.7	100%	7400.7	27.4%	7400.0	13.9%	7399.0	18.2%	7398.0
$(CopZ)_2$	14672.2	2.6%	14672.3	12.0%	14672.8	13.9%	14673.1	10.4%	14672.6
$Cu(CopZ)_2$	14735.7	0%	–	2.6%	14735.6	1.4%	14735.1	1.6%	14735.1
$Cu_2(CopZ)_2$	14799.2	7.1%	14802.0	3.7%	14801.2	0%	–	0%	–
$Cu_3(CopZ)_2$	14862.7	11.5%	14864.1	24.3%	14864.6	11.7%	14864.3	8.8%	14864.2
$Cu_4(CopZ)_2$	14926.2	4.8%	14924.4	39.7%	14927.2	85.1%	14927.0	83.9%	14926.9

In order to more clearly visualise this species distribution of CopZ, bar graphs are shown in **Figure 4.3.4**, illustrating the species present at each copper loading. Above 1.0 Cu/CopZ, the relative amount of monomer species was significantly reduced, accompanied by predominance of the tetra-copper species which indicated cooperative binding of Cu(I) to the CopZ dimer and relatively low amounts of the $Cu_2(CopZ)_2$ and $Cu_3(CopZ)_2$ species.

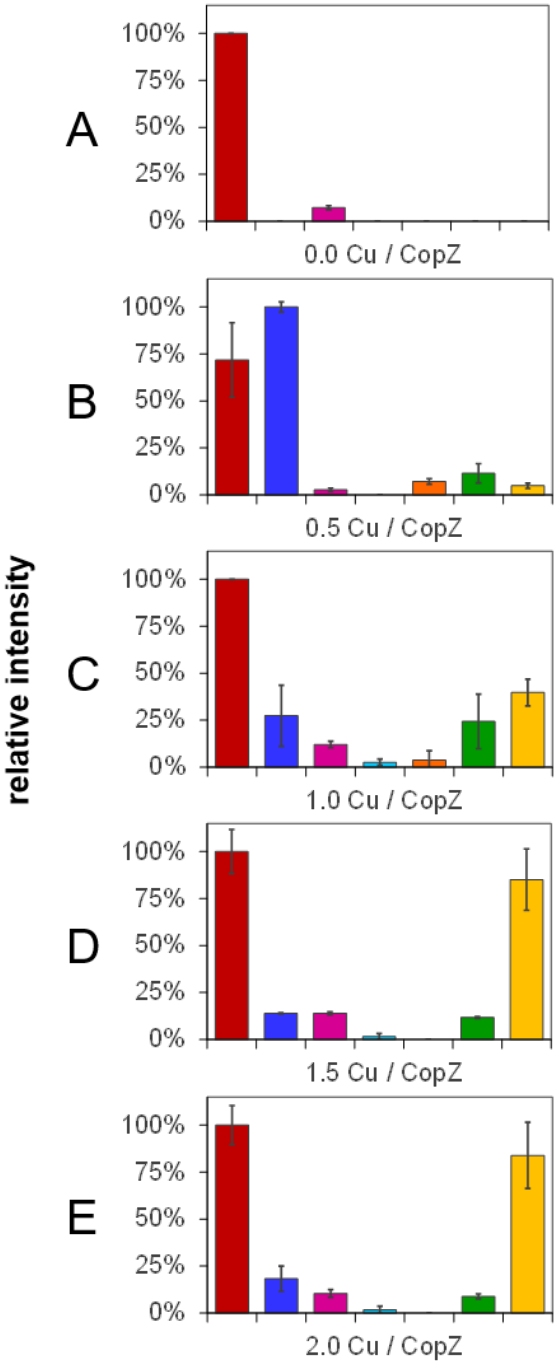

Figure 4.3.4: Species distribution via ESI-MS for CopZ at varied Cu(I) levels. Bar graph representation of species CopZ mass spectra prepared at Cu / protein ratio as labelled. Bars represent the CopZ species observed at each copper loading, with relative intensity from three experiments averaged and normalised to the greatest total ionisation intensity. Species represented in the following colours: Red, apo-CopZ; Blue, CuCopZ; Magenta, $CopZ_2$; Cyan, $Cu(CopZ)_2$; Orange, $Cu_2(CopZ)_2$; Green, $Cu_3(CopZ)_2$; Yellow, $Cu_4(CopZ)_2$.

4.4 Results: Cu(I) binding to CopZ In The Presence Of LMWT

4.4.1 Determination Of The Affinity Of Bacillithiol For Cu(I)

Affinities associated with Cu(I)-binding to thiolate ligands can be obtained through competition experiments with a high affinity Cu(I) ligand, such as bathocuproine disulfonate (BCS). BCS forms a coloured complex with Cu(I), $Cu(BCS)_2^{3-}$, that displays an A_{max} at 483 nm, which enables its concentration to be monitored during competition with BSH. Previously, a similar approach was used to determine the binding affinities of Cu(I) for both CopZ and the soluble domains of its cognate membrane protein, CopAab [84] [147].

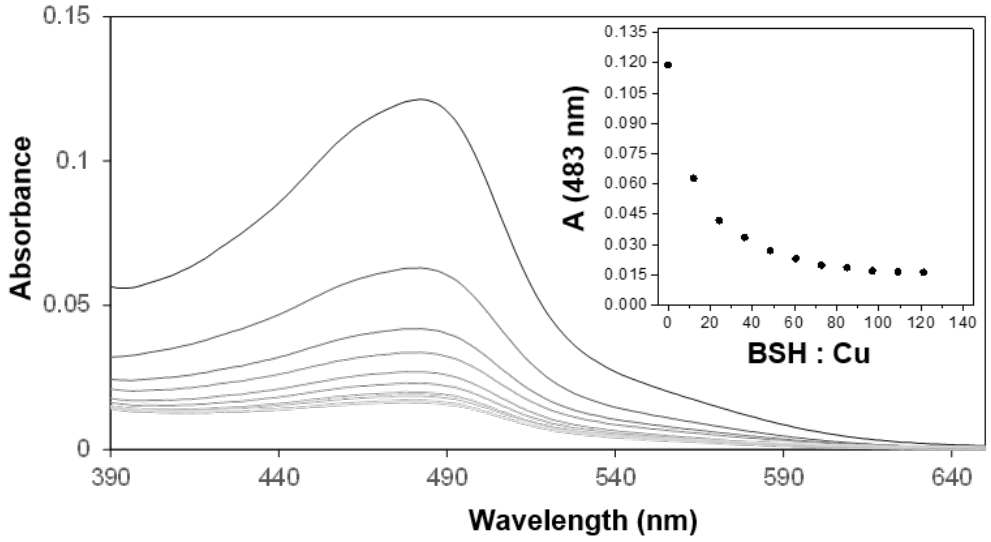

Figure 4.4.1: Competition for Cu(I) between BCS and BSH monitored by UV-vis. Overlaid absorbance spectra from competition assay where BSH was titrated into sample containing 8.95 μM $Cu(BCS)_2^{3-}$, 2 μM sodium dithionite. Decrease in A_{483} as BSH is titrated into solution indicates transfer of Cu(I) from BCS to BSH. Inset: plot of A_{483} against BSH / Cu(I) ratio.

By analogy with other LMWTs, it was expected that BSH would bind Cu(I) in a 2:1 ratio to form $Cu(BSH)_2$. The UV-visible absorbance spectra recorded during titration of BSH into the solution containing $Cu(BCS)_2^{3-}$ illustrated a steady decrease in A_{483} nm as shown in **Figure 4.4.1**, which indicated the transfer of copper from BCS to BSH. Because titrations of BSH alone into the same buffer did not exhibit absorbance in this region (data not shown), absorbance changes were attributed to loss of Cu(I) from $Cu(BCS)_2^{3-}$. Data were analysed according to Eqn 4.1 and Eqn 4.2, giving an apparent formation constant at pH 7.5 of $\beta_{2(BSH)} = 4.1 \pm 1.5 \times 10^{17}$ M^{-2} (see Table 4.2).

Table 4.2: Calculation of BSH Affinity for Cu(I). After titration of BSH into a solution containing $[Cu(BCS)_2]^{-3}$, the A_{483nm} values were used to calculate changes in concentration of $[Cu(BCS)_2]^{-3}$ (as copper was transferred to $Cu(BSH)_2$). From this, the concentrations of $Cu(BSH)_2$, free BSH and free BCS could be determined. The starting concentrations were: $[BCS]_T = 23.7$ μM, $[Cu]_T = 9.88$ μM.

BSH/Cu(I)	$[BSH]_T$	$[Cu(BSH)_2]$	$[Cu(BCS)_2]^{3-}$	$\beta_{2,\ BSH}$ x 10^{17}	$\beta_{2,\ BSH,\ AVG}$ (M^{-2})
0	0	0	8.95		
24	240	6.74	3.14	8.03	
36	359	7.34	2.52	5.40	
48	477	7.82	2.02	4.38	
61	595	8.09	1.73	3.57	
73	713	8.31	1.49	3.07	
85	830	8.38	1.40	2.44	
97	947	8.49	1.28	2.12	
					4.1 ± 1.5 x 10^{17}

During this experiment, as BSH is titrated in excess of copper, the ratio of free BSH to $Cu(BSH)_2$ decreases. Because the total proportion of BSH that binds copper decreases, there appears to be a decreasing trend across the β_2 values throughout the experiment

(see Equation 4.1). Previous examples of this type of competition assay using BCS have not been found to be influenced by formation of ternary complexes or intial formation of the 1:1 complex [148]. In addition, the variation observed here appears to be small and thus the reported formation constant is the average of these values.

4.4.2 Bacillithiol Reduces Number of CopZ Cu(I)-binding Phases

Previous spectroscopic studies of the effects of the LMWTs DTT, cysteine and GSH revealed that, though initial Cu(I)-binding behaviour was not perturbed, the formation of higher order Cu(I)-bound forms of dimeric CopZ is inhibited [89] [52]. These studies predated the discovery of BSH as the major LMWT in the *B. subtilis* cytoplasm [27]. To investigate the effects of BSH on Cu(I)-binding to CopZ, similar methods to those previously employed were used. UV-visible spectra arising from additions of 0 – 2 Cu / CopZ in the presence of 20-fold excess BSH are shown in **Figure 4.4.2A**, along with a plot of $\triangle A_{265nm}$ against increasing Cu / protein ratio **Figure 4.4.2B**.

Addition of Cu(I) ions led to a gradual essentially linear increase with respect to Cu(I) in A_{265nm}. Cu(I)-binding in the absence of LMWTs has been well-characterised, consisting of a series of distinct binding phases with break points at $\sim$0.5, 1.0, 1.5 and 2.0 Cu(I) per protein [89]. Clearly, here, multiphasic Cu(I) binding to CopZ was not observed in the presence of excess BSH. However, because Cu(I) bound to LMWT gives rise to absorbance in this spectral range, absorbance does not discriminate between protein-associated and non-protein-associated copper. CD spectroscopy, which provides more discriminating information about Cu(I)-binding to the protein was therefore used.

CD spectra of CopZ in the presence of 20-fold excess BSH resulting from anaerobic additions of Cu(I) in the range of 0 – 2 Cu / protein are shown in **Figure 4.4.3A**, and **Figure 4.4.3B** shows plots of $\triangle\triangle\varepsilon$ values at 265 nm, 290 nm and 335 nm as a function of Cu(I) added.

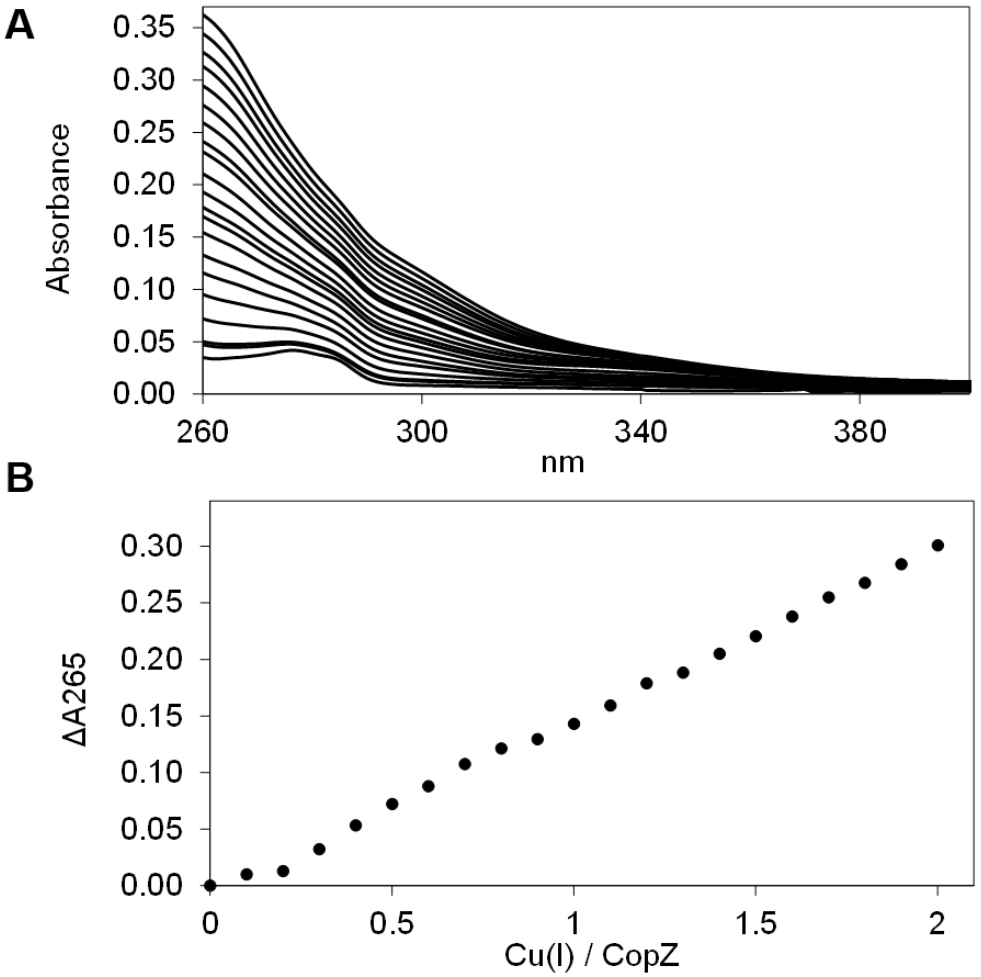

Figure 4.4.2: Cu(I) titration into CopZ, in the presence of BSH, monitored by UV-vis. Titration of Cu(I) into 35 μM CopZ in 100 mM MOPS, 100 mM NaCl, pH 7.5, and 20-fold excess BSH monitored by UV-visible absorbance, presented as: **A)** Overlaid spectra **B)** ΔA_{265nm} against the Cu(I)/CopZ ratio.

The initial Cu-free spectrum of CopZ with BSH was consistent with the previously reported spectrum of apo-CopZ with only a very shallow signal around 276 nm, due to its two tyrosine residues. Thus, CD intensity changes were attributed to Cu(I) ions bound at chiral centres within the protein. Initially, additions of Cu(I) gave rise to signal intensity changes at (+)265 nm and (-)295 nm, due to ligand-metal charge transfer bands. A plot of intensity versus Cu(I) depicted binding in the range from 0 – 0.7 Cu(I)/CopZ, after which

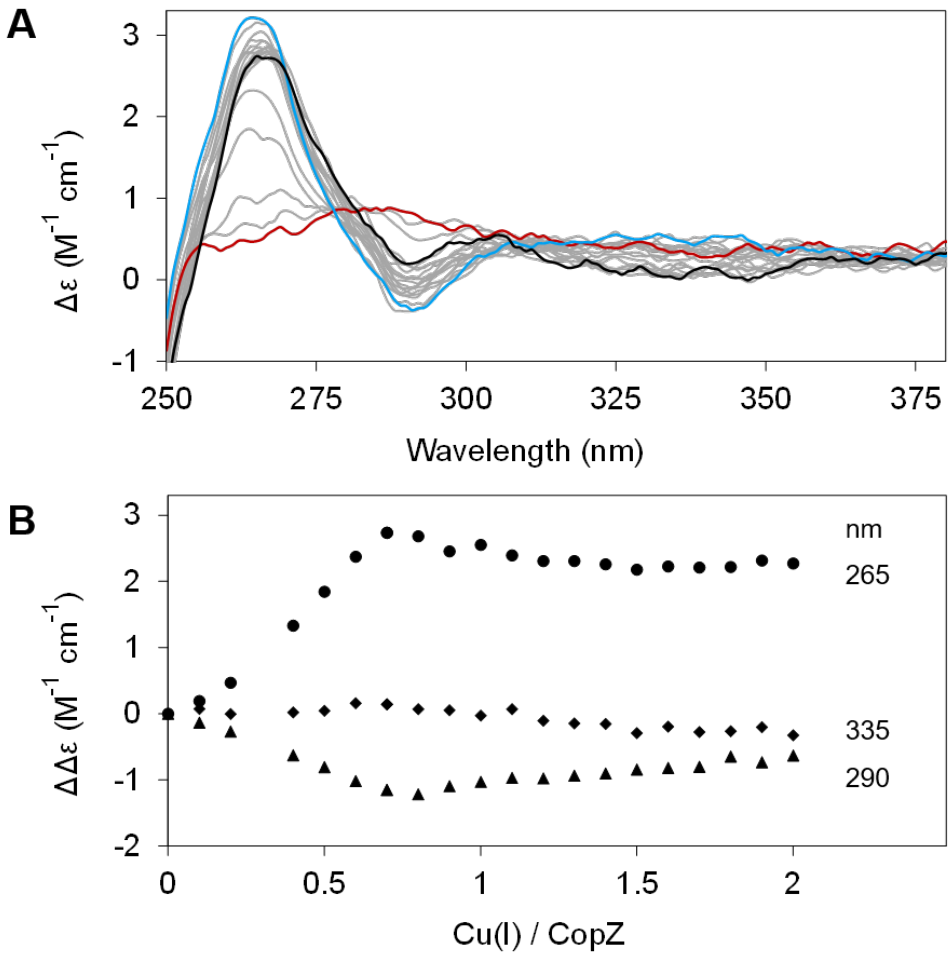

Figure 4.4.3: Cu(I) titration into CopZ, in the presence of BSH, monitored by CD. Titration of Cu(I) into 35 μM CopZ in 100 mM MOPS, 100 mM NaCl, pH 7.5, and 20-fold excess BSH monitored by CD, presented as: **A)** Overlaid spectra with colour scheme as follows: **Red**, initial copper-free spectrum; **Blue**, 0.7 Cu / protein; **Black**, 2 Cu / protein. **B)** $\Delta\Delta\varepsilon$ against the Cu(I)/CopZ ratio.

there were only minor changes in intensity at (-)265 nm, (+)295 nm and (-)335 nm, in each case levelling off at $\sim$ 2 Cu(I)/CopZ. Intensity at 335 nm was previously attributed to spin forbidden 3d – 4s metal cluster-centred transitions arising due to Cu(I)–Cu(I) interactions in multinuclear Cu(I) complexes [149] [150]. This behaviour was broadly similar to that previously observed for Cu(I)-binding to CopZ in the presence of the same excess of GSH and cysteine [52].

4.4.3 DTT and GSH Inhibit Higher Order Cu(I)-Forms Of CopZ

Native MS affords the opportunity to gain high resolution insight into the effects of LMWTs on Cu(I)-binding. Therefore mass spectra were recorded of CopZ prepared with 1 Cu / protein and progressively increasing concentrations of DTT, GSH and BSH (see Section 4.2.3).

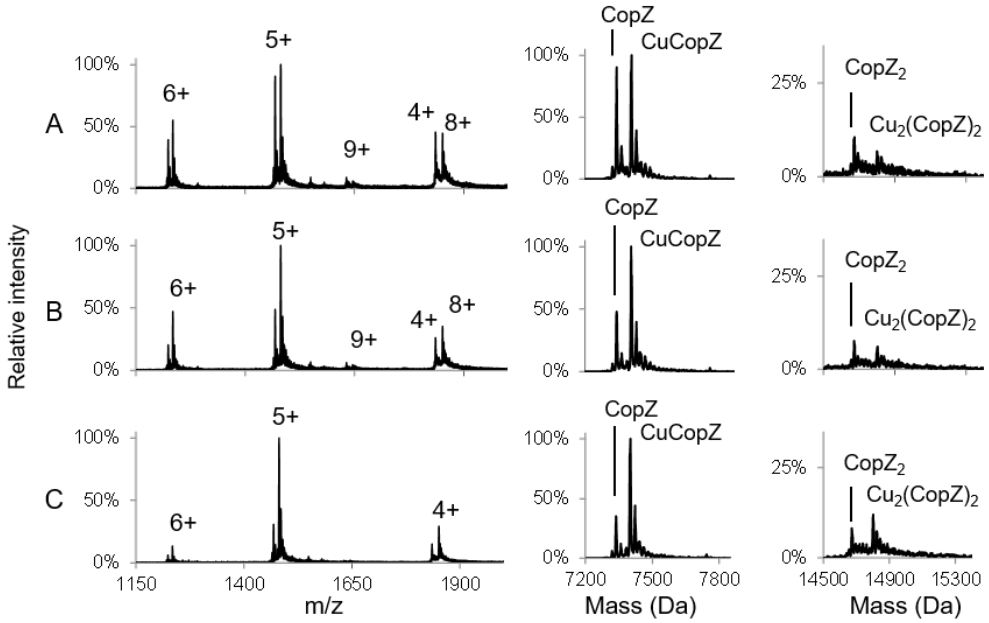

Figure 4.4.4: Mass spectra for 1 Cu/CopZ with varied DTT levels. Native m/z and mass spectra acquired of CopZ in 20 mM ammonium acetate, pH 7.4, reconstituted with 1 Cu / protein in the presence of **A)** 5 DTT/CopZ, **B)** 10 DTT/CopZ, **C)** 25 DTT/CopZ. The m/z spectra on the left with charge states labelled; on the right, monomer and dimer regions of the mass spectra expanded, with the protein species labelled. Peaks shift as DTT level increases, illustrating decreased dimerised CopZ species, favouring CuCopZ.

The mass spectra of 1 Cu / CopZ in the presence of DTT, before and after deconvolution, are shown in **Figure 4.4.4**. The spectra at all DTT loadings (5, 10 and 25 per CopZ) contained a monomer CopZ envelope (charge states +4, +5 +6) and a small amount of dimer envelope. In addition to the charge states observed in the absence of DTT (+8, +9),

these contained an additional peak at +7, suggesting that DTT causes a reduction in the number of charges on the CopZ dimer, perhaps resulting in a slightly more tightly folded conformation of CopZ dimer.

The species present in the mass spectrum can be seen in the deconvoluted spectra and in **Table 4.3**. The deconvoluted spectra illustrated that at 5 DTT/protein (**Figure 4.4.4A**), the peaks corresponding to dimer CopZ species, $Cu_3(CopZ)_2$ (14864.7 Da) and $Cu_4(CopZ)_2$ (14925.0 Da) were significantly decreased in intensity compared to spectra in the absence of the thiol (**Figure 4.2.3B**), with a corresponding increase in the CuCopZ peak (7400.4 Da) which was the most prominent copper-bound species, and apo-CopZ (7336.6 Da) the second most abundant (89% relative intensity).

Table 4.3: Species observed via ESI-MS for 1 Cu/CopZ at varied DTT levels. Exact masses and relative intensities of species observed in native mass spectra of CopZ prepared at 1.0 Cu / protein in the presence of DTT (5, 10 and 25 / protein).

Species	Pred (Da)	5 DTT / CopZ		10 DTT / CopZ		25 DTT / CopZ	
CopZ	7336.1	87.3%	7336.6	47.3%	7336.9	36.0%	7337.6
CuCopZ	7399.7	100%	7400.7	100%	7400.7	100%	7400.7
$(CopZ)_2$	14672.2	12.0%	14673.0	8.0%	14673.0	8.2%	14673.0
$Cu(CopZ)_2$	14735.7	$<$3%	–	$<$3%	–	3.5%	14738.2
$Cu_2(CopZ)_2$	14799.2	7.9%	14802.0	6.2%	14801.9	11.6%	14801.3
$Cu_3(CopZ)_2$	14862.7	3.0%	14864.7	$<$3%	–	3.2%	14863.4
$Cu_4(CopZ)_2$	14926.2	0%	–	0%	–	0%	–

At 10 DTT/protein and 25 DTT/protein (**Figures 4.4.4B** and **C**), the intensity of dimeric CopZ peaks were further reduced, and the most prominent peak was that of CuCopZ (7400.8 Da), while the relative intensity of the apo-CopZ monomer (7337.0 Da) decreased to 55% and 37% at 10 and 25 DTT/protein, respectively. This suggested the presence of DTT had a stabilising effect on the CuCopZ species. Also with increasing DTT levels, the intensity of $Cu_2(CopZ)_2$ increased slightly, perhaps due to increased stability of CuCopZ which facilitated the formation of this dimeric species.

The mass spectra of 1 Cu / CopZ in the presence of GSH, before and after deconvolution, are shown in **Figure 4.4.5**. The effect upon the mass spectra of GSH can be seen where, as for DTT, near elimination of the dimer envelope is observed at the final level of 25 GSH / protein. The charge state distribution was similar to that found in the mass spectra in the absence of thiol but, in the presence of GSH a great deal of adduct formation occurred, with additional peak envelopes at 25 GSH / protein due to clusters of GSH, which obtained multiple charges and overlapped with the CopZ peak envelope.

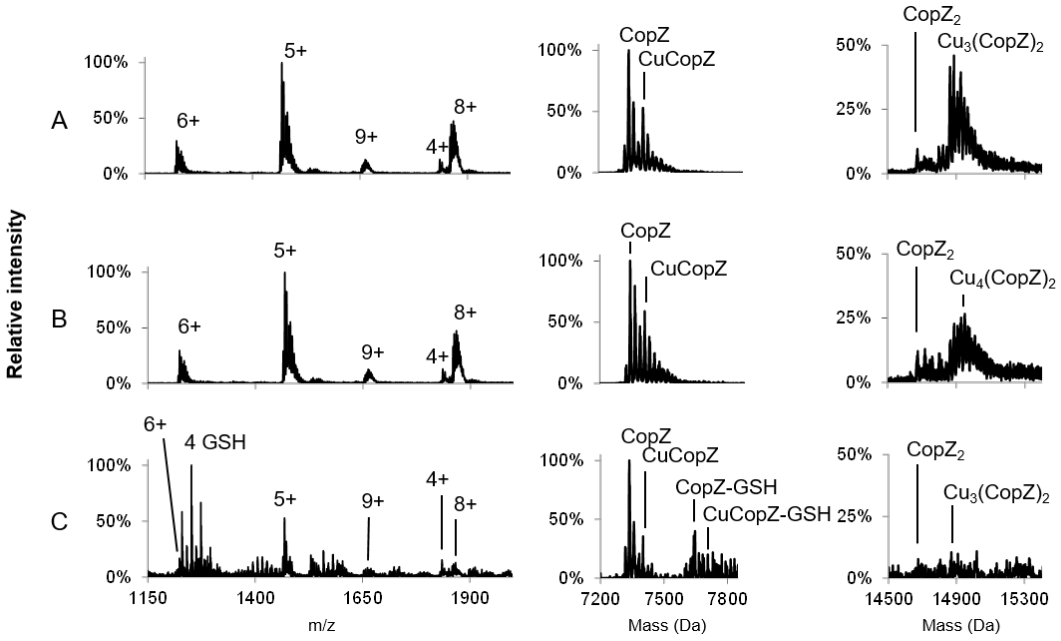

Figure 4.4.5: Mass spectra for 1 Cu/CopZ at varied GSH levels. Native mass spectra of CopZ at 1 Cu / protein, after addition of **A)** 5 GSH/CopZ, **B)** 10 GSH/CopZ, **C)** 25 GSH/CopZ. Mass spectra on the left with charge states labelled; on the right, monomer and dimer regions of the mass spectra expanded, with the protein species labelled. GSH ionises readily, leading to peak clusters which affect relative protein ionisation and therefore the deconvoluted mass spectra contain a lower signal-to-noise, particularly at high thiol ratio.

These effects can be seen after deconvolution and by the relative intensities and observed masses in **Table 4.4** where CopZ species contained a much higher proportion

of sodium adducts than observed previously. At 5 GSH / CopZ (**Figure 4.4.4A**), there was a slight increase in relative intensity of CuCopZ (7400.5 Da), relative to the dimerised $Cu_3(CopZ)_2$ (14864.1 Da) and $Cu_4(CopZ)_2$ (14926.2 Da). Further reduction in intensity of dimerised species was observed at 10 GSH / CopZ (**Figure 4.4.4B**), and finally at 25 GSH / CopZ (**Figure 4.4.4C**), the intensity of dimerised species was minimal ($<$10%), where the most intense Cu-bound species was CuCopZ. In addition, peaks corresponding to the addition of a glutathione molecule (+306.3 Da) were observed for CuCopZ (see below). Furthermore, the intensity of the monomeric CuCopZ species also decreased relative to the apo-CopZ peak, suggesting that these thiols might have competed with CopZ for Cu(I).

Table 4.4: Species observed via ESI-MS for 1 Cu(I)/CopZ at varied GSH levels. Exact masses and relative intensities of species observed in mass spectra of CopZ at 1.0 Cu / protein containing GSH (5, 10 and 25 per protein).

Species	Pred (Da)	5 GSH / CopZ		10 GSH / CopZ		25 GSH / CopZ	
CopZ	7336.1	100%	7336.8	100%	7336.7	100%	7336.2
CuCopZ	7399.7	50.5%	7400.5	57.7%	7400.2	34.0%	7400.7
CopZ-GSH	7643.4	0%	–	$<$3%	–	36.8%	7643.1
CuCopZ-GSH	7707.0	0%	–	0%	–	20.0%	7706.7
$(CopZ)_2$	14672.2	11.8%	14673.5	9.9%	14672.9	5.9%	14674.6
$Cu(CopZ)_2$	14735.7	0%	–	0%	–	$<$3%	–
$Cu_2(CopZ)_2$	14799.2	10.6%	14799.7	8.8%	14799.3	6.5%	14799.3
$Cu_3(CopZ)_2$	14862.7	41.6%	14864.1	16.6%	14863.9	6.9%	14864.8
$Cu_4(CopZ)_2$	14926.2	38.7%	14926.9	28.2%	14926.2	0%	–
$(CopZ)_2$-GSH	14979.5	0%	–	0%	–	7.8%	14980.7
$Cu_3(CopZ)_2$-GSH	15170.2	0%	–	0%	–	$<$3%	–
$Cu_4(CopZ)_2$-GSH	15233.7	0%	–	0%	–	$<$3%	–

4.4.4 BSH Inhibits Higher Order Cu(I)-Forms Of CopZ

In order to examine the effect of the physiological LMWT upon Cu-bound CopZ species distribution, mass spectra were recorded of CopZ prepared at 1 Cu / protein in the presence of 5, 10 and 25 BSH / protein. The mass spectra, prior to deconvolution are presented in **Figure 4.4.6A – C**.

Upon addition of 5 BSH / protein, the mass spectrum featured fairly similar intensities of CopZ peaks, compared to the thiol-free spectrum (**Figure 4.3.2C**). In addition, additional peaks corresponding to BSH adducts were observed. The mass spectrum at 10 BSH/protein revealed slightly reduced dimer peak intensity. In addition to appearing as adducts of CopZ, BSH also appeared on its own and, at 25 BSH/CopZ, these clusters overlapped with the CopZ peak envelope. A detailed view of the overlapped species is annotated in **Figure 4.4.6D**.

Despite the presence of many additional peaks in the m/z spectrum, the monomer and dimer charge states were still observed, as well as the trend where an increased proportion of BSH resulted in less intense peaks in the dimer envelope. The relative proportion of monomer/dimer peaks was hard to discern in the stacked mass spectra due to the overall decrease in protein peak intensity as BSH increased. This presumably arose due to BSH acting as an ion suppressant at higher concentration (25 BSH / protein = 250 μM BSH).

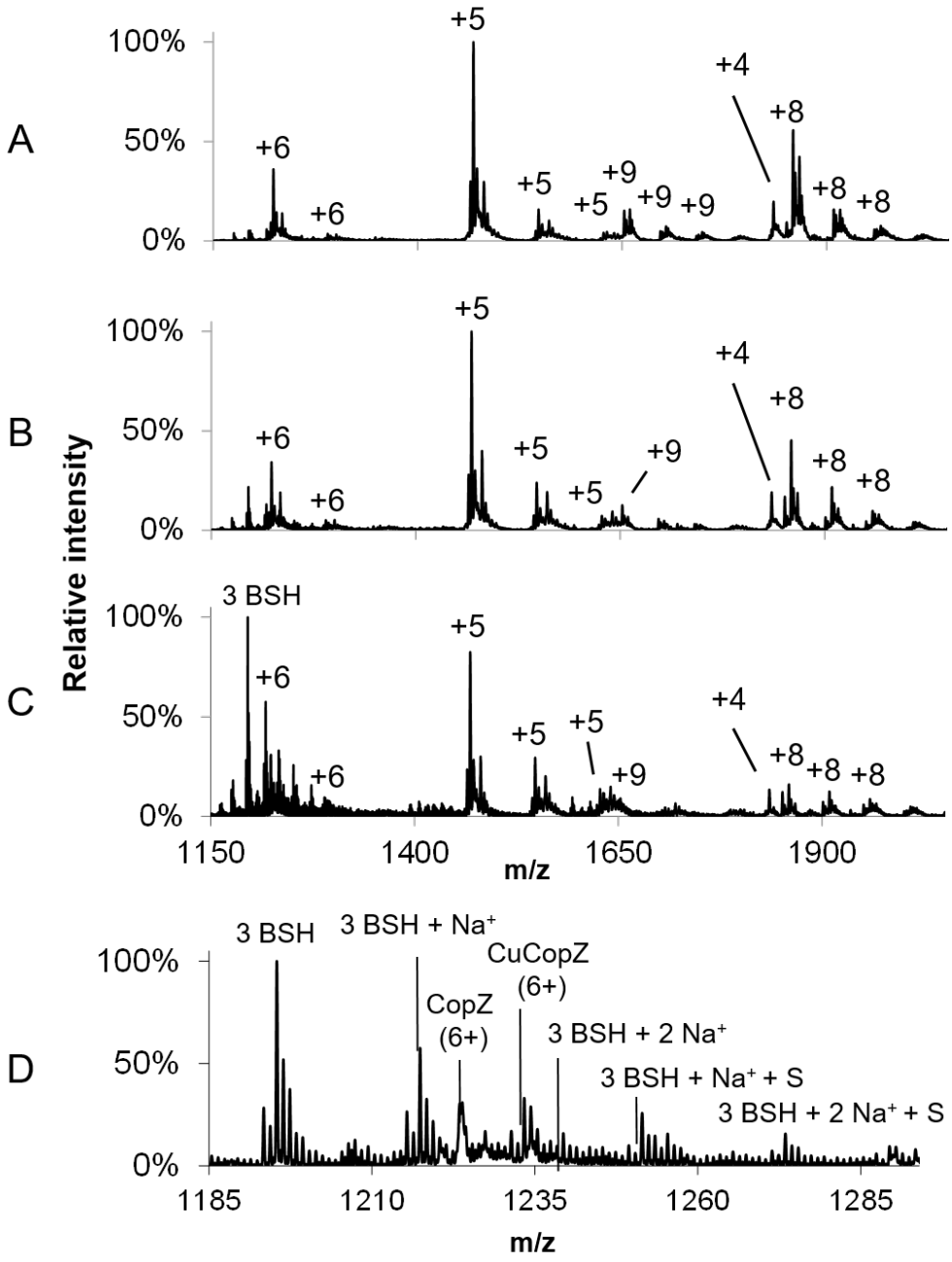

Figure 4.4.6: Mass spectra for 1 Cu/CopZ with varied BSH levels. Native m/z acquired of CopZ reconstituted with 1 Cu / protein, in the presence of: **A)** 5 BSH/CopZ, **B)** 10 BSH/CopZ, **C)** 25 BSH/CopZ. **D)** expanded view of 25 thiol/protein centred on m/z = 1220, where BSH peak clusters overlap with CopZ monomer peaks (+6 charge state). BSH ionises readily, affecting signal-to-noise. The intensity of charge states +8 and +9 (CopZ dimer peaks) decreases with increasing BSH.

After deconvolution, the monomer region (**Figure 4.4.7**) and the dimer region (**Figure 4.4.8**) of the mass spectra revealed additional information about the changes that occurred with increasing ratio of BSH/protein. The relative intensity of monomeric CuCopZ increased, and the predominant species in each spectrum was apo-CopZ. Also present were sodiated CopZ species and BSH adducts (+397.3 Da), CopZ-BSH and CuCopZ-BSH. Though the BSH adducts of apo-CopZ were likely disulfide-bonded, for CuCopZ, the cysteine thiols would be involved in copper coordination, suggesting that BSH served as an additional Cu(I) ligand, as observed in the solution structure in the presence of LMWT [40].

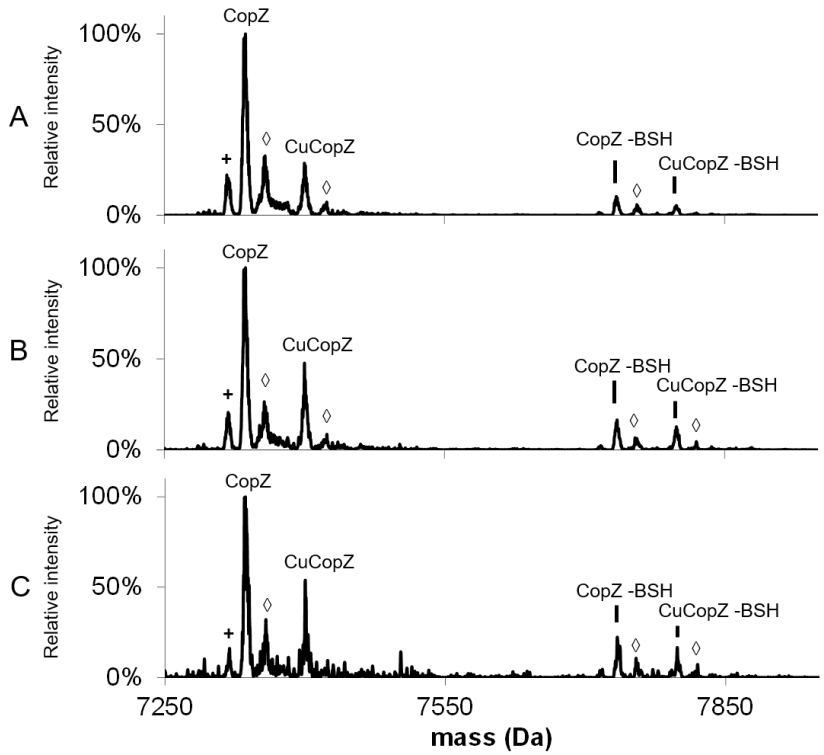

Figure 4.4.7: Deconvoluted mass spectra for 1 Cu/CopZ at varied BSH levels, monomer. Native mass spectra acquired for CopZ reconstituted with 1 Cu / protein, in the presence of **A)** 5 BSH/CopZ, **B)** 10 BSH/CopZ, **C)** 25 BSH/CopZ. Monomer region of the mass spectra expanded, with the protein species labelled and symbols used as followed: (◇) = Na^+ adduct, (+) = loss of H_2O. Peaks shift as thiol level increases, illustrating increased monomer peaks, favouring CuCopZ.

Alongside the increase in relative intensity of CuCopZ, a decrease was observed in peak intensity of dimer species, $Cu_3(CopZ)_2$ and $Cu_4(CopZ)_2$. However, this decrease was not to the extent observed above for DTT and GSH. BSH adducts were again observed which were likely to be involved in copper coordination for these higher order species.

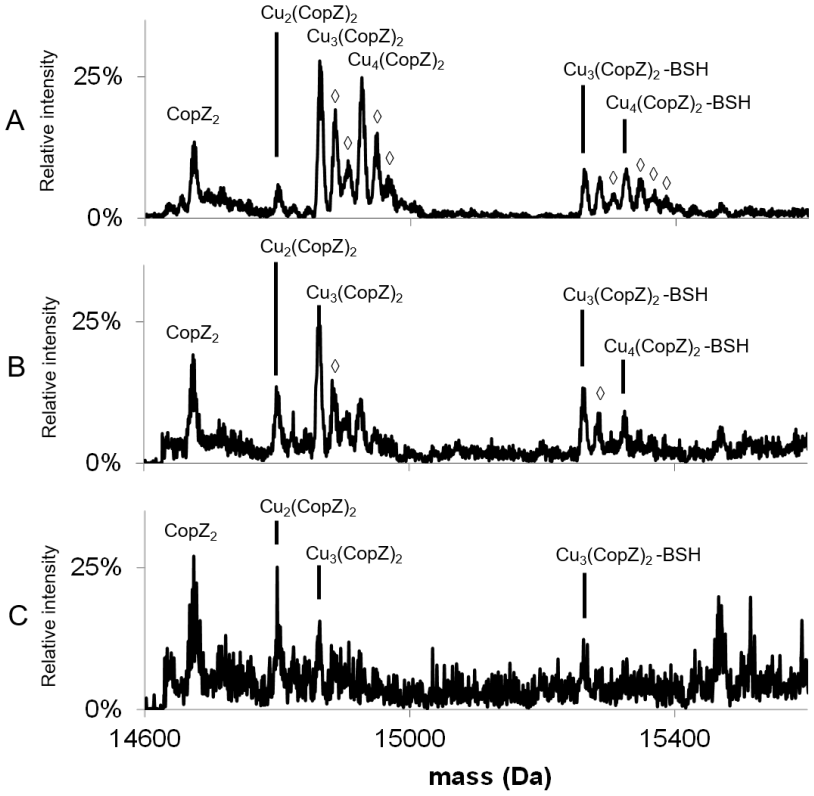

Figure 4.4.8: Deconvoluted mass spectra for 1 Cu/CopZ at varied BSH levels, dimer. Native mass spectra acquired for CopZ reconstituted with 1 Cu / protein, in the presence of **A)** 5 BSH/CopZ, **B)** 10 BSH/CopZ, **C)** 25 BSH/CopZ. Dimer region of the mass spectra, with the protein species labelled and symbol (◇) = Na^+ adduct. Peaks shift as thiol level increases, illustrating decreased dimerised CopZ species.

In addition, with increasing BSH level, the proportion of bacillithiolated protein increased, which may imply BSH exhibited a stabilising effect on the higher order species. These relative proportions are presented in Table 4.5.

Table 4.5: Proportion of BSH adducts observed for CopZ species. Results from ESI-MS experiments where CopZ was reconstituted with 1 Cu / protein, in the presence of three different ratios of BSH:CopZ. These values, representing the proportion of each species' BSH adduct relative to the total observed intensity of that particular species illustrate that the proportion of each species' BSH adduct increases as you progress from 5 10, 25 BSH/CopZ.

Species	5 BSH / CopZ	10 BSH / CopZ	25 BSH / CopZ
CopZ-BSH	8% $\pm$ 1%	13% $\pm$ 1%	18% $\pm$ 1%
CuCopZ-BSH	14% $\pm$ 3%	23% $\pm$ 1%	24% $\pm$ 7%
$Cu_3(CopZ)_2$-BSH	22% $\pm$ 2%	35% $\pm$ 1%	39% $\pm$ 3%
$Cu_4(CopZ)_2$-BSH	27% $\pm$ 1%	38% $\pm$ 4%	35% $\pm$ 21%

Table 4.6 contains the relative intensities and observed masses of species observed above. The masses were mostly in reasonable agreement with their predicted mass. As BSH is increased, the intensity of CuCopZ increased, accompanied by decreased intensity of the dimerised species. In addition, with increasing BSH, progressively fewer Cu(I) ions were coordinated by the dominant dimeric species, $Cu_3(CopZ)_2$ at 5 and 10 BSH/CopZ, followed by $Cu_2(CopZ)_2$ at 25 BSH/CopZ.

Table 4.6: Species observed via ESI-MS of 1 Cu/CopZ at varied BSH levels. Exact masses and relative intensities of species observed in native mass spectra of CopZ prepared at 1.0 Cu / protein in the presence of 5, 10 and 25 BSH per protein.

Species	Pred (Da)	5 BSH / CopZ		10 BSH / CopZ		25 BSH / CopZ	
CopZ	7336.1	100%	7336.2	100%	7336.3	100%	7336.2
CuCopZ	7399.7	28.5%	7400.4	44.2%	7400.5	47.3%	7400.3
CopZ-BSH	7734.3	8.9%	7734.3	15.3%	7734.5	22.5%	7734.7
CuCopZ-BSH	7797.9	4.6%	7798.5	12.9%	7798.6	14.2%	7798.6
$(CopZ)_2$	14672.2	13.5%	14673.2	17.6%	14674.1	28.4%	14674.3
$Cu_2(CopZ)_2$	14799.2	7.5%	14800.0	14.4%	14800.8	23.2%	14800.2
$Cu_3(CopZ)_2$	14862.7	32.7%	14864.5	25.9%	14864.8	19.3%	14864.5
$Cu_4(CopZ)_2$	14926.2	27.2%	14926.7	12.8%	14925.7	11.5%	14926.0
$(CopZ)_2$-BSH	15070.6	0%	–	0%	–	0%	–
$Cu_2(CopZ)_2$-BSH	15197.7	0%	–	0%	–	5.2%	15198.6
$Cu_3(CopZ)_2$-BSH	15262.3	9.2%	15262.3	13.6%	15262.8	12.5%	15265.8
$Cu_4(CopZ)_2$-BSH	15324.8	10.0%	15325.1	7.8%	15322.0	6.3%	15323.9

4.4.5 Glutathionylation, Bacillithiolation and CopZ-thiol Complex Formation

In order to aid the comparison of the relative distribution of CopZ species when 1 Cu / CopZ was loaded progressively increasing proportions of LMWT, bar graph representaions of the mass spectra peaks are presented in **Figure 4.4.9**. These bar graphs more clearly represent the overall trend observed: with an increase in thiol the major copper-bound species becomes CuCopZ accompanied by a decrease in dimerised species, though a more substantial amount of dimer remains at 25 BSH / protein compared to GSH and DTT. Also, in some cases, thiolation or thiol coordination was observed; this is indicated by a darker shaded bar beside each species.

Experiments conducted in the presence of GSH and BSH resulted in the observation of thiol adducts of CopZ, whereas in the presence of DTT no such adducts were observed. For apo-CopZ species, these adducts correspond to glutathionylation (+306.3 Da) or bacillithiolation (+397.3 Da), whereby a mixed disulfide forms between a Cys residue of CopZ and the LMWT. For Cu(I)-bound forms of CopZ, the adducts are unlikely to be mixed disulfides, as the Cys side chains are involved in coordination of the metal (as demonstrated through previous crystal structures and EXAFS studies [81] [38]). The extent to which these species were observed was different for GSH and BSH, with significantly more adducts observed with the physiologically relevant BSH.

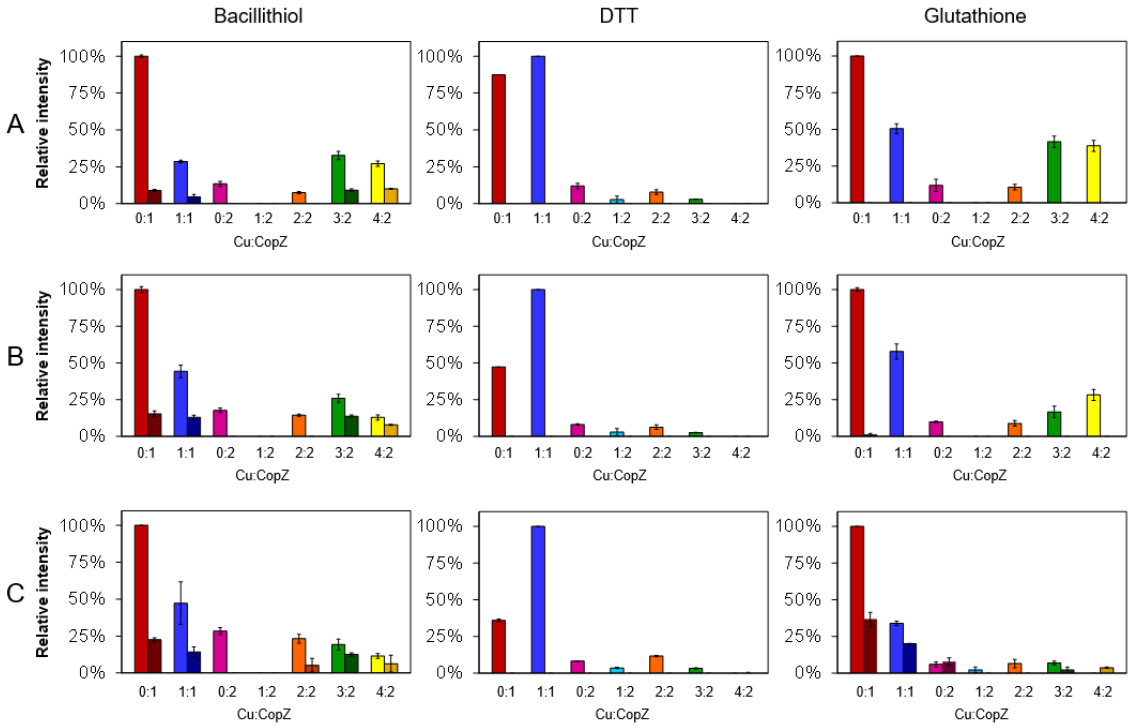

Figure 4.4.9: Species distribution observed via ESI-MS for 1 Cu / CopZ at varied thiol levels. Relative proportion of CopZ species in ESI-MS experiments of CopZ reconstituted with 1 Cu / protein in the presence of: **A)** 5 thiol/CopZ, **B)** 10 thiol/CopZ, **C)** 25 thiol/CopZ, according to the following colour code: Red, apo-CopZ; Blue, CuCopZ; Magenta, $CopZ_2$; Cyan, $Cu(CopZ)_2$; Orange, $Cu_2(CopZ)_2$; Green, $Cu_3(CopZ)_2$; Yellow, $Cu_4(CopZ)_2$. The darker portion represents the proportion of species containing a thiol adduct. With increasing thiol proportion, the intensity of dimerised CopZ peaks decrease, favoring CuCopZ; also the proportion of BSH/GSH adducts increases.

4.5 Discussion

Cu(I)-binding to *B. subtilis* CopZ has been previously shown to be complex. Initial binding of Cu(I) results in dimerisation of CopZ to form a $Cu(CopZ)_2$ species, which has the capacity to bind three further Cu(I) ions at the monomer-monomer interface [84]. While spectroscopic studies have revealed the different phases of Cu(I)-binding, and X-ray crystallography has provided a high resolution structure of the $Cu_4(CopZ)_2$ species [81], none of these techniques provided detailed information about the nature of the range of species present under different conditions of copper loading. Here it is illustrated that native MS can provide detailed, high resolution information about the distribution of CopZ and its metallo-forms that exist at different stoichiometric ratios of Cu(I) in solution.

No Cu(I)-bound CopZ species were observed when the Cu-loaded CopZ sample was subjected to the denaturing conditions of LCMS. Here, both the increased number of charge states and greater average charge state reflect the unfolding of the protein in acidified solvent, disrupting the Cu-binding site.

Under native conditions, apo-CopZ was, or was close to, the most abundant species even in copper-loaded samples. This despite the fact that previous equilibrium sedimentation and gel filtration revealed that CopZ exists predominately as a dimer in the presence of copper [89]. For a loading of 0.5 Cu/CopZ, this can be understood because solution studies previously showed that CuCopZ recruits a second CopZ molecule to form the dimeric species $Cu(CopZ)_2$ [89]. However, the association constant for the binding of the second CopZ is not high (estimated to be $\sim 10^5$ M^{-1}) [84] and so it is not surprising

that the $Cu(CopZ)_2$ species was observed only at low intensity in the mass spectrum, with apo-CopZ and CuCopZ the major species, resulting from dissociation of the $Cu(CopZ)_2$ species. At higher levels of Cu(I), the appearance of apo-CopZ may in part be a consequence of the cooperative formation of the $Cu_4(CopZ)_2$ species. However, even at a loading of 2 Cu/CopZ, which should saturate the formation of the $Cu_4(CopZ)_2$ species, significant amounts of apo-CopZ were observed. Although unexpected because electrostatic interactions are normally strengthened in the gas phase, the data appear to suggest that the Cu(I)-CopZ interaction does not efficiently survive the ionisation process.

Though it has been demonstrated that apo-CopZ exhibits reduced thermal and chemical stability [151], no change in ESI-MS charge state distribution was observed between apo-CopZ and Cu-loaded CopZ. This indicates that no major protein conformational change occurs upon addition of copper, and the reduced charge state distribution compared to denatured CopZ indicates that both apo-CopZ and Cu(I)-bound CopZ remain folded upon ionisation. Addition of higher amounts of Cu resulted in the emergence of a dimer peak envelope with charges +8, +9, centered upon higher m/z values than the monomer or denatured protein peak envelopes. This change in charge state behaviour is consistent with the well characterised relationship between protein association state and charge state [152].

At low Cu(I) loadings (0.5 Cu/CopZ), the major Cu(I)-bound species detected in the mass spectrum was CuCopZ, at higher levels of Cu(I) ($\geq$1 Cu/CopZ), several dimeric forms of CopZ were readily detected. This is consistent with previous solution studies which showed that binding of $\geq$ 1 Cu(I) at the monomer-monomer interface stabilised the complex significantly [89]. $Cu_2(CopZ)_2$, $Cu_3(CopZ)_2$ and $Cu_4(CopZ)_2$ species were all detected, with

$Cu_3(CopZ)_2$ marginally the most abundant of these dimeric species at 1 Cu / CopZ.

At Cu(I)-loadings above 1 per CopZ, the major Cu(I)-bound form of CopZ was $Cu_4(CopZ)_2$, at the expense of the other dimeric forms. This demonstrates a cooperativity of Cu(I)-binding to the dimeric form of CopZ, indicating that the arrangement of four Cu(I) ions in a cluster at the monomer interface is a particularly thermodynamically stable form. This is consistent with previous structural studies, in which the structure of $Cu_4(CopZ)_2$ was solved, but from crystallisation solutions containing a 1:1 ratio of Cu:CopZ (i.e., the $Cu_2(CopZ)_2$ species was the intended structural target of that study) [81]. *E. hirae* CopZ was previously studied by native MS [141], with a similar narrow charge state distribution observed for both apo- and Cu(I)-bound protein. In that case, although dimeric CopZ was detected in solution it was not observed by MS.

An especially diverse mixture was observed at 1.0 Cu/CopZ, where the increased number of species reflects the point of transition from monomeric CuCopZ to dimeric $Cu_4(CopZ)_2$. This transitionary Cu(I)-binding behaviour accounts, at least in part, for relatively large error bars in the 1.0 Cu/CopZ bar graphs (**Figure 4.2.4**), where slight variation of Cu(I) concentration between experiments has a significant effect on the equilibrium distribution of Cu(I)-bound CopZ species. Overall, the data demonstrate the distribution of metalloforms which exist as the major Cu(I)-bound species shifts from CuCopZ to $Cu_4(CopZ)_2$.

Previous spectroscopic and bioanalytical studies of the effect of LMWTs showed that DTT, GSH and Cys interfere with Cu(I)-binding to CopZ, inhibiting the formation of higher order Cu(I)-bound forms of the CopZ dimeric forms [89] [52], but the specific CopZ species which arose could not be identified. In addition, these studies pre-dated the discovery of

BSH, the recently discovered physiological LMWT in *B. subtilis* [27]. Therefore, it was desirable to continue previous spectroscopic studies using the physiologically relevant BSH, and probe the specific distribution via ESI-MS of CopZ species in the presence of LMWTs.

Data presented in this chapter generally agree with the observations from previous spectrocopy studies i.e., that the initial binding phase of Cu(I) to CopZ in the presence of LMWT is similar to that in the absence of thiol but, with subsequent Cu(I) additions, a significant departure from thiol-free behaviour was observed. Furthermore, the native MS data revealed more detail about the effects of thiols, demonstrating the decreased relative proportion of higher order dimerised CopZ in the presence of LMWT.

This was the case in the ESI-MS experiments in the presence of DTT, which severely inhibited the formation of higher order Cu(I)-bound forms of CopZ. However, because the intial species formed upon copper-binding, $Cu(CopZ)_2$, was not detected at significant abundance in the spectrum, the effect of DTT (and other thiols) on the formation of this species cannot be discerned. In addition, though DTT and DTT adducts of CuCopZ were not observed, perhaps the capability of DTT to serve as an additional ligand for the CuCopZ monomer species [40] is reflected by the increased proportion of CuCopZ with increasing DTT levels.

The effects of BSH, along with GSH, were similar but less severe, with a marked decrease in the abundance of dimer observed only at the highest ratio of GSH. The data are consistent with previous investigations which indicated the presence of thiols (particularly GSH and Cys) does not appreciably disrupt the initial binding of Cu(I) to CopZ, but does inhibit the formation of higher order Cu(I)-bound CopZ species [52]. Here, however, in the

presence of GSH and BSH, dimeric CopZ species persisted even at the highest ratios of thiol to protein tested here.

It is likely that, at higher levels of Cu(I), LMWTs may compete for Cu(I) because stepwise binding of Cu(I) to $Cu(CopZ)_2$ is weaker than the initial binding step [89]. Because of the high Cu(I)-binding affinities involved, competition effects would most likely occur through the formation of transient hetero-complexes in which Cu(I) is at least temporarily coordinated by both CopZ and a LMWT. For GSH and particularly BSH, it was found that such hetero-complexes are stable and can be readily detected. Interestingly, in addition to hetero-complexes formed between BSH and CuCopZ, BSH adducts of all the dimeric species were readily observed, suggesting that Cu(I) bound in clusters at the CopZ monomer-monomer interface can accommodate BSH coordination as well.

The high affinity of BSH for Cu(I), determined here as $\beta_2 = 4.1 \pm 1.5 \times 10^{17}$ M^{-2}, is consistent with a potential role in buffering Cu(I) levels in the cell. GSH was unable to compete with BCS for Cu(I) [138], suggesting that BSH has a higher affinity for Cu(I). This affinity, however, is $\sim$3 orders of magnitude lower than that of CopZ [84], and so it is unlikely that BSH alone buffers Cu(I). Consistent with this, *B. subtilis* cells lacking BSH were recently found to be unaffected in their overall sensitivity to Cu(I) stress compared to wild-type cells under equivalent conditions, but the expression of copZA was found to be elevated [23]. These data suggest that BSH is not an essential component of the copper trafficking pathways of *B. subtilis*, but are consistent with BSH playing a role in copper-buffering. Perhaps the observation of BSH adducts of Cu(I)-bound CopZ species indicates that BSH could function together with CopZ (and possibly CopA) via the formation of hetero-

complexes to buffer Cu(I) levels. Interestingly, BSH was recently found to be a major buffer of the cytoplasmic zinc pool in *B. subtilis* [23] in which a dedicated Zn(II) chaperone has not been identified.

Also, apo-CopZ was observed as a BSH adduct; this is the S-bacillithiolated form of the protein. Bacillithiolation of proteins in *B. subtilis* is known to occur as a reversible, protective response against over-oxidation of functionally important Cys residues resulting from oxidative stress. Bacillithiolation is known to protect proteins such as redox-sensor OhrR [153] and the methionine synthase MetE [154]. Though it is not clear what the oxidative driving force is in our experiments, a potential source could be a small amount of O_2 introduced during acquisition, or the ionisation process itself. Regardless, the ease with which these species are observed, even at relatively low ratios of BSH to protein, suggests that this would be a physiologically important process for the protection of CopZ.

Chapter 5

Studies of Cu(I) Binding to CopAab

5.1 Introduction

Translocation of Cu(I) across the *Bacillus subtilis* cell membrane takes place by way of CopA, the integral membrane P-type ATPase CopA. The P-type ATPase protein family typically contain a central core of transmembrane helices, multiple soluble cytoplasmic domains (MBDs), an actuator domain (A-domain) and an ATP-binding domain (ATP-BD), comprising two distinct sub-domains involved in nucleotide-binding (N) and phosphorylation (P) [47]. The P-type ATPases are further divided into subclasses based upon several structural features [155]. The P_{1B}-type ATPases contain an additional two helices in the transmembrane core. The P_{1B1}-type ATPase subclass also is distinguished by possession of a CPC transmembrane metal-binding motif (TMBS) located in helix 4, and one or more soluble MBDs at the N- and, sometimes, C-termini.

The two N-terminal cytoplasmic MBDs in *B.sutbilis* CopA, CopAab, possess the same $\beta\alpha\beta\beta\alpha\beta$ fold as the Atx1-like metallochaperone CopZ. Each individual domain, CopAa and CopAb, contains a conserved MXCXXC copper binding motif with two solvent-exposed cysteines located between the end of the first loop and the beginning of the first α-helix [156]. Cu(I) is not bound by the CopAab from the cytoplasm directly but, rather, by interaction with CopZ which helps to ensure specific transfer of copper, as the CXXC motif is capable

of binding other metals, such as zinc [157].

The exact role of MBDs in ATPase function is unclear, though it has been demonstrated they are required for copper transfer activity [158] [159], and interaction between MBD and the catalytic domains suggest they play a regulatory role [160]. In the absence of copper, one MBD interacts with one of the catalytic domains and is released upon copper binding [161]. Though Cu(I) binding to the MBDs is required for catalytic activation, it seems that copper-bound to the MBD at the start of the catalytic cycle remains bound, while Cu(I) bound to the TMBS is extruded across the membrane [162].

Cu(I) binding to CopAab has been characterised previously [147], with CopAab shown to undergo Cu(I)-mediated dimerisation above 1 Cu / protein and accommodate multiple Cu(I) ions. Copper binding by CopAab at a ratio of 2 Cu / protein was observed via luminescence, predicted to be $Cu_4CopAab_2$. However, luminescence quenching beyond a raio of 2:1 suggests that dimeric CopAab may be able to bind additional Cu(I) ions [163]. CopAab binds Cu(I) with high affinity, leading to dimerisation at 1 Cu / protein. Data from AUC and SEC suggested that a small portion of dimer (¡5%) is present at 1 Cu / protein and by 2 Cu / protein the association state is fully dimeric. [80].

In addition, Cu(I) binding to CopAa [83] and CopAb [82] has been characterised previously. Solution-phase studies demonstrated continual binding of Cu(I) by CopAa and CopAb between 0 and 2 Cu / protein.SEC and AUC data suggested the association state of CopAa is tetramer/monomer equilibrium at 0.5 Cu / protein, tetramer/dimer at 1 Cu / protein and a dimer at 2 Cu / protein. The association state of CopAb observed via AUC to be monomeric at 0.5 Cu / protein and dimeric at 1.0 and 2.0 Cu / protein.

Though apo-CopAa was observed to be folded (CD) and stable over 48 hours observed (NMR) [164], instability was observed upon copper binding, which did not occur when copper was bound by CopAab or CopAb [82]. In addition, instability was not observed in a mixed sample (CopAa/Ab) suggesting their physical connection may influence the stability and potentially structure and function of the protein *in vivo*.

The regulation of Cu(I) levels could be influenced by cytoplasmic low molecular weight thiol-containing species (LMWT). For example, it has been demonstrated that glutathione may serve as a copper-binding intermediate between the eukaryotic importer Ctr1 and cytoplasmic chaperones [165]. Though this influence upon Ctr1 may not be the same as in Cu(I) transfer to a Cu(I) export protein, a role in metal trafficking has been suggested for the cytoplasmic LMWT in *B. subtilis*, bacillithiol (BSH). Therefore understanding of Cu(I)-binding to *B. subtilis* CopAab, in the presence of LMWT, may help to further elucidate the role these domains play in Cu(I) export.

Despite previous studies characterising Cu(I) binding to CopAab, the nature of species and mixtures of species which form as Cu(I) levels fluctuate is unknown. In addition, the influence of LMWT upon Cu(I) binding by CopAab is not clear, nor is the influence of the two domain linker upon binding of Cu(I) by CopAab. In order to investigate these endpoints, native ESI-MS of CopAab in the absence and presence of LMWT was carried out, in addition to an experiment monitoring Cu(I) binding to a mixture of individual domains CopAa and CopAb by LCMS and ICP-AES.

5.2 Materials And Methods

5.2.1 ESI-MS Of CopAab

Mass spectrometry samples of CopAab were prepared using protein aliquots purified as described in section 2.2.3. ESI-MS samples of CopAab were prepared by first adding 15 mM DTT (Formedium) and removing reductant by passage down a G25 Sephadex column (PD10, GE Healthcare) in an anaerobic glovebox (Faircrest Engineering, O_2 concentration $<$ 2 ppm) using 20 mM ammonium acetate (Sigma), pH 7.4, as the elution buffer. Protein concentrations were calculated using an extinction coefficient, ε_{276nm}, of 5800 M^{-1} cm^{-1} [147], before anaerobic addition of Cu(I) using a microsyringe (Hamilton). UV-visible absorbance spectra were recorded on a Jasco V-550 spectrophotometer. To prepare Cu(I)-bound CopAab samples, a deoxygenated solution of Cu(I)Cl prepared in 100 mM HCl (Sigma), 1 M NaCl was added to anaerobic, reduced CopAab using a microsyringe (Hamilton) in an anaerobic glovebox. Unbound Cu(I) was removed by passage of the sample down a G25 Sephadex column (PD10, GE Healthcare) equilibrated with 20 mM ammonium acetate, pH 7.4. The protein sample was diluted with 20 mM ammonium acetate to a working sample concentration of 5 μM. Thiol experiments were carried out using dithiothreitol (DTT) (Formedium) or BSH (synthesised as described previously [143]; for structures see Section 4.2.3) prepared anaerobically using deoxygenated LC-MS grade water (HiPerSolv, VWR). Solutions of CopAab were prepared at 4.0 Cu(I) / protein (as described above), where thiol solution was added to yield ratios of 1, 5, 10, or 25 thiol per

protein.

Mass spectra were acquired using a Bruker micrOTOF-QIII electrospray ionisation (ESI) time-of-flight (TOF) mass spectrometer (Bruker Daltonics, Coventry, UK), in positive ion mode. The ESI-TOF was calibrated in the m/z range 300 – 2200 using ESI-L Low Concentration Tuning Mix (Agilent Technologies, San Diego, CA). Native protein samples were introduced to the ESI source at 4 °C via a syringe pump (Cole-Parmer) at 5 μL/min, and data acquired for 2 min, with ions scanned between 500 – 3000 m/z. MS acquisition was controlled using Bruker oTOF Control software, with parameters as follows: dry gas flow 5 L/min, nebuliser gas pressure 0.8 Bar, dry gas 180 °C, capillary voltage 4500 V, offset 500 V, isCID energy 0 eV, quadrupole RF stepping set at 2000 Vpp (25%) and 3200 Vpp (75%). Processing and analysis of MS experimental data was carried out using Compass DataAnalysis version 4.1 (Bruker Daltonik, Bremen, Germany). The spectra were deconvoluted using the ESI Compass version 1.3 Maximum Entropy deconvolution algorithm over a mass range of 15000 – 35000 Da. Exact masses were determined from peak centroids, with 3-point Gaussian smoothing applied only to spectra acquired in the presence of BSH.

5.2.2 Cu(I) Binding to CopAa/Ab Mixture

Samples were prepared under anaerobic conditions containing 100 μM of each CopAa and CopAb (prepared as described in Sections 2.2.4 and 2.2.5) in 100 mM MOPS, 100 mM NaCl, pH 7.5, at 0, 0.5, 1.0 and 2.0 Cu(I) per domain. Each 500 μL sample was loaded onto a Superdex G75 10/300 GL column (GE Healthcare), with a total column vol-

ume (V_t) of 24 mL and a void volume (V_0) of 7.6 mL, as determined using blue dextran. The column was equilibrated and operated using thoroughly deoxygenated buffer at a flow rate of 0.3 mL min^{-1}. Elution fractions were collected every 0.5 mL and analysed for Cu^+ and protein. For metal analysis of the elution fractions from the G75 column, an ICP-OE (inductively coupled plasma optical emission) spectrometer (Varian Vista) was used, calibrated with ICP grade Cu standards (Fisher) diluted to appropriate concentrations. After overnight incubation in 50% nitric acid (Primar Plus, Fisher) at 60 °C, elution buffer (as baseline) and protein samples were diluted to appropriate concentrations in a final volume of 10 mL using HiPerSolv water (VWR) for a final concentration of 4% nitric acid. Spectral line at 324.754 nm was used to determine Cu^+ concentrations. Data analysis was performed using ICP Expert version 4.1. For protein analysis, HPLC-MS experiments were performed using an UltiMate 3000 HPLC system (Dionex, Sunnvale, CA, USA), and a Bruker micrOTOF-QIII electrospray ionisation (ESI) time-of-flight (TOF) mass spectrometer (Bruker Daltonics, Coventry, UK), in positive ion mode. Protein samples were diluted 50-fold into 2% acetonitrile and a 1 μL injection volume was applied to a ProSwift® reversed phase RP-1S column (4.6 × 50mm; Dionex) at 25°C. Gradient elution was performed at a flow rate of 200 μL/min using solvents A (0.1% formic acid) and B (acetonitrile, 0.1% formic acid), with the following chromatographic method: isocratic wash (2% B, 0–1 min), linear gradient from 2–100% B (1–3 min), followed by an isocratic wash (100% B, 3–7 min) and column re-equilibration (2% B, 7–11 min). Mass spectra were recorded in the range 500 – 3400 m/z, using Bruker oTOF Control software with parameters as follows: dry gas flow 8 L/min, nebuliser gas pressure 1.8 Bar, dry gas 240°C, capillary voltage 4500 V, offset 500

V, collision RF 650 Vpp. The ESI-TOF was calibrated in the m/z range 300 – 2200 using ESI-L Low Concentration Tuning Mix (Agilent Technologies, San Diego, CA). Processing and analysis of MS experimental data was carried out using Compass DataAnalysis version 4.1 (Bruker Daltonik, Bremen, Germany). The spectra were deconvoluted using the ESI Compass version 1.3 Maximum Entropy deconvolution algorithm over a mass range of 7000 – 20000 Da. Exact masses were determined from peak centroids.

5.3 Results: ESI-MS of Cu(I) Binding To CopAab

It has been demonstrated previously that copper binding to CopAab is complex, with several different Cu(I)-bound forms observed including a dimer. In order to assess the mixture of species arising when CopAab binds copper, ESI-MS was carried out of CopAab at varied stoichiometric ratios of Cu(I).

5.3.1 Cu(I) Binding To CopAab

The mass spectra prior to deconvolution of CopAab at 0.5, 1.0, 2.0 and 4.0 Cu / protein are presented in **Figure 5.3.1**. The changes in intensity of the charge envelopes arise due to progressive increase of dimerised CopAab peaks, which occurs as copper level is increased.

The mass spectra revealed three charge state envelopes, one monomer (+8, +9) and two dimer (+11 – +14; and +16 – +18). The dimer charge states comprise two separate envelopes, suggesting the presence of two forms of the dimer species. The first charge envelope (11+, 12+, 13+, 14+) has fewer charges, suggesting a more compact dimer structure while the second charge envelope with more charges (16+, 17+, 18+) likely corresponds to a more open structure susceptible to greater protonation during ionisation. These two species appear to coordinate the same total number of copper ions.

At 0.5 and 1.0 Cu / CopAab (**Fig 5.3.1A** and **B**, respectively), the monomer charge envelope (8+, 9+) is predominant, with a small dimer envelope emerging. At 2.0 Cu / CopAab (**Fig 5.3.1C**), an increased intensity of dimer peaks is observed with monomer

envelope (8+, 9+) still the most prominent. At 4.0 Cu / CopAab (**Fig 5.3.1D**), the dimer peaks increase further in relative intensity, with both envelopes in approximately equal proportion to each other.

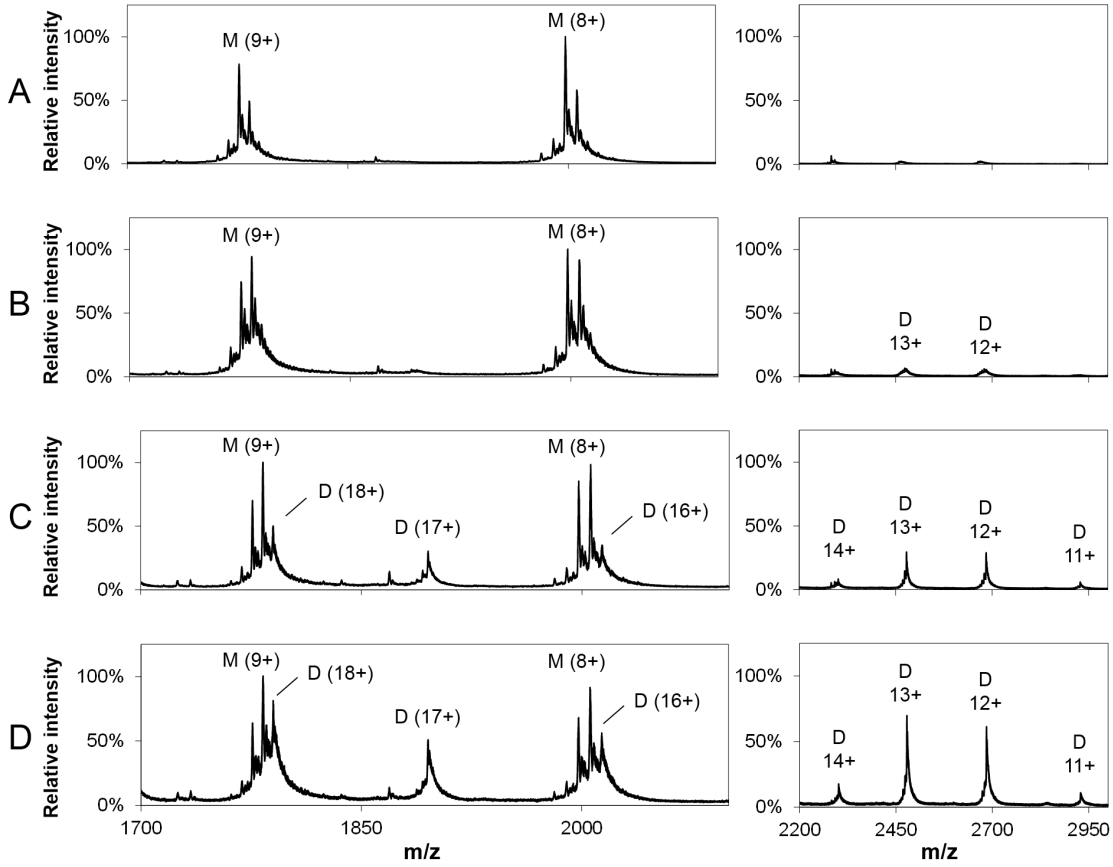

Figure 5.3.1: Mass spectra for CopAab at varied Cu(I) levels. The mass spectra prior to deconvolution of CopAab reconstituted with Cu(I) at: **A)** 0.5 Cu / protein, **B)** 1 Cu / protein, **C)** 2 Cu / protein, **D)** 4 Cu / protein.

The mass spectra after deconvolution presented in **Figure 5.3.2** focus on the monomer and dimer regions. They confirm the trend observed across the mass spectra in **Figure 5.3.1**, monomer dominates at 0.5 and 1 Cu / CopAab, leading to a dimer/monomer mixture at 2 and 4 Cu / CopAab. The only species observed in the spectra were different forms of CopAab, and some sodium adducts.

At 0.5 Cu / CopAab, the copper-bound species observed were CuCopAab and also Cu_2CopAab. Each domain (Aa and Ab) has a copper-binding motif and thus could co-ordinate metal ions independently. With increasing copper level, the relative intensity of Cu_2CopAab increases to become the dominant copper-bound peak at 2 Cu / protein. At 4 Cu / protein, the mass spectra reveal that the dimeric form $Cu_6(CopAab)_2$ is the predominant copper-bound species, accompanied by a decrease in Cu_2CopAab. At all levels of copper, apo-CopAab, $Cu_4(CopAab)_2$, and $Cu_5(CopAab)_2$ are observed, albeit at low intensity.

The exact masses and relative intensities of the species observed are presented in **Table 5.1**. The observed masses in Table 5.1 are mostly within 1 Da of the predicted mass. The observed masses of $Cu_6(CopAab)_2$ and $Cu_5(CopAab)_2$ are 2 – 4 Da higher than predicted; the reason for this is unclear.

Table 5.1: Species observed via ESI-MS for CopAab at varied Cu(I) levels. Exact masses and relative intensities of species observed in native mass spectra of CopAab prepared at 0.5, 1.0, 2.0 and 4.0 Cu / protein. Exact masses not reported for low intensity peaks below 3% relative intensity.

Species	Pred (Da)	0.5 Cu / CopAab		1.0 Cu / CopAab		2.0 Cu / CopAab		4.0 Cu / CopAab	
CopAab	15909.0	31%	15910.8	33%	15908.0	11%	15907.8	6%	15908.3
CuCopAab	15972.6	100%	15974.8	100%	15973.5	74%	15973.2	57%	15973.4
Cu_2CopAab	16036.1	60%	16037.9	68%	16037.5	100%	16037.3	51%	16037.6
$Cu_3(CopAab)_2$	32008.7	<3%	–	<3%	–	<3%	–	0%	–
$Cu_4(CopAab)_2$	32072.2	<3%	–	<3%	–	6%	32072.6	16%	32071.4
$Cu_5(CopAab)_2$	32135.8	<3%	–	8%	32138.7	17%	32138.6	13%	32139.5
$Cu_6(CopAab)_2$	32199.3	0%	–	10%	32201.3	33%	32201.4	100%	32202.3

In order to more clearly visualise changes occurring with copper level, **Figure 5.3.3** presents the distribution of species at each copper loading as bar graphs, obtained by averaging three independent measurements. **Figure 5.3.2** presents a single data set and,

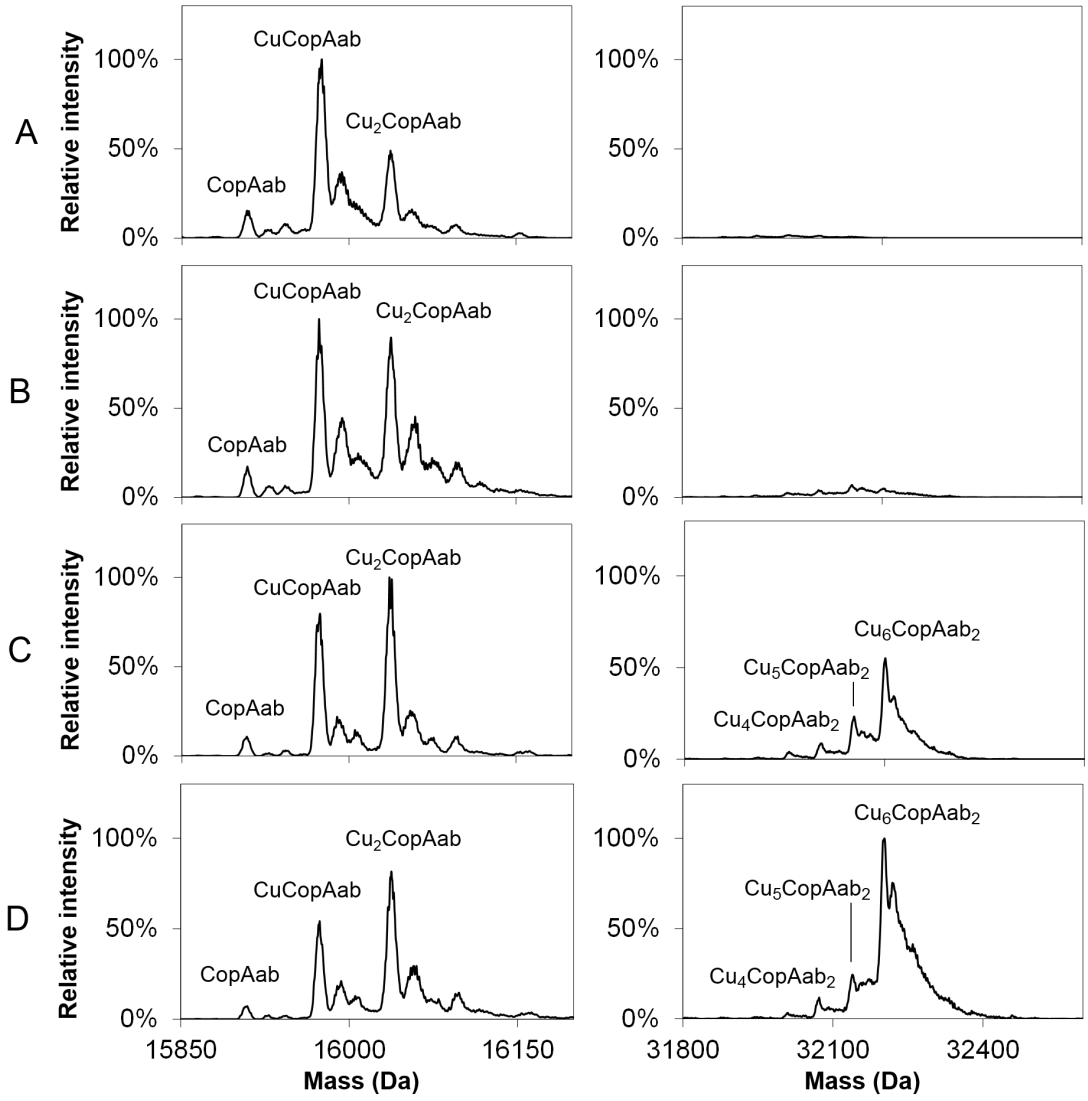

Figure 5.3.2: Deconvoluted mass spectra for CopAab at varied Cu(I) levels. The deconvoluted mass spectra of CopAab reconstituted with Cu(I) at: **A)** 0.5 Cu / protein, **B)** 1 Cu / protein, **C)** 2 Cu / protein, **D)** 4 Cu / protein.

thus, the relative intensities may not be identical to those in Table 5.1; this is represented by a few large error bars in **Figure 5.3.3**.

As copper level increases from 0.5 – 4 Cu / CopAab, the bar graphs illustrate an increase in intensity of CuCopAab and Cu_2CopAab, followed by a decrease in intensity of these species with increase of $Cu_6(CopAab)_2$ peak. The consistently low intensity of the

other dimeric forms implies a cooperativity of Cu-binding to the dimeric form $Cu_6(CopAab)_2$, which likely arises from the assembly of Cu_2CopAab protomers.

The Cu_3CopAab species is unexpected, as each domain possesses just a single CXXC motif and intra-domain Cu(I) coordination is not possible due to the short linker length between domains. This peak could represent a transient species arising from breakdown of $Cu_6(CopAab)_2$, which would agree with its low relative intensity and (proportionately) high error bar.

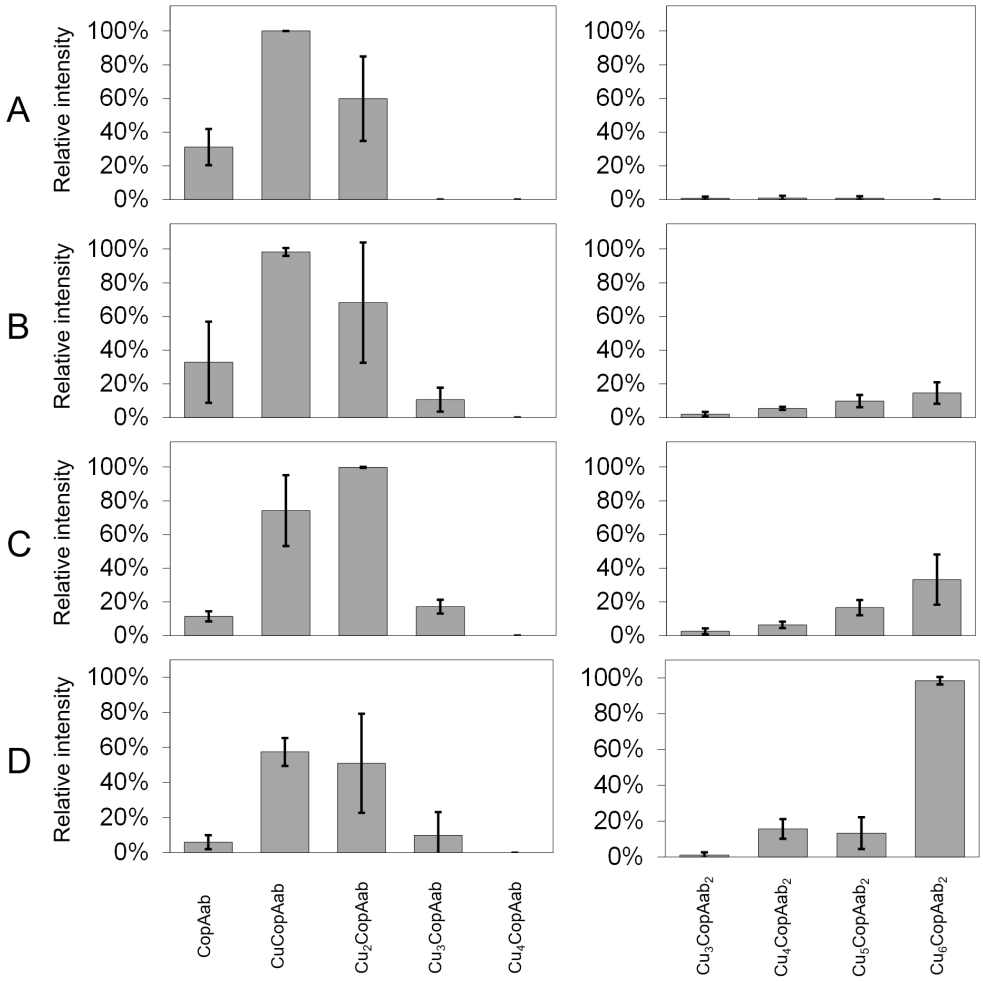

Figure 5.3.3: Species distribution observed via ESI-MS of CopAab with increasing levels of Cu(I). Species distribution in the deconvoluted mass spectra of CopAab reconstituted with Cu(I) at: **A)** 0.5 Cu / protein, **B)** 1 Cu / protein, **C)** 2 Cu / protein, **D)** 4 Cu / protein.

5.3.2 Cu(I) Binding To CopAab in the Presence of LMWT

To assess the effect of LMWT upon CopAab species distribution at elevated copper loadings, ESI-MS were recorded of CopAab (prepared at 4 Cu / protein) in the presence of DTT and BSH at 1, 5, 10 and 25 per protein (for structural representations, see Section 4.2.3). Compared to the experiments in Chapter 4 for CopZ, the effect of LMWT was more drastic at 5 / protein and, therefore, an additional experiment at a level of 1 thiol / protein was carried out.

CopAab + DTT

The mass spectra, prior to deconvolution, are presented in **Figure 5.3.4** of CopAab prepared with 4 Cu / protein, in the presence of 1, 5, 10 and 25 DTT per protein. Two peak envelopes are observed, monomer (+8, +9) and dimer (+12, +13). The dimer peak envelope is of low intensity, and represents the more compact of the two dimeric forms of CopAab observed in **Figure 5.3.1**.

Compared to the thiol-free spectrum (Fig 5.3.1.D), there are fewer peaks, with only a small amount of dimer envelope at 1 DTT / protein. The subsequent thiol loadings display a fairly similar peak distribution, with a slight increase in proportion of the monomer peak with increasing thiol. The presence of DTT caused neither the position nor number of peaks in either peak envelope to shift, suggesting no major conformational changes in the protein in the presence of thiol.

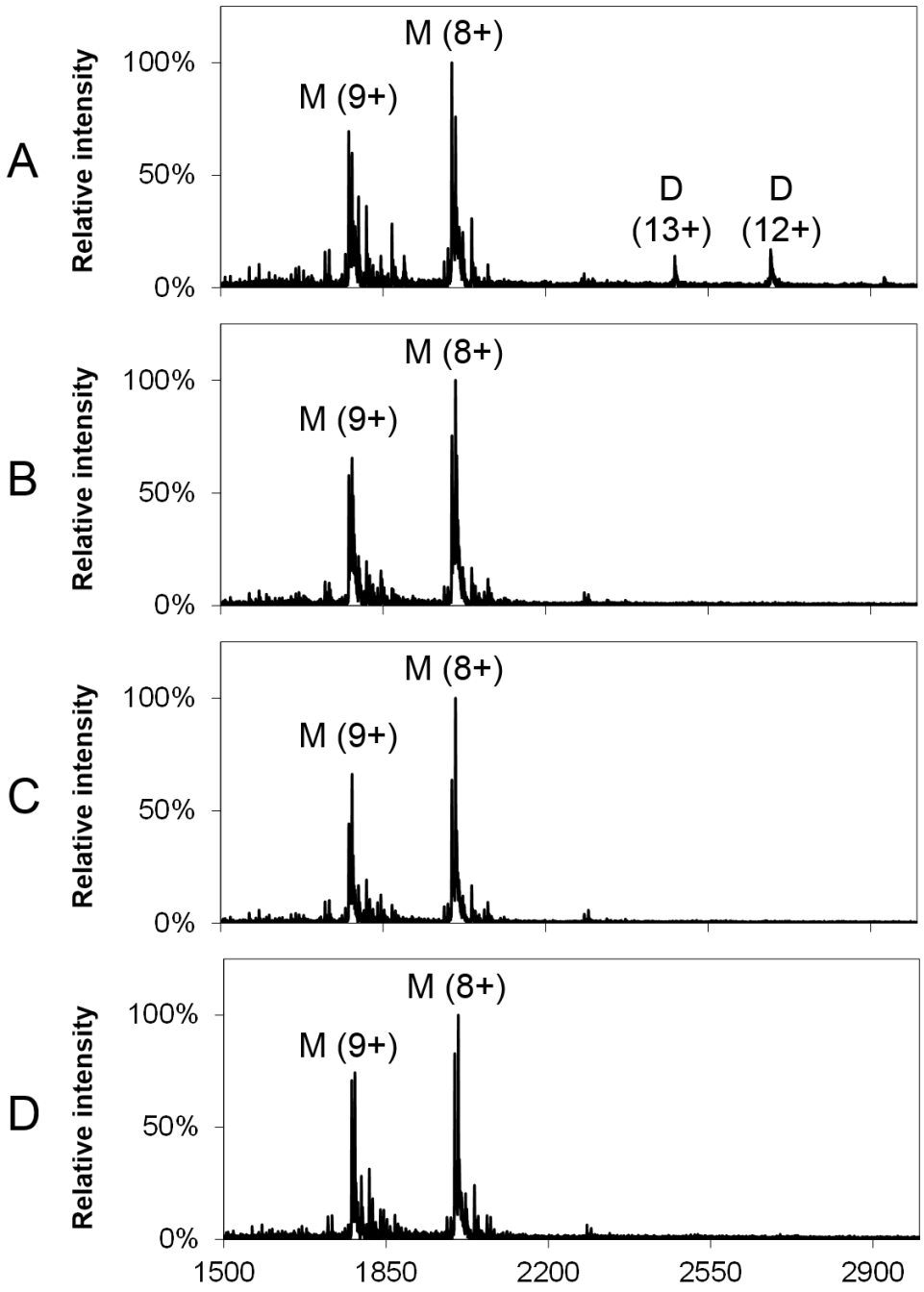

Figure 5.3.4: Mass spectra for 4 Cu/CopAab at varied DTT levels. The mass spectra prior to deconvolution of 4 Cu / CopAab in the presence of: **A)** 1 DTT / protein, **B)** 5 DTT / protein, **C)** 10 DTT / protein, **D)** 25 DTT / protein.

.

The deconvoluted mass spectra are presented in **Figure 5.3.5** and stand in agreement with the trend observed in the mass spectra above: at and above a thiol level of 5 / protein, the spectra contain a similar peak distribution, with dimeric species abolished. Unlike for CopZ in the presence of DTT (see Chapter 4), thiol adducts are observed for CopAab. These adduct species feature one or two DTT molecules, which are likely to serve as additional Cu(I) ligands given the higher than expected copper loadings (4, 5 and 6 per monomer). These species could somehow give rise to the peaks with unexpected Cu/protein ratios, Cu_3CopAab and Cu_4CopAab.

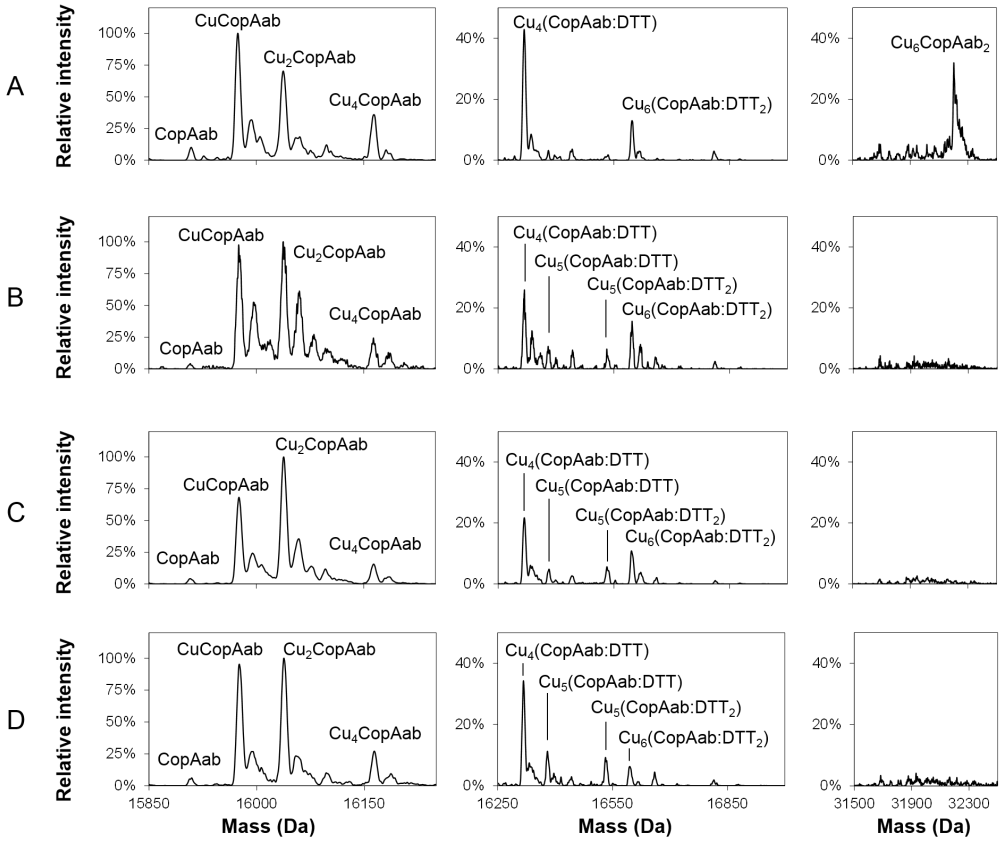

Figure 5.3.5: Deconvoluted mass spectra for 4 Cu/CopAab at varied DTT levels. Mass spectra of 4 Cu / CopAab in the presence of: **A)** 1 DTT / protein, **B)** 5 DTT / protein, **C)** 10 DTT / protein, **D)** 25 DTT / protein. The regions of the mass spectra, from left to right, are: CopAab monomer, DTT adducts of CopAab monomer, and CopAab dimer.

The observed masses and relative intensities of species in the mass spectra are presented in **Table 5.2**. The masses are mostly within 1 Da of the predicted masses. Cu_2CopAab and Cu_6(CopAab)$_2$ are approximately 3 Da greater than their predicted masses; the reason for this discrepancy is unclear.

Table 5.2: Species observed via ESI-MS for 4 Cu/CopAab at varied DTT levels. Exact masses and relative intensities of species observed in native mass spectra of CopAab prepared at 4.0 Cu / protein in the presence of DTT. Exact masses not reported for species below 3% relative intensity.

Species	Pred (Da)	1 DTT / CopAab		5 DTT / CopAab		10 DTT / CopAab		25 DTT / CopAab	
CopAab	15909.0	9%	15909.0	0%	–	4%	15908.2	<3%	–
CuCopAab	15972.6	100%	15974.1	98%	15975.6	73%	15975.7	95%	15975.9
Cu_2CopAab	16036.1	69%	16037.4	95%	16038.1	100%	16038.1	95%	16038.0
Cu_3CopAab	16099.6	11%	16097.8	0%	–	0%	–	6%	16099.5
Cu_4CopAab	16163.1	41%	16163.9	28%	16163.3	19%	16163.6	26%	16163.7
Cu_4(CopAab:DTT)	16317.4	37%	16317.5	27%	16317.4	24%	16317.6	35%	16317.3
Cu_5(CopAab:DTT)	16381.6	0%	–	10%	16382.5	6%	16381.6	10%	16379.8
Cu_6(CopAab:DTT)	16444.3	0%	–	4%	16443.2	4%	16444.3	<3%	–
Cu_5(CopAab:DTT)$_2$	16535.2	0%	–	4%	16532.3	<3%	–	6%	16534.3
Cu_6(CopAab:DTT$_2$	16598.8	9%	16597.3	13%	16597.3	7%	16599.4	9%	16595.8
Cu_4(CopAab)$_2$	32072.2	23%	32071.6	0%	–	0%	–	0%	–
Cu_5(CopAab)$_2$	32135.8	12%	32135.8	0%	–	0%	–	0%	–
Cu_6(CopAab)$_2$	32199.3	61%	32202.4	0%	–	0%	–	0%	–

In order to more clearly visualise the species distribution, the relative intensities observed the mass spectra are presented as bar graphs in **Figure 5.3.6**, taken as an average of three independent measurements. The bar graphs clearly depict the dominance of the monomeric forms CuCopAab and Cu_2CopAab at and above a level of 5 DTT / protein. The absence of of dimeric forms of CopAab suggests that DTT has competed for Cu(I).

The presence of DTT adduct species illustrates that DTT interacts with CopAab, with the most intense adduct species ($\sim$ 25%) Cu_4(CopAab:DTT). This likely represents an arrangement where DTT is acting as an additional ligand to Cu(I) at one of the CopAab

domains, though it is unclear which domain (Aa or Ab). It also is not clear how many coppers each domain has bound. Without the possibility for intra-protein domain interaction, the domain not experiencing the influence of DTT likely only binds one Cu(I).

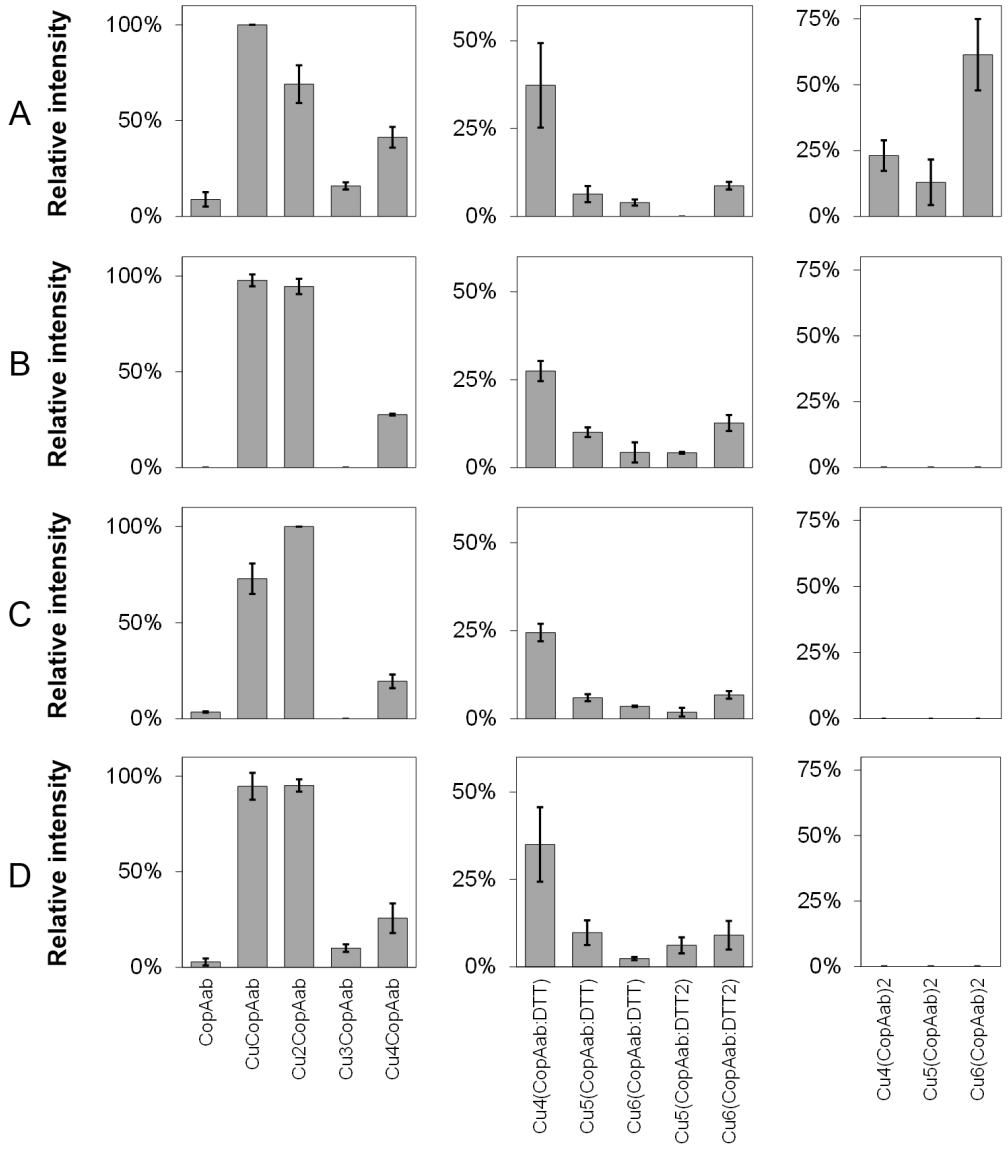

Figure 5.3.6: Species observed via ESI-MS for 4 Cu/CopAab at varied DTT levels. Species distribution in deconvoluted mass spectra of 4 Cu / CopAab in the presence of: **A)** 1 DTT / protein, **B)** 5 DTT / protein, **C)** 10 DTT / protein, **D)** 25 DTT / protein. Bar graphs generated from the average of three independent measurements.

CopAab + BSH

The mass spectra, prior to deconvolution, of CopAab prepared with 4 Cu / protein, in the presence of 1, 5, 10 and 25 BSH per protein are presented in **Figure 5.3.7**.

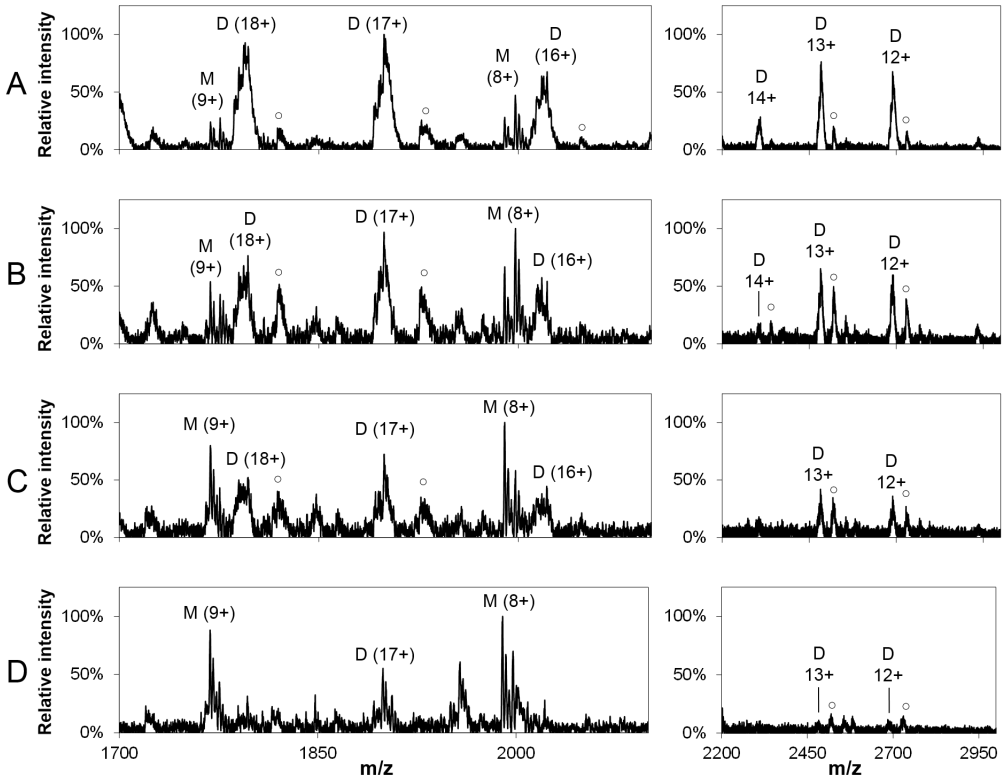

Figure 5.3.7: Mass spectra for 4 Cu/CopAab at varied BSH levels. The mass spectra prior to deconvolution of 4 Cu / CopAab in the presence of: **A)** 1 BSH / protein, **B)** 5 BSH / protein, **C)** 10 BSH / protein, **D)** 25 BSH / protein. Upon increase in BSH level, the dimer envelopes are diminished, with the formation of BSH adducts of copper-bound CopAab species, denoted by (°).

As seen for CopZ in Chapter 4, BSH ionises readily leading to ion suppression in the mass spectrum, affecting signal to noise ratio. For CopAab however, the peaks occur higher on the m/z axis and do not overlap with BSH clusters even at the highest BSH level tested. Three peak envelopes are observed, monomer (+8, +9) and two forms of dimer

(+12 – +14; and +16 – +18). As the BSH level increased, the relative intensity of the dimer peaks decreased; the response was quicker for the less compact, dimeric form (+12 – +14)

After deconvolution, the mass spectra presented in **Figure 5.3.8** provide further insight into the CopAab species present at increasing levels of BSH. Though the dimer species dominate at 1 BSH / protein, their relative intensity declines leading to CuCopAab as the dominant copper-bound species, and apo-CopAab the most intense peak at 25 BSH / protein. The presence of BSH has facilitated higher copper loadings by the dimeric species, with the coordination of 7 and 8 Cu(I) ions. In addition, BSH adducts are observed: $Cu_5(CopAab_2{:}BSH)$ and $Cu_6(CopAab_2{:}BSH)$.

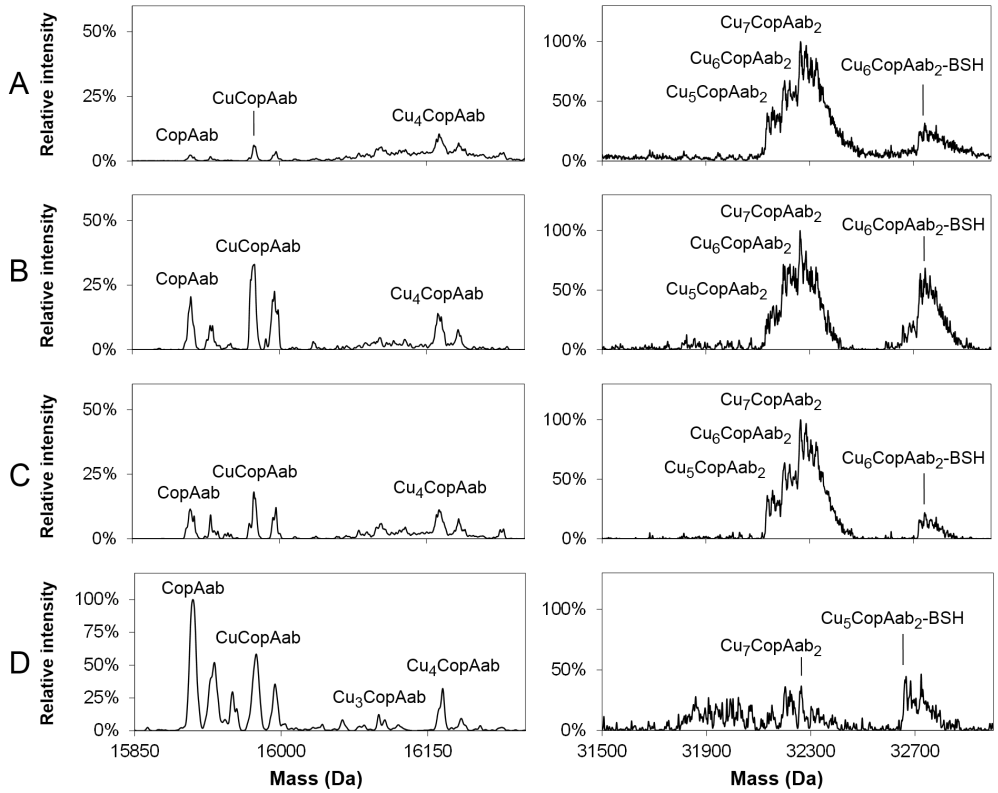

Figure 5.3.8: Deconvoluted mass spectra for 4 Cu/CopAab at varied BSH levels. The deconvoluted mass spectra of 4 Cu / CopAab in the presence of: **A)** 1 BSH / protein, **B)** 5 BSH / protein, **C)** 10 BSH / protein, **D)** 25 BSH / protein.

The relative intensities and masses observed in the mass spectra are presented in **Table 5.3**. As observed in the presence of DTT, the mass of CuCopAab is greater than its predicted mass (here, $\sim$ 2 Da). The observed mass of $Cu_6(CopAab)_2$ is greater than predicted ($\sim$ 2 –3 Da) whereas the masses of $Cu_7(CopAab)_2$ and $Cu_8(CopAab)_2$ are lower ($\sim$ 2 –5 Da). In addition, a substantial mass difference is observed for the adduct species, $Cu_6(CopAab_2$:BSH) ($\sim$ 7 Da). The reason for these large mass discrepancies is not entirely clear, but could arise due to the broadened peak shapes.

Table 5.3: Species observed via ESI-MS for 4 Cu/CopAab at varied BSH levels. Exact masses and relative intensities of species observed in native mass spectra of CopAab prepared at 4.0 Cu / protein in the presence of BSH.

Species	Pred (Da)	1 BSH / CopAab		5 BSH / CopAab		10 BSH / CopAab		25 BSH / CopAab	
CopAab	15909.0	<3%	15909.3	18%	15909.3	15%	15909.1	100%	15909.6
CuCopAab	15972.6	5%	15974.5	33%	15973.4	9%	15973.4	58%	15974.3
Cu_2CopAab	16036.1	0%	–	<3%	–	0%	–	0%	–
Cu_3CopAab	16099.6	0%	–	0%	–	0%	–	12%	16099.8
Cu_4CopAab	16163.2	9%	16163.2	13%	16162.6	10%	16163.1	32%	16165.2
$Cu_4(CopAab)_2$	32072.2	0%	–	0%	–	0%	–	21%	32073.8
$Cu_5(CopAab)_2$	32135.8	42%	32136.7	21%	32134.5	51%	32137.5	0%	–
$Cu_6(CopAab)_2$	32199.3	69%	32203.2	69%	32202.5	72%	32200.6	36%	32201.5
$Cu_7(CopAab)_2$	32268.9	100%	32265.1	100%	32264.2	92%	32265.9	37%	32263.7
$Cu_8(CopAab)_2$	32332.4	85%	32326.3	69%	32325.3	76%	32329.4	0%	–
$Cu_5(CopAab_2$:BSH)	32692.4	0%	–	0%	–	0%	–	41%	32692.8
$Cu_6(CopAab_2$:BSH)	32756.0	36%	32745.3	68%	32745.7	79%	32745.3	23%	32753.0

The relative intensities of species in the mass spectra are presented as bar graphs in **Figure 5.3.9**, by averaging the results from three independent measurements.

Though monomeric species increase in intensity across these spectra, the dimeric peaks persist at all levels of BSH tested. The most intense dimeric form at lower BSH levels is $Cu_7(CopAab)_2$, a species not observed with DTT or in the thiol-free spectrum. A high proportion of $Cu_8(CopAab)_2$ is observed as well.

With increasing BSH levels, CuCopAab becomes the dominant copper-bound species. Instead of steadily increasing in intensity, a slight dip is observed at 10 BSH / protein for CuCopAab; the reason for this is unclear. In addition, accumulation of Cu_2CopAab is not observed, suggesting one of the domains (CopAa or CopAb) does not bind Cu(I) in the presence of BSH.

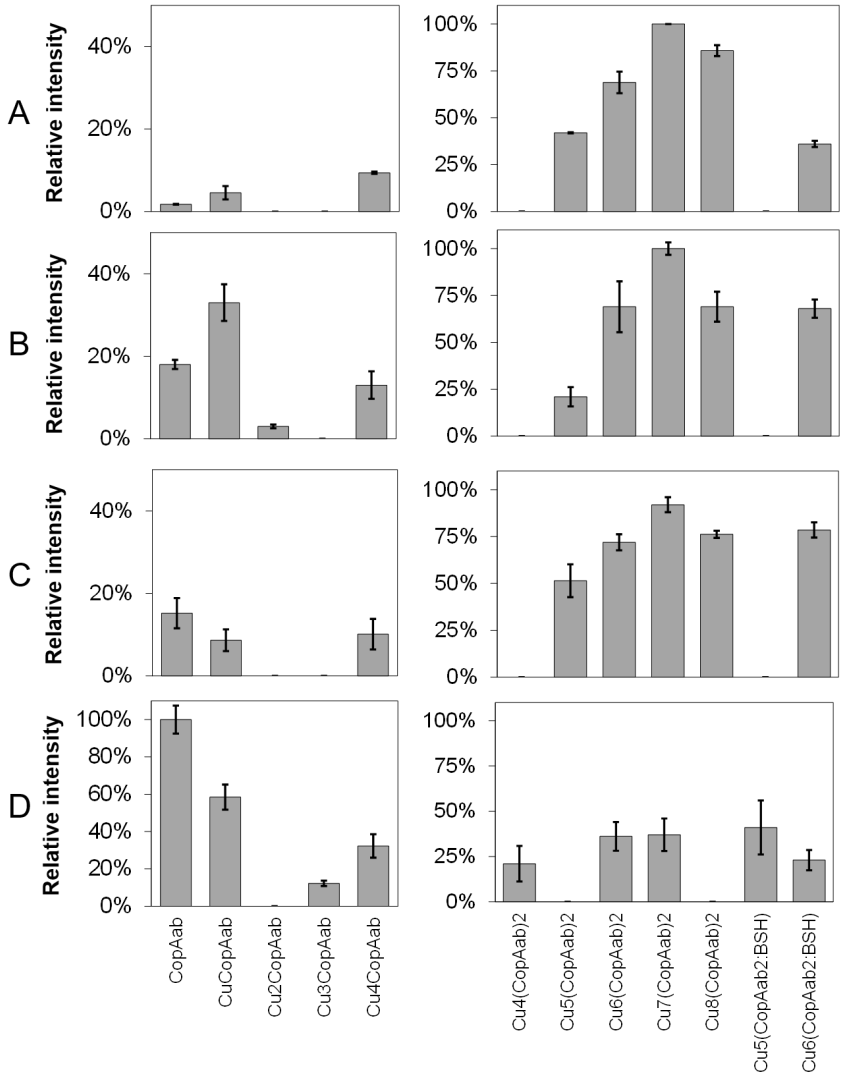

Figure 5.3.9: Species observed via ESI-MS for 4 Cu/CopAab at varied BSH levels. Species distribution in the deconvoluted mass spectra of 4 Cu / CopAab in the presence of: **A)** 1 BSH / protein, **B)** 5 BSH / protein, **C)** 10 BSH / protein, **D)** 25 BSH / protein.

5.4 Results: Cu(I) Binding To A Mixture Of CopAa And CopAb

Previous studies have demonstrated that CopAa exhibits instability in the presence of copper; this effect was mitigated by the presence of CopAb, suggesting it has a stabilising effect on the other domain [84]. To explore these observations, an experiment was carried out to compare the copper-binding behaviour of a mixture of CopAa and CopAb with the two domains in tandem CopAab. Copper was added to an equimolar mixture of CopAa and CopAb (at 1, 2 or 4 per domain), the solution components resolved by size exclusion chromatography (SEC), and the elution fractions analysed for metal (ICP-AES) and protein (LCMS).

The resulting copper distribution between CopAa and CopAb at each copper level is depicted in **Figure 5.4.1**. At 0.5 Cu / domain (**Figure 5.4.1A**), the gel filtration chromatogram (blue trace) reveals two overlapping peaks (12.8 mL and 13.8 mL). The LCMS analysis illustrates that CopAa (green bars) elutes between 12 mL and 15 mL, with a slight dip in relative intensity at 13.25 mL suggesting two different CopAa species are present. CopAb (magenta bars) elutes between 12.5 mL and 15 mL.

The results suggest three species whose peaks overlap considerably: dimeric CopAa (12.8 mL), and a mixture of monomeric CopAa and monomeric CopAb (13.8 mL). The metal analysis illustrates that the samples containing copper were distributed fairly symmetrically around 13.9 mL, suggesting that most of the copper is associated with the monomeric protein species, though it is difficult to say with certainty whether CopAa or CopAb.

At 1.0 Cu / protein (**Figure 5.4.1B**), the SEC trace contains three overlapping peaks

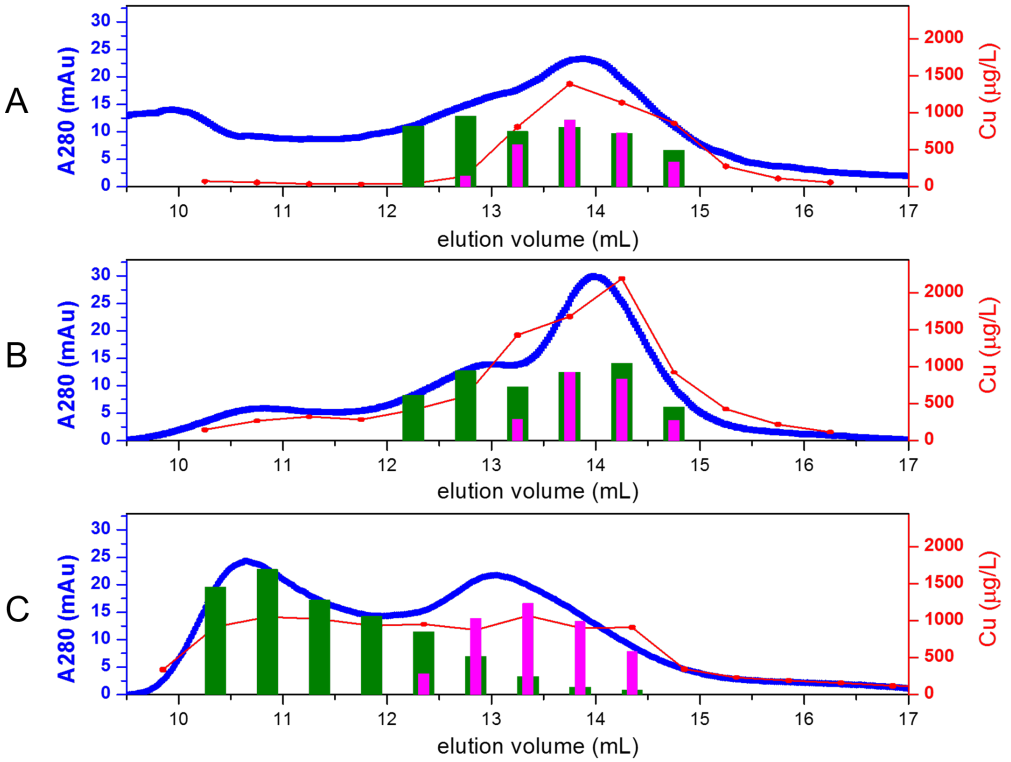

Figure 5.4.1: Cu(I) binding to the individual domains CopAa and CopAb Individual domains CopAa and CopAb were prepared at **A)** 0.5 Cu / protein, **B)** 1 Cu / protein, **C)** 2 Cu / protein. Figures depict the overlaid gel filtration chromatogram (**blue trace**), ICP-AE Cu^{+} analysis (**red trace**), bars represent the relative proportion of individual domains present CopAa (**green**) and CopAb (**magenta**) in each gel filtration fraction as determined by LC-MS analysis

(10.9 mL, 12.8 mL, 14.1 mL). LCMS illustrates CopAa eluting between 12 and 15 mL, again with a dip in relative intensity (13.25 mL) suggesting two different CopAa species overlapped, and CopAb eluting between 13 and 15 mL. The elution volumes coupled with LCMS suggest that present are: dimeric CopAa (12.8 mL), a mix of monomeric CopAb and CopAa species (14.1 mL). The metal analysis indicated that the majority of copper is distributed around 13.9 mL, suggesting it is associated with the monomeric species, though it is not possible to say whether CopAa or CopAb. Despite the presence of Cu(I) and $A_{280\ nm}$ at 10.9 mL, no protein was found via LCMS in the fractions at 10.9 mL; the

reason for this discrepancy is unclear. However, it could suggest that higher order forms are beginning to form / acquire copper at 1 Cu(I) per domain.

At 2.0 Cu / domain (**Figure 5.4.1C**) two overlapping peaks (10.9 and 13.1 mL) are observed in the SEC trace. LCMS illustrates CopAa eluting mostly between 10 and 13 mL suggesting trimeric and/or tetrameric CopAa, low intensity peak between 13 and 14.5 mL a dimeric form of CopAa, and CopAb eluting between 12 and 14.5 mL, suggesting dimeric and possibly monomeric CopAb. These results suggest the presence of tetramer CopAa (10.9 mL), trimer CopAa or an equilibrium between tetramer and monomer (11.2 mL) and dimer CopAb (13.1 mL). Metal analysis indicated that copper levels are relatively evenly distributed across all fractions and so associates with all protein species in this sample. However, peak overlap and difference in absorbance response observed when each protein binds copper [83] [82] makes it very difficult to say exactly which protein binds what amount of copper in this sample.

5.5 Discussion

Previous spectroscopic studies illustrated the complexity of the Cu(I)-binding behaviour of CopAab, with Cu(I)-mediated dimerisation occurring above a level of 1 Cu / protein. However, these methods cannot be used to resolve mixed species in the case of, for example, overlapping absorbance spectra or small mass differences. Here, ESI-MS was employed to investigate the species which form at progressively increasing Cu(I) levels. The range of copper-to-protein ratios, between 0.5 and 4.0 per protein, were chosen both to explore the mixture of species at lower Cu(I) levels and examine the dimeric species present at higher Cu(I) levels, as previously fluorescence quenching was observed beyond 2 per protein, suggesting copper binding occurs beyond $Cu_4(CopAab)_2$ [163].

The charge state envelopes which appear in the mass spectra prior to deconvolution illustrated the types of CopAab species present as Cu(I) levels are increased. Upon addition of Cu(I), the monomer envelope did not shift or take on additional charge states, suggesting no major conformational changes between apo- and Cu-bound CopAab.

At 0.5 and 1 Cu / CopAab, the predominant copper-bound species is CuCopAab, along with a sizable proportion of Cu_2CopAab, with only a minor amount of dimer species present. At 2.0 Cu / CopAab, the major copper-bound species is Cu_2CopAab, with a substantial proportion of CuCopAab present, along with copper-bound CopAab dimers, the most intense of which coordinates six Cu(I) ions. At 4.0 Cu / CopAab, the predominant species is $Cu_6(CopAab)_2$, with 20% relative intensity or less associated with the other copper-bound dimer species, and a decreased relative intensity of copper-bound CopAab monomers.

The two dimer envelopes suggest that two distinct dimeric CopAab species are present, each coordinating six Cu(I) ions. An arrangement to fulfill this requirement would be two monomers with one intra-domain interface coordinating four Cu(I) ions, and each of the remaining domains coordinating a single Cu(I) ion (**Figure 5.5.1**). A solvent-shielded tetranuclear cluster would agree with previously observed fluorescence quenching above 2 Cu / CopAab [163]. Because the dimeric structure with the greater number of charges acquired exactly double that of the CopAab monomer, this less compact version should have approximately the same surface area available as two CopAab monomers, which could be achieved by an asymmetric arrangement where the single copper domains are not interacting. The more compact dimer species with fewer charges could then be achieved if two intra-domain interactions formed coordinating multiple ions, shielding a portion of the dimer from protonation.

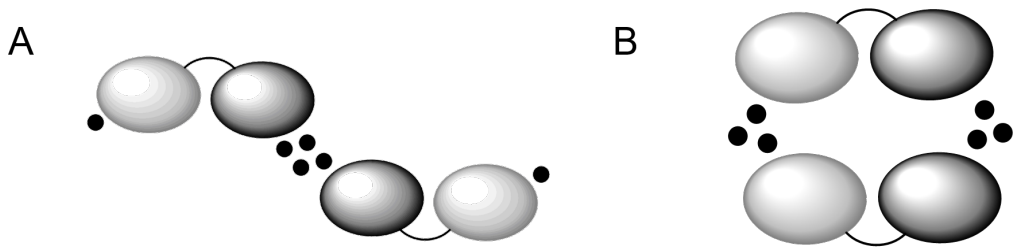

Figure 5.5.1: Possible structural representations of $Cu_6(CopAab)_2$. Structural arrangements $Cu_6(CopAab)_2$ where two CopAab monomers coordinate six Cu(I) ions with **A)** the same surface area as two monomers, generating an ESI-MS dimer envelope exactly double the number of charges **B)** less surface area than two monomers, generating an ESI-MS dimer envelope with fewer charges .

It was observed previously via NMR that the arrangement of the two domains is not affected when Cu(I) is transferred to CopAab from CopZ, and that copper transfer occurs simultaneously to Aa and Ab domain with no observable preference [80]. This behaviour can be corroborated by examining the copper binding behaviour of the monomeric CopAab. Upon addition of 1.0 and 0.5 Cu / CopAab, both one and two copper-bound monomers are observed. Though it is not possible to say for certain which domains have bound Cu(I), if binding of copper to a second site were to require saturation of the first copper-binding site, Cu_2CopAab would not be observed until above a level of 1 Cu / CopAab. Furthermore at 2.0 Cu / CopAab, Cu_2CopAab is the major copper-bound species. The relative intensity of Cu_2CopAab was observed to be quite variable, except at 2 Cu / CopAab, as dimers are beginning to form, where its relative intensity is 100% with small error bars. This perhaps suggests this species is an intermediate in cooperative formation of higher order dimeric CopAab species.

The lack of accumulation of dimer species coordinating fewer than six coppers suggests cooperative formation of $Cu_6(CopAab)_2$ upon increasing of copper levels. Though it cannot be ruled out that these species do not survive ionisation. For example, at higher copper-loadings, a small amount of Cu_3CopAab is observed. This species is not expected to form in solution and thus may be an artefact of breakdown of copper-bound dimer species. However, interpreting the role of dimerisation should be carried out with caution as, *in vivo*, these cytoplasmic MBDs are tethered to a membrane spanning ATPase. Each MBD has been shown to play different roles in copper export, where one MBD interacts with the A-domain to prevent phosphorylation in the absence of copper and is

released upon copper binding when catalytic activity is utilised for copper export. Performing different physiological roles would be reason to expect each domain to exhibit different copper-binding behaviour.

In order to compare the behaviour of tandem domains (CopAab) with individual domains (CopAa and CopAb) for binding Cu(I), a mixture of the individual domains was treated with 0.5, 1.0 or 2.0 Cu / domain. In order to determine the proportion of each domain with Cu(I) bound, the mixtures were separated by gel filtration, and each fraction subjected to ESI-MS and metal analysis. The solution structure of the individual domains demonstrated that they have nearly identical folds and secondary structural elements when in tandem or in isolation [164]. Though the fairly broad elution peaks from the gel filtration chromatogram illustrate the trouble arising in a mixture of two proteins of comparable mass (7692 and 8201 Da), both of which can form multimers even in the absence of copper, the LCMS helped to resolve the species present in each elution fraction.

At 0.5 Cu / domain (1 Cu / protein), the protein was mostly monomeric CopAa and CopAb and the copper was associated only with these fractions. This is supported by the ESI-MS experiment (**Figure 5.3.3B**) where the major copper-bound species were monomeric and very little dimer was present. Because tetrameric CopAa, previously observed in the presence of Cu(I), was not observed, this may suggests it does not preferentially form in the mixture of individual domains at low Cu(I) levels. It is not possible to tell from the SEC experiment whether Cu(I) has a higher preference for CopAa or CopAb.

At 1.0 Cu / domain (2 Cu / protein), a similar trend is observed where a small amount of dimeric CopAa was observed with the majority of protein monomeric. Most of the copper

is associated with the monomer though a small amount of copper is associated with the CopAa dimer. This does reflect the ESI-MS results at 2.0 Cu / CopAab, where the majority of protein is monomeric with a small amount of dimeric copper-bound species present.

At 2.0 Cu / domain (4 Cu / protein), the domains were resolved as the majority of CopAa formed a higher order species, and CopAb remained monomeric, or possibly a monomer/dimer mixture. The copper appeared to be relatively evenly spread amongst the protein containing fractions, suggesting the copper-bound species was a copper-bound CopAa tetramer, and CuCopAb. The ESI-MS results at 4.0 Cu / CopAab suggest the major copper-bound species to be $Cu_6(CopAab)_2$, which could arise from a tetra-copper cluster at the interface of two domains, with each of the remaining domains coordinating a single copper. Though it is difficult to compare directly the behaviour of the separated domains with the two-domain construct, this arrangement would support the mixture of individual domains forming a copper-bound dimer and monomer.

In order to examine the copper-binding behaviour of CopAab in the presence of LMWT, ESI-MS was employed using samples of CopAab at 4 Cu(I) per protein, in the presence of progressively increasing levels of DTT. Compared to the thiol-free spectrum, the mass spectra (before and after deconvolution) illustrated changes in speciation. Upon the addition of 1 DTT per protein, a substantial reduction in intensity of the peaks in the dimer envelopes is immediately seen, with entire removal of the dimer envelope at subsequent DTT loadings. The monomer envelopes acquire additional low-intensity adduct peaks in the presence of DTT.

Upon deconvolution, the peaks' masses demonstrate DTT adducts and dimer break-

down products. Seen at relative intensities of 40% and below are complexes formed between Cu-bound CopAab monomers and DTT. Due to the number of coppers bound (between 4 and 6), it can be inferred that DTT thiols serve as additional Cu(I) ligands in lieu of a second CopAab. DTT was not observed to form adducts or complexes with CopZ species (Chapter 4), though it is possible the increased proportion of CuCopZ with increasing DTT points to it acting as an additional Cu(I) ligand. Here, however a substantial proportion of complex with one and two DTT molecules were observed. The complexes with two DTT molecules bind a higher number of coppers, 5 and 6, rather than 4 or 5 with one DTT molecule. The presence of the species Cu_4CopAab would not be expected and is quite possiblly a breakdown artefact associated with the formation of Cu_4CopAab:DTT species. At each level of DTT / protein tested, the major copper-bound species remain CuCopAab and Cu_2CopAab, with somewhat proportionate relative intensities at each DTT loading. This suggests the presence of DTT drives the most prevalent copper-bound species to be monomeric with a fairly equal propensity for one or two copper-binding sites to be occupied, and additional coppers coordinated with DTT thiols serving as additional ligands.

When samples of CopAab at 4 Cu(I) per protein were in the presence of low levels of BSH, the mass spectra prior to deconvolution revealed a mixture of monomer and dimer species. Upon increasing the BSH level, both dimer envelopes decreased progressively, but the less compact structure consistently had a greater peak intensity than that of the more compact structure. This implies the presence of BSH affected these two dimer species differently, and may point to an increased stability of the less compact structure in the presence of BSH. Decreasing relative intensity of the dimer envelope led to

the monomer CopAab becoming the predominant species, a change which was also observed in the deconvoluted mass spectra. Unlike spectra recorded in the presence of DTT, no Cu_2CopAab was observed, making CuCopAab the major copper-bound species at higher copper loadings. Similarly to spectra recorded in the presence of DTT, small amounts of Cu_4CopAab were observed, which may be an artefact from the breakdown of dimeric BSH adduct species. In the presence of BSH the CopAab dimer accommodated additional Cu(I), with the dimer containing between 5 to 7 Cu(I) ions bound, rather than between 4 to 6 Cu(I) in the absence of BSH. However, no bacillithiolated CopAab monomer was observed, and potentially the only BSH-coordinated CopAab species observed was Cu_5(CopAab)$_2$:BSH (substantial mass difference for Cu_6(CopAab)$_2$:BSH makes this assignment tentative). This may suggest that, unlike that observed for cytoplasmic chaperone CopZ, bacillithiolation and LMWT Cu(I) coordination do not play a physiological role in the behaviour of CopA MBDs.

Chapter 6

Studies Of Cu(I) Transfer From CopZ To CopAab

6.1 Introduction

In order to prevent potential deleterious effects associated with Cu(I) ions, mechanisms of copper management have arisen which chelate and move copper ions safely between trafficking proteins. The Cu(I) P_{1B}-ATPases contain multiple N-terminal cytosolic metal-binding domains (MBDs), 1 – 2 in bacterial proteins and up to six in human ATP7A/B [47]. The function of these domains in copper transfer is not entirely clear, as they have been demonstrated to play roles both in copper transfer and regulation of transport activity [161] [166]. In the crystal structure of *Legionella pneumophila* CopA, a copper chaperone "docking station" was described [46], where copper could be transferred directly to the entrance of the transmembrane channel without involvement of the MBDs, in support of their function as a copper sensor regulator. In yeast, it has been demonstrated that, in the absence of copper, the MBDs of Ccc2 play a regulatory role by serving to inhibit the ATPase catalytic cycle. However, chaperone Atx1 was unable to transfer copper to a Ccc2 variant lacking its MBDs, supporting their necessity in copper transfer [159]. Similar results were found for *Thermotoga maritima* CopA, which was unable to undergo catalytic activation when the MBDs were deleted [167].

Atx1-like metallochaperones exhibit extremely high affinities for Cu(I) ($K_D \sim 10^{17}$M

[168] [144] [169]) in order to adeptly acquire cytoplasmic copper. The multiple types of coordination exhibited by the solvent-exposed cysteine-rich copper binding sites in these proteins may be related to the copper transfer mechanism to their partner ATPase MBDs. For monomeric human Atox1, two interconverting Cu(I) coordination geometries were found [170] a more solvent-shielded digonal arrangement, and a solvent-exposed trigonal arrangement. Two orientations of Cu(I)-binding cysteines also were observed in yeast Atx1 in its apo- and copper-bound states [41]. Tricoordination of Cu(I) has been observed previously for yeast [34] and *B. subtilis* [40], which may have emerged as an efficient way to "grab" Cu(I) at an outward orientation to then promote its transfer to target proteins [170]. As the target copper-acquiring sites are typically less solvent-exposed, copper transfer is facilitated by complementary electrostatic interactions between the proteins [171].

Because Cu(I) does not exist freely in the cytoplasm [34], the mechanism of copper transfer does not comprise release of Cu(I) by chaperones, followed by chelation by receptor proteins and/or enzymes. Rather, it has been demonstrated *in vitro* that copper transfer entails formation of a Cu-mediated heterocomplex to facilitate delivery of copper from the chaperone to the ATPase MBDs, and then breakdown of the complex into protein products [67] [57] [172]. Copper transfer within the complex is thought to involve rapid interconversion of two different three-coordinate, copper-sulfur intermediates [34] [173] [174]. Flexibility in linkers near the copper binding sites has been demonstrated to facilitate rapid copper transfer [171].

Copper exchange between the heteroprotein complex is not dictated by any substantial thermodynamic gradient for copper transfer [175] [168]. Previous *in vitro* work has

illustrated that, upon copper transfer, copper ends up almost equivalently distributed between CopZ and CopAab though, in some cases, a slightly larger amount was transferred from CopZ to CopAab [163] [176]. Copper transfer between CopZ and CopAab has been characterised by luminescence experiments [163] but, as a luminescent signal only arises when CopAab reaches a level greater than 1 Cu / protein, this method could not be used for lower copper loadings. Data characterising the thermodynamics of copper transfer between His_6CopZ and CopAab was obtained at low copper loadings, where one protein was copper-free and the other was prepared at 0.5 Cu / protein. Here, a Ni^{2+} IMAC affinity column was used to bind His_6CopZ and CopAab (apo- or 0.5 Cu / protein depending upon the His_6CopZ sample) was applied to the column; after separate elution of each protein, copper content was measured by ICP-AES. Regardless of whether CopZ or CopAab was loaded with 0.5 Cu / protein, it was found that copper was equally distributed between the two, suggesting a similar initial affinty for Cu(I) [177].

Because there is little thermodynamic drive for copper transfer, and transfer is reversible, more insight into the kinetic and structural aspects of copper transfer will be instrumental in defining the copper transfer mechanism between CopZ and CopAab, and more generally for establishing the principles of transfer for chaperone target protein interactions.

6.2 Materials And Methods

6.2.1 Preparation of Apo- and Cu-loaded CopZ and CopAab Samples

CopZ and CopAab were prepared as described in Sections 4.2 and 5.2, respectively. Mass spectrometry samples were prepared by first adding 15 mM DTT (Formedium) and removing reductant by passage down a G25 Sephadex column (PD10, GE Healthcare) in an anaerobic glovebox (Faircrest Engineering, O_2 concentration $<$ 2 ppm) using 20 mM ammonium acetate, pH 7.4 (Sigma) as the elution buffer. Protein concentrations were calculated using an extinction coefficient, $\varepsilon_{276\,nm}$, of 1450 M^{-1} cm^{-1} for CopZ [89] and 5800 M^{-1} cm^{-1} for CopAab [147]. UV-visible absorbance spectra were recorded on a Jasco V-550 spectrophotometer. To prepare Cu(I)-bound protein samples, a deoxygenated solution of Cu(I)Cl prepared in 100 mM HCl and 1 M NaCl was added to anaerobic, reduced protein using a microsyringe (Hamilton) in an anaerobic glovebox. Unbound Cu(I) was removed by passage of the sample down a G25 Sephadex column (PD10, GE Healthcare) equilibrated with working buffer. For solution-phase experiments, buffer was 100 mM MOPS, 100 mM NaCl, pH 7.5. For ESI-MS experiments, buffer was 20 mM ammonium acetate, pH 7.4 and the protein sample was diluted with 20 mM ammonium acetate to a working sample concentration of 15 μM.

6.2.2 Dialysis Assay Of CopZ Cu(I) off-rate

Cu-loaded and apo-proteins were prepared in an anaerobic glovebox as described previously (see Chapter 2) to generate 0.5 Cu/CopZ and apo-His_6CopZ each in 100 mM MOPS,

100 mM NaCl, pH 7.5, at a final concentration of 60 μM. Then 5 mL of each sample was placed into separate dialysis cassettes submerged in same buffer. In order to maximise diffusion within the beaker, gentle stirring was applied. UV-vis spectra were acquired at several time points over the course of 48 hours. At this point, 2.5 mL of each protein sample was mixed together and (after one hour incubation) applied to a 5 mL Ni^{2+} IMAC column equilibrated with 100 mM MOPS, 100 mM NaCl, 20 mM imidazole, pH 7.5. The column was washed with 3 $\times$ 5 mL fractions of binding buffer to elute CopZ and then 3 $\times$ 5 mL of elution buffer (binding buffer + 500 mM imidazole) to elute His_6CopZ. Protein-containing fractions (identified by SDS-PAGE) were pooled and buffer exchanged using a 3 kDa MWCO spin concentrator (Sartorius), generating 2 $\times$ 5 mL samples in $<$1 mM imidazole, 100 mM MOPS, 100 mM NaCl, pH 7.5, each 30 μM in protein.

6.2.3 Rapid Reaction Kinetics Of Cu(I) Transfer Between CopZ And CopAab

CopZ, His_6CopZ and CopAab were prepared as described in Section 2.2. Copper transfer experiments were carried out in 100 mM MOPS, 100 mM NaCl, pH 7.5. Prior to the addition of Cu(I), in an anaerobic glovebox (Faircrest Engineering, O_2 concentration $<$ 2 ppm), protein samples were treated with 15 mM DTT and excess reductant was removed via buffer exchange using a G25 Sephadex column (PD10, GE Healthcare). Additions of Cu(I) were made anaerobically using a solution of Cu(I)Cl in 1 M NaCl and 100 mM HCl. Reaction kinetics were monitored at 25 °C using an Applied Photophysics Bio-Sequential DX.17MV stopped-flow instrument. For each experiment, 2000 data points were collected over 0.5 seconds on a logarithmic time base, and three shots were averaged for each experiment.

Copper transfer reactions were monitored in both directions (apo-His_6CopZ + Cu(CopAab) or Cu(His_6CopZ)$_2$ + apo-CopAab) with varied concentration of one protein (20, 40, or 60 μM) mixed with its partner protein at a fixed concentration (40 μM). Copper transfer was monitored by detecting the change in $\Delta\varepsilon$ at 265 nm in units of M^{-1} cm^{-1}; Absorbance kinetic data were fitted using Origin software (OriginLab).

6.2.4 Native Electrospray Ionisation Mass Spectrometry of CopAab and CopZ Mixtures

Mass spectra were acquired using a Bruker micrOTOF-QIII electrospray ionisation (ESI) time-of-flight (TOF) mass spectrometer (Bruker Daltonics, Coventry, UK), in positive ion mode. The ESI-TOF was calibrated in the m/z range 300 – 2200 using ESI-L Low Concentration Tuning Mix (Agilent Technologies, San Diego, CA). Native protein samples were introduced to the ESI source via a syringe pump (Cole-Parmer) at 5 μL/min, and data acquired for 2 min, with ions scanned between 500 – 3000 m/z. MS acquisition was controlled using Bruker oTOF Control software, with parameters as follows: dry gas flow 5 L/min, nebuliser gas pressure 0.8 Bar, dry gas 180 °C, capillary voltage 4500 V, offset 500 V, isCID energy 0 eV, quadrupole RF set at 2000 Vpp (25%) and 3200 Vpp (75%). Processing and analysis of MS experimental data was carried out using Compass DataAnalysis version 4.1 (Bruker Daltonik, Bremen, Germany). The spectra were deconvoluted using the ESI Compass version 1.3 Maximum Entropy deconvolution algorithm over a mass range of 7200 – 35000 Da. Overlapping peak envelopes were deconvoluted manually. Exact masses were determined from peak centroids.

6.3 Results: Kinetics of Copper Transfer Between CopZ and CopAab

6.3.1 Kinetic Drive For Cu(I) Transfer Inhibited Without Protein Interaction

CopZ binds Cu(I) very tightly, as denoted by a high affinity constant, characteristic of a high on-rate constant and/or a low off-rate constant. Monitoring the off-rate separately requires an experimental design which allows dissociation of Cu(I) from CopZ to be measured in competition with the reassociation reaction. To achieve this, CopZ, prepared at 0.5 Cu / protein, and apo-His_6CopZ were placed into separate dialysis cassettes both submerged in buffer. This separation of the proteins allowed copper transfer to be monitored through absorbance changes occurring in either sample, contingent upon copper being released by CopZ into bulk solution first, and subsequently bound by His_6CopZ. A trial run of this experiment indicated that scattering due to protein precipitation began to occur on the third day (data not shown) and therefore absorbance spectra were recorded at several time points over 2760 minutes, or 46 hours. The overlaid spectra recorded for each protein are presented in **Figure 6.3.1**, and the values of absorbance intensity at 265 nm are plotted against time in **Figure 6.3.2**.

Monitoring the holo-CopZ sample revealed that during the first six hours, the four spectra acquired overlaid exactly and the A_{265nm} changed by -0.003, within the sensitivity limits of the instrument. After 30.5 hours, the A_{265nm} decreased by a further 0.028 AU, with slight changes in spectral shape. After 46 hours, the A_{265nm} of the holo sample had decreased

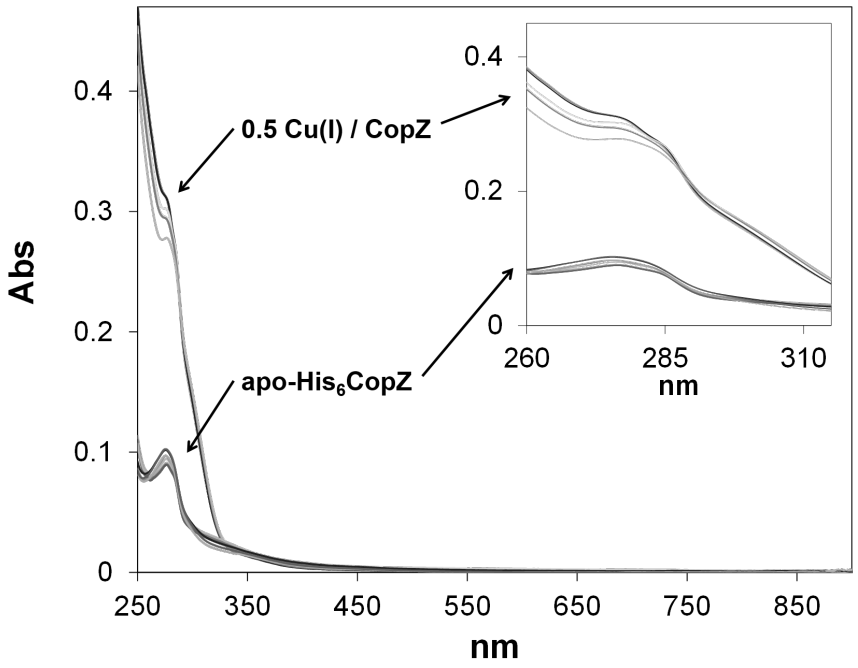

Figure 6.3.1: Off-rate of Cu(I) from CopZ monitored by UV-visible absorbance. Overlaid UV-visible absorbance spectra acquired of of 0.5 Cu / CopZ and apo-His_6CopZ over 46 hours. The similarity of spectra throughout the experiment illustrates that when the proteins are separated in dialysis cassettes and, therefore cannot interact, little if any copper transfer is observed.

by a total of -0.056, a loss of 16% of the signal intensity at 265 nm from the first spectrum recorded. The apo-His_6CopZ sample experienced very slight fluctuations in A_{265nm} during the first 6 hours of the experiment, when the absorbance intensity at 265 nm varied within 4% of its intial intensity. These small changes were not accompanied by a decrease in absorbance of the holo-CopZ sample. After 30.5 hours, the spectra showed slight shape changes but the A_{265nm} fluctuated by no more than 0.007 AU, 9% of the initial signal intensity.

Though these changes could have indicated transfer of a small amount of copper, at the end of the experiment, the samples were analysed for metal content via ICP-AES. The

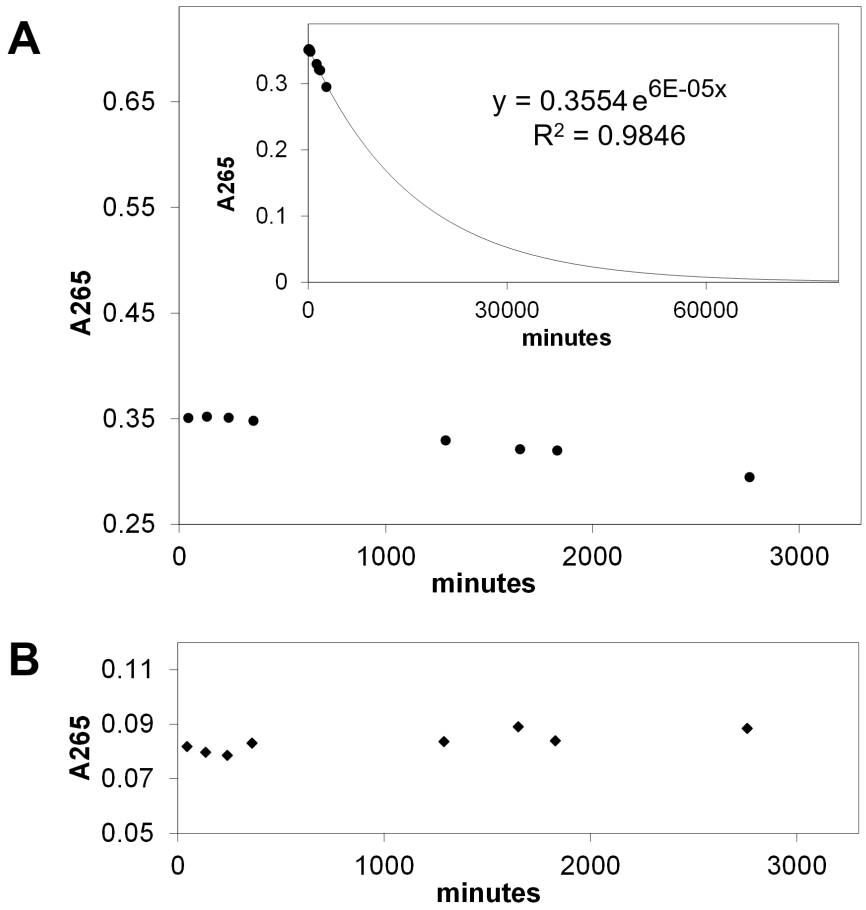

Figure 6.3.2: Off-rate (upper limit) of Cu(I) from CopZ. Change in absorbance intensity at 265 nm plotted as a function of time of: **A)** 0.5 Cu / CopZ and **B)** apo-His_6CopZ. When the proteins were separated in dialysis cassettes, little to no copper transfer was observed. The $A_{265\ nm}$ of 0.5 Cu / CopZ was fitted to a single exponential consistent with a first order dissociation process. This establishes an estimated upper limit of off-rate of Cu(I) from CopZ.

results revealed that the CopZ contained Cu(I), whereas no copper was found associated with the His_6CopZ sample, nor the buffer in the beaker. Thus absorbance changes are most likely not due to copper transfer and, are probably attributable to instrumental drift and/or loss of protein signal. If it were assumed that absorbance changes were due to holo-CopZ copper transfer, the data could represent the initial part of an exponential decay due to Cu(I) transfer (**Figure 6.3.2**). This allows the estimation of an upper limit of the off-rate to be established, $\sim 6 \times 10^{-5}\ s^{-1}$.

6.3.2 Kinetics Of Cu(I) Transfer Between CopZ And CopAab Detected By Stopped Flow Absorbance

The binding of Cu(I) to both CopZ and CopAab gives rise to high-energy absorbance bands, assigned to cysteine-to-copper ligand to metal charge transfer transitions (LMCT) [150]. **Figure 6.3.3** displays overlaid plots of the change in absorbance intensity during Cu(I) titration for each protein, as characterised by extinction coefficients at 265 nm. Compared to CopZ, the response of CopAab is shallower between 0 and 0.75 Cu(I) per protein, which enabled monitoring the direction of Cu(I) transfer between CopZ and CopAab at low Cu(I) levels.

Stopped flow absorbance was used to monitor absorbance changes at 265 nm which occurred upon mixing 0.5 Cu / CopZ with apo-CopAab and the reverse reaction, apo-CopZ mixed with 0.5 Cu / CopAab, see **Figure 6.3.4**. Due to the relative absorbance intensities of CopZ and CopAab in the range of copper loading below 0.5 Cu / protein, it is expected that copper transfer should be indicated clearly by the direction of change in ΔA_{265} absorbance. Copper transfer to CopZ from CopAab resulted in an increased absorbance of approximately 0.007 AU (**Figure 6.3.4A**). Based upon the relative absorbance responses of CopZ and CopAab, this increase in absorbance represents copper transfer from CopAab to CopZ. Conversely, the reverse reaction (0.5 Cu / CopZ and apo-CopAab, **Figure 6.3.4B**) results in a decrease in absorbance of approximately 0.005 AU, indicating that copper is being transferred from CopZ to CopAab.

Approximately equal magnitudes of ΔA_{265} were in agreement with reversible copper

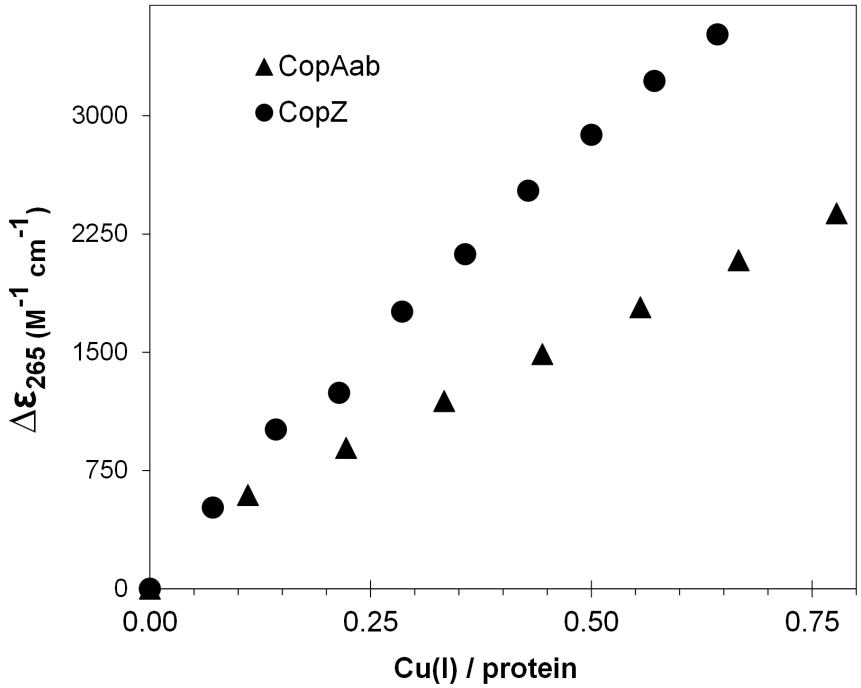

Figure 6.3.3: Divergent A_{265nm} responses during copper titration of CopAab and CopZ. Plot of absorbance intensity at 265 nm against Cu / protein ratio during titration of CopZ (40 μM) and CopAab (40 μM) with Cu(I). Overlaid plots depict the distinct absorbance intensities the proteins ellicit at each Cu(I) loading. These plots enable the prediction of the direction of absorbance change when apo- and Cu-loaded samples are mixed together.

transfer previously demonstrated, which also resulted in equal distribution between the two proteins [163]. In addition, this reaction, in both directions, is completed very quickly, within 0.02 seconds. The data were fitted with a single exponential function, and the rate constants determined; for copper transfer from CopAab to CopZ, k = 208 $\pm$ 2.6 s^{-1}, from CopZ to CopAab, k = 300 $\pm$ 3.8 s^{-1}.

Identical experiments were carried out using His_6CopZ to investigate whether the direction and rate of copper transfer is affected by the addition of the His tag, see **Figure 6.3.5**. Mixing of 0.5 Cu / CopAab with apo-His_6CopZ resulted in an absorbance increase

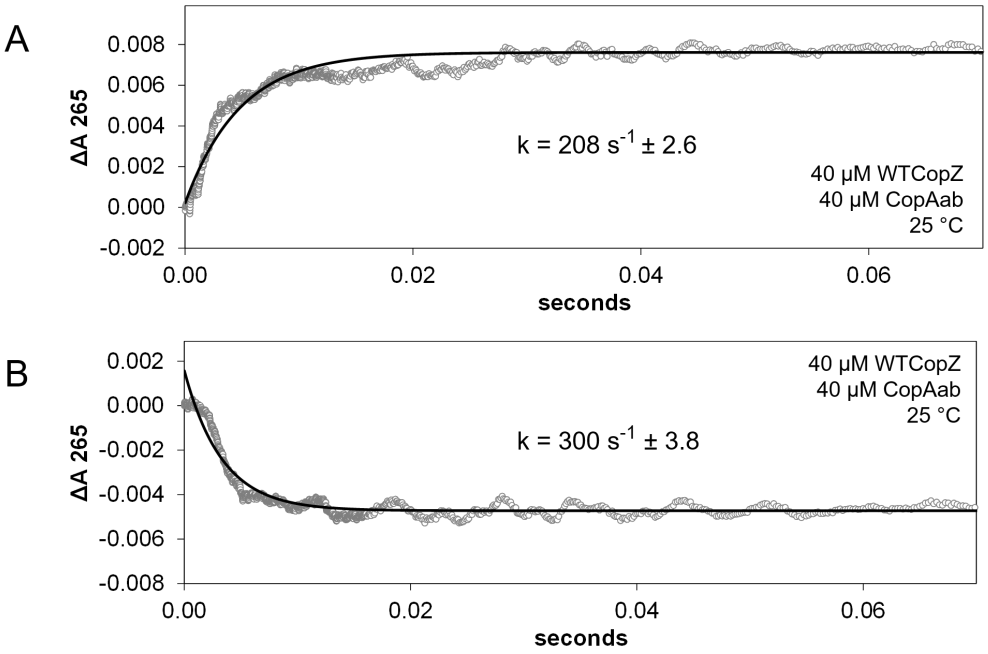

Figure 6.3.4: Kinetics of Cu(I) transfer between CopZ and CopAab. After rapid mixing at 25 °C of CopZ and apo-CopAab, the change in absorbance intensity at 265 nm was recorded and plotted against time. The samples mixed together contained: **A)** apo-CopZ (40 μM) and 0.5 Cu / CopAab (40 μM), and **B)** 0.5 Cu / CopZ (40 μM) and apo-CopAab (40 μM). The data were fit to a single exponential function from which the rate constant was derived, and is labelled on each plot.

of approximately 0.007 AU, in agreement with copper transfer from CopAab to His_6CopZ. Mixing of 0.5 Cu / His_6CopZ with apo-CopAab resulted in a decrease in absorbance of approximately 0.007 AU consistent with copper transfer in the opposite direction, from CopZ to CopAab. The magnitude of these changes is small, but a single exponential function fitted the data well and, again, the reactions were complete within 0.02 sec. The rate constant for copper transfer from CopAab to His_6CopZ was 258 $\pm$ 2.6 s^{-1}; from His_6CopZ to CopAab was 247 $\pm$ 2.2 s^{-1}.

The results indicate copper transfer between CopZ and CopAab at this copper load-

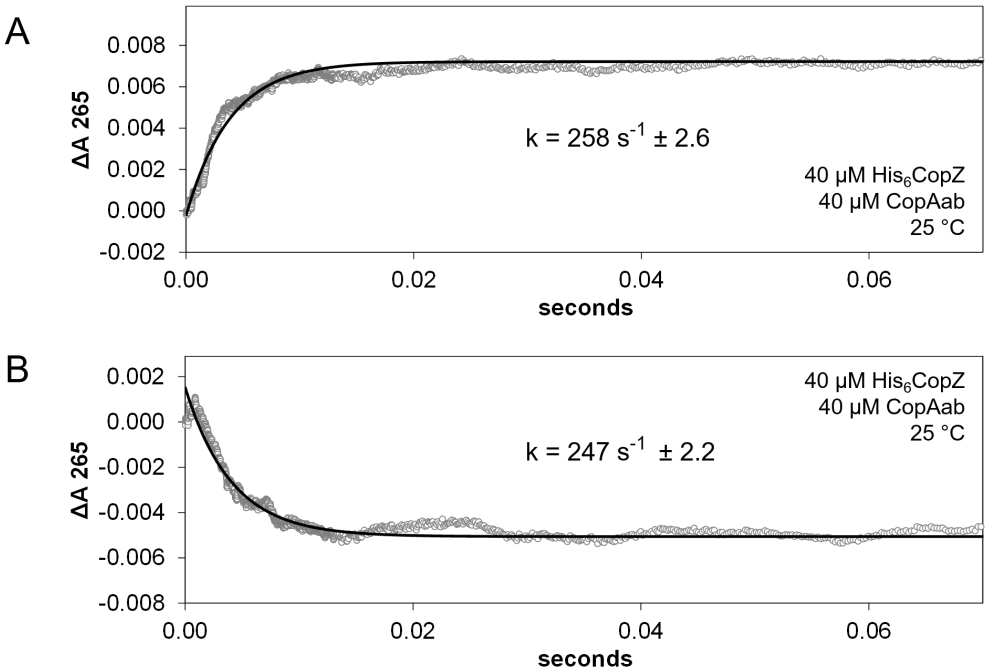

Figure 6.3.5: Kinetics of Cu(I) transfer between His_6CopZ and CopAab. After rapid mixing at 25 °C of His_6CopZ and apo-CopAab, the change in absorbance intensity at 265 nm was recorded and plotted against time. The samples mixed together contained: **A)** apo-His_6CopZ (40 μM) and 0.5 Cu / CopAab (40 μM), and **B)** 0.5 Cu / His_6CopZ (40 μM) and apo-CopAab (40 μM). The data were fitted to a single exponential function from which the rate constant was derived, and is labelled on each plot.

ing is reversible and extremely rapid. Though the transfer from CopAab to CopZ (**Figure 6.3.4B**) was slightly faster, nevertheless these results are in good agreement and it was decided to use the His_6CopZ to probe further the kinetics of copper transfer between these two proteins.

Kinetics of Cu(I) transfer at varied protein concentration

It is generally accepted that copper transfer between CopZ and CopAab proceeds by way of two steps: formation of a heteroprotein complex, followed by dissociation of the complex [178]. Were complex formation the rate-limiting step, it would be expected that the rate constant could be varied by changing the concentration of one of the reactants. Therefore, the dependence of the rate constant upon protein concentration was tested by carrying out the same reactions, at 25 °C, and varying either the concentration of His_6CopZ or CopAab (20, 40 or 60 μM) while holding the concentration of its partner protein constant (40 μM).

For the reaction 0.5 Cu / His_6CopZ + apo-CopAab, **Figure 6.3.6** presents the resultant plots when the protein concentrations were varied. Here, each of the curves depicts a decrease in absorbance at each concentration of His_6CopZ, as expected for copper transfer from His_6CopZ to CopAab.

A single exponential decay function was used to fit the data, resulting in the following constants for each concentration of CopZ: 280 $\pm$ 5.1 s^{-1} for 20 μM His_6CopZ, 263 $\pm$ 2.2 s^{-1} for 60 μM His_6CopZ. When the concentration of CopAab was varied, again, the resulting rate constants: 278 $\pm$ 3.5 s^{-1} for 20 μM CopAab, and 270 $\pm$ 2.8 s^{-1} for 60 μM CopAab. These values compare reasonably well with the rate constant (247 $\pm$ 2.2 s^{-1}) calculated for both His_6CopZ and CopAab at 40 μM (see **Fig 6.3.5**).

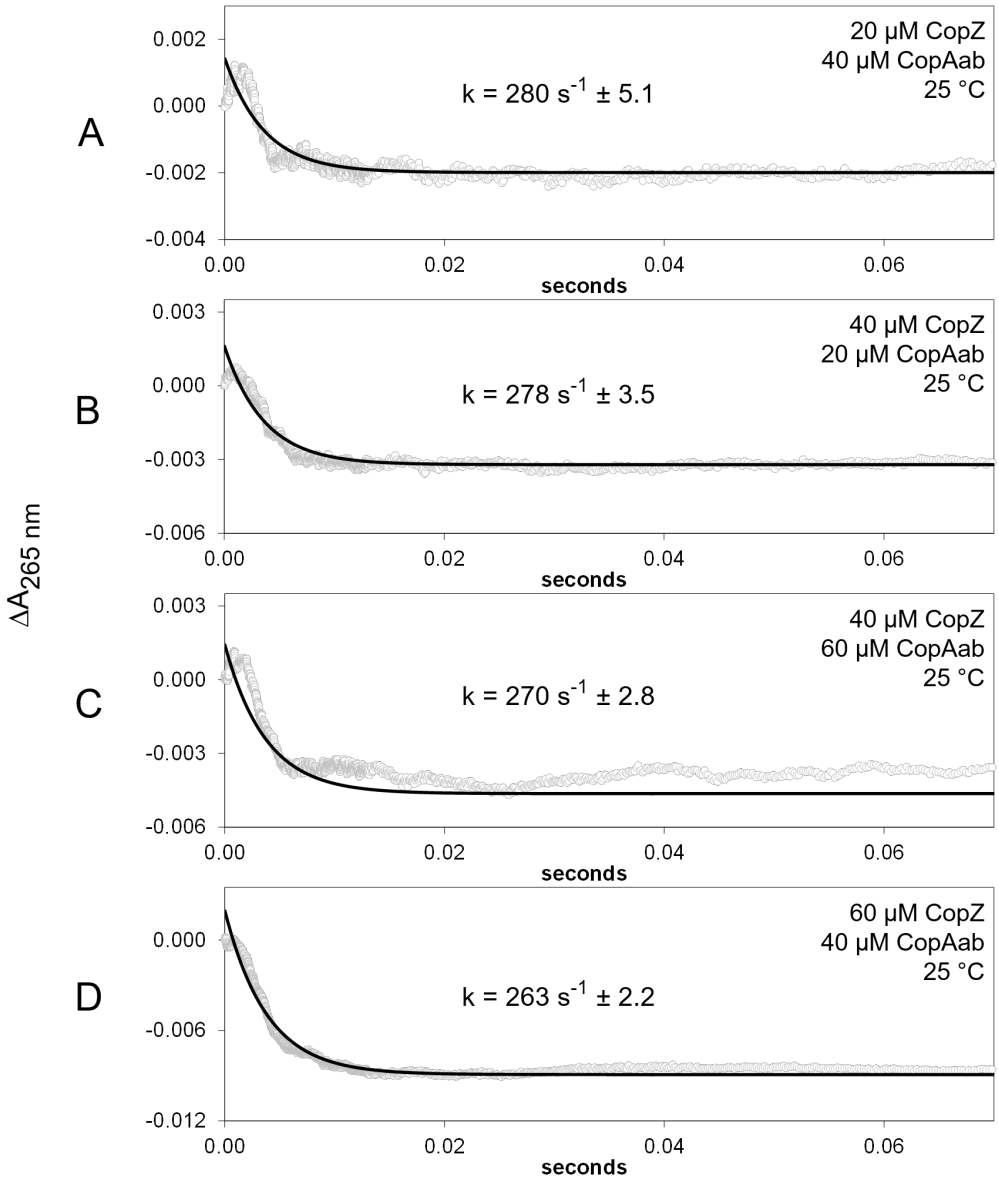

Figure 6.3.6: Kinetics of Cu(I) transfer of 0.5 Cu / His_6CopZ at varied concentrations mixed with apo-CopAab, 25 °C. Change in absorbance intensity at 265 nm plotted against time after rapid mixing of apo-CopAab at 40 μM mixed with: A) 60 μM 0.5 Cu / His_6CopZ B) 40 μM 0.5 Cu / His_6CopZ C) 20 μM 0.5 Cu / His_6CopZ. The data were fit to single exponential function from which the rate constant was derived, and is labelled on each plot. These plots illustrate that the rate constant is not dependent upon concentration of His_6CopZ.

Results from the reverse reaction, apo-His_6CopZ + 0.5 Cu / CopAab, at 25 °C are presented in **Figure 6.3.7**, where protein concentrations were varied as above. Each of the curves depicts a increase in absorbance, in accordance with copper transfer from CopAab to CopZ.

A single exponential decay function was fitted to each of the traces, giving rate constants for each concentration of CopZ: 243 $\pm$ 3.6 s^{-1} for 20 μM His_6CopZ, and 249 $\pm$ 3.5 s^{-1} for 60 μM His_6CopZ. The following rate constants were found when concentration of CopAab was varied: 231 $\pm$ 3.6 s^{-1} for 20 μM CopAab, and 321 $\pm$ 3.5 s^{-1} for 60 μM CopAab. These values compare reasonably well to that obtained when both proteins at 40 μM CopAab, 258 $\pm$ 2.6 s^{-1} (see **Fig 6.3.5**).

The plots of copper transfer between CopAab and His_6CopZ when one is loaded with 0.5 Cu(I) / protein illustrate that copper transfer in both directions is a rapid reaction complete within 20 milliseconds. In addition, the agreement between rate constants obtained in both directions of copper transfer indicates the same rate-limiting step occurs in both reactions. The fact that the rate does not change with protein concentration suggests it is a true first-order process.

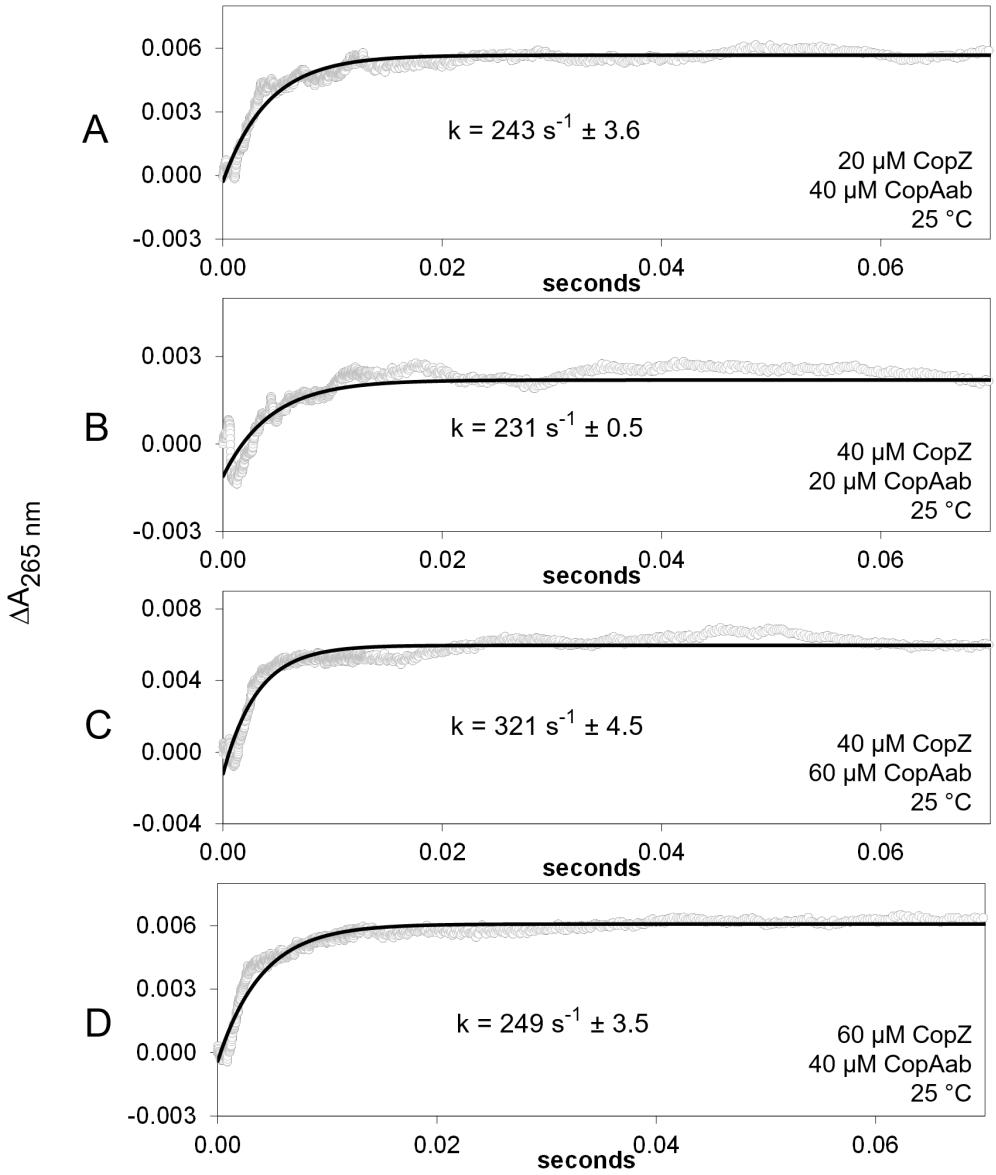

Figure 6.3.7: Kinetics of Cu(I) transfer of 0.5 Cu / His_6CopZ mixed with apo-CopAab at varied concentrations, 25 °C. Change in absorbance intensity at 265 nm plotted against time after rapid mixing of 0.5 Cu / His_6CopZ at 40 μM mixed with: A) 60 μM apo-CopAab B) 40 μM apo-CopAab C) 20 μM apo-CopAab. The data were fit to single exponential function from which the rate constant was derived, and is labelled on each plot. These plots illustrate that the rate constant is not dependent upon concentration of apo-CopAab.

Kinetics of Cu(I) transfer at varied temperature

At 25 °C, similar $\triangle$A values were obtained for forward/reverse directions for reactions carried out at complementary protein concentrations, suggesting that copper transfer is reversible. However, the change in absorbance did not represent the expected transfer of half the copper; given the rapidity of this reaction, that suggested that some transfer occurred within the dead time of the instrument. Therefore the reaction was carried out at lower temperature, with the aim of slowing the reaction in order to determine the extent of copper transfer.

For the reaction 0.5 Cu / His_6CopZ + apo- CopAab (**Figure 6.3.8**), the concentration of 0.5 Cu / His_6CopZ and apo-CopAab was varied for this reaction, at 15 °C. Each of the curves depicts an decrease in absorbance in each experiment, as expected for copper transfer from CopZ to His_6CopZ. A single exponential decay function was fitted to each of the traces, resulting in similar rate constants for each concentration, as labelled in the figure.

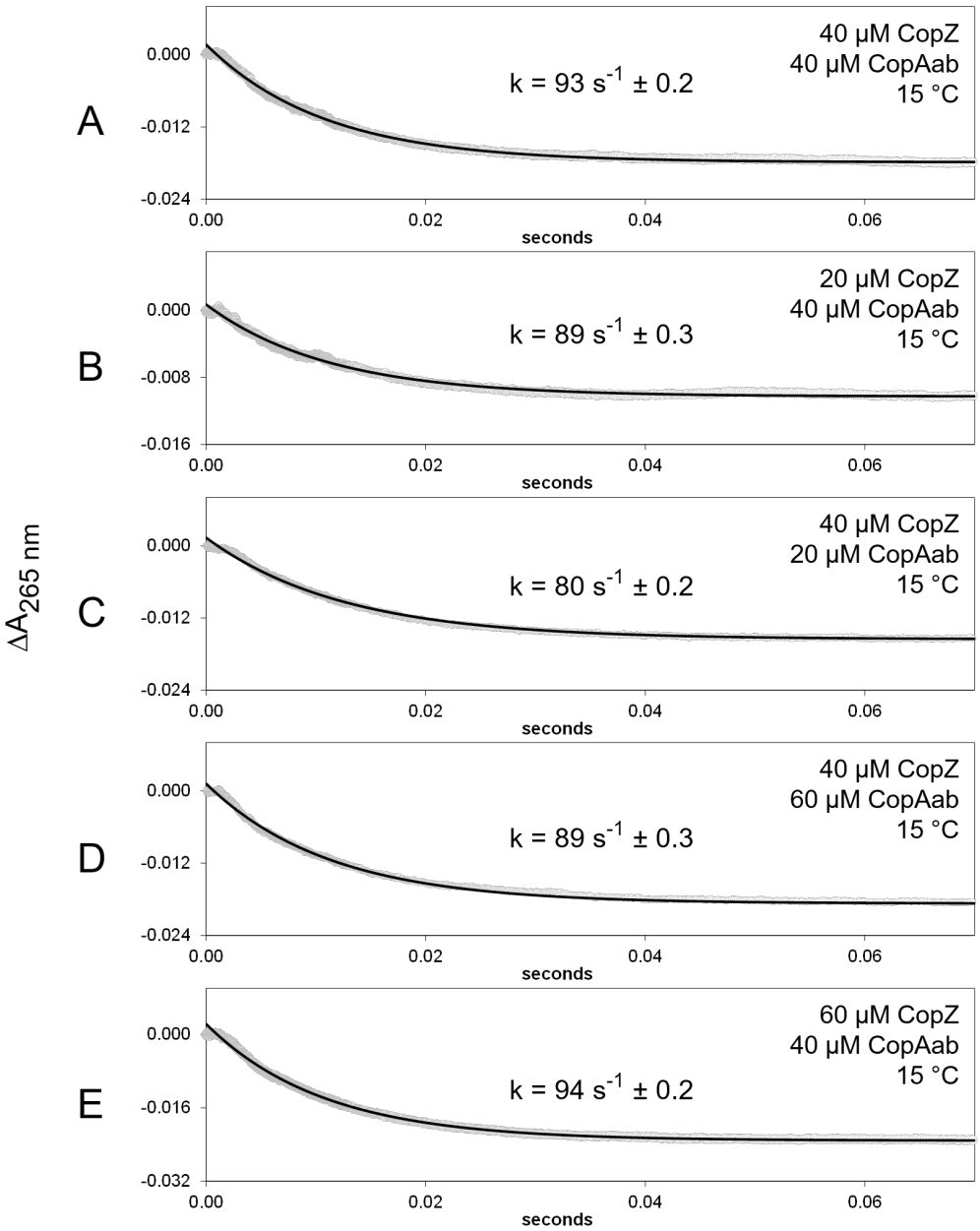

Figure 6.3.8: Kinetics of Cu(I) transfer of apo-His_6CopZ at varied concentrations mixed with 0.5 Cu / CopAab, 15 °C. Change in absorbance intensity at 265 nm plotted against time after rapid mixing of 0.5 Cu / CopAab at 40 μM mixed with: A) 60 μM apo-His_6CopZ B) 40 μM apo-His_6CopZ C) 20 μM apo-His_6CopZ. The data were fit to single exponential function from which the rate constant was derived, and is labelled on each plot. These plots illustrate that the rate constant is not dependent upon concentration of His_6CopZ.

Again, for the same reaction 0.5 Cu / His_6CopZ + apo- CopAab, the concentrations of 0.5 Cu / His_6CopZ and apo-CopAab were varied for this reaction, at 10 °C. Each of the curves depicted in (**Figure 6.3.9**) displays a decrease in absorbance in each experiment, as expected for copper transfer from CopZ to His_6CopZ. A single exponential decay function was fitted to each of the traces, resulting in rate constants as labelled in the figure.

Here, again, the calculated rate constants appeared to be independent of starting concentration of either reactant, suggesting that the formation of the heteroprotein complex is not the rate-limiting step. This would suggest that some element of copper transfer within the complex, or dissociation of the complex into constitutent proteins, is the rate-limiting step. Across these experiments, the rate decreases with decreasing temperature (as expected), enabling a greater extent of copper transfer to be visualised. However, the extent of copper transfer still does not seem to be represented by the ΔA_{265nm} values shown.

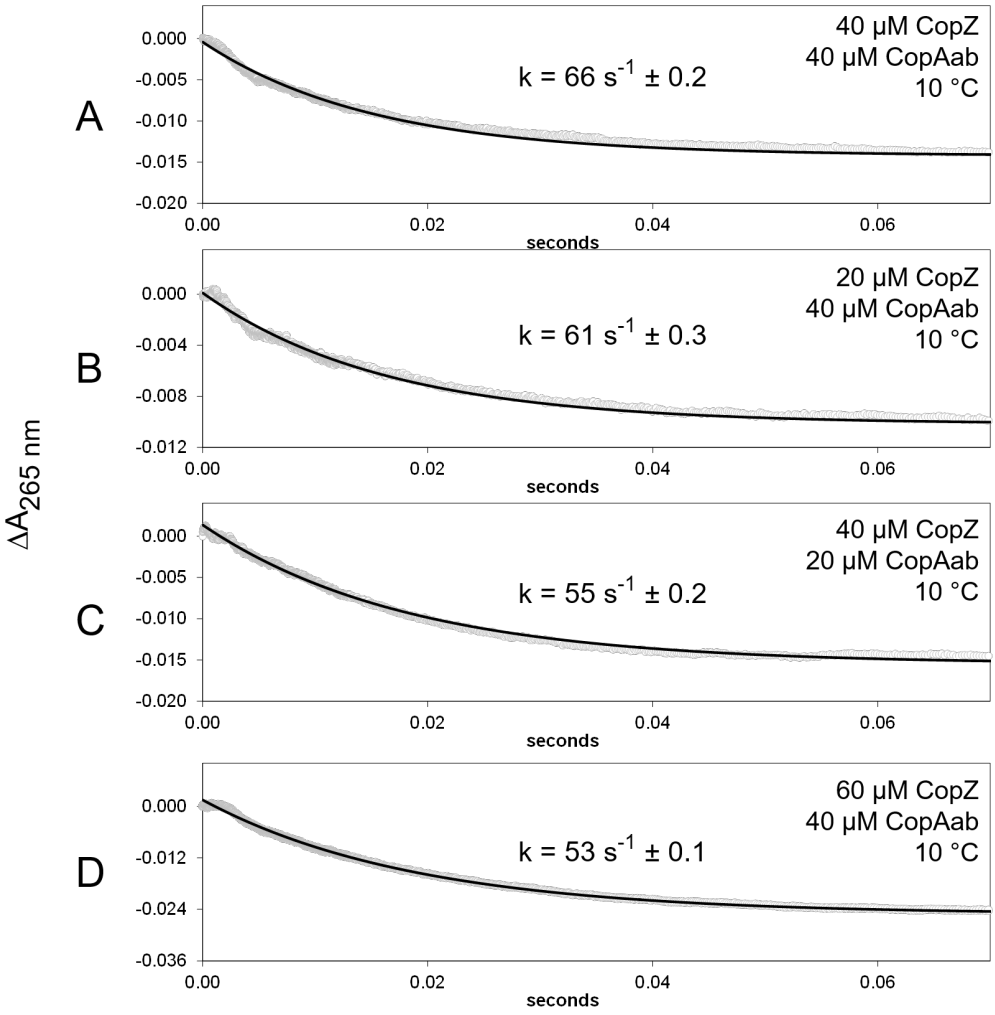

Figure 6.3.9: Kinetics of Cu(I) transfer of apo-His_6CopZ at varied concentrations mixed with 0.5 Cu / CopAab, 10 °C. Change in absorbance intensity at 265 nm plotted against time after rapid mixing of apo-His_6CopZ at 40 μM mixed with: A) 60 μM 0.5 Cu / CopAab B) 40 μM 0.5 Cu / CopAab C) 20 μM 0.5 Cu / CopAab. The data were fit to single exponential function from which the rate constant was derived, and is labelled on each plot. These plots illustrate that the rate constant is not dependent upon concentration of His_6CopZ.

6.4 Results: Copper Transfer Between CopZ and CopAab via ESI-MS

6.4.1 Mixture Of Species Detected In Mass-To-Charge Spectrum

The native ESI mass spectra prior to deconvolution are presented in **Figure 6.4.1** of samples containing: CopZ prepared at 0.5 Cu / protein and then mixed with apo-CopAab; apo-CopZ mixed with CopAab prepared at 0.5 Cu / protein. The mass spectrum prior to deconvolution of the sample containing 0.5 Cu / CopZ and apo-CopAab is shown in its entirety in **Figure 6.4.1A** with an expanded view of the low-intensity, lower charge state peaks. These spectra illustrate multiple peak envelopes which arise from the mixture of species in solution: CopZ, CopAab and a complex formed between CopZ and CopAab. The CopZ envelope comprises monomer with 3+, 4+, 5+ and 6+ charges, with a small amount of dimer peak with 7+ charges (peak m/z 2097.0) and a small amount of CopZ trimer peak with 10+ charges (m/z 2201.9). The CopAab envelope predominantly consists of monomer peaks with 8+ and 9+ charges, and a low-intensity monomer peak with 7+ charges. Also present is an additional set of peaks corresponding to a complex formed by CopZ and CopAab with 9+, 10+ and 11+ charges.

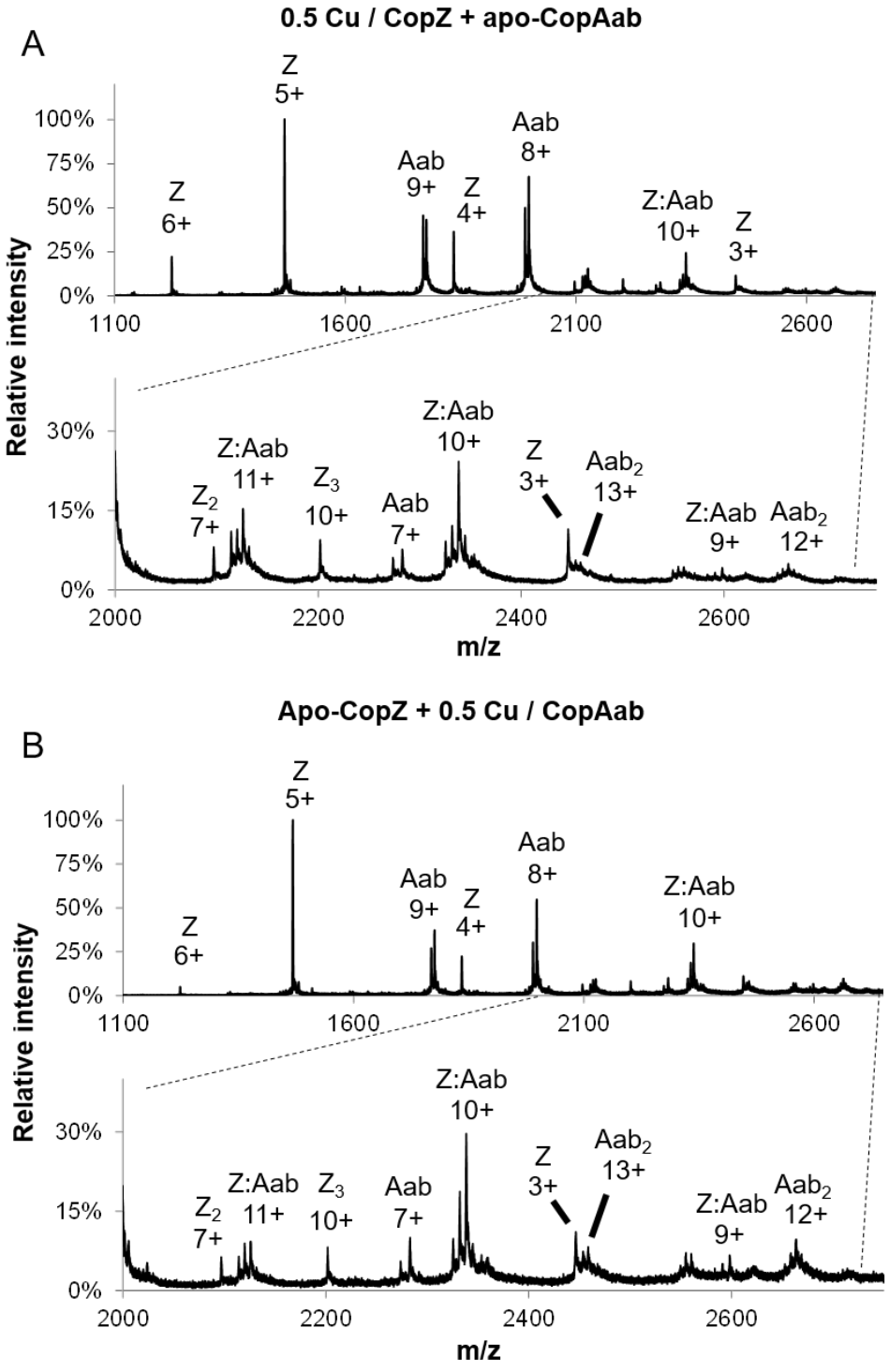

Figure 6.4.1: Mass spectra for mixtures of CopZ and CopAab. Mass spectra prior to deconvolution of samples containing: A) 0.5Cu / CopZ + apo-CopAab B) expanded view of 0.5 Cu/CopZ + apo-CopAab C) apo-CopZ + 0.5Cu/CopAab D) expanded view of apo-CopZ + 0.5 Cu/CopAab. Each protein envelope is labelled with the corresponding charge state of each peak, as follows: Aab, CopAab monomer; Aab_2, CopAab dimer; Z, CopZ monomer; Z_2, CopZ dimer; Z_3, CopZ trimer; Z:Aab, CopZ-CopAab complex. The spectra illustrate the mixture of peak envelopes arising in samples containing mixtures of the two proteins.

The mass spectrum prior to deconvolution of the other sample, which contained a mixture of apo-CopZ with CopAab prepared at 0.5 Cu / protein (**Figure 6.4.1B**) depict a similar distribution of individual species: mostly CopZ monomer (4+, 5+, 6+) and CopAab monomer (8+, 9+), with low-intensity peaks representing CopZ dimer (7+) and trimer (10+), and CopAab dimer (12+, 13+). Also observed, as above, are peaks due to the CopZ-CopAab complex (9+, 10+, 11+). The location and distribution of charge states agrees with that observed in native ESI-MS experiements carried out with the individual proteins (see Chapter 4 and 5), suggesting here that the proteins are folded in solution, with no major conformational changes when they exist in a mixture, apart from formation of a heteroprotein complex between them.

6.4.2 Copper-Bound CopZ:CopAab Complex Observed

The monomer and dimer species observed via ESI-MS in samples containing mixtures of CopZ and CopAab are presented in **Figure 6.4.2**. As seen above, the spectra after deconvolution reveal a mixture of CopAab and CopZ species. Despite the low intensity of some species, the peaks were resolved from the baseline with minimal applied smoothing, with sodium adduct formation observed.

Comparing the spectra from each sample reveals that, regardless of which protein is copper-loaded prior to mixing, a similar species distribution results and the predominant copper-bound peak is CuCopAab. Also present is a significant proportion of apo-CopAab, with the most intense species being apo-CopZ. Additional copper-bound peaks, both monomer and dimer, are observed at low intensity: CuCopZ, $Cu(CopAab)_2$, and $Cu_2(CopAab)_2$.

The relative intensities and exact masses of these species are presented in **Table 6.1**. The exact masses observed are mostly within 1 Da of the predicted mass. One exception is $Cu_2(CopZ)_2$; the reason for the observed mass difference of $\sim$ 5 Da is likely due to its low intensity.

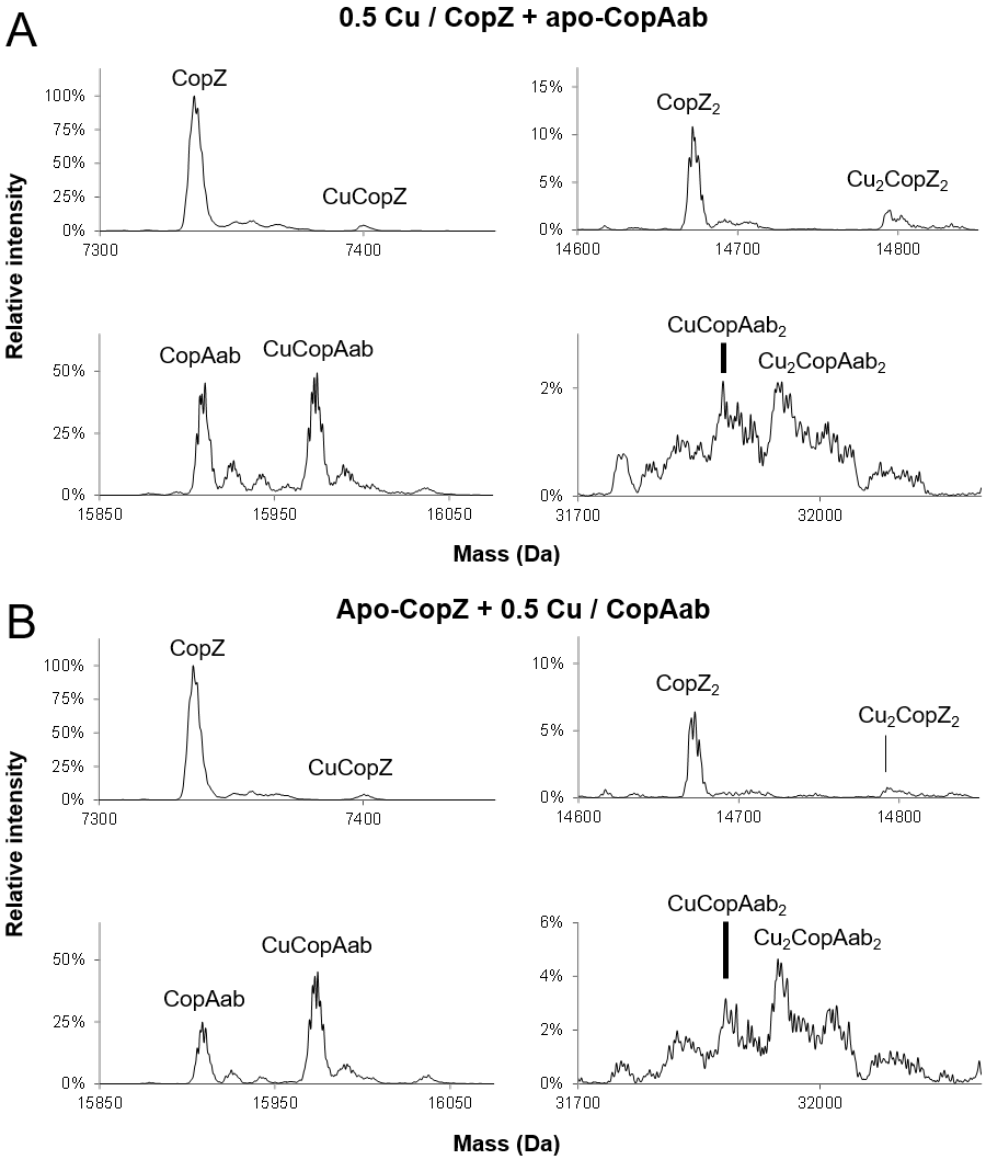

Figure 6.4.2: Deconvoluted mass spectra for mixtures of CopZ and CopAab. The mass spectra prior to deconvolution containing: **A)** 0.5 Cu / CopZ + apo-CopAab, and **B)** apo-CopZ + 0.5 Cu / CopAab. The species distribution resulting from copper transfer in either direction is similar, resulting in the predominant copper-bound species, CuCopAab. Additional low-intensity copper-bound species, including CuCopZ, are observed.

Table 6.1: Species observed via ESI-MS of mixtures of CopZ and CopAab. Relative intensities and observed masses of species appearing in native ESI-MS spectra where CopZ and CopAab were mixed, one apo- and one at 0.5 Cu / protein.

Species	Pred (Da)	0.5 Cu/CopZ + apo-CopAab		apo-CopZ + 0.5 Cu/CopAab	
CopZ	7336.1	100%	7336.2	100%	7336.0
CuCopZ	7400.5	5%	7400.2	5%	7400.5
$(CopZ)_2$	14673.2	11%	14672.6	7%	14671.7
$Cu(CopZ)_2$	14723	0%	–	0%	–
$Cu_2(CopZ)_2$	14799.3	2%	14794.0	0%	–
CopAab	15909.0	43%	15909.2	0%	–
CuCopAab	15972.6	44%	15973.5	0%	–
$CopZ_3$	22008.3	5%	22009.6	0%	–
CopZ:CopAab	23245.1	4%	23244.8	4%	23245.5
Cu(CopZ:CopAab)	23309.9	3%	23309.7	6%	23311.6
Cu_2(CopZ:CopAab)	23374.2	7%	23374.0	10%	23374.5

Figure 6.4.3 illustrates the region in each spectrum where a copper-bound complex between CopZ and CopAab was observed. These peaks are of low intensity, but this is reasonable as their formation is expected to be transient and relies on encounters between individual proteins. A small amount of copper-free complex may have arisen from disulfide-bonded proteins, and two copper-bound complex species are observed: Cu(CopZ:CopAab) and Cu_2CopZCopAab. It is unclear which domain(s) of CopAab (a or b) participate in coordination of copper, and it is possible that the Cu(CopZ:CopAab) species is disulfide bonded. However, the Cu_2(CopZ:CopAab) species suggests copper transfer between CopZ and one domain from CopAab.

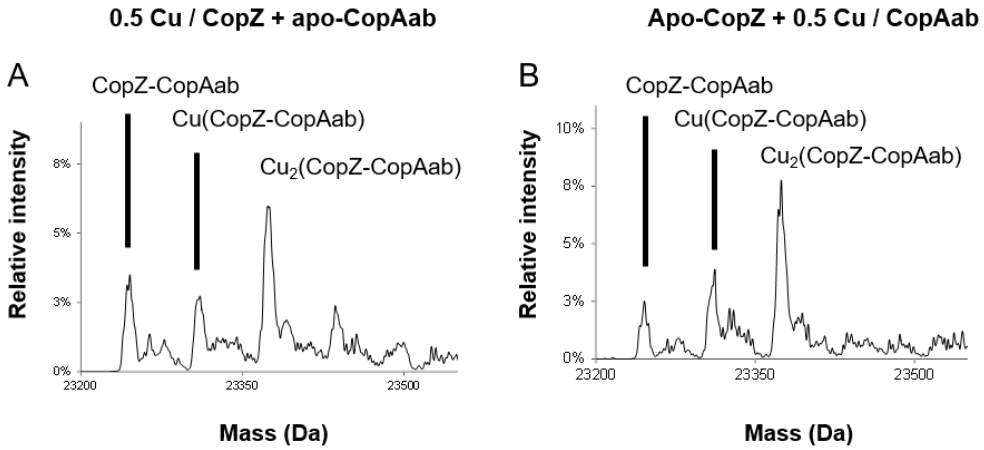

Figure 6.4.3: Deconvoluted mass spectra for mixtures of CopZ and CopAab, complex formation. The mass spectra depicting the CopZ:CopAab complex formed in samples containing: **A)** 0.5 Cu / CopZ + apo-CopAab, and **B)** apo-CopZ + 0.5 Cu / CopAab.

In order to compare the species distribution in these mixtures of CopZ and CopAab, the relative intensities of species present in these samples are plotted as bar graphs in **Figure 6.4.4**. Most of the peaks observed are at similar relative intensity in each sample. Regardless of which protein is copper-loaded prior to mixing, the predominant copper-bound species is CuCopAab, and its relative intensity is similar in both spectra. The intensities of the CopZ:CopAab complex species are fairly similar in each sample, with a slightly higher amount in the sample prepared by mixing apo-CopZ with 0.5 Cu / CopAab. The dominance of apo-CopZ may mask the extent of copper transfer by suppressing other peaks; mass spectra of CopZ (see Chapter 4) also revealed persistently high relative intensity of apo-

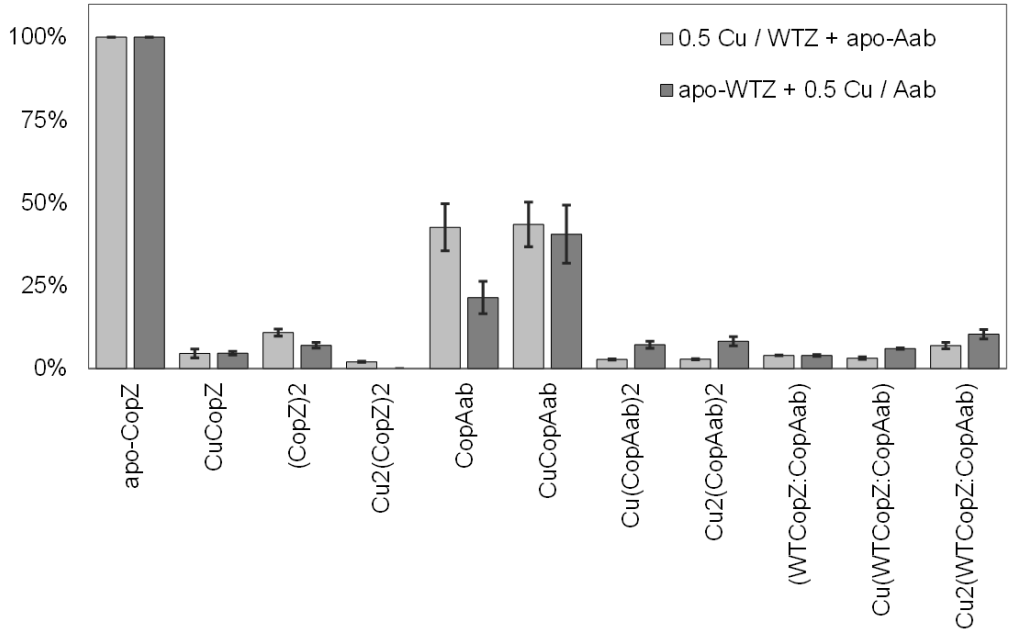

Figure 6.4.4: Species distribution observed via ESI-MS of mixtures of CopZ and CopAab. Bar graphs illustrating the relative intensity of each species present in the deconvoluted mass spectra of samples as labelled.

CopZ. In addition, for the mass spectra at 0.5 Cu / protein of CopZ (**Figure 4.2.3A**) and CopAab (**Figure 5.3.2A**), the relative intensity of the apo-protein peak was diminished. Here, it is possible that the relative proportions of apo-CopZ/CuCopZ and apo-CopAab/CuCopAab provide some indication of copper loading.

6.5 Discussion

Despite the extremely high affinity for Cu(I) displayed by CopZ and CopAab, copper transfer between the proteins is very rapid [163], with a transfer mechanism likely involving a protein-protein interaction. Heteroprotein complex formation for cognate Atx1-like/MBD pairs including CopZ and CopAab has been observed previously, leading to roughly equal distribution of copper between the proteins [163] [66] [67]. Though the weak thermodynamic drive for copper transfer implies copper exchange is under kinetic control [66], rate measurements have not been reported.

In order to gain further understanding of Cu(I) transfer between CopZ and CopA, it was desirable to measure the off-rate of Cu(I) from CopZ, in the absence of any influence of protein-protein interactions. The formation constant which defines the first Cu(I)-bound species, $Cu(CopZ)_2$, was established previously ($\beta_2 = \sim 10^{22}$ M^{-2}) and illustrates the extremely high affinity of CopZ for Cu(I). However, at a ratio of 0.5 Cu / CopZ, a small amount of CopZ monomer remains, suggesting that the affinity constant associated with binding of the second CopZ is not particularly high, $K_2 \sim 10^5$ M^{-1} [89]. Therefore, the tight binding is dominated by the stability constant K associated with binding of the first Cu(I) to form CuCopZ.

$$Cu(I) + CopZ \xrightarrow{K_1} CuCopZ \tag{6.1}$$

$$CopZ + CuCopZ \xrightarrow{K_2} CuCopZ_2 \tag{6.2}$$

The affinity constant represents the association and dissocation reactions between Cu(I) and CopZ as a ratio of the on-rate constant k_{on} and the off-rate constant k_{off}.

$$Cu(I) + CopZ \underset{k_{on}}{\overset{k_{off}}{\rightleftharpoons}} CuCopZ$$

Therefore the rate of change of concentration of the product, CuCopZ, can be expressed as a combination of the association and dissociation terms:

$$\frac{d[CuCopZ]}{dt} = [Cu][CopZ]k_{on} - [CuCopZ]k_{off} \tag{6.3}$$

At equilibrium, the forward and reverse binding transitions would be balanced, therefore these terms would be equal.

$$[Cu][CopZ]k_{on} = [CuCopZ]k_{off} \tag{6.4}$$

This expression can be rearranged to express the dissociation constant as a ratio of off-rate to on-rate constants, where k_{off} has units of s^{-1}, and k_{on} has units $M^{-1}\ s^{-1}$:

$$K_D = \frac{k_{off}}{k_{on}} = \frac{[Cu][CopZ]}{[CuCopZ]} \tag{6.5}$$

The maximum value of the on-rate constant is limited to that for a diffusion-controlled reaction, $k_{on} \sim 10^8\ M^{-1}\ s^{-1}$, suggesting the upper limit for the off-rate constant is very low (predicted to be $10^{-9}\ s^{-1}$). In order to measure the off-rate of Cu from CuCopZ "directly", reassociation was limited by placing the 0.5 Cu / CopZ sample into a dialysis cassette in a beaker of buffer. As a receptor to monitor Cu(I) release, a second dialysis cassette was im-

mersed containing apo-His_6CopZ, which has been demonstrated to have identical copper-binding behaviour as the non-tagged protein [179]. This experimental setup dictated that copper transfer would first take place via dissociation of Cu from CopZ in solution, rather than being facilitated by interaction between the two proteins.

Because of the extremely high affinity of copper chaperones for Cu(I) and the need to protect the cytoplasmic environment from the deleterious effects of copper, it was expected that very little, if any, copper would be released from CopZ over a measureable period. Though the absorbance of Cu-bound CopZ did decrease slightly between 24 and 48 hours, this was not accompanied by an appreciable increase in absorbance of apo-His_6CopZ. The beaker buffer was not found to contain any Cu(I), in agreement with previous studies demonstrating that cytoplasmic Cu(I) content is virtually zero [180].

Therefore, it is likely that the majority of the absorbance change is not attributable to loss of Cu(I) from CopZ but, rather, experimental constraints associated with measuring small amounts of slow transfer of copper, such as slight instrument drift or a small amount of protein loss due to adsorption to the dialysis membrane. The insignificant detection of copper transfer over the course of two days is supportive of the prediction that the off-rate constant in Equation 6.4 would have very small magnitude.

Although stability of CopZ was not sufficient to definitively determine the off-rate constant, the data acquired do have utility in establishing its upper limit. This was achieved by fitting a single exponential function to the data giving a rate constant of $\sim 10^{-5}$ s^{-1}. This would make the relationship between variables in Eqn 6.5 reasonable based upon the limitations of this experiment, i.e., a difference of several orders of magnitude between k_{off}

and K_D and an assumption of a diffusion-limited reaction ($\sim 10^{-9}$ s^{-1}). Regardless it can be concluded that, if the mechanism for copper transfer relied upon dissociation of Cu(I) from the $Cu(CopZ)_2$ or CuCopZ complex, the rate would be exceptionally slow.

This kinetic limitation is overcome by Atx1-like chaperones' interaction with their cognate ATPase MBDs, in which a complex that facilitates Cu(I) transfer is formed at least transiently. Such a complex has been observed for yeast Atx1 and Ccc2 [67], and B. subtilis CopZ and CopAab [163], and human Atox1 and ATP7A/B [49]. Although Cu(I) transfer occurs readily, the rate at which it occurs has not been determined for any chaperone transfer pair.

In order to characterise the kinetics of copper transfer between CopZ and CopAab at low copper loadings, a method was employed using stopped flow rapid mixing monitored by UV-visible absorbance, where the proteins' differing response in A_{265nm} upon binding of Cu(I) was exploited to monitor the direction and rate of copper transfer. Based upon the relative absorbance changes for the individual proteins, the direction of copper transfer was as expected: transfer from CopAab to CopZ resulted in an increase in signal, with a decrease in signal observed for the reverse transfer from CopZ to CopAab.

Stopped-flow experiments carried out with His_6CopZ here exhibited the same behaviour as the non-tagged construct, in agreement with previous data establishing its Cu(I)-binding behaviour [177]. Repeating the experiments with His_6CopZ and CopAab generated comparable plots, whose exponential fits revealed rate constants of k = 258 $\pm$ 2.6 s^{-1} and 247 $\pm$ 2.2 s^{-1}, in agreement with data obtained for non-tagged CopZ.

The observed changes in absorbance permitted the direct monitoring of copper trans-

fer between the species, $Cu(CopZ)_2$ and CopAab, and in the reverse direction between CuCopAab and CopZ. At 25 °C, the magnitude of absorbance intensity changes were approximately the same in both directions, $\sim$0.007 AU, suggesting that the same amount of copper was transferred in both reactions. These observations are in agreement with a previous experiments which found copper to be equally distributed between the proteins following equilibration and separation [177] and a shallow thermodynamic gradient for transfer at higher copper loadings [163]. Here, the transfer reaction was found to be rapid, being complete well within 20 milliseconds.

A single exponential function fitted the data well, with apparent first-order rate constants of 200 – 300 s^{-1} in both directions, suggesting the rate-limiting step in both directions is the same. Previous luminescence data at higher copper loadings suggested the rate constants differ for the “forward” and “reverse” direction of copper transfer, but this could be due to conformational changes required for CopAab which is a dimer at higher levels of copper [163]. Though CopZ is a dimer at this copper loading, the high affinity is dominated by K_1 as described above. Therefore, here the copper transfer measured is likely to be carried out within a CopZ:CopAab complex.

In order to determine whether the copper transfer reaction rate was dominated by formation or dissociation of the complex species, the concentration dependence of the reaction was explored. After varying the concentrations of both reactants, there appeared to be no effect upon the k_{obs}, suggesting that the rate-limiting step is not complex formation. These data concur with kinetics of copper transfer between CopZ and chelator BCS [84] where the rate constant in both directions of copper transfer was found to be the same,

suggesting that the same step was rate-limiting in both reaction directions.

Not only do the stopped flow data indicate that the rate of copper transfer is the same in both directions, they illustrate that copper transfer from CopZ to CopAab by way of complex formation proceeds at a $\sim 10^7$-fold increase in Cu(I) off-rate than in the absence of protein interaction.

To examine the species present at equilibrium upon transfer of copper between CopZ and CopAab, native ESI-MS was carried out using: apo-CopZ + 0.5 Cu/CopAab, and 0.5 Cu/CopZ + apo-CopAab. The charge state distribution observed in these mass spectra were in agreement to the individual proteins' mass spectra (see Chapter 4 and 5), suggesting the monomers remain folded without major structural changes when in a mixture. The resulting spectra from both directions of copper transfer contained a similar mixture of copper-bound and copper-free species. The major species observed was apo-CopZ, and the most intense copper-bound species is CuCopAab. Additional low-intensity peaks were observed, including a complex between CopZ and CopAab.

The dominance of CuCopAab in the ESI-MS spectra suggests that all copper is transferred to CopAab, but comparing these results to the individual mass spectra, the extent of copper transfer is unclear. Though the low peak intensity makes it difficult to interpret this spectrum with certainty, there are some indications that copper has been transferred between the proteins. At 0.5 Cu / protein, the most intense species observed were CuCopAab (**Figure 5.3.2A**) and CuCopZ (**Figure 4.2.2A**), and this would imply these species form first at low copper loadings (even below 0.5 Cu / protein). Thus, a high proportion of apo-CopZ and apo-CopAab would be expected. However, no appreciable amount of

Cu_2CopAab was observed, which was observed in the individual spectrum of CopAab prepared at 0.5 Cu / protein. Here, had all the copper been transferred to CopAab, its loading would be 0.5 Cu / protein and Cu_2CopAab species would be expected. This suggests that transfer of some, but not all copper has taken place.

Again, a sizeable proportion of apo-CopAab and apo-CopZ was expected, as the overall copper loading is 0.25 / protein. However, the apo-CopZ peak was always very intense even in the presence of copper (see Chapter 4). Here, in the mixed samples, a noticeable difference between the two spectra are the relative intensities of CopAab and CuCopAab peaks. ESI-MS of CopAab at 0.5 Cu / CopAab (**Figure 5.3.2A**) revealed the apo-CopAab peak to be of much lower intensity than CuCopAab. Here, that is not the case, perhaps suggesting not all copper is bound by CopAab.

An important observation in the ESI-MS experiment is a hetero-complex observed in both spectra, where CopZ:CopAab coordinates 1 or 2 copper ions. It is possible the complex species CuCopZCopAab represents exchange between CuCopZ and one of the CopAab domains (a or b). The species Cu_2CopZCopAab could depict the same exchange process with the other domain (a or b) in possession of copper. The expected products are observed, CuCopAab ($\sim$45%) and CuCopZ ($\sim$5%). The different relative intensities of these products could arise from dissimilar ionisation intensities, or from continual exchange to form CuCopAab which results in decreased proportion of CuCopZ. The presence of a complex species implies that that copper transfer indeed has taken place and is continually being exchanged in this equilibrium mixture.

The data presented in this chapter support a copper transfer mechanism that involves

rapid copper transfer between CopZ and CopAab, by way of a heteroprotein complex. Further work is needed to establish ESI-MS data which reveal the species present during copper transfer between these two proteins.

Chapter 7

Studies Of Cu(I) Binding To Copper Chaperones From *Streptomyces lividans* and *Saccharomyces cerevisiae*

7.1 Introduction

Metallochaperones are highly conserved throughout biology, transporting and effectively distributing potentially dangerous copper ions throughout the cell. The exact mechanisms of copper movement throughout the cell are not fully defined, but their action is known to rely on binding Cu(I) with high affinity/specificity, such that essentially none exists in free form in the cytoplasm.

The Atx1-like copper chaperones are $\sim$ 75 residue proteins, with a conserved $\beta\alpha\beta\beta\alpha\beta$ fold, exhibiting high affinity for Cu(I) ($K_d \sim 10^{18}$ M^{-1}). *Saccharomyces cerevisiae* Atx1 is the eponymous member of the Atx1-like copper chaperones demonstrated to transfer Cu(I) to the N-terminal domains of its cognate transport protein, Ccc2, in a direct and reversible manner [66] [34], similar to *B. subtilis* CopZ. *Streptomyces lividans* is a soil dwelling-bacterium which requires copper ions for development [72]. The *S. lividans* copper efflux system is upregulated through Cu(I) binding of copper sensitive operon repressor (CsoR). Under the transcriptional control of CsoR are CopZ-3079 and CopZ-1317, two Atx1-like proteins [73].

Like *B. subtilis* CopZ, these three copper chaperones have been characterised by

solution-phase biophysical studies, and demonstrated to form both a monomer and dimer *in vitro* with evidence of an effect of LMWT upon association state. In addition, examining their behaviour enables comparisons to be made across multiple kingdoms of biology and explore the effect of particular conserved residues. Comparing the amino acid sequences of some Atx1-like proteins (**Figure 7.1.1**) illustrates their conserved residues.

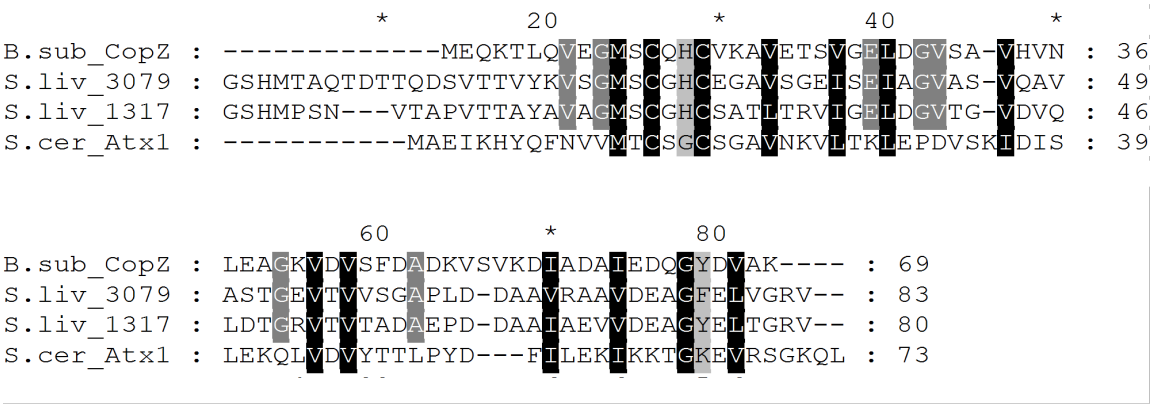

Figure 7.1.1: Aligned primary sequences of Atx1-like copper chaperones. The primary sequences of CopZ from *S. lividans*, *S. cerevisiae* and *B. subtilis* are aligned with residues highlighted: those conserved among all four (**black**); conserved among prokaryotic (**gray**); X_3 and loop 5 residues (**light gray**)

CopZ-1317 and CopZ-3079 were demonstrated via BCS competition to exhibit high affinity for Cu(I), with K_D(Cu(I)) of: 2.1×10^{-17} M for CopZ-1317, and 3.7×10^{-18} M for CopZ-3079 [74]. Transcription levels suggested that CopZ-3079 contributes far more to Cu(I) resistance, as during copper stress, CopZ-1317 is less than 2% of transcription. In titration experiments with a solution of BCA, this chelator was unable to remove any Cu(I) from either CopZ-1317 or CopZ-3079 beyond a level of 1 Cu / protein. However, this may indicate an overall copper / protein ratio within a mixture. Spectroscopic studies demonstrated these proteins can form higher order assemblies at elevated copper levels, and size

exclusion chromatography confirmed their inability to form in the presence of LMWT.

Residues other than cysteine in the conserved $MX_1CX_2X_3C$ motif typically do not participate in metal binding (**Figure 7.1.2**). The X_1 site usually contains a His, Thr, Asp or Ser; X_2 and X_3 are frequently small and hydrophobic, or polar uncharged residues, such as Ala, Gly, Ser [181]. However, many prokaryotic variants have a histidine at X_3 for example in *B. subtilis* CopZ whose crystal structure of $Cu_4(CopZ)_2$ revealed that this histidine serves as an additional Cu(I) ligand in the dimerised form of the protein [81]. This may indicate a greater propensity for prokaryotic Atx1-like chaperones, or at least those featuring histidine at X_3, to form dimers.

Another conserved residue thought to be functionally important is on loop 5 following the last conserved glycine, typically a lysine in eukaryotes and a tyrosine in prokaryotes. The cyanobacterial Atx1 contains a histidine, which acts as a Cu(I) ligand that is released upon complex formation with a partner protein [182]. In other organisms, though this residue does lie in proximity to the Cu(I) binding site, it does not serve as a Cu(I) ligand [171]. The prokaryotic Tyr has been shown to form a hydrophobic patch through its interaction with the conserved methionine, which may facilitate protein-protein recognition with CopA [81]. In eukaryotes the positive charge of the lysine is thought to stabilise the Cu(I) oxidation state through charge balance, and inhibit the need for dimerisation [183] [184] .

In addition, this residue may influence the solvent accessibility of the bound Cu(I) ion, making it more buried in eukaryotic proteins than in their prokaryotic counterparts; perhaps this limits the likelihood of dimerisation. For example, in *S. cerevisiae* Atx1, Lys65

affects solvent accessibility of the Cu(I) [41] with the mechanism for Cu transfer involving changes of the relative positioning of Lys65 and the Ccc2 MBD [185]. In human Atox1, the positioning of Lys60 creates two alternating configurations of the coordination site, where the copper is either more solvent-exposed or -buried. This arrangement is not present in bacterial and yeast Atx1 proteins, and is proposed to have evolved to effectively capture and then safely cradle Cu(I) ions [170]. Though this conserved Lys may confer a protective effect in eukaryotes precluded in the prokaryotic versions by protein dimerisation, both prokaryotic and eukaryotic proteins have been demonstrated to form higher order copper-bound assemblies *in vitro*. Examples include human Hah1 [57] [186], yeast Atx1 [187], *E. hirae* CopZ [188], *Synechocysis* PCC6803 Atx1 [139].

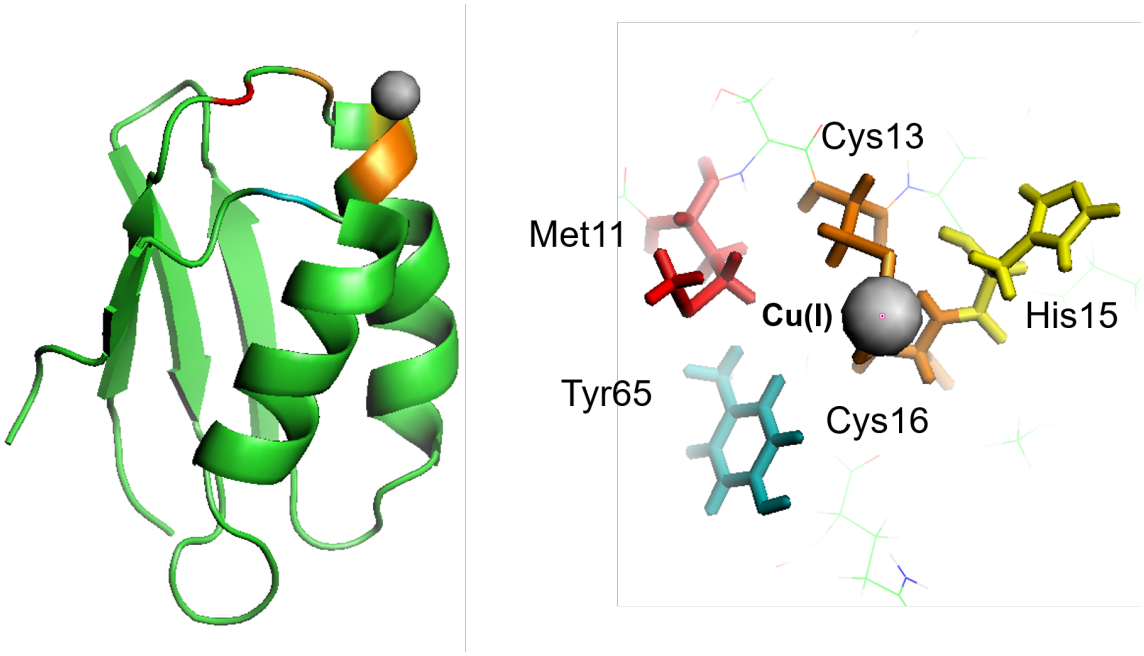

Figure 7.1.2: Cu(I)-binding site of *B. subtilis* CopZ. Ribbon structure of *B. subtilis* CopZ with a single Cu(I) bound, along with an expanded view of the Cu(I)-binding site. Residues from the conserved $MX_1CX_2X_3C$ motif are labelled: Met; copper-coordinating Cys; residue in the X_3 position (here, His15) and the conserved loop 5 residue (here, Tyr65). Figure adapted from NMR solution structure (PDB: 1K0V) [40].

The physiological relevance of these higher order assemblies is debatable, due to the influence of cytoplasmic low molecular weight thiols (LMWT), which exhibit moderately high Cu(I) affinities [138] and can serve as exogenous Cu(I) ligands [40] [186]. It is unclear whether the presence of a low molecular weight thiol species *in vitro* promotes or inhibits dimerisation, even in the presence of copper. Human Atox1 has been reported to bind Cu(I) as a monomer in a 1:1 ratio when prepared at 1 Cu / protein in the presence of DTT [189], but also has been observed to dimerise when prepared in the absence of LMWT [57] and again in the absence of LMWT though in the presence of tris(2-carboxyethyl)phosphine (TCEP) [186].

Monomeric yeast CuAtx1 was reported in the solution structure in the absence of LMWT [41] and also in the presence of LMWT, even when loaded with excess Cu(I) [66]. However, more recently the presence of LMWT was reported to induce dimerisation of Atx1 [187] when in the presence of glutathione (GSH), $Cu_2Atx1_2GSH_2$ formed, which was not observed in the absence of GSH [190]. In addition, a trimeric Cu(I)-bound form of Atx1 has also been reported in the presence of endogenous thiol ligands, in a crystal structure solved after treatment with copper chelator tetrathiomolybdate (TM) (MoS_{4-}) [191], though this trimeric form may only occur in the case of molybdenum toxicity.

The effect that varied Cu(I) and LMWT levels have upon the mixture of copper-bound species formed by copper chaperones is complex. Perhaps the prokaryotic histidine at X_3 favours dimerisation, but this effect may be inhibited by LMWT due to Cu(I) competition effects. In the absence of this histidine, the eukaryotic variants may not undergo dimerisation in the same way, also influenced by the conserved lysine residue at the copper-binding

site. Thus it would be expected that dimerisation might occur for the eukaryotic proteins at higher copper / protein levels. Observation of $Cu_2Atx1_2GSH_2$ combined with high intracellular GSH concentrations implies this, too, is a physiologically relevant copper-bound form of Atx1, with the LMWT serving as an additional Cu(I) ligand in the dimeric forms. Defining the physiologically relevant copper-bound forms of these proteins requires consideration of their copper-binding behaviour in the presence and absence of LMWT. To this end, ESI-MS was carried out to examine the copper-bound species present at varied copper levels with and without DTT of *S. cerevisiae* Atx1 and *S. lividans* CopZ-1317 and CopZ-3079.

7.2 Materials And Methods

7.2.1 Preparation Of CopZ-3079, CopZ-1317 And Atx1 For ESI-MS

Samples of *S. lividans* CopZ-1317 and CopZ-3079 were kindly provided by Dr Jonathan Worrall and *S. cerevisiae* Atx1 by Professor Christopher Dennison, which had been purified as described previously [74] [139]. Mass spectrometry samples were prepared with reagents prepared in deoxygenated LC-MS grade water (HiPerSolv, VWR) in an anaerobic glovebox (Faircrest Engineering, O_2 concentration $<$2 ppm). Protein disulfide bonds were reduced with 15 mM DTT (Formedium) and the protein was exchanged into 20 mM ammonium acetate, pH 7.4 (Sigma) using a G25 Sephadex column (PD10, GE Healthcare). Protein concentrations were determined by recording UV-visible absorbance spectra on a Jasco V-550 spectrophotometer and using extinction coefficients, $\varepsilon_{276\ nm}$, of 2980 M^{-1} cm^{-1} (CopZ-1317), 1490 M^{-1} cm^{-1} (CopZ-3079), and 4470 M^{-1} cm^{-1} (Atx1) [74]. Protein samples were diluted with 20 mM ammonium acetate to a working sample concentration of 5 – 10 μM. To prepare Cu(I)-bound protein samples, a deoxygenated solution of Cu(I)Cl prepared in 100 mM HCl,1 M NaCl was added using a microsyringe (Hamilton) to anaerobic, reduced protein exchanged into 250 mM HEPES, pH 7.5. Unbound Cu(I) was removed by passage of the sample down a G25 Sephadex column (PD10, GE Healthcare) equilibrated with 20 mM ammonium acetate, pH 7.4. For DTT experiments, anaerobically prepared DTT (Formedium) (for structural representation, see Section 4.2.3) was added to aliquots of protein containing 2 molar equivalents of Cu(I), to yield thiol/protein ratios described for

each protein.

7.2.2 Electrospray Ionisation Mass Spectrometry

Mass spectra were acquired using a Bruker micrOTOF-QIII electrospray ionisation (ESI) time-of-flight (TOF) mass spectrometer (Bruker Daltonics, Coventry, UK), in positive ion mode. The ESI-TOF was calibrated in the m/z range 300 – 2200 using ESI-L Low Concentration Tuning Mix (Agilent Technologies, San Diego, CA). Native protein samples were introduced to the ESI source via a syringe pump (Cole-Parmer) at 3 μL/min, and data acquired for 2 min, with ion scans between 50 – 3400 m/z. MS acquisition was controlled using Bruker oTOF Control software, with parameters as follows: dry gas flow 5 L/min, nebuliser gas pressure 0.8 Bar, dry gas 180 °C, capillary voltage 4500 V, offset 500 V, quadrupole RF energy 1000 Vpp and 2575 Vpp (50:50), and transfer time 136 μs and 146 μs (50:50). The spectra were deconvoluted using the ESI Compass version 1.3 Maximum Entropy deconvolution algorithm version 4.1 (Bruker Daltonik, Bremen, Germany) over a mass range of 7000 – 30,000 Da. Overlapping peak envelopes were deconvoluted manually. Exact masses were determined from peak centroids, with minimal (no more than 3-point Gaussian) smoothing applied.

7.3 Results: Cu(I) Binding Of Copper Chaperones From *Streptomyces lividans*

7.3.1 ESI-MS Of Cu(I) Binding To CopZ-3079

In order to investigate its copper-binding behaviour, mass spectra were recorded of CopZ-3079 prepared at 0, 1 and 2 Cu / protein (**Figure 7.3.1**). The mass spectrum of apo-CopZ-3079 (**Figure 7.3.1A**) contained three peaks comprising the monomer envelope with 4+, 5+ and 6+ charges; the peak with 6+ charges was most intense. At a copper level of 1 / protein, the monomer peak envelope was present, along with a dimer peak envelope with the predominant peak possessing 9+ charges, and some overlap between monomer and dimer envelope at 4+/8+ and 5+/10+. When the copper level was increased to 2 Cu / protein, the dimer peak containing 9+ charges became the most intense, with a decrease in the monomer peaks' intensities. The charge state distribution is very similar to that observed for *B. subtilis* CopZ in its apo- and Cu-bound forms. In addition, the charge state envelope does not shift upon Cu-binding, suggesting CopZ-3079 is folded before and after copper binding occurs.

The deconvoluted mass spectra (**Figure 7.3.2**) illustrate the species present at each copper loading, while their exact neutral masses and relative intensities are presented in Table 7.1. The mass spectrum of CopZ-3079 prepared at 0 Cu / protein contains apo-CopZ-3079 as its predominant peak. A low intensity CuCopZ-3079 peak has been assigned ($\sim$ 13%) but this is not very pronounced above the noise and could overlap with a trisodiated

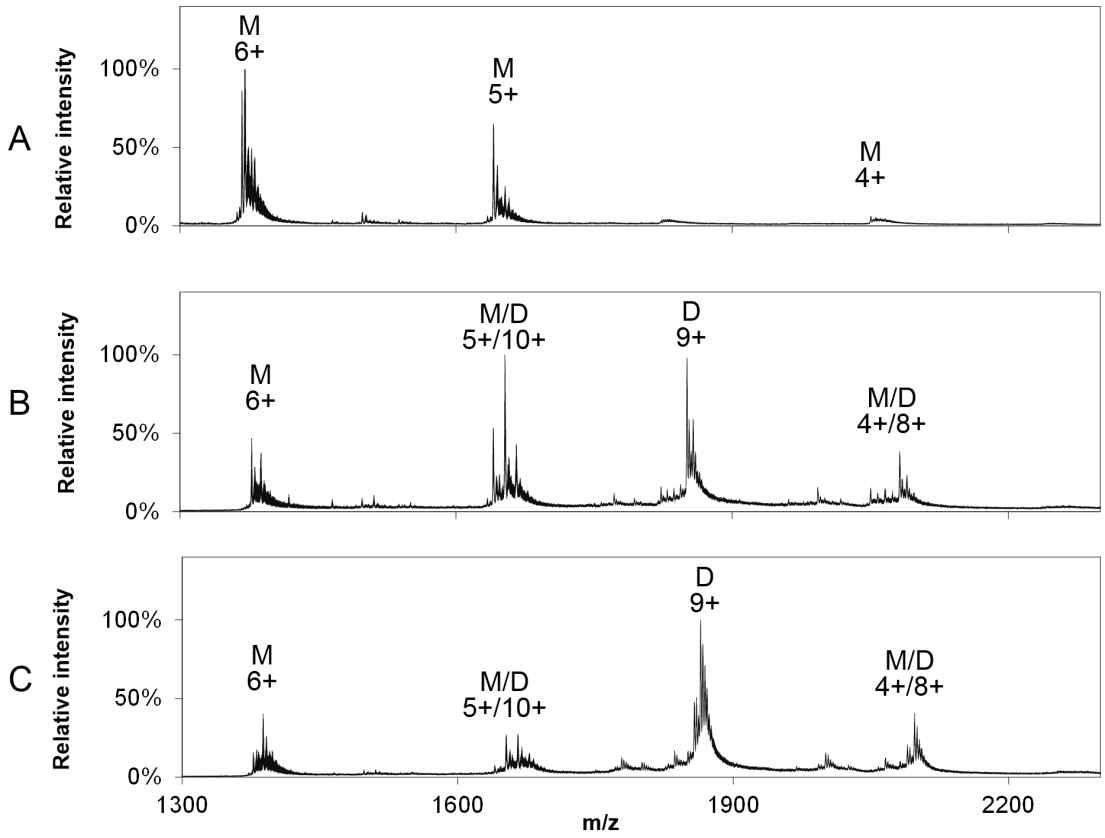

Figure 7.3.1: Mass spectra for CopZ-3079 at varied Cu(I) loadings. The mass spectra prior to deconvolution of CopZ-3079 prepared at a level of: **A)** 0.0 Cu / protein, **B)** 1 Cu / protein, **C)** 2 Cu / protein.

adduct of apo-CopZ-3079.

In the presence of copper, at a level of 1 Cu / protein, the most intense copper-bound species are CuCopZ-3079 and Cu_4(CopZ-3079)$_2$, both near 100% relative intensity. The next most intense copper-bound peak is Cu_5CopZ-3079$_2$ at 34 % relative intensity. The peaks for other dimeric forms, as well as apo-CopZ-3079 and Cu_2Atx1 have diminished to 20% relative intensity.

When the copper level is raised to 2 Cu / protein, the most intense species is the

dimeric copper-bound $Cu_6CopZ\text{-}3079_2$. Also present are monomeric CuCopZ-3079 and $Cu_2CopZ\text{-}3079$, along with a diverse mixture of dimeric species. Among these copper-bound dimeric peaks, $Cu_2(CopZ\text{-}3079)_2$ and $Cu_5CopZ\text{-}3079_2$ are of elevated intensity compared to the others, which could indicate that these species are intermediates favoured during the formation of $Cu_6CopZ\text{-}3079_2$.

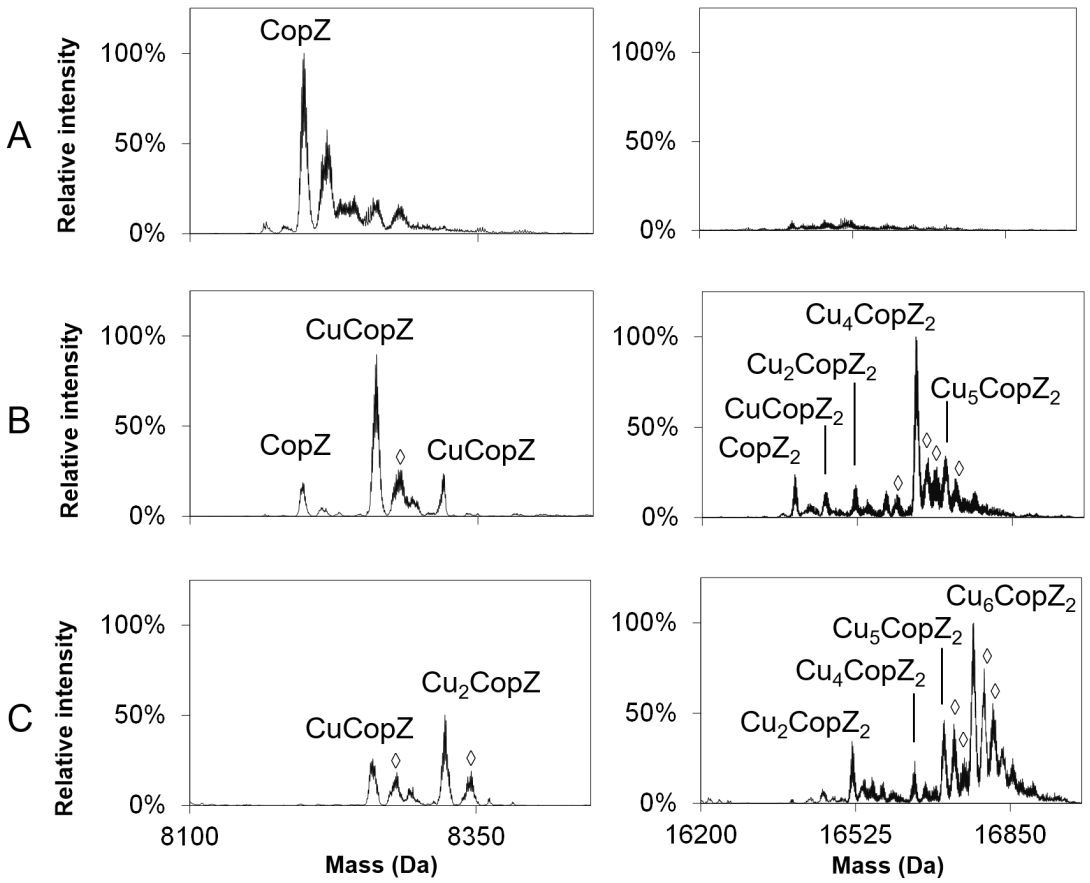

Figure 7.3.2: Deconvoluted mass spectra for CopZ-3079 at varied Cu(I) loadings. Deconvoluted mass spectra of CopZ-3079 prepared at a level of: **A)** 0.0 Cu / protein, **B)** 1 Cu / protein, **C)** 2 Cu / protein. Diamond symbols represent Na+ adducts.

The observed masses are mostly within 1 Da of their predicted mass, with some slight

Table 7.1: Species observed via ESI-MS of CopZ-3079 at varied Cu(I) loadings. Relative intensities and masses observed when CopZ-3079 prepared at 0, 1, and 2 Cu / protein.

Species	Pred (Da)	0 Cu / CopZ		1.0 Cu / CopZ		2.0 Cu / CopZ	
CopZ	8199.9	100%	8198.9	20%	8197.8	0%	–
CuCopZ	8262.4	13%	8261.6	93%	8261.6	26%	8259.2
Cu_2CopZ	8324.9	0%	–	28%	8320.1	40%	8322.9
$(CopZ)_2$	16399.9	7%	16396.6	26%	16394.6	0%	–
$Cu(CopZ)_2$	16462.4	0%	–	23%	16458.3	9%	16456.2
$Cu_2(CopZ)_2$	16524.9	0%	–	22%	16521.5	34%	16518.6
$Cu_3(CopZ)_2$	16587.4	0%	–	18%	16585.5	11%	16583.5
$Cu_4(CopZ)_2$	16649.9	0%	–	96%	16648.8	24%	16649.4
$Cu_5(CopZ)_2$	16712.4	0%	–	34%	16709.8	45%	16710.9
$Cu_6(CopZ)_2$	16774.9	0%	–	0%	–	96%	16772.5

discrepancies. At 2 Cu / CopZ-3079, the masses of CuCopZ-3079 is 3.2 Da less than predicted. The mass of Cu_2CopZ-3079 is 2 – 4.8 Da less than predicted. The mass of CopZ-3079_2 is 3.3 – 5.3 Da less than expected which most likely reflects the loss of hydrogens during disulfide formation, but is still slightly less than expected. Cu(CopZ-$3079)_2$ is 3.9 – 6.2 Da less than expected, perhaps reflecting overlap with a trisodiated adduct, and its ability to form one intramolecular disulfide while binding Cu(I) with another two cysteines. The observed masses of the other dimeric forms are also 1.1 – 6.0 Da less than predicted for reasons which are not clear. The size of the mass difference generally decreases with increasing peak intensity, suggesting perhaps lower intensity peaks are less accurate due to poorer peak shape/adduct overlap.

The bar graphs in **Figure 7.3.3** illustrate that, as the Cu(I) level is increased, the proportion of dimerised Cu(I)-bound CopZ-3079 increases. Two major species form at 1 Cu / CopZ-3079: CuCopZ-3079 and Cu_4(CopZ-$3079)_2$; the low intensity of other dimer peaks

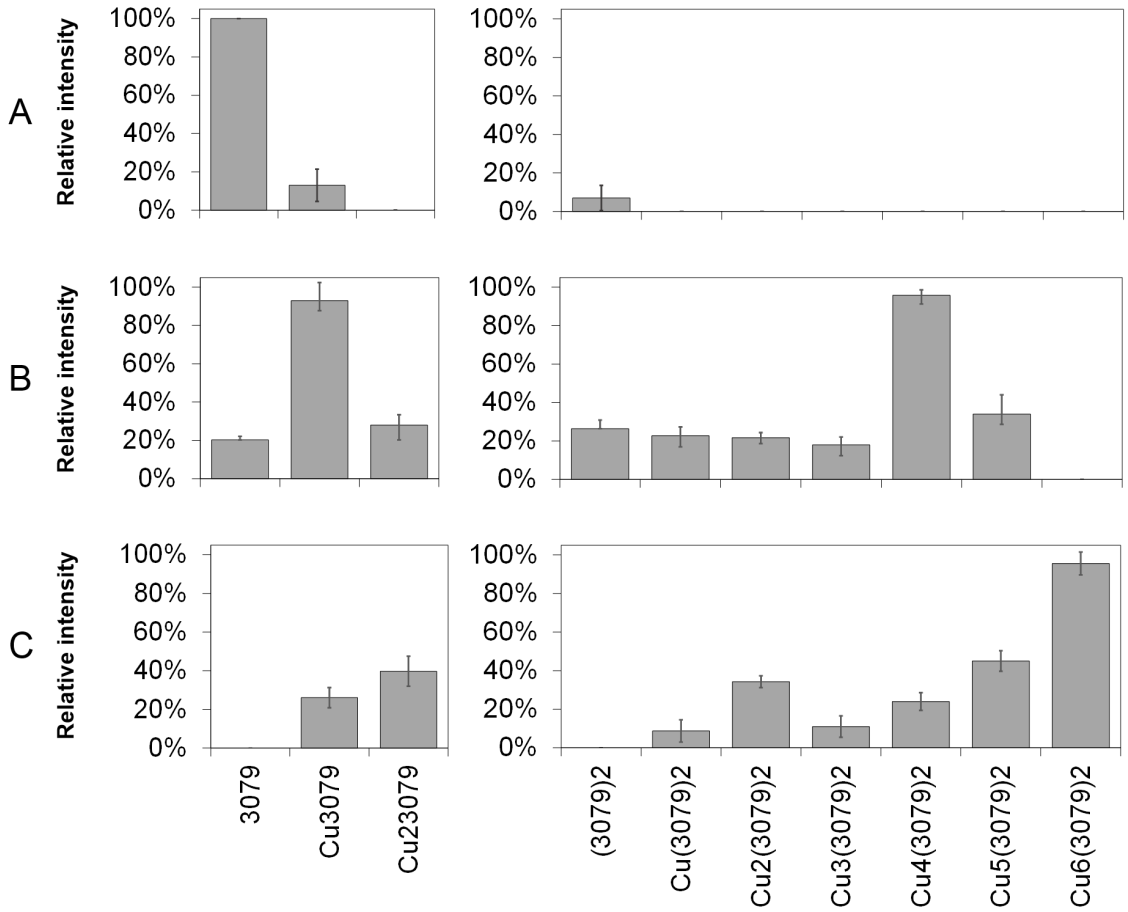

Figure 7.3.3: Species observed via ESI-MS of CopZ-3079 at varied Cu(I) loadings. Species present in deconvoluted mass spectra of CopZ-3079 prepared at a level of: **A)** 0 Cu / protein, **B)** 1 Cu / protein, **C)** 2 Cu / protein.

suggests cooperative formation of the tetra-copper species. At 2 Cu / CopZ-3079, the relative intensities of CuCopZ-3079 and Cu_4(CopZ-3079)$_2$ decrease, favouring formation of Cu_6(CopZ-3079)$_2$. This implies an additional cooperative mechanism involved in formation of a hexanuclear CopZ-3079 dimer species.

In order to compare the above data to solution-phase experiments, **Figure 7.3.4** presents unpublished data, acquired previously [192], size exclusion chromatography (SEC) of CopZ-3079 at multiple copper loadings, and a plot representing change in absorbance occurring

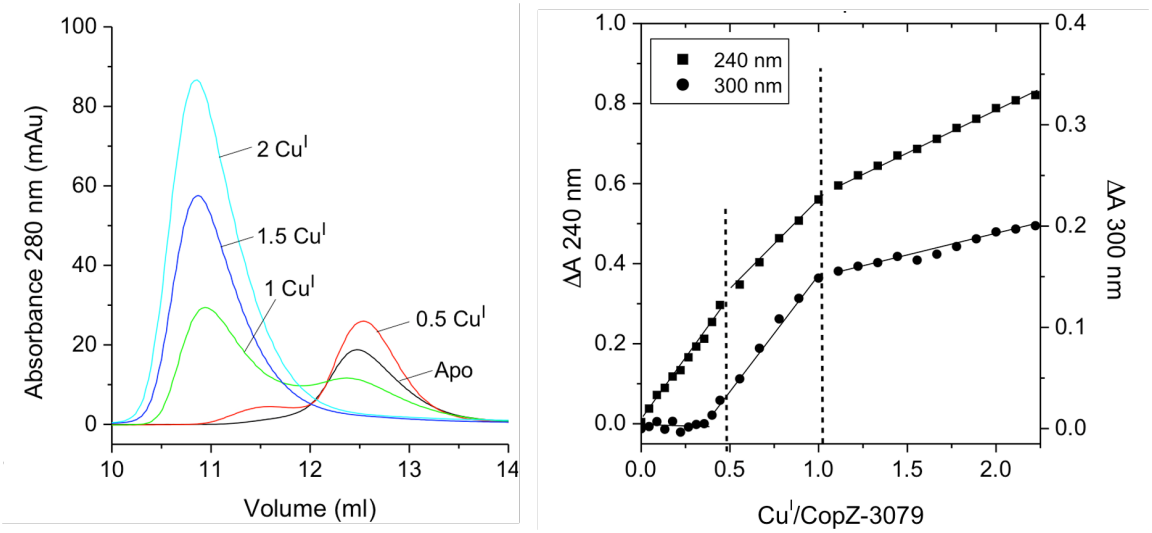

Figure 7.3.4: Size exclusion chromatography at multiple Cu(I) levels and UV-vis Cu(I) titration for CopZ-3079. Unpublished data, acquired previously [192] of: **A)** Size exclusion of CopZ-3079 prepared at molar equivalents of Cu(I) as labelled **B)** Cu(I) binding by CopZ-3079 monitored using UV-visible absorbance changes at 20 °C, pH 7.5. The absorbance changes observed for CopZ-3079 at 240 nm and 300 nm plotted as a function of Cu(I)/CopZ-3079 (CopZ-3079, 45 μM). Samples of CopZ-3079 were prepared in 10 mM MOPS pH 7.5, 150 mM NaCl under anaerobic conditions, adding 0.5, 1.0, 1.5 or 2 molar equivalents of Cu(I) to reduced CopZ-3079. Apo-CopZ-3079 concentrations were determined at 280 nm using extinction coefficients based upon ProtParam ExPASy and concentrations calculated using the Beer Lambert law. Size exclusion elution profiles created by monitoring the absorbance at 280 nm on a 10/300 GL G-75 Superdex column (GE-Healthcare) equilibrated in sample buffer. Absorbance measurements were carried out on a a Varian Cary 50 UV-visible spectrophotometer set at 20 °C.

at selected wavelengths as Cu(I) was titrated into a solution of CopZ-3079. **Fig 7.3.4A** displays the SEC chromatograms at 280 nm of CopZ-3079 at increasing ratios of Cu / protein, where it can be seen that CopZ-3079 forms higher order complexes when the Cu(I) level is increased. The apo-protein elutes entirely as monomer ($\sim$ 12.5 mL), at 0.5 molar equivalent a small amount of dimer is present ($\sim$ 11.5 mL), and above 0.5 molar equivalent dimer is the majority species. At 1 Cu / protein, a small amount of monomeric protein is present ($\sim$ 12.5 mL), with the most intense peak ($\sim$ 10.9 mL) according to the calibration

curve corresponding to a molecular weight of $\sim$ 20 kDa. At 1.5 and 2 Cu / protein, the monomeric peak is missing with only dimeric species present ($\sim$ 10.9 mL). This species distribution is similar to that observed in the mass spectra above.

The titration of Cu(I) into CopZ-3079 monitored by absorbance (**Figure 7.3.4B**) shows changes in A_{240nm} and A_{300nm} with increasing Cu(I) level, which are in agreement with the gel filtration data. At 1 Cu / CopZ-3079 distinct breakpoints are seen at both wavelengths, and beyond this point the absorbance continually increases until a level of 2 Cu / protein is reached. These trends are consistent with the ESI-MS data above, where a decrease in monomer peak intensity was observed beyond 1 Cu / protein, favouring formation of dimeric Cu_6CopZ-3079_2.

7.3.2 ESI-MS of Cu(I) Binding To CopZ-3079 In The Presence Of DTT

In order to examine the effect of LMWT upon Cu(I) binding by CopZ-3079, mass spectra were recorded of 2 Cu / CopZ-3079 in the presence of 5, 10 and 40 DTT / protein. The mass spectra prior to deconvolution are presented in **Figure 7.3.5**, revealing a fairly similar peak distribution at all levels of DTT. Compared to the spectrum in the absence of DTT (Fig 7.3.1), the monomer and dimer peak envelopes have not shifted, suggesting that CopZ-3079 does not undergo major conformational changes in the presence of DTT and no DTT adduct envelopes are observed. The dimer envelope intensity has greatly diminished, though there is a low-intensity dimer peak with 9+ charges. The monomer peaks are most intense with 5+ and 6+ charges being predominant, and a low intensity peak with 4+ charges.

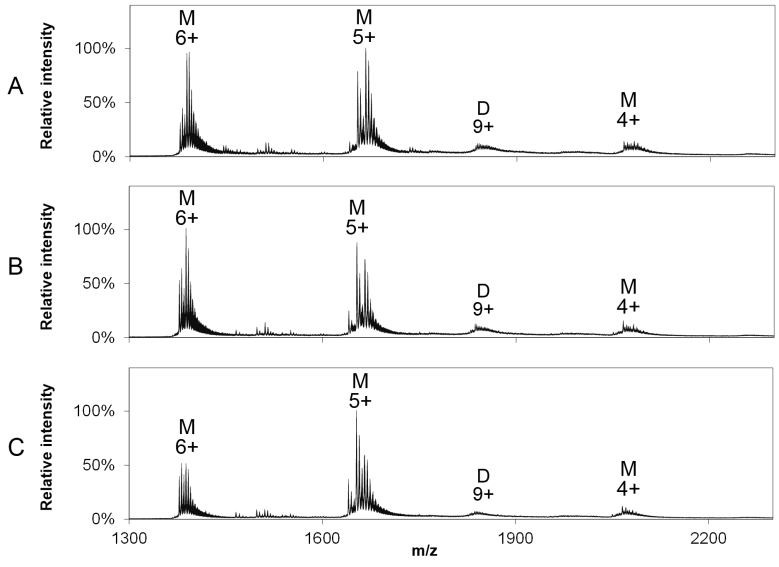

Figure 7.3.5: Mass spectra for 2 Cu / CopZ-3079 at varied DTT levels. The mass spectra prior to deconvolution of CopZ-3079 prepared at 2 Cu / protein in the presence of: **A)** 5 DTT / protein, **B)** 10 DTT / protein, **C)** 40 DTT / protein.

The deconvoluted mass spectra in **Figure 7.3.6** illustrate the mixture of species present, and their observed masses and intensities are presented in **Table 7.2**, and the relative intensities of species present in the deconvoluted mass spectra are presented as bar graphs in **Figure 7.3.7**. The spectra illustrate that a substantial proportion of the protein appears as sodiated adducts. However, because these peaks occur in roughly equal proportion to the protein species themselves, the relative intensities have been assigned based upon the protein peaks alone. The species distribution is fairly similar at all levels of DTT, with the dimer species being suppressed in favour of formation of Cu_2CopZ-3079 at first (5 and 10 DTT / protein) and then the formation of CuCopZ-3079 (40 DTT / protein). Low-intensity dimer peaks remain with a small amount of Cu_2(CopZ-3079)$_2$.

The observed masses, on average, are slightly less than the predicted masses. For CopZ-3079 and Cu(CopZ-3079)$_2$ this could be explained by intramolecular disulfide formation. However, for the other copper-bound species the reason for these mass shifts is not entirely clear.

Table 7.2: Species observed via ESI-MS of 2 Cu / CopZ-3079 at varied DTT levels. Observed masses and relative intensities for CopZ-3079 prepared at 2 Cu / protein in the presence of 5, 10 and 40 DTT / protein.

Species	Pred (Da)	5 DTT / CopZ		10 DTT / CopZ		40 DTT / CopZ	
CopZ	8199.9	2%	8198.6	8%	8198.6	14%	8199.0
CuCopZ	8262.4	44%	8261.3	67%	8261.5	100%	8261.6
Cu_2CopZ	8324.9	100%	8323.6	100%	8323.1	76%	8323.9
Cu(CopZ)$_2$	16462.4	0%	–	5%	16459.6	4%	16459.4
Cu_2(CopZ)$_2$	16524.9	11%	16518.9	18%	16519.8	14%	16521.4
Cu_3(CopZ)$_2$	16587.4	7%	16582.6	8%	16583.0	6%	16586.9
Cu_4(CopZ)$_2$	16649.9	8%	16651.6	0%	–	4%	16649.2

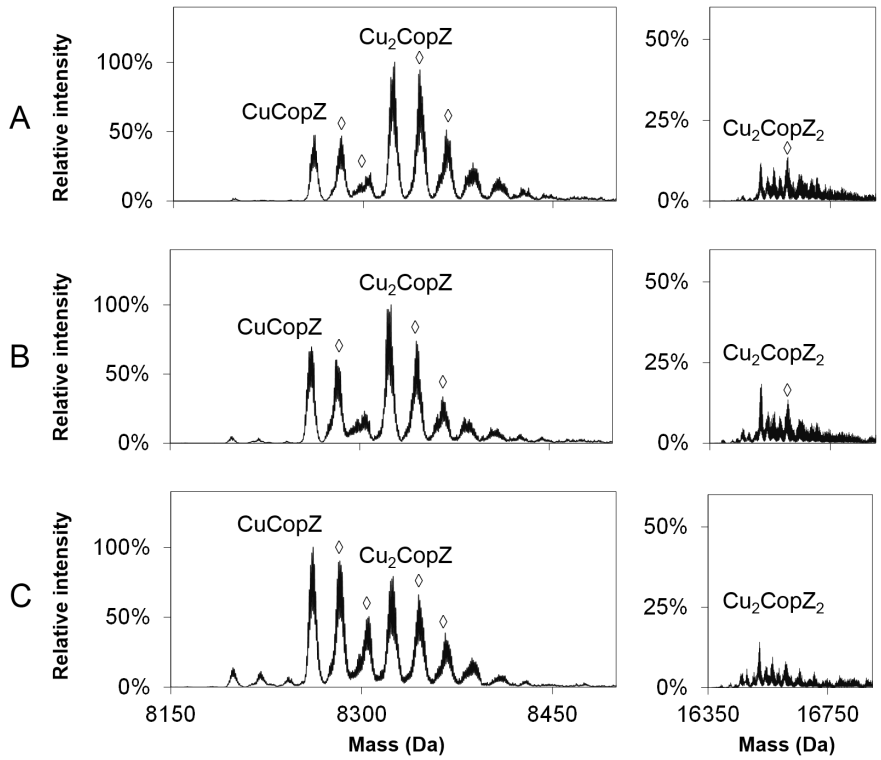

Figure 7.3.6: Deconvoluted mass spectra for 2 Cu / CopZ-3079 at varied DTT levels. Deconvoluted mass spectra of CopZ-3079 prepared at 2 Cu / protein in the presence of: **A)** 5 DTT / protein, **B)** 10 DTT / protein, **C)** 40 DTT / protein. Na+ adducts indicated by ◊ symbols.

Bar graphs in **Figure 7.3.6** illustrate the species distribution at each DTT loading. In the absence of DTT, the most intense species present was Cu_6CopZ-3079_2, but in the presence of DTT, this and other dimer species are not present. With increasing DTT level, the dimer species distribution shows slight tendency toward formation of Cu_2(CopZ-$3079)_2$, but overall the dimer species have been abolished. At 5 and 10 DTT / protein, the dominant species is Cu_2CopZ-3079 with a progressive increase in intensity of CuCopZ-3079 until it becomes the most intense peak at 40 DTT / protein.

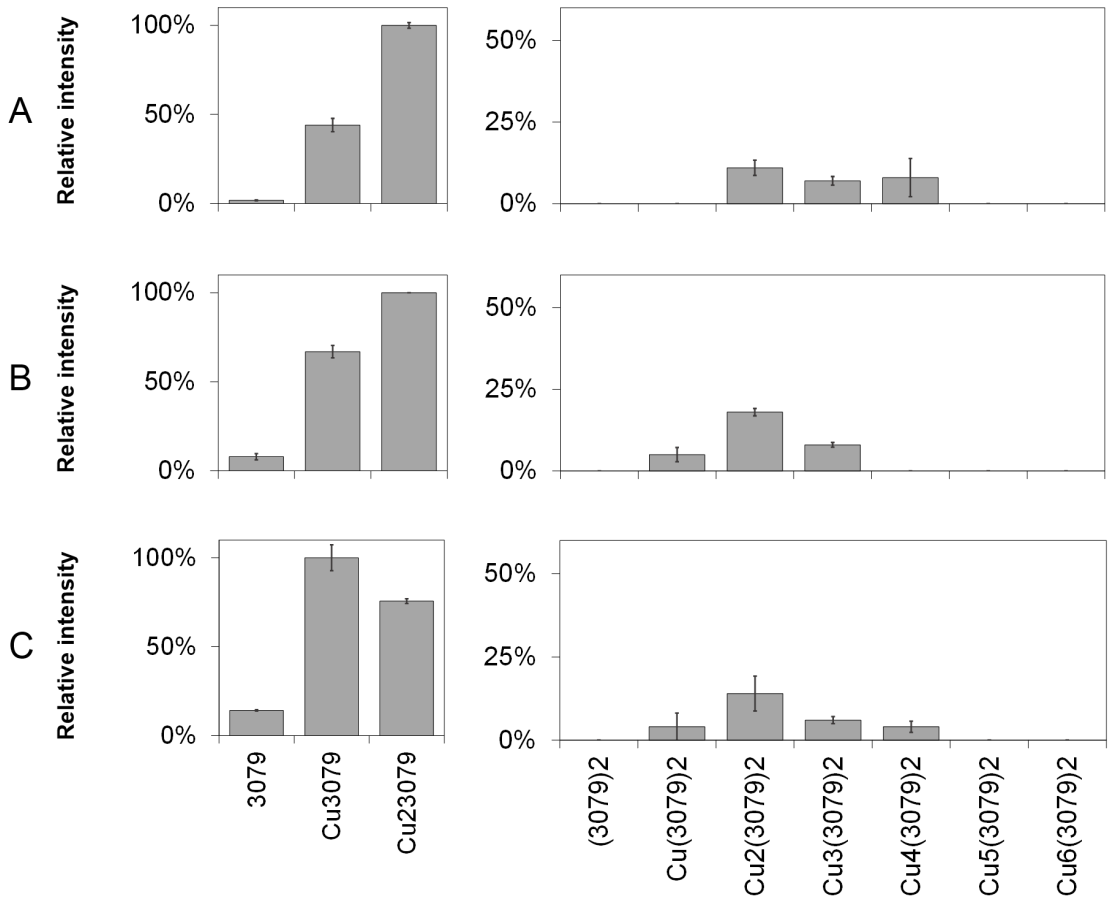

Figure 7.3.7: Species observed via ESI-MS of 2 Cu / CopZ-3079 at varied DTT levels. Species present in deconvoluted mass spectra of 2 Cu / CopZ-3079 prepared at a level of: **A)** 5 DTT / protein, **B)** 10 DTT / protein, **C)** 40 DTT / protein.

7.3.3 ESI-MS Of Cu(I) Binding To CopZ-1317

In order to investigate the Cu(I)-binding behaviour of CopZ-1317, mass spectra were recorded of CopZ-1317 in the presence of 0, 1 and 2 Cu / protein (**Figure 7.3.8**). In the absence of copper, the monomer peak envelope was predominant with 5+ and 6+ charges, with low intensity dimer peaks present possessing 8+ and 9+ charges. In the presence of copper, the position of these charge state envelopes did not shift suggesting no major conformational changes in the presence of copper. The intensities of the dimer peaks increased, and a trimeric peak envelope emerged with 11+, 12+ and 13+ charges. This suggests a diverse mixture of CopZ-1317 metalloforms.

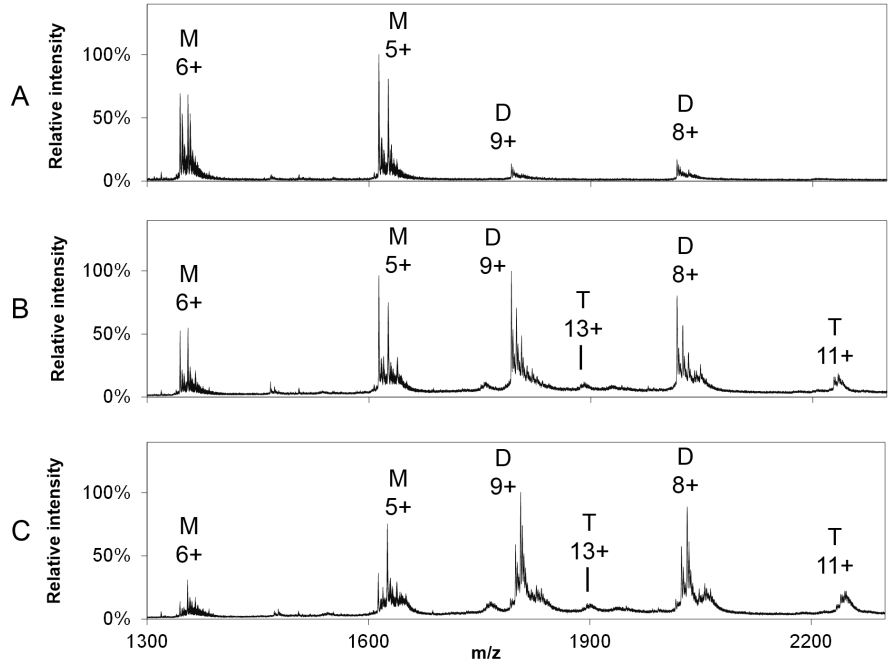

Figure 7.3.8: Mass spectra for CopZ-1317 at varied Cu(I) levels. The mass spectra prior to deconvolution of CopZ-1317 prepared at a level of: **A)** 0.0 Cu / protein, **B)** 1 Cu / protein, **C)** 2 Cu / protein.

The deconvoluted mass spectra (**Fig 7.3.9**) illustrate the CopZ-1317 species which form in the presence of increasing Cu(I) levels. In the absence of copper, the major species is apo-CopZ-1317. However, the presence of a significant CuCopZ-1317 peak suggests that the sample contained some copper despite being prepared without copper added. At 1 Cu / protein, the most intense species is disulfide-bonded CopZ-1317_2; the copper-bound species present are CuCopZ-1317, Cu(CopZ-$1317)_2$ and Cu_2(CopZ-$1317)_2$. These are the major copper-bound species at 2 Cu / protein as well, though their intensities shift to favour Cu_2(CopZ-$1317)_2$, with the intensity of the CopZ-1317_2 peak having decreased substantially.

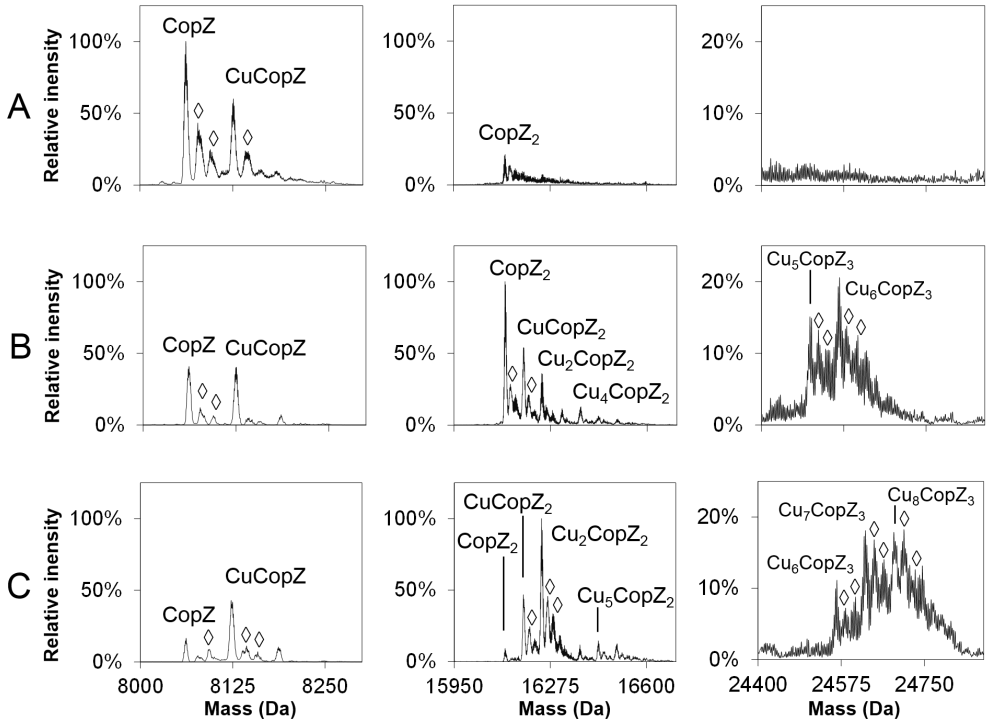

Figure 7.3.9: Deconvoluted mass spectra for CopZ-1317 at varied Cu(I) levels. Deconvoluted mass spectra of CopZ-1317 prepared at a level of: **A)** 0.0 Cu / protein, **B)** 1 Cu / protein, **C)** 2 Cu / protein. Na+ adducts indicated by ◊ symbols.

Most of the monomer peaks have an exact mass within a 1 – 2 Da of their predicted mass. For the dimeric species, the agreement is variable between predicted and observed exact mass, see **Table 7.3**. The reduced mass of CopZ-1317_2 could be explained by disulfide bond formation. The dimeric species with 3, 4, 5 and 6 coppers bound are mostly within 2 – 3 Da of their predicted mass. The species Cu(CopZ-$1317)_2$ and Cu_2(CopZ-$1317)_2$ are $\sim$ 6 Da less than their predicted mass, despite being of high relative intensity. Typically the mass becomes closer to the expected mass with increasing peak intensity but, here, that is not the case. The intensity of trimeric species is roughly within 2 Da except for Cu_8CopZ-1317_3.

Table 7.3: Species observed via ESI-MS for CopZ-1317 at varied Cu(I) levels. Observed masses and relative intensities when CopZ-1317 prepared at: 0, 1 and 2 Cu / protein.

Species	Pred (Da)	0 Cu / CopZ		1.0 Cu / CopZ		2.0 Cu / CopZ	
CopZ	8063.8	100%	8061.7	46%	8061.5	5%	8061.8
CuCopZ	8126.3	59%	8125.6	34%	8124.7	29%	8124.4
Cu_2CopZ	8188.8	0%	–	6%	8185.8	4%	8188.2
$CopZ_2$	16127.7	22%	16123.6	100%	16123.0	21%	16121.9
$Cu(CopZ)_2$	16190.2	0%	–	73%	16184.4	53%	16184.5
$Cu_2(CopZ)_2$	16252.7	0%	–	53%	16245.6	100%	16246.0
$Cu_3(CopZ)_2$	16315.2	0%	–	20%	16313.9	0%	–
$Cu_4(CopZ)_2$	16377.7	0%	–	24%	16376.7	13%	16375.5
$Cu_5(CopZ)_2$	16440.2	0%	–	15%	16440.1	26%	16437.4
$Cu_6(CopZ)_2$	16502.7	0%	–	10%	16502.1	24%	16500.0
$Cu_5(CopZ)_3$	24504.0	0%	–	24%	24502.6	8%	24502.2
$Cu_6(CopZ)_3$	24566.5	0%	–	35%	24565.1	18%	24565.0
$Cu_7(CopZ)_3$	24629.0	0%	–	0%	–	27%	24626.8
$Cu_8(CopZ)_3$	24691.5	0%	–	0%	–	27%	24686.7

The bar graphs in **Figure 7.3.10** illustrate the distribution of CopZ-1317 species with increasing Cu(I) levels. At 1 Cu / protein, a diverse mixture of species is observed with the major species being disulfide bonded CopZ-1317_2. This would not likely form under

the reducing conditions of the cell and most likely indicates some sort of oxidative driving force in the sample. The next most intense species is $Cu(CopZ\text{-}1317)_2$ with a substantial intensity of CuCopZ-1317 and $Cu_2(CopZ\text{-}1317)_2$ as well. Also observed are trimeric species with 5 and 6 coppers bound. When the copper level is increased to 2 Cu / protein, the major species shifts to $Cu_2(CopZ\text{-}1317)_2$, with approximiately equal proportions of CuCopZ-1317 and $Cu(CopZ\text{-}1317)_2$. The relative intensity of other dimeric copper-bound species has not increased. The relative intensity of the trimeric copper-bound species also has not increased but has shifted to form higher copper loaded trimeric species.

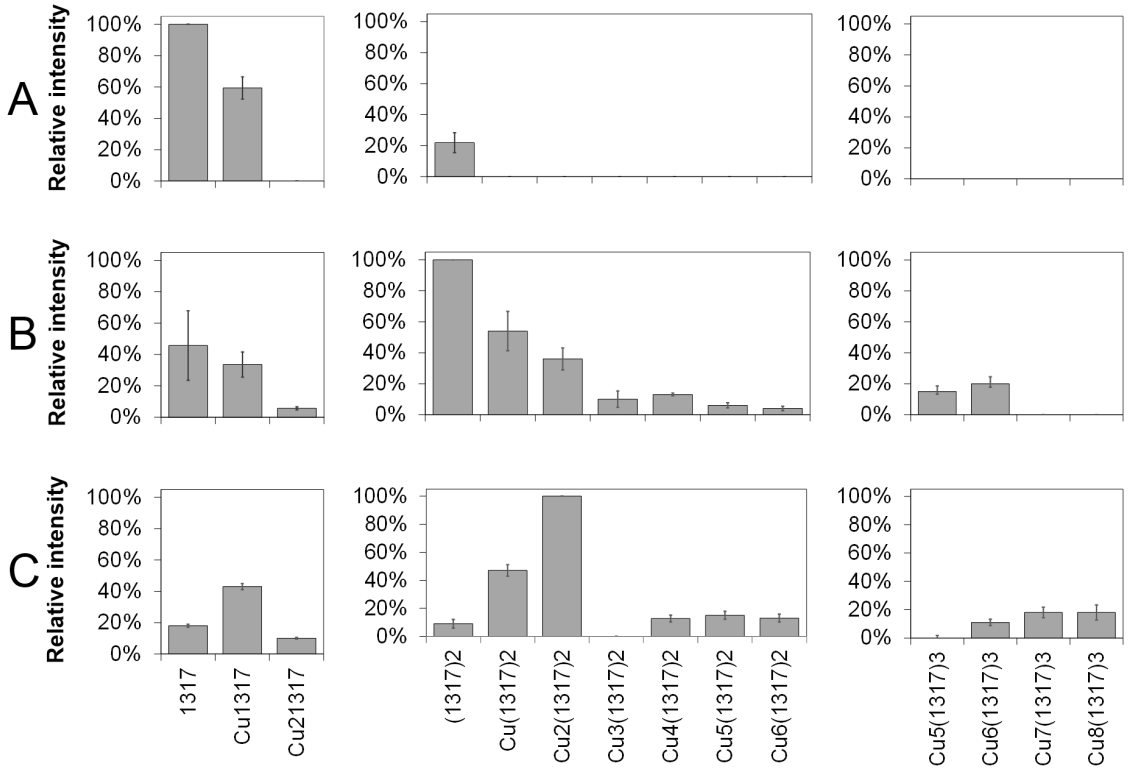

Figure 7.3.10: Species observed via ESI-MS of CopZ-1317 at varied Cu(I) loadings. Species present in deconvoluted mass spectra of CopZ-1317 prepared at a level of: **A)** 0.0 Cu / protein, **B)** 1 Cu / protein, **C)** 2 Cu / protein.

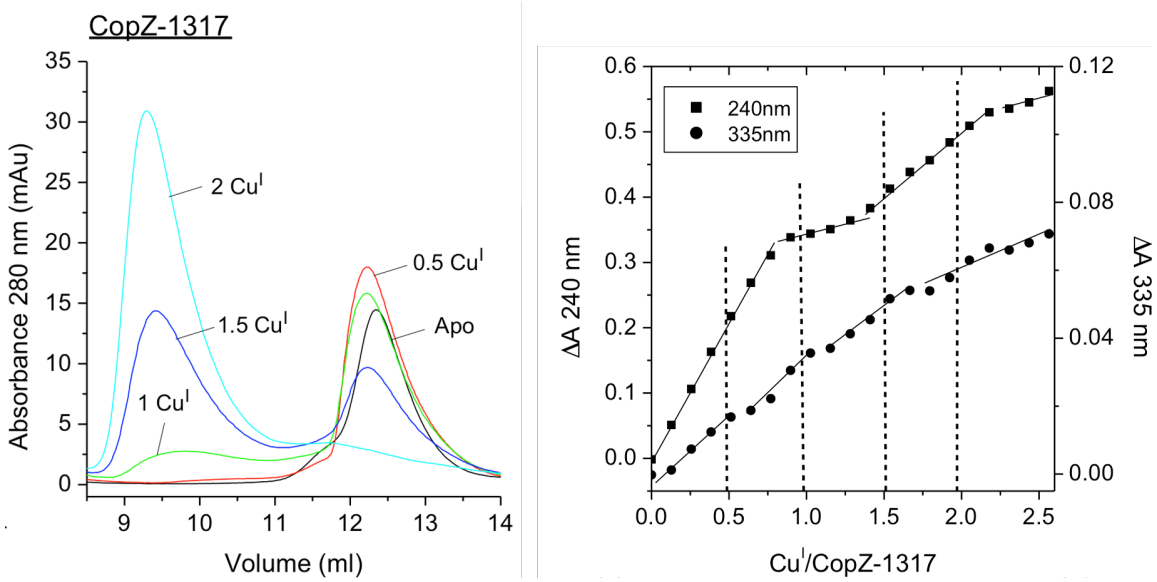

Figure 7.3.11: Size exclusion chromatography at multiple Cu(I) levels and UV-vis Cu(I) titration for CopZ-1317. Previous data, acquired previously [192], of: **A)** Size exclusion of CopZ-1317 prepared at molar equivalents of Cu(I) as labelled **B)** Cu(I) binding by CopZ-1317 monitored using UV-visible absorbance changes at 20 °C, pH 7.5. The absorbance changes observed for CopZ-1317 at 240 nm and 335 nm plotted as a function of Cu(I)/CopZ-1317 (CopZ-1317, 39 μM). Samples of CopZ-1317 were prepared in 10 mM MOPS pH 7.5, 150 mM NaCl under anaerobic conditions, adding 0.5, 1.0, 1.5 or 2 molar equivalents of Cu(I) to reduced CopZ-1317. Apo-CopZ-1317 concentrations were determined at 280 nm using extinction coefficients based upon ProtParam ExPASy and concentrations calculated using the Beer Lambert law. Size exclusion elution profiles created by monitoring the absorbance at 280 nm on a 10/300 GL G-75 Superdex column (GE-Healthcare) equilibrated in sample buffer. Absorbance measurements were carried out on a a Varian Cary 50 UV-visible spectrophotometer set at 20 °C.

In order to compare the above data to solution-phase experiments, **Figure 7.3.11** presents unpublished data, acquired previously [192]: size exclusion chromatography of CopZ-1317 at multiple copper loadings, and UV-vis absorbance data obtained when Cu(I) was titrated into a solution of CopZ-1317.

The size exclusion chromatography elution profiles of CopZ-1317 at increasing ratios of Cu / protein illustrate that this protein forms higher order complexes in the presence

of increased Cu(I) level. According to the column calibration, the apo protein is entirely monomer. CopZ-1317 remains predominantly monomeric at 1 molar equivalent of Cu(I) with a peak at $\sim$ 12.3 mL elution volume. At 2 molar equivalents of Cu(I) CopZ-1317 exists primarily as a higher order assembly at an elution volume of $\sim$ 9.4 mL corresponding to a molecular weight of $\sim$ 43 kDa. This suggests that CopZ-1317 is some form of higher-order assembly (trimer or tetramer) upon addition of 2 molar equivalents of Cu(I), however the higher order peak centred on $\sim$ 9.4 mL has a shoulder, perhaps illustrating a mixture of higher-order species.

The titration of Cu(I) into CopZ-1317 monitored by absorbance (**Figure 7.3.11B**) shows changes in A_{240nm} and A_{335nm} with increasing Cu(I) level. The absorbance changes are complex and it is difficult to make predictions of the species distribution. The progressively increased absorbance suggests continuing binding of Cu(I) by CopZ-1317. There is a slight breakpoint at 1 Cu / protein which could support the speciation change observed in the mass spectra between 1 and 2 Cu / protein where the dimeric copper-bound forms of CopZ-1317 become predominant.

7.3.4 ESI-MS Of Cu(I) Binding To CopZ-1317 In The Presence Of DTT

In order to examine the effects of LMWT on Cu(I) binding, mass spectra were recorded for CopZ-1317 prepared with 2 molar equivalents copper, plus 1, 5 and 20 DTT / protein (**Figure 7.3.12**). At 1 DTT / protein, the relative intensities of the monomer and dimer peak envelope are similar to those observed in the absence of thiol. When the DTT level is increased to 5 / protein, a decrease in intensity of dimer peaks (8+ and 9+ charges) is accompanied by an increase in relative intensity of the monomer peaks (5+ and 6+ charges). There is a further decrease in the dimer peaks' relative intensity at 20 DTT / protein. Also present are adduct peaks at +405 Da (monomer) and +812 Da (dimer), suggesting each monomer has acquired an adduct species of $\sim$ 405 – 406 Da. With increasing DTT levels, the relative intensity of these adduct peaks progressively decreases.

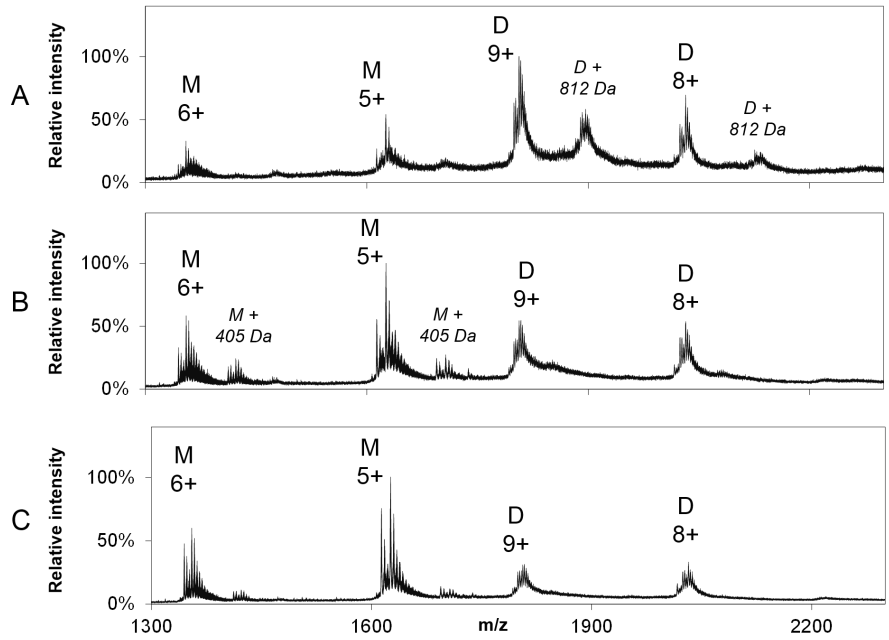

Figure 7.3.12: Mass spectra for 2 Cu/CopZ-1317 at varied DTT levels. The mass spectra prior to deconvolution of CopZ-1317 prepared at 2 Cu / protein in the presence of: **A)** 1 DTT / protein, **B)** 5 DTT / protein, **C)** 20 DTT / protein.

The deconvoluted mass spectra (**Figure 7.3.13**) illustrate changes in CopZ-1317 species distribution with increasing levels of DTT. The relative intensities of species present in the deconvoluted mass spectra of CopZ-1317 in the presence of DTT are presented as bar graphs in **Figure 7.3.14**, with the exact masses and relative intensities presented in **Table 7.4**.

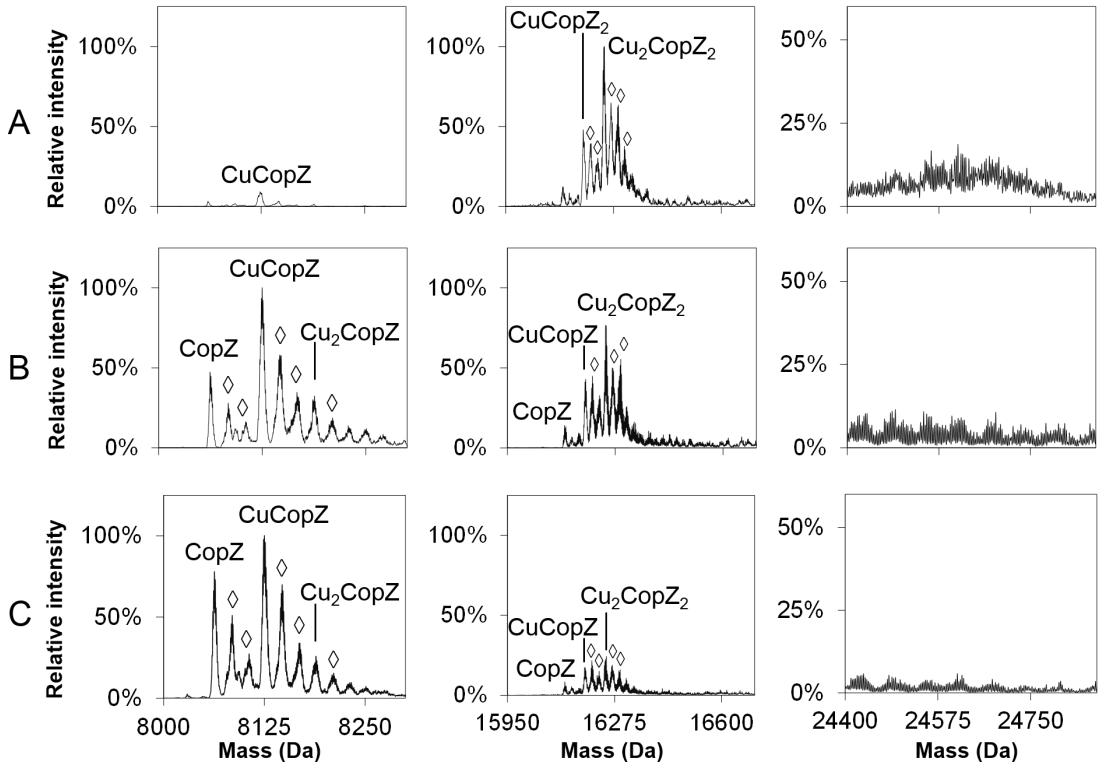

Figure 7.3.13: Deconvoluted mass spectra for 2 Cu/CopZ-1317 at varied DTT levels. Deconvoluted mass spectra of CopZ-1317 prepared at 2 Cu / protein in the presence of: **A)** 1 DTT / protein, **B)** 5 DTT / protein, **C)** 20 DTT / protein. Diamond symbols represent Na+ adducts.

At 1 DTT / protein, the species distribution is similar to that recorded in the absence of thiol at 2 molar equivalents of copper (**Fig 7.3.9**). The distinct differences are that the low-intensity copper-bound dimeric and trimeric species are not observed, and the relative intensity of CuCopZ-1317 has decreased. However, similarly, the predominant copper-

bound species is Cu_2(CopZ-1317)$_2$, the intensity of Cu(CopZ-1317)$_2$ peak is sizable, and low intensity peaks of apo-CopZ-1317 and disulfide bonded (CopZ-1317)$_2$ can be seen.

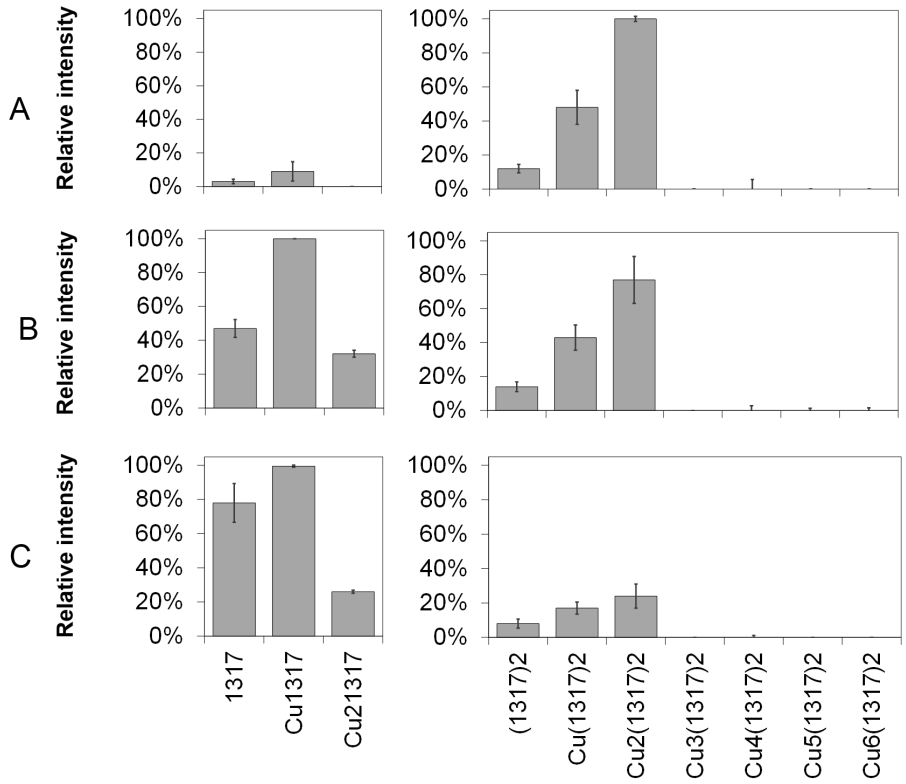

Figure 7.3.14: Species observed for 2 Cu/CopZ-1317 at varied DTT levels. Species present in deconvoluted mass spectra of 2 Cu / CopZ-1317 prepared at a level of: **A)** 1 DTT / protein, **B)** 5 DTT / protein, **C)** 20 DTT / protein.

When the DTT level is increased to 5 / protein, the intensity of the monomeric peaks increases, though a substantial proportion of copper-bound dimeric species is present. The major copper-bound species is CuCopZ-1317, with a large proportion of Cu(CopZ-1317)$_2$ and Cu_2(CopZ-1317)$_2$ are present.

At 20 DTT / protein, the dimer peaks are almost eliminated entirely, with copper-bound monomer species prevailing. The intensity of dimeric species Cu(CopZ-1317)$_2$ and Cu_2(CopZ-1317)$_2$ has diminished. The predominant peak is CuCopZ-1317, and the pro-

Table 7.4: Species observed for 2 Cu/CopZ-1317 at varied DTT levels. Observed masses and relative intensities for CopZ-1317 prepared at 2 Cu(I) / protein in the presence of 1, 5 and 20 DTT / protein.

Species	Pred (Da)	1 DTT / CopZ		5 DTT / CopZ		20 DTT / CopZ	
CopZ	8063.8	3%	8061.3	47%	8062.6	78%	8063.2
CuCopZ	8126.3	9%	8124.7	100%	8124.7	100%	8125.2
Cu_2CopZ	8188.8	0%	–	32%	8188.0	26%	8188.5
$CopZ_2$	16127.7	12%	16122.7	14%	16123.8	8%	16123.8
$Cu(CopZ)_2$	16190.2	48%	16185.0	43%	16185.3	17%	16185.6
$Cu_2(CopZ)_2$	16252.7	100%	16246.6	77%	16247.0	24%	16247.6

portion of apo-CopZ-1317 increased.

The exact masses observed for the monomeric species are within $\sim$ 2 Da of the expected mass. The dimeric species are lower than that expected, by $\sim$ 4 – 5 Da. Though intra- and intermolecular disulfide bonds are possible for apo-CopZ-1317 and $(CopZ\text{-}1317)_2$, respectively, the reason for the other mass differences is not clear.

Increasing the proportion of DTT seems to favour formation of CuCopZ-1317 as the major copper-bound species, and results in a large apo-CopZ-1317 peak. This species distribution does not account for the initial copper level of the sample, and suggests that DTT competes against the protein for copper, but does not ionise, leaving the highest-affinity species to form, CuCopZ-1317.

7.4 Results: Cu(I) Binding To Atx1 From *Saccharomyces cerevisiae*

7.4.1 ESI-MS Of Cu(I) Binding To Atx1

In order to investigate the copper-binding behaviour of Atx1, mass spectra were recorded for Atx1 prepared with Cu(I) at 0, 0.5, 1.0, 1.5 and 2.0 Cu / protein. The mass spectra prior to deconvolution (**Figure 7.4.1**) illustrate a series of overlapping peak envelopes corresponding to monomer, dimer and trimer species. In the absence of copper, the monomer peaks (4+, 5+, 6+) are predominant. Upon addition of 0.5 Cu / protein, additional peak envelopes emerge corresponding to dimer (7+, 8+, 9+) and trimer (10+, 11+, 12+, 13+). The subsequent copper loadings contain a similar distribution of species, indicating a mixture of monomeric, dimeric and trimeric Atx1 is present. The positions of these peak envelopes are in accord with that observed for the prokaryotic copper chaperones. The location of these envelopes do not shift upon addition of copper suggesting no major conformational changes upon binding of copper. As the copper level is increased, the monomer peak envelope decreases in intensity with a concomitant increase in the intensity of the dimeric peaks, while the intensity of the trimeric peaks remains consistently low.

The deconvoluted mass spectra of Atx1 in the presence of copper (**Figure 7.4.2**) reveal the mixture of species present. The intensities and exact neutral masses observed are reported in **Table 7.5**, and the peak intensities are presented as a bar graph in **Figure 7.4.3**.

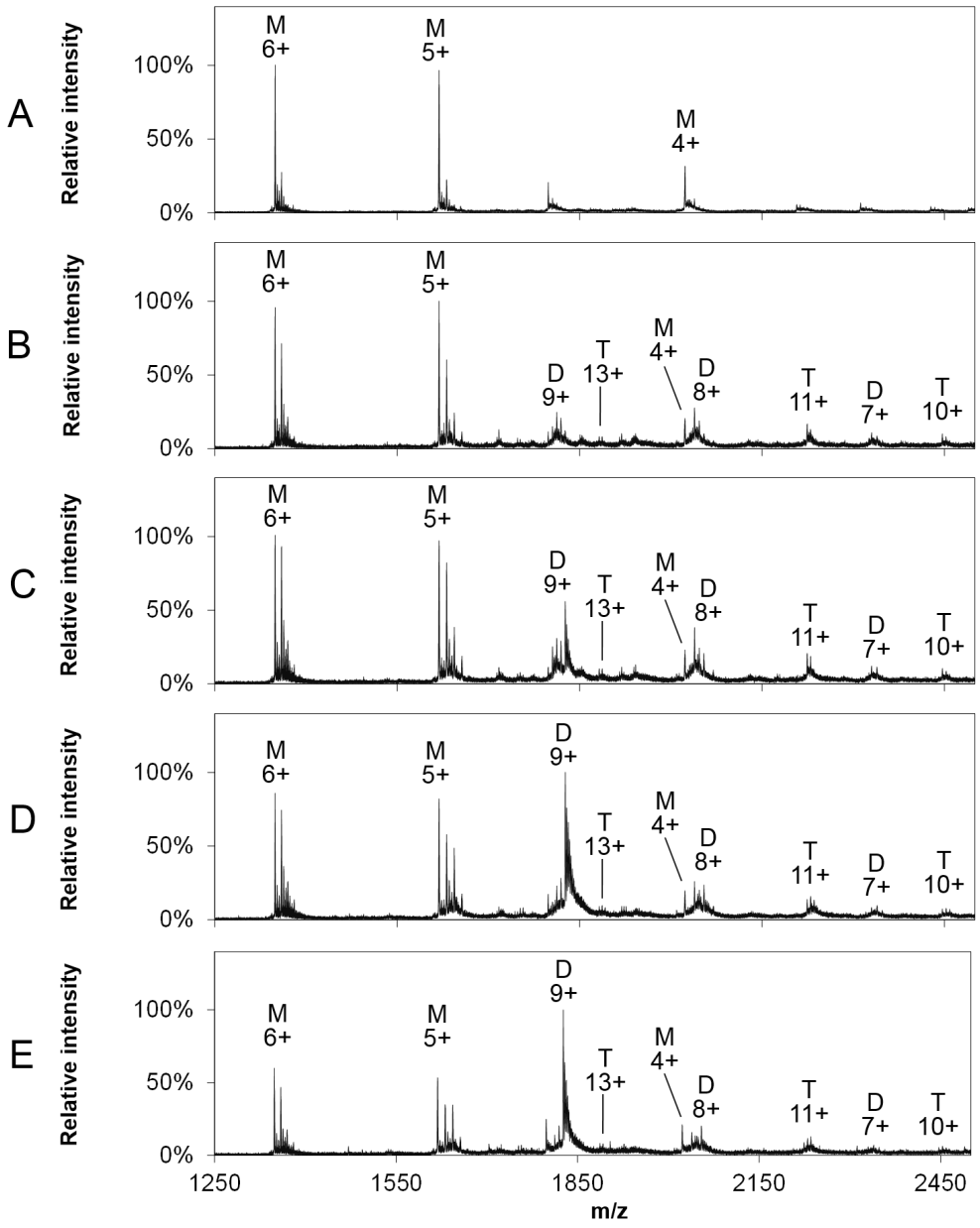

Figure 7.4.1: Mass spectra for Atx1 at varied Cu(I) levels. Species present in the mass spectra prior to deconvolution of Atx1 prepared at a level of: **A)** 0 Cu(I) / protein, **B)** 0.5 Cu / protein, **C)** 1.0 Cu / protein, **D)** 1.5 Cu / protein, **E)** 2.0 Cu / protein.

In the absence of copper, the Atx1 mass spectrum contains mostly apo-Atx1 whose mass (8089.4 Da) reflects the loss of the N-terminal methionine, a typical eukaryotic post-translational modification. Also observed are low-intensity peaks for disulfide bonded species: $(Atx1)_2$ and $(Atx1)_3$. Also present is a low-intensity peak ($\sim$ 19%) in agreement with the predicted mass of CuAtx1, suggesting that, despite that no copper was added, a small amount of copper is present in the sample.

Table 7.5: Species observed via ESI-MS for Atx1 at varied Cu(I) levels. Observed masses and relative intensities for Atx1 prepared at 0, 0.5, 1, 1.5 and 2 Cu / protein.

Species	Pred (Da)	0 Cu / Atx1		0.5 Cu / Atx1		1.0 Cu / Atx1		1.5 Cu / Atx1		2.0 Cu / Atx1	
Atx1	8089.4	100%	8088.5	100%	8087.5	100%	8088.4	100%	8088.4	85%	8088.3
CuAtx1	8151.9	19%	8151.8	53%	8151.2	66%	8151.2	75%	8151.2	69%	8150.6
Cu_2Atx1	8214.4	0%	-	13%	8214.0	13%	8210.3	20%	8211.6	15%	8210.6
$(Atx1)_2$	16178.8	23%	16176.4	15%	16174.5	16%	16174.5	35%	16174.9	57%	16174.9
$Cu(Atx1)_2$	16241.3	10%	16240.1	9%	16238.6	9%	16238.6	7%	16239.6	7%	16238.6
$Cu_2(Atx1)_2$	16303.8	6%	16303.7	23%	16302.6	28%	16302.6	23%	16303.9	19%	16303.4
$Cu_3(Atx1)_2$	16366.3	0%	-	16%	16365.4	18%	16365.7	30%	16366.1	23%	16366.3
$Cu_4(Atx1)_2$	16428.8	0%	-	14%	16428.2	41%	16428.8	93%	16428.8	100%	16428.8
$(Atx1)_3$	24268.1	13%	24267.3	5%	24261.9	5%	24259.1	13%	24264.2	12%	24262.3
$Cu_3(Atx1)_3$	24455.6	0%	-	17%	24454.0	19%	24456.8	24%	24455.2	14%	24455.6
$Cu_4(Atx1)_3$	24518.1	0%	-	12%	24516.2	19%	24519.3	36%	24518.9	32%	24518.8
$Cu_5(Atx1)_3$	24580.6	0%	-	0%	-	6%	24579.6	30%	24580.4	34%	24581.1
$Cu_3(Atx1)_4$	32545	0%	-	7%	32544.8	7%	32545.1	6%	32544.8	7%	32544.8
$Cu_4(Atx1)_4$	32607.5	0%	-	14%	32604.8	16%	32609.1	22%	32609.4	14%	32609.4
$Cu_5(Atx1)_4$	32670	0%	-	0%	-	8%	32673.2	11%	32673.2	10%	32673.2
$Cu_4(Atx1)_5$	40696.9	0%	-	4%	40698.7	4%	40701.8	7%	40702.4	7%	40702.1
$Cu_5(Atx1)_5$	40759.4	0%	-	6%	40756.5	7%	40766.4	8%	40766.4	6%	40766.4

With the addition of 0.5 Cu / protein, a mixture of monomeric, dimeric and trimeric species is observed, with the major copper-bound species being CuAtx1 and the most intense peak overall is apo-Atx1. The proportion of disulfide-bonded $(Atx1)_2$ and $(Atx1)_3$ has decreased slightly. In addition to CuAtx1 ($\sim$ 53% relative intensity), a second monomeric copper-bound species, Cu_2Atx1 is present. A variety of dimeric/trimeric copper-bound species are observed, all below 25% relative intensity, the most intense of which is Cu_2Atx1_2.

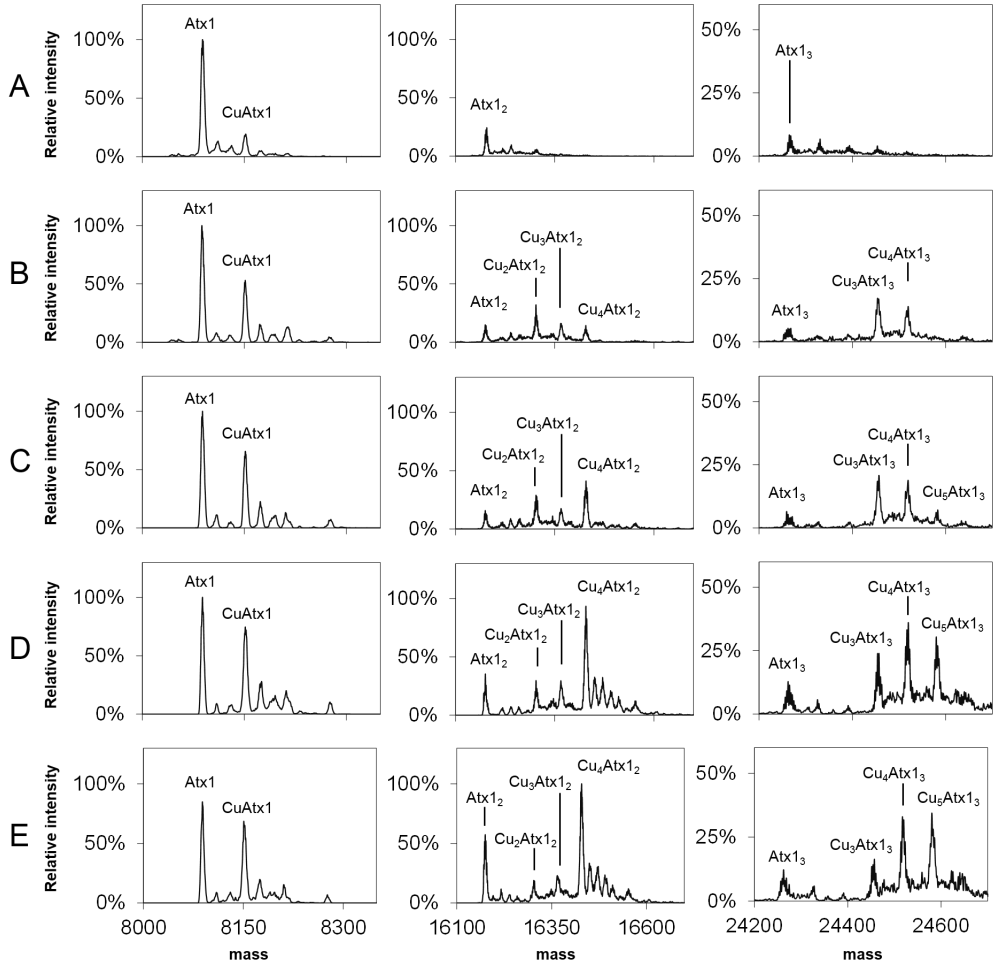

Figure 7.4.2: Deconvoluted mass spectra for Atx1 at varied Cu(I) levels. Deconvoluted mass spectra of Atx1 prepared at a level of: **A)** 0 Cu(I) / protein, **B)** 0.5 Cu / protein, **C)** 1.0 Cu / protein, **D)** 1.5 Cu / protein, **E)** 2.0 Cu / protein.

At 1.0 Cu / protein, the species distribution is similar to that at 0.5 Cu / Atx1. The predominant species is apo-Atx1, and the most prominent copper-bound peak is CuAtx1, though its relative intensity has now increased to $\sim$ 66%. Again, a diverse mixture of dimeric and trimeric copper-bound peaks is observed, mostly below 25% relative intensity. One distinct change at this copper loading, is the increase in intensity of Cu_4Atx1_2 to 41% relative intensity.

At 1.5 Cu / protein, the predominant species is still marginally apo-Atx1, with the inten-

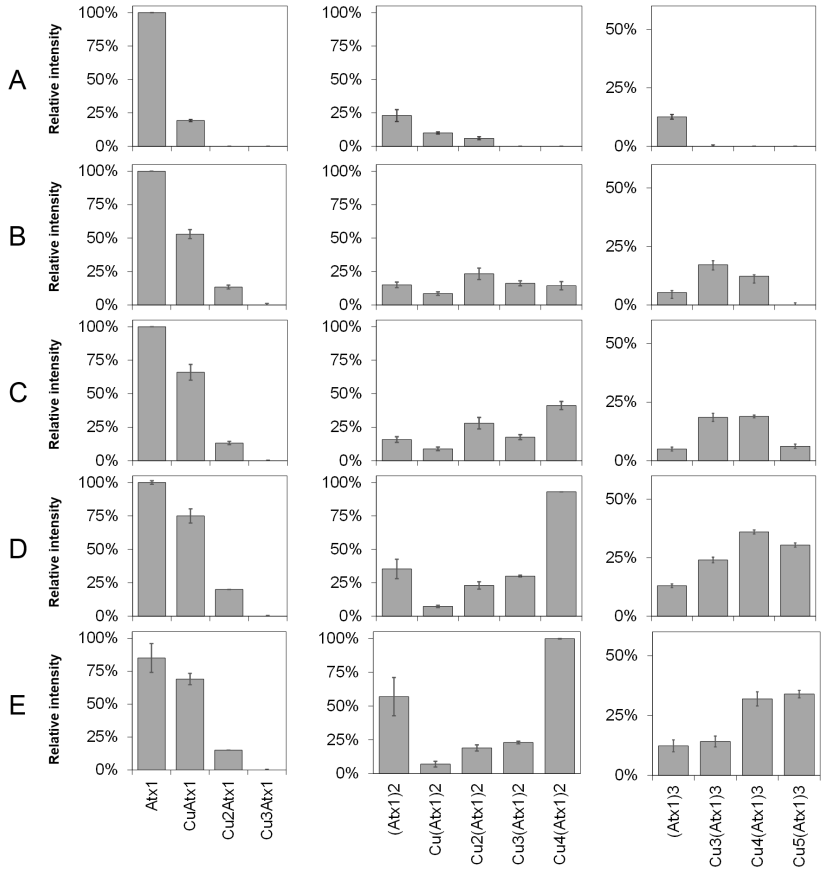

Figure 7.4.3: Species observed via ESI-MS for Atx1 at varied Cu(I) levels. Species present in deconvoluted mass spectra of Atx1 prepared at a level of: **A)** 0 Cu(I) / protein, **B)** 0.5 Cu / protein, **C)** 1.0 Cu / protein, **D)** 1.5 Cu / protein, **E)** 2.0 Cu / protein.

sity of the Cu_4Atx1_2 peak having increased to 93% relative intensity. The intensities of the other dimeric forms have stayed relatively similar to that observed at 1.0 Cu / protein, as does the monomeric Cu_2Atx1. The intensities of the peaks for disulfide-bonded $Atx1_2$ and $Atx1_3$ have increased slightly. The relative intensities of the trimeric copper-bound peaks have increased, with the most intense species being Cu_4Atx1_3.

At 2.0 Cu / protein, the most intense species becomes Cu_4Atx1_2, with still a large proportion of apo-Atx1. The intensities of the peaks for disulfide-bonded $Atx1_2$ and $Atx1_3$ have increased further from that observed at 1.5 Cu / protein. The intensities of monomeric

CuAtx1 and Cu_2Atx1, and also the 1-, 2-, and 3-copper dimeric forms have stayed relatively similar to that observed at 1.5 Cu / protein. The peak intensities of the copper-bound trimeric peaks stays fairly similar to that observed at 1.5 Cu / protein, except for a slight decrease in the Cu_3Atx1_3 species.

The exact masses observed for Atx1 species are mostly within $\sim 1 - 2$ Da of their predicted mass. The decreased mass observed for apo-Atx1, $Atx1_2$, and $Atx1_3$ are likely due to intra- and intermolecular disulfide bond formation. The decreased mass observed for the Cu_2Atx1 peak could be attributed to its low intensity, in which case overlap with a trisodiated adduct of CuAtx1 influences the peak position. A similar influence could occur for the trimeric Atx1 peaks. For example, Cu_4Atx1_3 occurs at a lower mass than expected when at 12% relative intensity (0.5 Cu/protein), but in subsequent spectra, when the peak relative intensity is higher, the observed mass is close to the predicted mass.

7.4.2 ESI-MS Of Cu(I) Binding To Atx1 In The Presence Of DTT

In order to observe the species present when copper-loaded Atx1 is mixed with progressively increasing levels of thiol, mass spectra were recorded for 2 Cu / Atx1 at 5, 10 and 20 DTT / protein and are presented in **Figure 7.4.4**. The mass spectrum prior to deconvolution in the absence of thiol revealed a mixture of monomer, dimer and trimer peaks with the dimer envelope being predominant. In the presence of DTT, the same species can be seen as the peak envelopes are not shifted appreciably: monomer (4+, 5+ 6+), dimer (7+, 8+, 9+) and trimer (10+, 11+, 12+, 13+) observed. However, the intensities of the dimer and trimer envelopes are diminished significantly reflecting loss of intensity of these species.

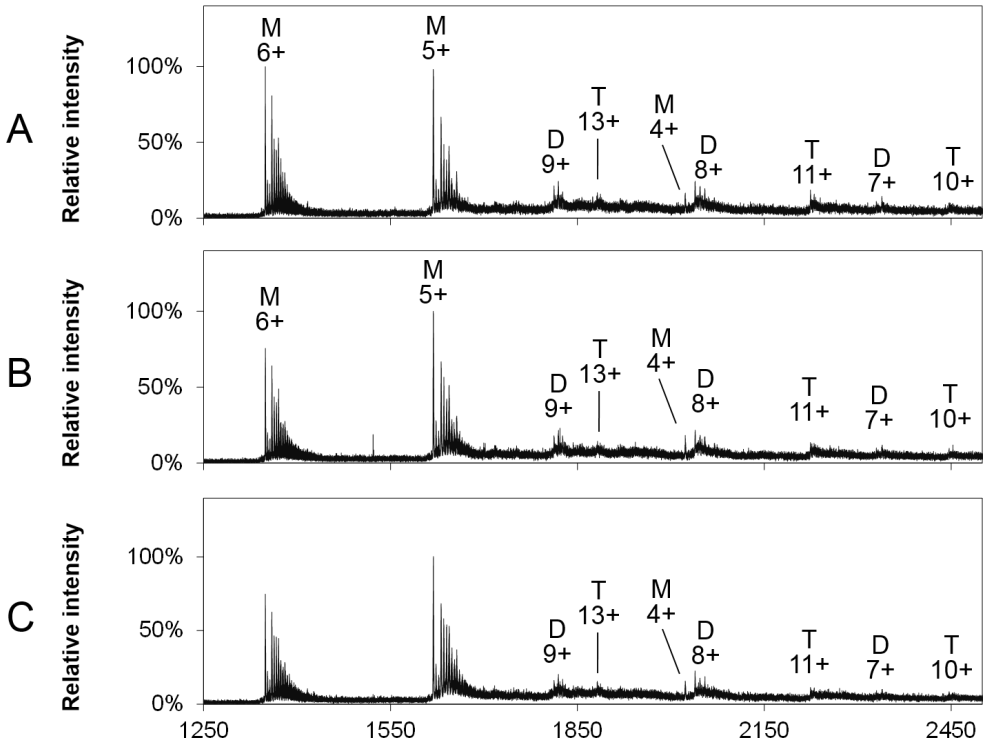

Figure 7.4.4: Mass spectra for Atx1 prepared at 2 Cu(I) / protein with varied DTT levels. Mass spectra prior to deconvolution of Atx1 prepared at 2 Cu(I) / protein in the presence of: **A)** 5 DTT / protein, **B)** 10 DTT / protein, **C)** 20 DTT / protein

Deconvolution of these mass spectra (**Figure 7.4.5**) reveals the species present, the exact neutral masses and relative intensities are presented in **Table 7.6**. The relative intensities are presented as bar graphs in **Figure 7.4.6**.

The species distribution at each level of DTT is fairly similar, with the most intense species being apo-Atx1, the most intense copper-bound species is CuAtx1, with a sizeable proportion of Cu_2Atx1. Though, in the absence of thiol, the proportion of disulfide-bonded $Atx1_2$ was high, very little is observed in the presence of DTT, presumably due to the presence of this reducing agent in the sample.

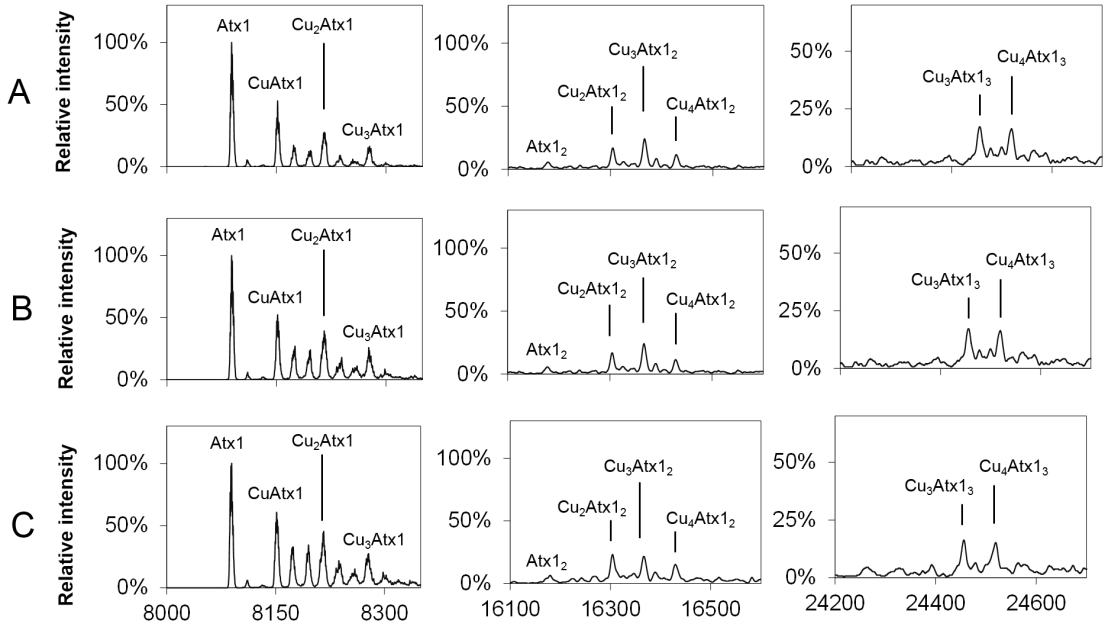

Figure 7.4.5: Deconvoluted mass spectra for Atx1 prepared at 2 Cu(I) / protein with varied DTT levels. Deconvoluted mass spectra of Atx1 prepared at 2 Cu(I) / protein in the presence of: **A)** 5 DTT / protein, **B)** 10 DTT / protein, **C)** 20 DTT / protein

Table 7.6: Species observed via ESI-MS for Atx1 at varied DTT levels. Observed masses and relative intensities for Atx1 prepared at 2 Cu / protein in the presence of: 5, 10 and 20 DTT / protein.

Species	Pred (Da)	5 DTT / Atx1		10 DTT / Atx1		20 DTT / Atx1	
Atx1	8089.4	100%	8089.1	100%	8089.1	100%	8089.0
CuAtx1	8151.9	52%	8151.7	52%	8151.6	67%	8151.5
Cu_2Atx1	8214.4	29%	8215.3	40%	8215.2	45%	8215.8
Cu_3Atx1	8276.9	16%	8277.0	24%	8277.0	26%	8277.9
$(Atx1)_2$	16178.8	34%	16177.7	35%	16175.5	34%	16179.6
$Cu(Atx1)_2$	16241.3	0%	–	0%	–	0%	–
$Cu_2(Atx1)_2$	16303.8	52%	16304.4	58%	16304.2	54%	16303.8
$Cu_3(Atx1)_2$	16366.3	37%	16366.5	44%	16366.7	28%	16366.3
$Cu_4(Atx1)_2$	16428.8	35%	16428.5	49%	16428.3	42%	16429.0
$(Atx1)_3$	24268.1	0%	–	0%	–	0%	–
$Cu_3(Atx1)_3$	24455.6	47%	24455.8	52%	24456.3	50%	24456.4
$Cu_4(Atx1)_3$	24518.1	42%	24519.2	47%	24518.6	47%	24519.7
$Cu_5(Atx1)_3$	24580.6	0%	–	0%	–	0%	–

In contrast to the spectrum in the absence of DTT, here in the presence of DTT, the intensity of the dimeric copper-bound species are diminished to 25% relative intensity and below. This could be explained by DTT binding Cu(I) and reducing the likelihood of dimeric species formation. However, in the presence of DTT the intensity of Cu_2Atx1 has also increased and the species Cu_3Atx1 appears around 20% relative intensity at all levels of DTT. Both of these species, which possess unexpected copper:protein ratios, could arise as breakdown products of dimeric species which do not readily survive the ionisation process.

The observed masses of all Atx1 species are very close to their predicted masses, mostly within $\sim 1 - 2$ Da. The mass of apo-Atx1 is nearly exact in all cases, perhaps reflecting the effect of DTT preventing an intramolecular disulfide bond formation. Again, the decreased mass observed for disulfide bonded $Atx1_2$ species (present at much lower levels than in the presence of DTT) is expected due to loss of cysteine hydrogens. The

masses of copper-bound monomeric, dimeric and trimeric species are all very close to that expected mass. The only differences greater than 1 Da are at 20 DTT / protein, where Cu_2Atx1 and Cu_{43} are $\sim$ 1.4 Da and 1.8 Da greater than expected. Both peaks are of moderate intensity and the reason for this mass difference is not clear.

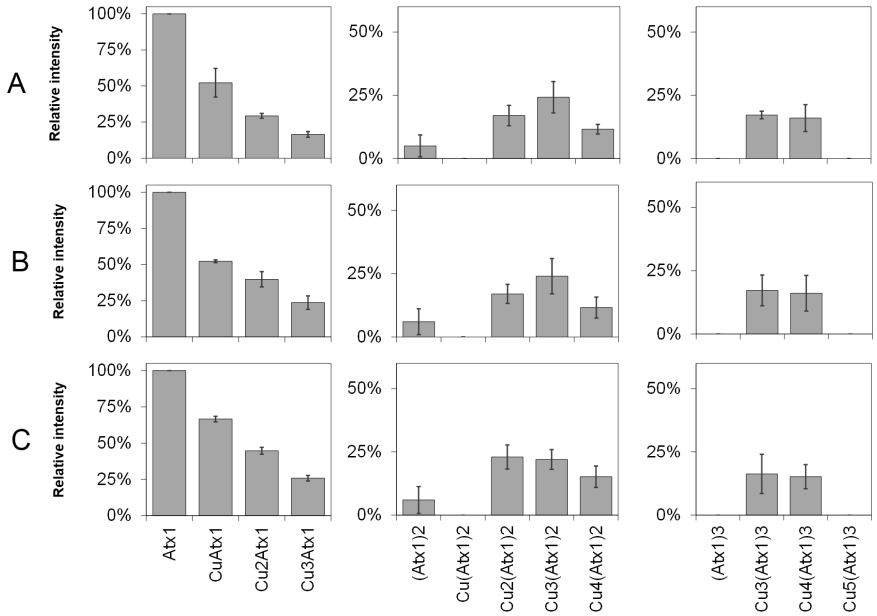

Figure 7.4.6: Species observed via ESI-MS for 2 Cu / Atx1 at varied DTT levels. Species distribution observed in deconvoluted mass spectra of Atx1 prepared at 2 Cu(I) / protein in the presence of: **A)** 5 DTT / protein, **B)** 10 DTT / protein, **C)** 20 DTT / protein

The mass of Cu_2Atx1 is as expected at first (0.5 Cu / CopZ), but subsequently is $\sim$ 4 Da lower (at 1.0, 1.5, 2.0 Cu / CopZ), a mass change suggesting these peaks could shift slightly due to overlap with a tri-sodiated adduct peak of CuAtx1. Though the dimeric Atx1 species with 2, 3 and 4 coppers bound are all within 2 Da of their predicted mass, the mass of $CuAtx1_2$ is lower than expected, perhaps reflecting the potential for a single disulfide to be formed while one copper is coordinated by the other cysteine pair.

7.5 Discussion

Atx1-like copper chaperones function in such a way that cellular copper is entirely sequestered, with none ”free” in the cytoplasm. Defining the physiologically relevant copper-bound forms of these proteins is essential to understanding the mechanisms of cellular copper management. Though higher order copper-bound assemblies have been reported for several members of the Atx1-like chaperone family, their physiological relevance is unclear, particularly due to the potential influence of cytoplasmic LMWT. ESI-MS experiments using prokaryotic CopZ-1317 and CopZ-3079 from *S. lividans*, and eukaryotic Atx1 from *S. cerevisiae* have demonstrated that these proteins form a variety of copper-bound species, both in the presence and absence of LMWT.

ESI-MS of *S. cerevisiae* Atx1

The mass spectra of *S. cerevisiae* Atx1 contained monomeric apo-protein as the major species in the absence of copper, though showed evidence of a low level of Cu(I) present as a low-intensity CuAtx1 peak was observed. Low intensity $Atx1_2$ and $Atx1_3$ peaks suggest disulfide bonded protein arising from a small amount of oxygen in the sample, or driven by the ESI process itself [101]. The observed masses of the Atx1 species present are in close proximity to their predicted masses, mostly within $\sim 1 - 2$ Da, including the most intense copper-bound species CuAtx1 and Cu_4Atx1_2. Deviations could be accounted for by loss of hydrogen in disulfide bond formation ($Atx1_2$ or $Atx1_3$) or low-intensity peaks shifting slightly due to overlap with other adduct peaks (Cu_2Atx1). Upon addition of Cu(I), the

monomeric peak envelope did not shift appreciably suggesting no major structural changes upon copper binding, which was also observed in the solution structure [41].

The major species formed in the presence of copper were CuAtx1 (0.5 and 1 Cu / protein) and Cu_4Atx1_2 (1.5 and 2.0 Cu / protein). The Atx1 NMR solution structure [41] was solved using a sample prepared at 0.9 Cu(I) / Atx1 in the absence of LMWT, where the only species observed was CuAtx1. Though the mass spectrum at a similar stoichiometric ratio of 1 Cu / protein displayed the same major peak (66 % relative intensity), a mixture of additional dimeric and trimeric species also are present (e.g., Cu_4Atx1_2, 41% relative intensity). Though the reason these higher order assemblies were not observed via NMR is not entirely clear, protein dimerisation can lead to loss of signals (as observed previously for *B. subtilis* [80]), meaning that this portion of the sample may have been not visible by NMR.

At higher copper levels, except for a slight bump in intensity of the Cu_2Atx1_2 peak, no significant accumulation of any copper-bound dimeric or trimeric Atx1 species was observed, suggesting cooperativity in formation of Cu_4Atx1_2. It is noted that $Atx1_2$ accumulates with increasing copper, perhaps as a results of the cooperative formation of the tetranuclear species from two Cu_2Atx1_2 yielding apo-Atx1.

The effect of LMWT upon the Atx1 species distribution was illustrated by the mass spectra of 2.0 Cu / Atx1 prepared at 5, 10 and 25 DTT / protein. Here, Cu_4Atx1_2 is no longer the most intense peak but, rather, the monomeric species apo-Atx1 and CuAtx1. The presence of DTT appeared to reduce disulfide bonds, with reduced intensity observed for $Atx1_2$and $Atx1_3$ peaks. In addition, here the observed apo-Atx1 mass was closer to the

predicted mass (within 0.4 Da), suggesting decreased capacity for it to form an intramolecular disulfide in the presence of DTT.

Some of the observed changes in the presence of DTT arise due to its ability to compete for Cu(I), such as the reduced intensity of dimeric Atx1 species. In addition, the dominance of the apo-Atx1 peak could reflect loss of copper to DTT. Previously, it has been demonstrated that Atx1 prepared with 2.5 molar equivalents of copper, in the presence of 20 DTT / protein, generated a CuAtx1 species, but with the sample containing a final Cu / protein ratio of 0.75 [34]. Though it is difficult to infer species distribution from the total Cu / protein ratio, this result could arise from competition for Cu(I) by DTT. Here, the ESI-MS data did not show CuAtx1 as the stable copper-bound species, displaying dimeric species at all levels of copper and thiol tested. However, the dominance of monomer species CuAtx1 was observed at lower copper loadings (0.5 and 1.0 Cu / protein) in the absence of thiol, and at higher copper loadings (2.0 Cu / protein) in the presence of thiol. The persistent drive toward formation of this species suggests it is stable and perhaps dominant under a variety of solution-phase conditions.

More recently, it was reported that the presence of LMWT induces Atx1 dimerisation, as $Cu_2Atx1_2GSH_2$ was formed *in vitro* in the presence of GSH [187]. However, here, dimeric species were not dominant at any DTT level and time constraints did not allow testing in the presence of GSH. Instead, the mass spectra of 2 Cu / Atx1 contained a diverse mixture of monomeric Atx1 species at all thiol levels tested, with dimeric and trimeric peaks of consistently low-intensity.

Though trimeric species were observed at all copper and thiol levels tested, their rela-

tive intensities peaked upon formation of Cu_4Atx1_3, and were consistently low. It is unclear what role they play in the copper binding mechanism of Atx1, but could suggest that trimeric forms are an intermediate, perhaps in cooperative formation of Cu_4Atx1_2 in the absence of thiol ligands. Previously, an Atx1 trimer has been observed in a crystal structure after treatment with tetrathiomolybdate (TM), MoS_4^-, where each Atx1 in the cluster retains the canonical $\beta\alpha\beta\beta\alpha\beta$ fold [191]. This illustrates the possibility for a stable trimeric Atx1 species to form in the presence of endogenous thiol ligands.

The proposed Cu(I)-binding arrangement of $Cu_2Atx1_2GSH_2$ was one copper coordinated only by cysteine, and the other more exposed with GSH as exogenous ligands, perhaps mimicking or facilitating the process of copper transfer [190]. It is possible that DTT would not be able to induce formation of a similar dimeric species, perhaps due to its differing properties to GSH (such as charge). If $Cu_2Atx1_2DTT_2$ were present in solution, the thiol competition could result in removal of a DTT-Cu(I) species prior to or during ionisation. Alternately, the thiol affinity could be too low for this thiol adduct species to survive ionisation. In either case, possible products could be $CuAtx1_2$ or Cu_2Atx1_2. These species were not observed here, but also were not present in the absence of LMWT suggesting they may not be amenable to ionisation. In that case, the formation of DTT adducts may ultimately result in the observation of apo-Atx1 and CuAtx1, which here are the most intense species observed in the spectra at all levels of DTT.

ESI-MS of *S. lividans* CopZ-1317 and CopZ-3079

The mass spectra of apo-CopZ-1317 led to a typical peak distribution for a metallochaper-

one of this size, with no peak shifts upon binding of Cu(I). Addition of 1 Cu(I) /CopZ-1317 led to a mixture of copper-bound forms, predominantly CuCopZ-1317, CuCopZ-1317_2, and Cu_2CopZ-1317_2. The prominent peak corresponding to disulfide-bonded $CopZ_2$ likely arose due to the introduction of oxygen or was facilitated by the oxidising ESI process itself, as this species would be unexpected.

Upon increase of Cu(I) level from 1 to 2 molar equivalents, the dominant species shifted from CuCopZ-1317_2 to Cu_2CopZ-1317_2, in agreement with the absorbance changes above 1 Cu / protein at 335 nm, indicative of formation of a multinuclear Cu(I) interaction. The SEC chromatogram (**Figure 7.3.11**) suggested that at 1 Cu / CopZ-1317, there was more monomeric than dimeric protein present, though this would be the case, too, in the mass spectra if the disulfide bonded $Atx1_2$ existed as monomeric apo-protein. The changes observed in the SEC chromatogram between a level of 1 and 2 Cu / CopZ-1317 are also consistent with the mass spectra, as the higher order assemblies become dominant as the Cu level is increased above 1 / protein. However, unlike in the SEC where this higher order CopZ-1317 species appeared to be tetrameric, no such peak envelope was observed in the mass spectrum of CopZ-1317 prior to deconvolution. Some trimeric CopZ-1317 was observed as a component of a diverse mixture of various higher order assemblies. Cu_2CopZ-1317_2 could simply arise from being amenable to ionisation, as a breakdown product of Cu_4CopZ-1317_4.

At the lowest level of DTT tested, the low-intensity dimeric and trimeric peaks are abolished, suggesting these species do not bind Cu(I) with very high affinity. In addition, the monomeric forms are not present, supporting the idea that the most stable species at 2 Cu /

protein in the absence of LMWT is Cu_2CopZ-1317_2, or the presence of thiols somehow stabilises this species. In the presence of 10 – 20-fold excess of DTT, the SEC data revealed that higher order CopZ-1317 assemblies were unable to form with elution peaks being entirely monomeric at all levels of copper loading tested. The ESI-MS corroborates these results, where with increasing DTT levels up to 20-fold excess, the dimeric CuCopZ-1317_2 and Cu_2CopZ-1317_2 were suppressed with increase in monomeric forms CuCopZ-1317 and apo-CopZ-1317.

CopZ-3079 is the principal copper chaperone in *S. lividans* as it is present at higher cellular concentration, and with a slightly higher affinity for Cu(I), than CopZ-1317. The ESI-MS data suggested that in the absence of thiol the copper-bound species observed are CuCopZ-3079 and Cu_4CopZ-3079_2 (at 1 Cu/CopZ-3079), leading to the formation of Cu_6CopZ-3079_2 (at 2 Cu/CopZ-3079). At 1 Cu / CopZ-3079, the mass spectra displayed a diverse mixture of copper-bound forms with CopZ-3079 and Cu_4CopZ-3079_2 predominant and of equal intensity. The species distribution observed in the mass spectra of CopZ at 1 Cu / protein fits with the absorbance titration data, suggesting that the monomer CuCopZ-3079 forms up until 0.5 Cu / protein, with subsequent copper additions leading to formation of Cu_4CopZ-3079_2. Though ESI-MS data was not acquired at 0.5 Cu / CopZ-3079, this pattern was observed for the ESI-MS data for *B. subtilis* CopZ (Section 4.3.2). This is in reasonable agreement with the SEC chromatogram at 1 Cu / protein, although SEC suggests that more dimer than monomer was present. This slight discrepancy could easily be explained by slightly different ionisation efficiencies of the monomeric and dimeric forms, or variations in absorbance changes due to multinuclear centres, compared with that for

the monomeric CuCopZ-3079 species.

At 2 Cu / protein the mass spectrum of CopZ-3079 revealed a diverse mixture which is almost entirely dimeric with Cu_6CopZ-3079$_2$ clearly predominant. This is in agreement with the SEC chromatogram revealing entirely dimeric species at 2 molar equivalents of copper. The mass spectral and SEC data can be juxtaposed with the absorbance titration data, where beyond 1 Cu / protein the shallower absorbance changes could arise from loss of monomer as Cu_6CopZ-3079$_2$ becomes the predominant species.

The presence of DTT led to near entire removal of dimerised species in the mass spectrum, though with increasing DTT level from 10 to 20-fold excess the major copper-bound species becomes CuCopZ-3079. At approximately the same DTT level, SEC confirmed that no higher order assemblies were formed, suggesting that Cu_2CopZ-3079 is not representative of some breakdown product as no dimers should exist in solution. This would suggest that DTT is somehow acting as a ligand to support CopZ-3079 to coordinate an additional copper ion, but does not survive ionisation to be observed as a DTT adduct species. This conclusion was also made in the mass spectra of *B. subtilis* CopZ containing DTT.

The ability of DTT to inhibit dimerisation may be due in part to its ability to compete for Cu(I). The affinity of DTT is lower (Kd $\sim 10^{-15}$ M) than that of CopZ-1317 (Kd $\sim 10^{-17}$ M), CopZ-3079 (Kd $\sim 10^{-18}$ M) [74], and Atx1 (Kd $\sim 10^{-18}$ M) [138], but at increasing levels of DTT, it would become more competitive, leading to the formation of the monomeric copper-bound forms. These were observed for each protein.

In addition, the relative affinities of the individual proteins fell in line with the extent to which DTT abolished the dimeric assemblies. For CopZ-1317, with the lowest affinity for

Cu(I), 20-fold excess of DTT was sufficient to remove the dimeric species entirely. However, for Atx1, with a slightly higher affinity than CopZ-1317, a 20-fold excess of DTT did diminish the dimeric species but they were not removed entirely. Perhaps, a greater proportion of DTT would have accomplished this, such as observed for CopZ-3079 (with similar Cu(I) affinity to Atx1), where at a 40-fold excess of DTT did, in fact, lead to a near entire removal of dimeric species.

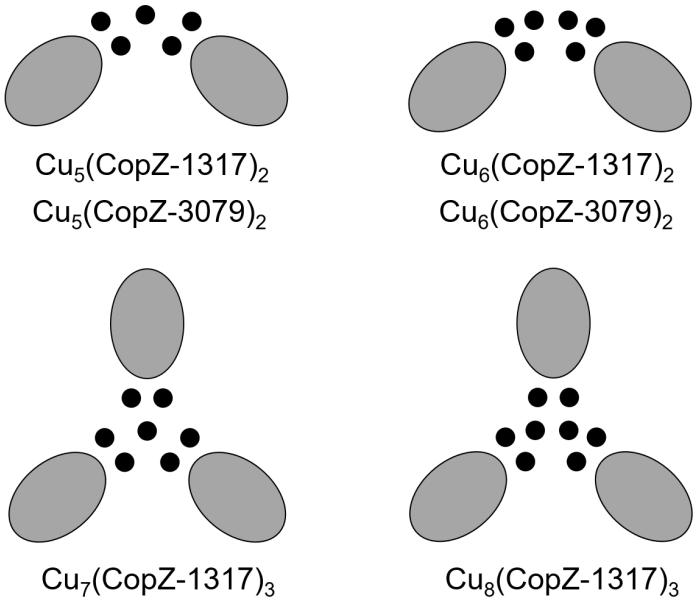

Figure 7.5.1: Chaperone complexes with a high proportion of copper Structural representations of higher-order copper chaperone complexes with copper-to-protein ratios greater than 2:1. Here, the number of available Cys per copper ion is less than one, suggesting that additional residues would be involved in Cu(I) coordination.

The spectra presented here illustrate a diverse mixture of species as the copper / protein ratio in each sample is fluctuated. Higher-order copper chaperone complexes featuring multicopper clusters typically involve no greater than a 2:1 ratio of copper to protein. This is influenced by the number of available Cys ligands per protomer (here, two), and is true

for the majority of species observed in the mixtures of copper chaperone species. At and above this 2:1 copper-to-protein ratio, additional ligands may be involved, as observed for *B. subtilis* Cu_4CopZ_2 (His15) [81] and the CuA site of Thermus thermophilus cytochrome c oxidase [193], where the carbonyl oxygen of a nearby Gln served as a weak ligand to a Cu_2S_2 cluster.

A few species with copper-to-protein ratios above 2:1 (**Figure 7.5.1**) were observed in mass spectra presented here. As described in Section 3.2.1, the relative intensity scale is based upon peaks normalised to the most intense species. This means that, as an example, a moderate relative intensity ($\sim$ 15 – 20%) could actually represent quite a low proportion of the molecular population ($\sim$ 2 – 4%). In addition, the ESI-MS data obtained represent a snapshot of the equilibrium mixture of coordinate complexes under different conditions. Here, nearly all the species at elevated copper-to-protein ratios were observed below 30% relative intensity suggesting they are transient intermediates, and at low concentration in solution.

The exceptions were Cu_5CopZ-3079_2 and Cu_6CopZ-3079_2. CopZ-3079 does feature some sequence differences to CopZ-1317, such as Lys just before the conserved MXCXXC motif which could charge balance the Cu(I) centre as for Atx1, or several Gln in its sequence which have been observed elsewhere as weak copper ligands as described above. However, without a solution or crystal structure, it is unclear which residues would lie proximal to the copper-binding site.

Despite some divergent structural features between prokaryotic and eukaryotic copper chaperones, all proteins formed higher association state assemblies at higher levels of

copper. The conserved Lys65 in yeast Atx1 is located close to the metal ion, and is thought to provide a balancing positive charge to stabilise the Cu(I) oxidation state that inhibits the need for protein dimerisation. In addition, its MXCXXC motif lacks the histidine at X_3 found to coordinate Cu(I) in the dimeric copper-bound forms of CopZ [81], which may limit the likelihood of dimerisation. Nonetheless, here, in the absence of LMWT, Atx1 was able to dimerise and also formed trimeric species though this required a higher copper / protein ratio than observed for other prokaryotic versions, as Atx1 dimeric species were not dominant until above a level of 1 Cu / protein. Studies of CopZ where Tyr65 was mutated to Lys did not prevent CopZ association into a trimer, but did require a higher copper level as Y65K CopZ remained monomeric below 0.5 Cu / protein [179].

This may then be consistent with the idea that Lys65 inhibits multimer formation. It is in agreement with the fact that here, the yeast Atx1 dimeric form dominated at a higher Cu / protein level than for the prokaryotic variants. Also, the lack of histidine may be overcome by the abundance of LMWT in the cytosol and explain the enhancement of dimerisation observed in the presence of GSH, which was able to serve as a Cu(I) ligand. The fact that these species were not observed i.e., $Cu_2Atx1_2DTT_2$, could result from the low ionisation efficiency of this DTT-bound complex resulting, rather, in loss of CuDTT and observation of a mixture of Atx1 and CuAtx1 in the mass spectra.

In *B. subtilis* CopZ, Tyr65 may be involved in copper binding or affect the protein association state as it forms a hydrophobic contact with Met11, (of the MXCXXC motif) and this hydrophobic patch is thought to interact with CopA, facilitating protein-protein interaction with CopA [171] [81]. CopZ-3079 contains a phenylalanine residue at this location.

Interestingly, this is typically the conserved residue at the complementary position within ATPase MBDs [194]. CopZ-3079 formed dimeric species with 4 and 6 Cu(I), suggesting that neither a Tyr nor a Lys are required for dimerisation. CopZ-1317 contains a conserved Tyr71, and exhibits a slightly lower affinity for Cu(I), which was not affected by mutating this Tyr71 to a Phe [74]. Here, CopZ-1317 protein dimerisation occurred at 1 Cu / protein and trimeric forms were observed as well. All three of these prokaryotic versions of Atx1-like proteins contain histidine at the X_3 position; perhaps this residue facilitates dimerisation at slightly lower copper / protein ratios compared to eukaryotic homologues. Of particular note is that the two *S. lividans* CopZ proteins exhibit quite distinct Cu(I)-binding behaviour, which may well be connected to different phsyiological roles.

Chapter 8

Purification Of Integral Membrane Protein, CopA

8.1 Introduction

In *Bacillus subtilis*, copper is exported from the cell by way of the integral membrane ATPase, CopA, which utilises energy harvested from ATP hydrolysis to drive copper translocation (see Chapter 1). CopA in *B. subtilis* is an 803 amino acid protein, encoded by the gene *copA* [78], whose major structural features are depicted in **Figure 8.1.1**. These include cytoplasmic metal-binding domains (MBDs), eight transmembrane helices, an actuator domain (A-domain), and the ATP-binding region (P- and N-domains) [47]. Most, but not all, P_{1B}-type ATPases contain two additional TM helices at the N-terminal side of the core domain, MA and MB [47].

P_{1B}-type ATPases engage in catalytic phosphorylation coupled with active transport of a Cu(I) ion across a transmembrane channel, which follows the major conformational states of the Albers-Post catalytic cycle: E1 (ATP and metal-binding) and E2 (phosphorylation and metal release). In the E1 state, ATP binds the N-domain while metal binds the cytoplasmic TM transport site (TMBS). In the E2 state, the metal is translocated across the membrane and, as metal is released, aspartic acid of a conserved DKTGT sequence in CopA is phosphorylated. One ATP is coupled with transport of up to two Cu^+ ions [195] and the rate-limiting step appears to be metal release, with slower rates observed for P_{1B}-

ATPases ($<$10 s^{-1}) than for other ion subclasses P_2- and P_3-ATPases [167].

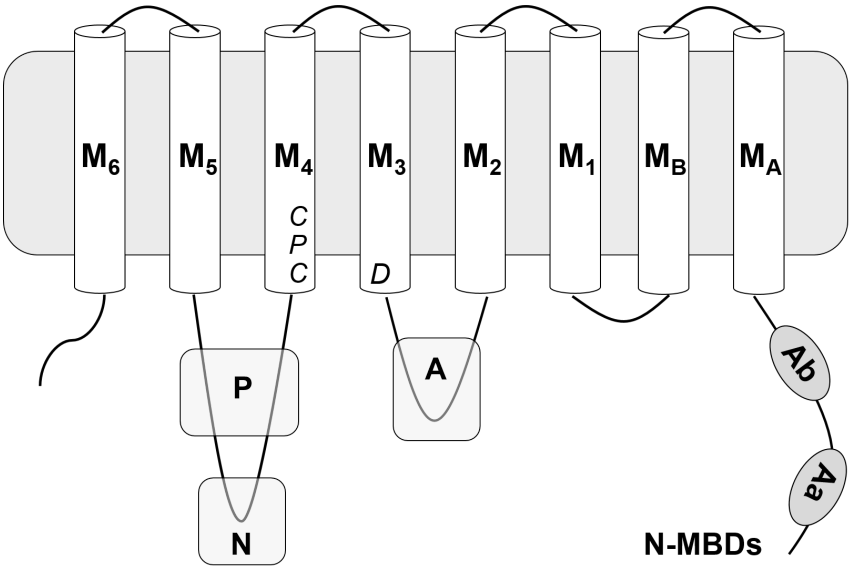

Figure 8.1.1: Structural representation of CopA. Conserved structural features of CopA include: eight transmembrane helices (MA and MB at the N-terminus, and M1-M6), an ATP-binding region comprising the nucleotide-binding (N) and phosphorylation (P) domains, and the actuator domain (A). As a member of the P_{1B}-1 family of P-type ATPases, CopA contains a CPC transmembrane copper-binding motif in M4. In addition, the conserved DKTGT domain found in M3 contains the aspartate that is phosphorylated during the catalytic cycle. The soluble MBDs, CopAa and CopAb, are located at the N-terminus.

The two soluble MBDs of CopA, CopAa and CopAb are located at the N-terminus and contain conserved MXCXXC copper-binding motifs. Thus far, copper transfer from the cytoplasmic metallochaperone CopZ to *B. subtilis* CopA has been characterised using a truncated construct comprising these two MBDs, CopAab. In *Thermotoga maritima*, copper transfer to the CopA MBDs was demonstrated to be required for enzyme function [167] but it has not yet been demonstrated copper transfer out of the cell occurs by way of binding to the MBDs. A regulatory role has been proposed [160] for MBDs in copper trafficking. For example, in the human ATP7A, it has been demonstrated *in vitro* that the MBDs interact with

the ATP-binding domain; this interaction is ablated upon Cu(I) binding by the MBDs [196].

Thus, understanding the physiological mechanisms of copper export in *B. subtilis* involves the characterising the behaviour of the full-length integral membrane protein. To this end, a plasmid construct has been generated to heterologously express the full-length CopA (CopA-FL).

Purification of integral membrane proteins requires a specialised procedure whereby, after overexpression, the membrane-bound protein is first isolated via differential centrifugation and then the membrane-spanning regions are solubilised using buffer systems containing detergent [197]. Detergents generally consist of a hydrophobic moiety (often an alkane chain or aromatic hydrocarbon) with a polar or charged head group, and form micelles around the hydrophobic regions, leaving the hydrophilic regions exposed to solution [198]. The minimal concentration for micelle formation (CMC) varies among detergents. Generally speaking, the CMC is determined by the length of the alkyl chain, while the head group affects the detergent's interaction with the protein, i.e., the resulting stability [199]. To guarantee complete micelle formation, solubilisation is usually carried out at substantial concentrations above the CMC (established experimentally) and subsequent experiments carried out at a decreased working concentration of detergent.

In addition to purification and solubilisation of CopA-FL, its capacity as an enzyme must be established by a functional assay. As ATP is turned over by CopA, the resulting inorganic phosphate (P_i) can be quantified through its reaction with acidified ammonium molybdate, to form the phosphomolybdate anion, $PMo_{12}O_{40}{}^{3-}$ [200]. The $Mo^{(VI)}$ is reduced to generate an α-Keggin molydenum heteropoly complex, with a blue color that can be

monitored spectroscopically at 710 nm to quantify P_i [201]. Carrying out this activity assay tests the ability of CopA to turn over ATP and ensures the enzyme is active in its purified, solubilised form.

The desired outcomes of this work were to: establish that the heterologous host is able to overexpress CopA, effectively isolate membrane-bound CopA via cell lysis and centrifugation, solubilise CopA from the membranes using a suitable type and concentration of detergent, purify the solubilised CopA using Ni^{2+} IMAC, develop and carry out an assay to establish the enzyme activity of CopA.

8.2 Materials and Methods

8.2.1 Overexpression of His_6CopA

The plasmid construct for expression of full-length CopA, pBSCOPA1, was prepared by Genscript (Piscataway, NJ, USA), shown in **Figure 8.2.1** where *copA* is encoded in the expression vector pET21a under control of the inducible T7 promotor, containing a C-terminal hexa-histidine tag. For overexpression of CopA in *E. coli* BL21(DE3), 2.5 L (5 $\times$ 500 mL) of LB medium with 100 μg/mL ampicillin was inoculated with 5 $\times$ 5 mL of an overnight culture containing pBSCOPA1, and incubated at 37 °C and 200 rev/min. When OD_{600} reached 0.4 – 0.6, IPTG (Formedium) was added to a final concentration of 0.5 mM and the cultures were incubated at 37 °C and 200 rev/min for a further 4 hours. Cells were harvested by centrifugation at 5,000 $\times$ g for 20 min at 4 °C and pellets frozen at -20 °C.

8.2.2 Solubilisation of CopA with Brij-35 and Triton X-100

For Brij-35 and Triton X-100 solubilisation trials, the pellets were resuspended in 40 mL of resuspension buffer (here, 50 mM sodium phophate, 200 mM NaCl, 1 mM DTT, 10% glycerol, pH 7.2). After adding DNAse I (Sigma) to a final concentration of 2 μg/mL, the cells were lysed by 2 passes through a French pressure cell at 1000 psi, with breaks on ice between cycles. The lysate was centrifuged at 20,000 $\times$ g for 30 min at 4 °C using a Beckman Coulter Avanti J25 centrifuge (Beckman Coulter Inc., USA), and the supernatant was centrifuged at 105,000 $\times$ g for 120 min at 4 °C using a Beckman Coulter Optima LE-80K Ultracentrifuge and 70Ti Rotor (Beckman Coulter Inc., USA). Cell pellets were

His_6CopA-FL

MLSEQKEIAM QVSG**MTCAAC** AARIEKGLKR MPGVTDANVN LATETSNVIY DPAETGTAAI
QEKIEKLGYH VVTEKAEFDI EG**MTCAAC**AN RIEKRLNKIE GVANAPVNFA LETVTVEYNP
KEASVSDLKE AVDKLGYKLK LKGEQDSEAA AKKKEERKQT ARLIFSAVLS FPLLWAMVSH
FTFTSFIWVP DIFLNPWMQF ALATPVQFLI GWPFYVGAYK ALRNKSANMD VLVALGTTAA
YAYSLYLTFQ SIGSHGHTDG LYYETSAILL TLILLGKLFE TKAKGRSSDA IKKLMKLQAK
TATVVRDGQE QIIPIDEVLV NDIVYVKPGE RIPVDGEVVE GRSAVDESMI TGESLPVDKN
PGDSVTGSTV NANGFLKIKA VNVGKDTALS HIIKIVEEAQ GSKAPIQRLA DQISGIFVPI
VLGIAVLTFL IWYLWAAPGD FAEAISKFIA VLVIA**CPC**AL GLATPTSIMA GSGRAAEFGI
LFKGGEHLEK THRLDTIVLD KTGTVTNGKP RLTDAIPFGR FEEKDLLQFA AAAETGSEHP
LGEAIIAGVK DKGLEIPKLT RFEAKVGAGI LAEAGGKSIL VGTRKLMESE QVEHGALLAQ
MEELEAEGKT VMLVSIDGEA AGLVAVADTI KDTSRKAVAR LKELGLDVIM MTGDNRRTAE
AIAKEAGIAN IIAEVLPEQK AAEIARLQKE GRQTAMVGDG INDAPALATA DIGMAIGTGT
DIAMETADIT LIRGDLNSIA DAIRMSRLTM KNIKQNLFWA LGYNSLGIPI AALGFLAPWI
AGAAMAFSSV SVVLNALRLQ KVKLEHHHHH H

Isotopically Averaged Molecular Mass = 87089.555 Da

Figure 8.2.1: Sequence encoded by pBSCOPA1. The isotopically averaged molecular mass and primary sequence of full-length CopA, as produced using pBSCOPA1.

resolubilised for 60 min at 4 °C, in 4 × 25 mL solubilisation buffer, i.e., resuspension buffer containing final concentrations (where % is w/v) of: Brij-35 at 1 mM (0.125%), Brij-35 at 10 mM (1.25%), Triton X-100 at 1 mM (0.06%), or Triton X-100 at 10 mM (0.6%). The samples were centrifuged at 200,000 × g for 45 min at 4 °C. CopA solubilised in Brij-35 (both 1 and 10 mM, supernatant fraction) was applied to a 5 mL IMAC HiTrap FF Ni-NTA column (GE Healthcare) equilibrated with 25 mL (5 × CV) of solubilisation buffer containing 50 mM imidazole, and eluted with a 30 mL (6 × CV) imidazole gradient of 50 – 500 mM imidazole, with CopA eluting at approximately 100 mM imidazole.

8.2.3 Solubilisation of CopA with DDM

For the second purification trial, incorporating a high salt wash to remove nucleic acid, and a more commonly used detergent, n-dodecyl-β-D-maltoside (DDM), cell pellets were resuspended in 6 mL/g (here, $\sim$ 55 mL) of resuspension buffer (100 mM HEPES, 200 mM NaCl, 1 mM DTT, 10% glycerol, pH 7.2). After adding DNAse I (Sigma) to a final concentration of 2 μg/mL, the cells were lysed by 2 passes through a French pressure cell at 1000 psi, with breaks on ice between cycles. The lysate was centrifuged at 20,000 $\times$ g for 20 min at 4 °C using a Beckman Avanti J25 centrifuge (Beckman Coulter Inc., USA), and the supernatant was centrifuged at 105,000 $\times$ g for 120 min at 4 °C using Beckman Coulter Optima Max Ultracentrifuge with MLS-50 rotor (Beckman Coulter Inc., USA). Pellets were resuspended in 4 $\times$ 5 mL solubilisation buffer, i.e., resuspension buffer containing 15 mM DTT and final concentrations (where % is w/v) of DDM at: 0.3 mM (0.03%), 1.2 mM (0.08%), 2.5 mM (0.15%) and 5 mM (0.30%). These samples were incubated for 14 hours at 4 °C, and then centrifuged at 200,000 $\times$ g for 2 hours at 4 °C. After selecting the most effectively solubilised CopA sample (5 mM DDM, based on SDS-PAGE analysis), this sample was loaded onto a 5 mL IMAC HiTrap FF Ni-NTA column (GE Healthcare), previously equilibrated with 25 mL (5 $\times$ CV) of binding buffer (100 mM HEPES, 200 mM NaCl, 10% glycerol, 50 mM imidazole, 15 mM DTT, 5 mM DDM, pH 7.2). The column was washed with 100 mL (20 $\times$ CV) of binding buffer containing 1 M NaCl to remove nucleic acid, before eluting CopA with a 50 mL (10 $\times$ CV) gradient of 50 – 500 mM imidazole (in binding buffer). Semi-pure CopA fractions were pooled and frozen at -20 °C.

8.2.4 ATPase activity assay

All reagents were prepared in plastic. The stop solution was prepared on ice with stirring, by adding 15 mL of 1 M HCl to 10.5 mL of 0.5 mM ascorbic acid, and incubating for 10 minutes, then adding 1.5 mL 10% w/v $(NH_4)_2MoO_4$ (from stock prepared in a volumetric flask), and 4.5 mL sodium dodecyl sulfate (SDS) (10% w/v), ensuring the solution appeared yellow and not blue-green. The reducing solution is prepared by first dissolving 1.75 g bismuth citrate, and then 1.75 g sodium citrate, in 1 M HCl to a final volume of 50 mL. For the standard calibration curve, 500 μL samples of K_2HPO_4 (stock prepared in a volumetric flask) were prepared at a final concentration of P_i between 0 and 200 μM, in 3 mL spectrophotometric cells. For the protein samples, CopA was exchanged into assay buffer: 100 mM HEPES, 200 mM NaCl, 1 mM Brij-35, 10% glycerol, pH 7.2, using a G25 Sephadex column (PD-10, GE Healthcare). Then 450 μL of CopA was mixed in a 3 mL spectrophotometric cell with 50 μL 1 mM Na_2ATP (stock prepared in volumetric flask), and incubated for 15 minutes before assay. The assay was carried out in duplicate by adding 1 mL of stop solution to each spectrophotometric cell, followed by 10 minutes of incubation on ice. Then 1.5 mL reducing solution is added followed by 10 minutes incubation at 37 °C. Absorbance was then measured at 710 nm.

8.3 Results

With the aim of characterising full-length CopA *in vitro*, a protocol was established to purify solubilised, functionally active CopA. First, pBSCOPA1 encoding CopA with a C-terminal hexa-histidine tag was overexpressed in *E. coli* BL21(DE3). The growth conditions described in the methods section were used in this host for the production of other proteins from the same expression vector (pET21a), and were first tested on a small (10 mL) scale (data not shown), before carrying out a full 2.5 L overexpression.

After overexpression, the isolation of membrane-bound CopA from the *E. coli* cell pellets using a French pressure cell and centrifugation are depicted in **Figure 8.3.1**, lanes 1 – 5. Here, SDS-PAGE analysis illustrates CopA (mol. wt. $\sim$87.1 kDa) under the molecular weight marker at 100 kDa.

The lysate generated by the pressure cell (**Figure 8.3.1**, lane 1) was centrifuged at 20,000 $\times$ g with a high proportion of CopA then found in the pellet (lane 2) suggesting it was contained in large insoluble sections of membrane or unbroken cells. Sonication was also attempted as an alternate lysis method, but resulted in only small quantities of CopA in the centrifugation supernatant (data not shown). The pressure cell supernatant (lane 3) was then centrifuged at 105,000 $\times$ g in order to separate the membrane-bound CopA into the pellet (lane 4). This step was moderately effective as half (or less) of CopA remained in the supernatant (lane 5).

Solubilisation trials were carried out using three nonionic detergents typically used in purification of integral membrane proteins; their structures are depicted in **Figure 8.3.2**,

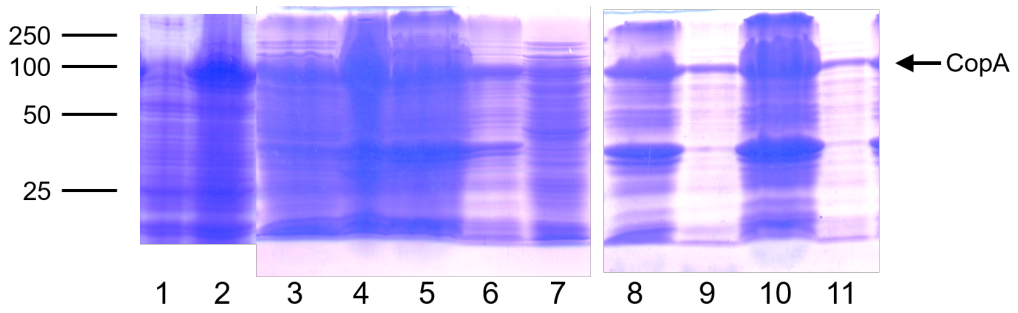

Figure 8.3.1: Isolation of CopA and solubilisation in Triton X-100. After over-expression, CopA was isolated via centrifugation at 20,000 × g and then 105,000 × g. SDS-PAGE analysis reveals proteins present in: **1)** Pre-induction culture, **2)** Post-induction culture, **3)** Cell lysate, **4)** pellet after centrifugation at 20,000 × g, **5)** supernatant after centrifugation at 20,000 × g, **6)** pellet after centrifugation at 105,000 × g, **7)** supernatant after centrifugation at 105,000 × g. After isolation, the semi-pure CopA (Lane 4) was solubilised in two different concentrations of Triton X-100 (1 mM and 10 mM) and centrifuged at 200,000 × g, generating: **8)** Soluble fraction at 1 mM (0.06%) Triton X-100, **9)** Insoluble fraction at 1 mM (0.06%) Triton X-100, **10)** Soluble fraction at 10 mM (0.6%) Triton X-100, **11)** Insoluble fraction at 10 mM (0.6%) Triton X-100.

along with the reported CMC value for each detergent. Solubilisation of CopA was carried out using a concentration 4- to 40-fold in excess of the CMC.

SDS-PAGE analysis of solubilisation of membrane-bound CopA using Triton X-100 and Brij-35 are depicted in **Figure 8.3.1** and **Figure 8.3.3**, respectively. The semi-pure, solubilised CopA samples were applied to a Ni^{2+} IMAC column. The samples solubilised in Triton X-100 did not bind to the column (data not shown). At both concentrations of Brij-35, CopA did bind the IMAC column, the column flow-through (lanes 3 and 8) did not contain a large amount of CopA, and CopA eluted in 2 × 5 mL fractions (lanes 4, 5, 8, and 9), at approximately 100 mM imidazole. Though SDS-PAGE indicated these fractions were fairly pure, the absorbance spectrum revealed an A_{max} = 260 nm, suggesting nucleic

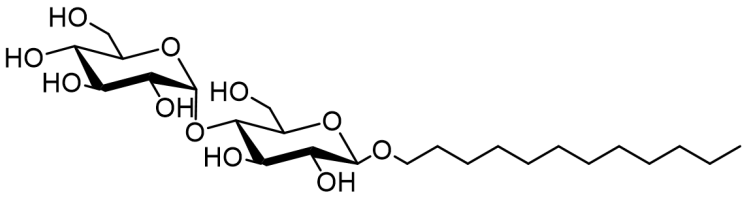

DDM (N-dodecyl-β-D-maltoside)
CMC: ~0.170 mM (0.009%)

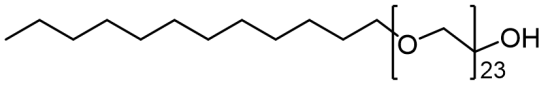

Brij-35 (Polyoxyethylene(23) lauryl ether)
CMC: ~0.098 mM (0.012%)

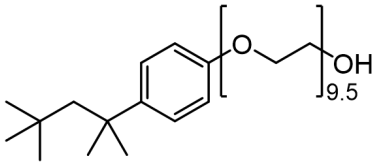

Triton X-100 (4-octylphenol polyethoxylate)
CMC: ~0.220 mM (0.016%)

Figure 8.3.2: Detergents tested for the solubilisation of CopA. DDM, Brij-35 and Triton X-100 are all nonionic detergents used in solubilisation trials of CopA. The CMC for Triton X-100 is reported to be $\sim$ 0.220 mM (0.016% w/v). The CMC for Brij-35 is reported to be $\sim$ 0.10 mM (0.012% w/v) [202]. The CMC for DDM is reported to be $\sim$ 0.170 mM (0.009% w/v) [203].

acid contamination (**Figure 8.3.4**).

The ATPase assay was tested using fractions containing CopA solubilised in Brij-35, but a large absorbance intensity at 710 nm arose, suggesting the presence of phosphate, which likely was carried over from the phosphate buffer used in the purification of the protein (data not shown). Therefore the protein was buffer exchanged, and the enzyme activity of CopA was assessed using the ATPase functional assay in a HEPES buffer system. The results are presented in **Figure 8.3.5**, with the standard curve reporting on the presence of inorganic phosphate. The samples containing combinations of buffer, water and ATP did not exhibit absorbance at 710 nm, suggesting no phosphate was found in those materials.

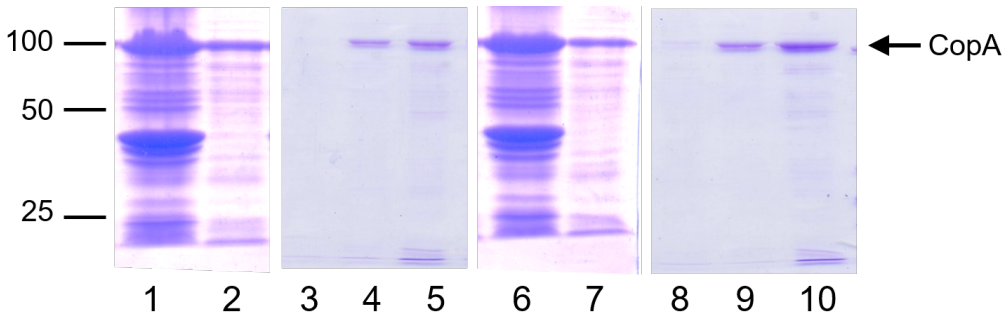

Figure 8.3.3: Purification of CopA in Brij-35. After CopA overexpression and isolation, semi-pure CopA (**Figure 8.3.1**, Lane 4) was solubilised in Brij-35 and applied to a Ni^{2+} IMAC column. Here, SDS-PAGE analysis depicts the results in both concentrations of Brij-35 (1 mM and 10 mM). After solubilisation at 1 mM Brij-35, **1)** Soluble fraction, **2)** Insoluble fraction, **3)** IMAC flow-through, **4)** IMAC F2, **5)** IMAC F3. A similar proportion of CopA was solubilised and recovered from the Ni^{2+} IMAC column after solubilisation at 10 mM Brij-35: **6)** Soluble fraction, **7)** Insoluble fraction, **8)** IMAC flow-through, **9)** IMAC F2, **10)** IMAC F3.

The sample containing CopA and ATP exhibited an absorbance of 1.58 at 710 nm suggesting the presence of 1.96 mmoles P_i. Though P_i could have arisen partially due to ATP turnover, the level measured exceeds the molar quantity of ATP added to the sample (0.05 μmoles). This suggests additional phosphate was present in the sample, perhaps further carryover from the phosphate buffer, thus the assay results cannot confirm ATPase activity of the protein.

With the aim of improving the protocol, a second overexpression was carried out and the purification modified in the following ways: use of HEPES buffer instead of phosphate, use of n-dodecyl-β-D-maltoside (DDM) for solubilisation which was found to be common in protocols for P-type ATPase purification [46], [204], [205], along with addition of a salt

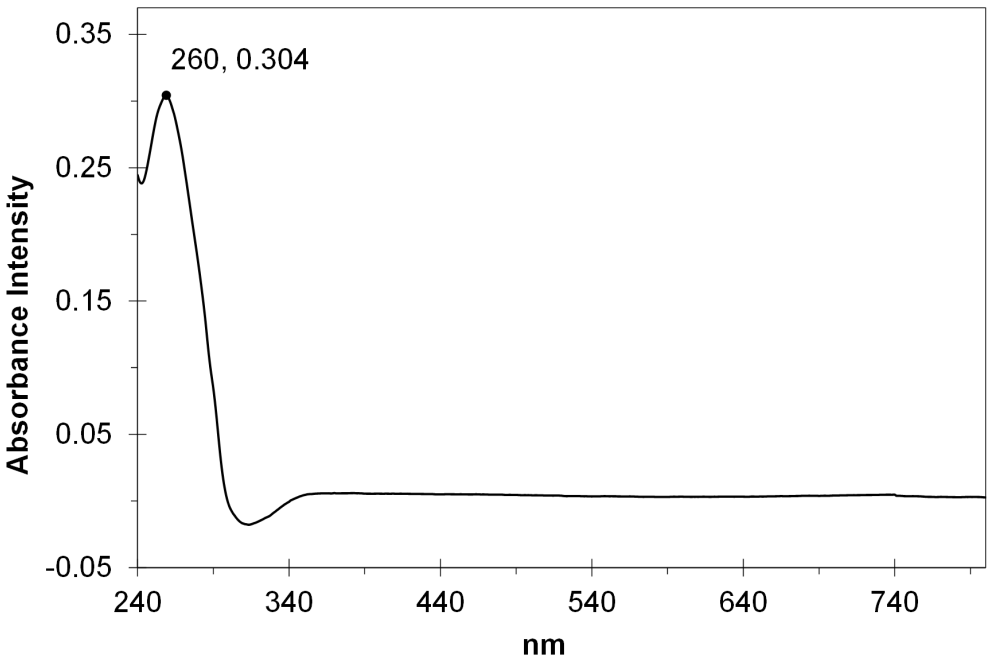

Figure 8.3.4: UV-visible absorbance of CopA in Brij-35. Absorbance spectrum of elution fractions from Ni^{2+} IMAC column containing CopA. The A_{max} = 260 nm suggests nucleic acid contamination in these fractions. The baseline anomaly at approximately 325 nm likely arises due to the baseline and sample cells containing different levels of oxidised DTT, which causes a yellow-brown colour and absorbance at $\sim$ 325 nm.

wash during IMAC in order to remove nucleic acid.

The SDS-PAGE analysis of the second purification of CopA using DDM is depicted in **Figure 8.3.6**. Centrifugation of the lysate at 20,000 $\times$ g generated a pellet (lane 2) containing a high proportion of CopA, but a substantial amount of CopA was also found in the supernatant fraction (lane 3). This suggests that approximately half the CopA remained in unbroken cells or very large insoluble membrane sections. Centrifugation of the supernatant at 105,000 $\times$ g resulted in half of the CopA being isolated in the pellet (lane

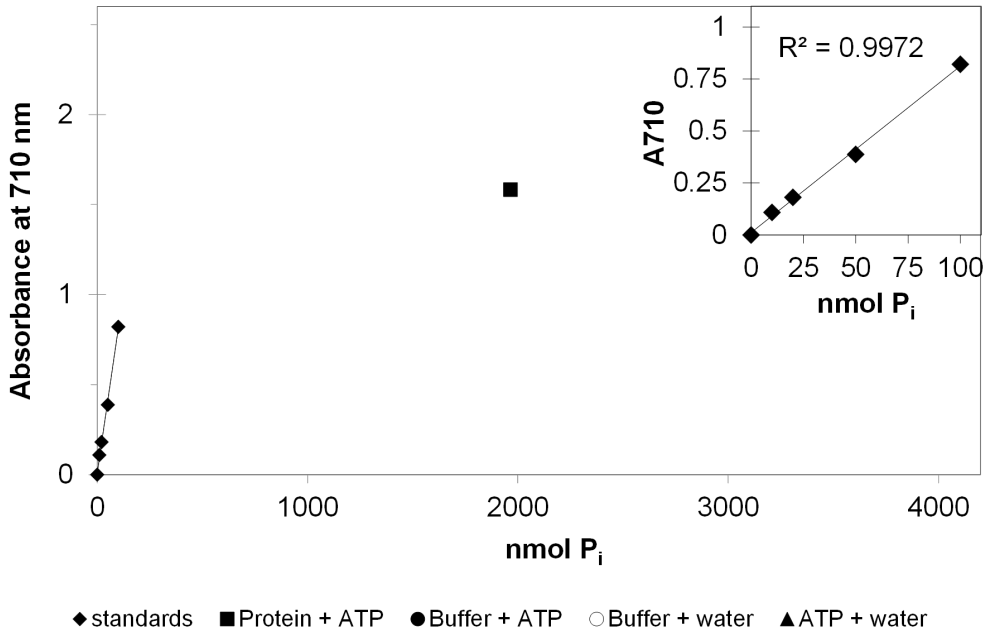

Figure 8.3.5: ATPase activity assay of CopA. ATPase assay where inorganic phosphate reacts with $(NH_4)_2MoO_4$ and is quantified by monitoring absorbance at 710 nm. Inset: standard curve samples. The standard curve (filled diamonds) establishes the absorbance expected at increasing levels of phosphate. The samples containing Buffer + ATP (filled circle) or Buffer + water (hollow circle) or ATP + water (filled triangle) generated zero absorbance at 710 nm. The absorbance observed for CopA + ATP (filled square) illustrates that $\sim$ 2 mmoles P_i is present. However, rather than indicating ATPase activity it is likely that this is due to carry-over from the purification protocol where a phosphate buffer was used.

4).

After solubilising the membranes in DDM for 14 hours (at 0.03%, 0.08%, 0.15% or 0.3%), the remaining insoluble material was removed via centrifugation (200,000 $\times$ g). SDS-PAGE analysis illustrates that, with increasing DDM concentration, a progressively increasing amount of CopA was recovered in the supernatant (**Figure 8.3.6**, lanes 6 – 9). The semi-pure CopA solubilised at 5 mM (0.3%) DDM was applied to a Ni^{2+} IMAC column,

and CopA was the primary species observed in the elution fractions (2 × 5 mL), but was not the only species present. Thus, the purification protocol described above generated only semi-pure CopA. To continue studies of CopA, the yield and purity resulting from this protocol should be improved upon in future.

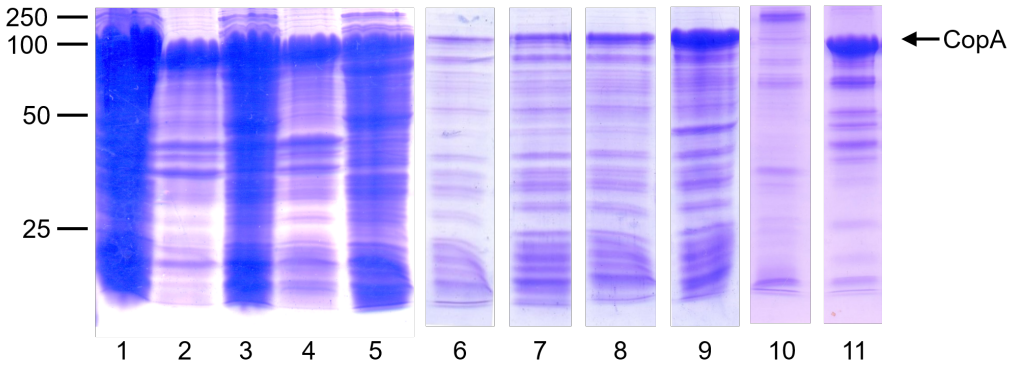

Figure 8.3.6: Purification of CopA in DDM. SDS-PAGE analysis of CopA lysis and centrifugation, solubilisation in DDM, and Ni^{2+} IMAC: **1)** Cell lysate, **2)** Pellet after centrifugation at 20,000 × g, **3)** Supernatant after centrifugation at 20,000 × g, **4)** Pellet after centrifugation at 95,000 × g, **5)** Supernatant after centrifugation at 95,000 × g, **6)** Supernatant after solubilisation in 0.5 mM (0.03 %) DDM, **7)** Supernatant after solubilisation in 1.2 mM (0.08 %) DDM, **8)** Supernatant after solubilisation in 2.5 mM (0.15 %) DDM, **9)** Supernatant after solubilisation in 5 mM (0.30 %) DDM, **10)** IMAC flow through, **11)** IMAC elution fraction.

8.4 Discussion

The lysis and isolation portion of the protocol resulted in good recovery of membrane-bound CopA, but this could perhaps be improved as the lysate pellet contained a large proportion of CopA. The centrifugation speeds chosen here were consistent with those reported in established protocols [46] [204], with low speed aimed at removal of debris/unbroken cells in the pellet, and the high speed included to isolate the membrane fraction from soluble unwanted proteins or unfolded CopA. Though reduction of the first centrifugation speed [205] perhaps could result in improved recovery of the membrane fraction (and thus CopA), this also may lead to contamination with unbroken cells/debris.

It is also possible that amending the lysis step could improve the yield of CopA. Other established purification protocols including P-type ATPases [206] [207] utilise a pressure cell for cell lysis. Accordingly, here, the pressure cell liberated a high proportion of the membrane fraction compared to sonication. In both instances of using the pressure cell, two passes at 1000 psi were used. Perhaps a greater number of passes or increased pressure would improve the membrane fraction yield.

For intact protein analysis, it is generally better to use a mild detergent with low CMC, preferably nonionic, and/or one with a larger headgroup or longer hydrocarbon chain [198]. With this in mind, three nonionic analytical grade detergents were selected. Triton X-100 is a mild, low CMC detergent used for solubilisation of membrane and ATP-binding proteins [208]. Despite its success at solubilisation, CopA in Triton X-100 did not bind the IMAC column. It would not have been an ideal choice due to its absorbance in the UV

region which interferes during purifcation [197]. Brij-35 is a low CMC detergent similar in structure to octaethylene glycol (OG; C12E8), a detergent used in solibilising membrane proteins including a P_{1B}-type ATPase [46]. While solubilisation was effective in Brij-35 with recovery of nearly all CopA at both concentrations, its use is not as prevalent in purification of ATPase proteins, and therefore for the second purification in non-phosphate buffer, a third detergent, DDM, was tested.

After incubation of the ultracentrifugation pellet in DDM, the solubilisation seemed to recover less CopA compared to Brij-35 and Triton X-100 at similar proportions (10 $\times$ CMC, Brij-35; 5 $\times$ CMC, Triton X-100; 3 and 9 $\times$ CMC, DDM). Increased concentration to 17 $\times$ CMC improved recovery and for 33 $\times$ CMC (0.3%) approximately half the CopA was solubilised; perhaps a further increase in DDM concentration would be worth exploring. It has been demonstrated in certain cases, the detergent concentration during solubilisation can be up to 100-fold excess DDM [209] and sometimes 200-fold in excess of the CMC [46].

It was expected that the interaction between the His-tag and the IMAC resin may be obstructed due to the large micelles formed by DDM [210]. However, this was not the case as the column-flow through contained little protein, with nearly all protein including CopA found in the IMAC elution fractions. However, additional proteins solubilised by DDM also were recovered via IMAC. This could suggest that additional, small proteins are incorporated into the micelle. Employing a step gradient could be effective in isolating CopA from other proteins, but would be difficult as CopA elutes at a fairly low imidazole concentration ($\sim$100 mM). Lowering the detergent concentration may lead to CopA binding the column more tightly, and enable better separation from other protein species. Because IMAC is

usually effective at isolating the target His-tagged protein, it is possible that some other proteins are degradation products of CopA. Addition of a protease inhibitor could reduce protein degradation, and the length of time spent on this purification procedure ($\sim$ two weeks) should naturally be reduced to $\sim$ 2 –3 days once an optimised protocol is established.

The ATPase assay calibration curve suggests that this assay is an effective quantitative measure of inorganic phosphate. Phosphate cross-contamination during CopA purification was alleviated, but not eradicated, via preparation of assay solutions in plastic and sample buffer exchange, which led to an accurate standard curve and control samples free of P_i. The absorbance intensity of the sample containing CopA and ATP suggested that this sample contained 1.96 mmoles P_i, far exceeding the quantity of ATP present in the sample (0.05 μmoles). Because phosphate was not found in samples containing buffer, water or ATP, this suggests that though buffer exchange did significantly lower the P_i concentration, the protein sample may have contained residual phosphate carryover and additional buffer exchange steps are likely required. Therefore, though this small-scale trial demonstrates the workings of the assay, the results here cannot reliably validate the ATPase function of the protein.

Clearly this work is unfinished and time constraints meant that it was not possible to continue these investigations. However, they map out the successful over-expression and purification of significant quantities of CopA (albeit in a semi-pure state) and, as such, lay the ground work for future studies of the full length CopA protein.

Chapter 9

General Discussion

Copper trafficking proteins have previously been characterised by spectroscopic and biophysical methods, which revealed information about their copper-binding behaviour. To further this, here, ESI-MS and kinetic studies were employed using *Bacillus subtilis* copper chaperone (CopZ) and the soluble N-terminal domains (CopAab) of the integral membrane export ATPase CopA. Cu(I)-binding behaviour in the presence and absence of low molecular weight thiols (LMWT) was explored, as was the Cu(I) binding behaviour of other copper chaperones from *Saccharomyces cerevisiae* and *Streptomyces lividans*.

The binding of Cu(I) to CopZ is complex with dimerisation occurring in the presence of copper. Here, native ESI-MS was employed to examine the species distribution of each of these proteins with changing copper levels. Previous data supported a model where CopZ dimerised upon binding Cu(I), forming $Cu(CopZ)_2$ at 0.5 Cu / protein, with binding of additional Cu(I) ions to form $Cu_4(CopZ)_2$ at 2 Cu / CopZ [89]. The ESI-MS data at 0.5 / CopZ presented here revealed the major species to be monomeric CuCopZ with a large amount of apo-CopZ present; given the previous solution studies, this is likely to arise as a result of breakdown of $Cu(CopZ)_2$. At 1 Cu / protein, the relative intensity of CuCopZ decreased, with a diverse mixture of CopZ species present, both monomeric and dimeric; the most intense copper-bound species being $Cu_4(CopZ)_2$. The tetranuclear species was observed previously, as a crystal structure generated from a CopZ sample prepared at 1

Cu / protein [81]; this suggests that $Cu_4(CopZ)_2$ is a thermodynamically stable form. The continued dominance of $Cu_4(CopZ)_2$ in mass spectra at higher copper levels (1.5 and 2 / protein) without accumulation of $Cu_2(CopZ)_2$ or $Cu_3(CopZ)_2$ is indicative of cooperative formation of $Cu_4(CopZ)_2$ by CopZ as the Cu(I) level is increased.

The role low molecular weight thiols (LMWT) play *in vivo* is multifaceted and complex as they participate in redox buffering, and form protective mixed disulfides with cellular proteins under oxidative stress [154]. The high affinity of their thiol groups for soft metals also potentially makes them influential in metal trafficking. Here, an interesting aspect was the ability to use the physiologically relevant LMWT, bacillithiol (BSH) [211]. To assess its capacity for Cu(I) binding, through competition with $Cu(BCS)_2^{3-}$, the affinity of BSH for Cu(I) was established to be $\beta_{2(BSH)} = 4.1 \pm 1.5 \times 10^{17}\ M^{-2}$. A Cu(I) titration of CopZ in the presence of 20-fold excess BSH was monitored by UV-visible spectroscopy and circular dichroism, yielding similar results to previous data acquired using Cys and GSH [52]: little effect upon Cu(I) binding up to 0.5 Cu / CopZ, beyond which a departure from thiol-free behaviour was observed, including a reduction in number of binding phases.

ESI-MS revealed the effect of LMWT upon the species distribution observed in the thiol-free spectrum of CopZ prepared at 1 Cu / protein. In the presence of all thiols tested (BSH, GSH, DTT), a reduced intensity of higher order Cu(I)-bound forms was observed, presumably due to competition of LMWT for Cu(I). The effect was seen immediately using DTT, as CuCopZ was the predominant species observed at low levels of DTT. With increasing DTT, a decreasing proportion of apo-CopZ was observed, which could indicate some stabilising effect of DTT upon CuCopZ. DTT has been demonstrated to serve as an

additional ligand for Cu(I) in CuCopZ *in vitro* [40], but no DTT adducts were observed here by ESI-MS to directly confirm this.

GSH and BSH led to reduction in dimeric CopZ forms but unlike observed for DTT, the effect was gradual as the ratio of thiol/protein was increased. In addition, glutathionylation and bacillithiolation were observed, where thiol adducts are formed between LMWT and protein; *in vivo* this process is a safeguard against irreversible overoxidation of sulfide. In higher order CopZ complexes, the Cys thiols are involved in Cu(I) coordination; here it is therefore likely that BSH and GSH are serving as additional Cu(I) ligands.

The process of dimerisation by prokaryotic copper chaperones is thought to be influenced by two residues (see Figure 7.1.2). One is the X_3 residue in the conserved $MX_1CX_2X_3C$ binding motif, where prokaryotes have a conserved histidine that can act as an additional Cu(I) ligand in higher order complexes. Another residue is found at the end of loop 5, typically a tyrosine in prokaryotes, which is thought to facilitate protein-protein interaction and dimerisation through its proximity to the Cu(I)-binding site. Here, eukaryotes typically possess a lysine, which is thought to preclude the need for dimerisation by reducing the bound copper's solvent-accessibility, and stabilise the cysteine thiolate by way of charge balancing the metal centre. To explore the potential effect of these residues upon the copper-bound species distribution of prokaryotic and eukaryotic copper chaperones, ESI-MS was carried out upon *S. lividans* CopZ-1317 and CopZ-3079, and *S. cerevisiae* Atx1.

The *S. lividans* copper chaperones are predicted to play different roles in copper trafficking and, consistent with this, ESI-MS revealed rather different distributions of copper-

bound species. For CopZ-3079 prepared at 1 Cu / protein, a diverse mixture of species was present with CuCopZ-3079 and Cu_4CopZ-3079_2 dominant (in agreement with SEC data [192] that showed a mixture of monomer/dimer). At 2 Cu / protein, monomeric species were diminished with Cu_6CopZ-3079_2 dominant (supported by absorbance titration which revealed rising absorbance $\geq$ 1.5 Cu / protein, and SEC where dimeric species dominated $\geq$ 1.5 Cu / protein). The species distribution observed implies cooperative formation of Cu_6CopZ-3079_2, with progressively elevated intensity of Cu_2CopZ-3079 and Cu_2CopZ-3079_2 suggesting they exist as intermediates. It is unclear how a dimeric form coordinating five or six Cu(I) ions would be arranged.

The ESI-MS data of CopZ-1317 was more complex. At 1 Cu / protein mass spectra illustrated a diverse mixture of monomeric, dimeric and trimeric species. Assuming the dominant peak CopZ-1317_2 represents disulfide bonded apo-protein, the species distribution observed in ESI-MS could be supported by the SEC elution profile [192] that demonstrated monomeric forms dominate in solution at 1 Cu / protein. At 2 Cu / protein, the predominant species observed was Cu_2CopZ-1317_2, with a diverse mixture of low-intensity species, including trimeric forms which coordinated up to 8 Cu(I) ions. Previous data revealed multiphasic increases in absorbance intensity between 1 and 2 Cu / protein [192] (which could support this diverse mixture of species) and elevated copper levels resulting in formation of a higher order form at a stoichiometry of 1:1, proposed to be Cu_4CopZ-1317_4 [74]. The ESI-MS species distribution suggests that elevated copper levels leads to formation of Cu_2CopZ-1317_2 either instead of, or as a breakdown of Cu_4CopZ-1317_4.

Due to higher transcription levels and five-fold higher affinity for Cu(I), CopZ-3079 is

proposed to be more involved in buffering cellular Cu(I) than CopZ-1317 [74]. In line with their proposed divergent cellular roles in copper trafficking, CopZ-3079 and CopZ-1317 displayed different copper-binding behaviour. Both possess the X_3 histidine in their conserved $MX_1CX_2X_3C$ copper-binding motifs, but at the end of loop 5 CopZ-1317 (like *B. subtilis* CopZ), possesses a conserved tyrosine where CopZ-3079 has a phenylalanine, unusual for a prokaryotic copper chaperone. Despite this, for both proteins, dimeric copper-bound forms dominated at elevated copper levels: CopZ-3079 with a higher Cu(I) affinity formed Cu_6CopZ-3079$_2$; for CopZ-1317 with the lower Cu(I) affinity, Cu_2CopZ-1317$_2$ dominated. Thus the lack of conserved tyrosine at the end of loop 5 for CopZ-3079 did not inhibit dimerisation; in fact, dimeric forms dominated at a lower copper/protein ratio for CopZ-3079 in agreement with SEC data. Perhaps the X_3 histidine is a key factor in stabilisation of dimeric forms, which has been demonsrated in its ability to serve as an additional ligand in the tetranuclear copper cluster observed for *B. subtilis* Cu_4(CopZ)$_2$ [81]. It cannot be ruled out that the tyrosine somehow affects the stability of higher order forms as trimeric forms here were only observed for CopZ-1317. Previously, a trimeric complex of *B. subtilis* CopZ containing a trinuclear Cu(I) cluster was observed in a high-resolution crystal structure [163], where Tyr65 played a central role in stabilising the structure.

ESI-MS of *S. cerevisiae* Atx1 in the presence of increasing Cu(I) revealed monomeric CuAtx1 as the major species at low copper levels (0.5 and 1.0 Cu / protein) followed by cooperative formation of Cu_4Atx1$_2$ (1.5 and 2.0 Cu / protein). Atx1 lacks an X_3 histidine and at the end of loop 5 possesses a lysine. In agreement, the dominance of the dimeric form Cu_4Atx1$_2$ was observed at a higher Cu / protein ratio than for the prokaryotic coun-

terparts. This idea can be supported by mutagenesis experiments involving Y65K CopZ which demonstrated a higher Cu / protein ratio required for dimerisation [179].

Spectroscopic studies demonstrated *S. lividans* CopZ-1317 and CopZ-3079, at elevated copper levels, can form higher order assemblies, which were demonstrated via SEC not to form in the presence of LMWT. In the presence of low levels of LMWT, the spectrum of 2 Cu / CopZ-1317 predominantly contained a mixture of $Cu(CopZ)_2$ and $Cu_2(CopZ)_2$, suggesting the dimeric and trimeric species with higher copper loadings observed in the thiol-free spectrum were low-affinity complexes. With increasing LMWT, no higher order complexes were observed suggesting DTT competes effectively for Cu(I) at higher loadings. Though the predominant peaks observed were a mixture of CopZ-1317 and CuCopZ-1317, the dimeric Cu_2(CopZ-1317)$_2$ persisted ($\sim$ 20% relative intensity) even at the highest level of DTT tested. This is in contrast to the presence of LMWT in a spectrum of 2 Cu / CopZ-3079, which resulted in immediate near complete removal of all dimerised species' peaks. The predominant species observed were a mixture of CuCopZ and Cu_2CopZ. No apo-CopZ-3079 was observed, perhaps reflecting the higher Cu(I) affinity of this protein compared to CopZ-1317. For both CopZ-3079 and CopZ-1317, in the presence of elevated levels of LMWT, this unexpected stoichiometry Cu_2CopZ were observed, which may indicate a stabilising effect or that DTT can provide additional ligands to the Cu(I), but which does not survive the ionisation process.

A similar species distribution was observed for Atx1 at all DTT levels tested though this differed from the thiol-free spectrum of 2 Cu / Atx1. This suggests that the presence of DTT redistributes Cu(I). Some of the species observed have unexpected stoichiometric

ratios of Cu:protein, which could suggest that DTT serves as an additional Cu(I) ligand. In addition, the high intensity of apo-Atx1 would be in agreement that DTT competes for copper. Despite the fact that $Cu_2Atx1_2GSH_2$ was observed previously, the equivalent species $Cu_2Atx1_2DTT_2$ was not observed. Although no DTT adducts were observed directly, perhaps the stabilised intensity of Cu_2Atx1 and Cu_2Atx1_2 points to the presence of this species in solution.

Prior to undertaking the ESI-MS based studies, substantial spectroscopic data supported a model where CopAab binds Cu(I) with high affinity as a monomer up to a ratio of 1 Cu / protein, beyond which a multinuclear, dimerised form of CopAab was observed [80]. Between 1 – 4 Cu / protein, the model proposes gradual formation of $Cu_8(CopAab)_2$ [147]. The ESI-MS data between 0 and 1 Cu / protein confirmed CopAab to be monomeric, as either CuCopAab or Cu_2CopAab. Between 1 – 2 Cu / protein, the ESI-MS data depart from the previous model by showing that CopAab is primarily monomeric with the major species Cu_2CopAab. However, a $Cu_4(CopAab)_2$ species was detected. The Cu_2CopAab species does possess the same stoichiometric ratio as the sample (2:1) and is in agreement with previous NMR data demonstrating that both the a and b domains bind Cu(I) with equal preference [80]. However, CopAab was demonstrated to be dimeric at 2 Cu / protein by analytical ultracentrifugation and size exclusion chromatography. This could indicate poor ionisation efficiency/gas-phase stability of $Cu_4(CopAab)_2$, which is supported by low peak intensity of this species in the mass spectrum, and the lack of $Cu_2(CopAab)_2$ or $Cu_3(CopAab)_2$ species. The previous model based upon fluorescence and circular dichroism data illustrated that dimeric CopAab continually binds Cu(I) ions beyond a level of 2

Cu / protein. Though it was not explicitly demonstrated, this model suggested that, ultimately, $Cu_8(CopAab)_2$ was formed. ESI-MS confirmed the binding of Cu(I) ions by the CopAab dimer beyond 2 / protein, but at 4 Cu / CopAab the observed major species was $Cu_6(CopAab)_2$.

Two different dimeric species were indicated by separate ESI-MS peak envelopes, each with equal copper-to-protein ratios; the lower charge state peaks likely resulted from a more compact arrangement. This led to the proposal of a compact, symmetric form with two trinuclear Cu(I) clusters, and also a less compact asymmetric form, where a domain from each monomer jointly coordinates a tetranuclear Cu(I) cluster and the remaining two domains each coordinate a single Cu(I) ion. Previous NMR data have shown that domain a is less stable, and is subject to unfolding upon binding of copper [83] [212]. Thus, it is also a possibility that the less compact structure could result from the symmetric dimer undergoing partial unfolding.

Though CuCopAab and Cu_2CopAab were both observed via ESI-MS, it was unclear which domains participated in higher order copper-bound CopAab species, and whether Cu(I) binding is equivalent to both domains of CopAab as copper levels are increased. Intraprotein multinuclear cluster formation cannot occur due to the short length of the linker tethering the domains of CopAab. Thus when a multinuclear cluster is formed, it can only result from interaction of domains from two different proteins. Therefore though a CopAab dimer does involve four domains, it is not possible for them to all act as ligands to the same copper ion. This would imply that each domain functions independently within CopAab, exhibiting its own copper-binding behaviour and, potentially, its own function in the copper

trafficking pathway.

Previous spectroscopic studies have established the Cu(I) binding behaviour of the individual domains, CopAa [83] and CopAb [82]. Each of the individual domains binds Cu(I) with high affinity and forms multinuclear copper centers. Independently, CopAa exhibits instability upon Cu(I) binding, particularly at high levels ($>$ 1 Cu / protein), but this instability is lessened within a mixture of CopAa and Ab, suggesting the two domains interact in solution.

In order to assess whether a mixture of the individual domains (CopAa and CopAb) behave differently when combined as separate domains in solution compared to the two domain protein CopAab, Cu(I) was added (at 0.5, 1, or 2 per domain) to an equimolar CopAa/CopAb mixture. The solution composition was resolved by SEC and fractions analysed for protein by ESI-MS, and metal by ICP-OES. The data at 0.5 and 1.0 Cu / domain revealed mostly monomeric CopAa and CopAb (with copper associated) and, in agreement with the ESI-MS data, revealed mostly monomeric CopAab. A small amount of homodimeric CopAa (with little copper associated) implied that initial dimeric species observed at low Cu(I) loadings in ESI-MS of CopAab involve copper coordination by the CopAa domains.

At 2 Cu / domain (4 Cu / protein), the ESI-MS data (Fig 5.3.3D) depicted a high proportion of dimeric CopAab with a multinuclear copper cluster. The SEC data revealed that copper was evenly distributed among the tetrameric CopAa and dimeric species (mostly CopAb). Here, it is not entirely clear whether the dimeric species are homodimeric, whether any of the tetrameric CopAa has exhibited loss of secondary structure, or whether a multi-

nuclear cluster has formed. Further work establishing the speciation of individual domains CopAa and CopAb would be useful to determine (qualitatively) the level of secondary structure preserved, and also what copper-bound forms of CopAa exist at high Cu(I) levels.

The effect of DTT upon copper binding of CopAab was assessed by ESI-MS. Because we wanted to explore the species distribution at higher copper levels, which did not fully support the binding model established using previous spectroscopic data, 4 Cu / CopAab was chosen. Unlike in the mass spectra of CopZ, DTT adducts were observed for several monomeric CopAab species. Higher levels of DTT (5, 10 and 25 molar equivalents) did lead to loss of the dimer peak envelope. However, at the lowest level of DTT (1 molar equivalent), dimeric species were still present. A slight increase in intensity of CopAab species containing 4 Cu(I) may indicate a stabilising effect upon $[Cu_2CopAab]_2$, the species which previously had been suggested to bind additional Cu(I) and lead to formation of other higher order species [163]. This stabilising effect may be corroborated by the appearance of DTT adducts on monomer CopAab containing 4 – 6 Cu ions, not observed in the absence of thiol. One of these peaks persisted ($\sim$ 25%, Cu_4CopAab:DTT) even at the highest level of DTT tested.

Compared to the thiol-free mass spectra, the physiologically relevant BSH appeared to confer a stabilising effect on dimeric forms of CopAab, which appeared at much higher relative intensity than in the absence of thiol, and persisted to the highest thiol level tested. In addition, CuCopAab was the only copper-bound monomeric form present; this could occur as Cu_2CopAab was present in thiol-free spectra as a breakdown product of $[Cu_2CopAab]_2$. No bacillithiolation of monomeric CopAab was observed. The copper-binding capacity of

the dimer appeared to be higher in the presence of BSH, as $Cu_7(CopAab)_2$ and $Cu_8(CopAab)_2$ were observed. Concomitantly, the monomer peak intensity was much lower with $Cu_7(CopAab)_2$ being the major copper-bound species at the lower three BSH levels tested. This stabilising effect is also suggested by the observation of BSH adducts on dimeric forms of CopAab containing 5 and 6 Cu(I) ions. The more compact dimeric form of CopAab diminished more readily in the presence of BSH, which could occur because BSH is able to penetrate the less compact structure more easily to serve as a stabilising force.

Despite the extremely high affinity for Cu(I) displayed by CopZ and CopAab, copper transfer between the proteins is rapid and reversible [163]; previously a weak thermodynamic drive for exchange [66] has been reported for these types of proteins. Because copper transfer is thought to occur within a protein:protein complex under kinetic control, rate measurements were carried out of copper transfer between CopAab and CopZ.

To confirm that protein interaction is required for copper transfer, complex formation was prevented by loading apo- and copper-bound CopZ into separate dialysis cassettes, submerged in the same buffer. The intention was that monitoring absorbance would enable direct measurement of the dissociation of Cu(I) from CopZ. No absorbance increases were observed for apo-CopZ, and copper analysis revealed copper only to be associated with holo-CopZ, not with the (original) apo-protein or in the buffer itself. The absorbance of the copper-loaded CopZ sample did decrease slightly over the course of the experiment but this probably, at least partially, indicates loss of protein on the dialysis membrane rather than loss of copper. The results confirmed that the offrate of Cu(I) from CopZ is extremely low; extrapolation of the data established an upper limit of 6×10^{-5} s^{-1}. This is consistent

with the proposal that copper transfer does not involve release of free Cu(I) and requires protein-protein interaction.

The low dissociation rate of copper from CopZ is due to a large kinetic barrier which is offset when protein complex formation is permitted. Copper transfer between CopZ and CopAab, measured by stopped flow absorbance, revealed extremely rapid reactions, complete within 0.02 s under the conditions tested, consistent with the prediction that protein-protein interaction facilitates expedient copper transfer. The reversibility of copper transfer was confirmed based upon $\triangle A_{265}$ with the sign of the change in accordance with the direction of copper transfer.

Varying the concentration of both proteins revealed that, in both directions of copper transfer, the calculated rate constant was approximately equal: $247 \pm 2.2\ s^{-1}$ from CopZ to CopAab, and $258 \pm 2.6\ s^{-1}$ from CopAab to CopZ. The approximate equivalence of these rate constants indicates the rate limiting step is the same in both directions. In addition, varying the concentration of each reactant revealed the rate constant to be concentration-independent, indicative of a true first-order process. This eliminates the possibility that it could be complex formation, which would be a second order process. This is consistent with predictions of it being rearrangement of a three-coordinate thiolate-Cu site (2 chaperone/1 MBD to 1 chaperone/2 MBD) or dissociation of the complex [34] [213].

This complex involves an interaction between CopZ and one of the domains of CopAab. Both of these proteins reveal dimerised species via ESI-MS, thus in order to explore the utility of ESI-MS for revealing complexes of CopZ/CopAab, mass spectra were acquired of 0.5 Cu/CopZ + apo-CopAab, and also of apo-CopZ + 0.5 Cu/CopAab. The charge state

distribution of these spectra were comparable to each other, and similar also to the spectra of the individual proteins at 0.5 Cu / protein, suggesting there are no major structural differences occurring within the mixture. Because copper transfer has been demonstrated to be rapid and reversible and, very little dimerised protein was observed in either individual protein spectra at this copper level, it was expected that an equal mixture of CuCopAab and CuCopZ would be observed. Though the most intense copper-bound species observed was CuCopAab, this should be interpreted with caution as the relative intensities of copper-bound peaks could be overshadowed by the high intensity of apo-CopZ. Slight differences between the mixed and individual spectra may indicate that copper transfer has taken place: the intensity of CuCopZ peak was lower than apo-CopZ (not the case in the 0.5 Cu/CopZ mass spectrum), and no Cu_2CopAab was observed.

An important observation from this experiment was addditional peaks corresponding to copper-bound CopZ:CopAab complex, which contained 1 or 2 copper ions bound; in addition, apo-complex was observed. The low intensity of the complex peaks is plausible as transfer would be dependent upon encounters between individual proteins. Regardless, further work needs to be done to establish the mixture of species resulting from copper transfer between these proteins.

Fully defining the mechanism of copper export from the cell will involve characterisation of the function of the full-length, membrane-bound CopA, including the role of the MBDs. To further this aim, here, purification of a CopA-FL using new construct pBSCOPA1 was carried out and a purification was developed to generate partially pure, solubilised CopA. Recovery of CopA could perhaps be improved by optimisation of the lysis step in order to

break more cells. It was unclear whether contamination of CopA with other proteins arose due to degradation of CopA, or additional proteins being incorporated into the micelles. In future, completion of the protocol more quickly and addition of a protease inhibitor could inhibit protein degradation. Also, it is possible that other proteins could be released from the micelles by reducing the concentration of DDM during IMAC while the CopA was bound to the column. Quantification of ATPase turnover relies on absorbance arising from the presence of inorganic phosphate; the initial use of phosphate buffers resulted in carryover which confounded the results. Nonetheless, a method was developed to carry out this quantitative assay in future.

In order to continue the study of copper trafficking proteins, some subsequent work to be carried out includes modelling the cooperativity of copper binding to CopZ in formation of higher order complexes. Too few data points were recorded here to effectively complete this analysis, but possibly could be achieved by gradually introducing copper into a CopZ sample and monitoring real-time formation of $Cu_4(CopZ)_2$ via ESI-MS. This approach has been carried out elsewhere via ESI-MS [214], and could be taken to further investigate the copper-bound forms of CopZ (or other chaperones) at high metal-to-protein ratios and/or and mixture of higher order forms. Refer to Appendix for plots illustrating a summary of species distribution from each set of ESI-MS data; with additional data points these types of plots could allow binding cooperativity to be modelled in future.

Additional future studies could be carried out to characterise complex formation during copper transfer between CopZ and CopAab. This could be accomplished via ESI-MS for samples of CopAab/CopZ mixtures, where one protein is copper-free, and and the other at

varied Cu/protein ratios. To further explore the physiological relevance of the higher order complexes, these experiments could be carried out in the absence and presence of BSH.

Another facet of copper transfer to examine would be conformational changes that may take place in CopAab upon binding copper, and their effect upon the function and ATPase activity of CopA. It has been proposed that CopAab may serve to sense copper, or ”switch” on ATPase activity (see Chapter 6). This work could be carried out using the full-length construct of catalytically active CopA.

Further goals could be to quantify the amount of copper transferred between the proteins via ESI-MS and stopped-flow absorbance. To further define the role of each individual domain CopAa and CopAb, ESI-MS could be used to investigate the copper-bound complexes formed by the individual and mixed proteins.

Bibliography

[1] Hodgkinson, V.; Petris, M. J., "Copper Homeostasis at the Host-Pathogen Interface," *Journal of Biological Chemistry*, vol. 287, no. 17, pp. 13549–13555, 2012.

[2] Crichton, R. R.; Pierre, J. L., "Old Iron, Young Copper: from Mars to Venus," *Biometals*, vol. 14, no. 2, pp. 99–112, 2001.

[3] Cordano, A.; Baertl, J. M.; Graham, G. G., "Copper Deficiency in Infancy," *Pediatrics*, vol. 34, pp. 324–336, 1964.

[4] Waddell, J.; Elvehjem, C. A.; Steenbock, H.; Hart, E. B., "Nutritional Anemia on Whole Milk Diets and its Correction with the Ash of Beef Liver," *Science*, vol. 67, no. 1727, pp. 139–140, 1928.

[5] Ridge, P. G.; Zhang, Y.; Gladyshev, V. N., "Comparative Genomic Analyses of Copper Transporters and Cuproproteomes Reveal Evolutionary Dynamics of Copper Utilization and its Link to Oxygen," *PLoS One*, vol. 3, no. 1, p. e1378, 2008.

[6] Rubino, J. T.; Franz, K. J., "Coordination Chemistry of Copper Proteins: How Nature Handles a Toxic Cargo for Essential Function," *Journal of Inorganic Biochemistry*, vol. 107, no. 1, pp. 129–143, 2012.

[7] Solioz, M.; Abicht, H. K.; Mermod, M. and Mancini, S., "Response of Gram-positive Bacteria to Copper Stress," *Journal of Biological Inorganic Chemistry*, vol. 15, no. 1, pp. 3–14, 2010.

[8] Pushie, M. J.; Zhang, L.; Pickering, I. J.; George, G. N., "The Fictile Coordination Chemistry of Cuprous-thiolate Sites in Copper Chaperones," *Biochimica et Biophysica Acta*, vol. 1817, no. 6, pp. 938–947, 2012.

[9] Hu, J.; Dong, L.; Outten, C. E., "The Redox Environment in the Mitochondrial Intermembrane Space is Maintained Separately from the Cytosol and Matrix," *Journal of Biological Chemistry*, vol. 283, no. 43, pp. 29126–29134, 2008.

[10] Silver, S.; Phung le, T., "A Bacterial View of the Periodic Table: Genes and Proteins for Toxic Inorganic Ions," *Journal of Industrial Microbiology and Biotechnology*, vol. 32, no. 11-12, pp. 587–605, 2005.

[11] Macomber, L.; Imlay, J. A., "The Iron-Sulfur Clusters of Dehydratases are Primary Intracellular Targets of Copper Toxicity," *Proceedings of the National Academy of Science USA*, vol. 106, no. 20, pp. 8344–8349, 2009.

[12] Bertini, I.; Cavallaro, G.; and McGreevy, K. S., "Cellular Copper Management - a Draft User's Guide," *Coordination Chemistry Reviews*, vol. 254, no. 5, pp. 506–524, 2010.

[13] Festa, R. A.; Thiele, D. J., "Copper: an Essential Metal in Biology," *Current Biology*, vol. 21, no. 21, pp. R877–883, 2011.

[14] Robinson, N. J.; Winge, D. R., "Copper Metallochaperones," *Annual Review of Biochemistry*, vol. 79, pp. 537–562, 2010.

[15] Tapiero, H.; Townsend, D. M.; Tew, K. D., “Trace Elements in Human Physiology and Pathology. Copper,” *Biomedical Pharmacotherapy*, vol. 57, no. 9, pp. 386–398, 2003.

[16] Peterson, R. L.; Galaleldeen, A.; Villarreal, J.; Taylor, A. B.; Cabelli, D. E.; Hart, P. J.; Culotta, V. C., “The Phylogeny and Active Site Design of Eukaryotic Cu-only Superoxide Dismutases,” *Journal of Biological Chemistry*, 2016.

[17] Gleason, J. E.; Galaleldeen, A.; Peterson, R. L.; Taylor, A. B.; Holloway, S. P.; Waninger-Saroni, J.; Cormack, B. P.; Cabelli, D. E.; Hart, P. J.; Culotta, V. C., “Candida albicans SOD5 Represents the Prototype of an Unprecedented Class of Cu-only Superoxide Dismutases Required for Pathogen Defense,” *Proceedings of the National Academy of Science USA*, vol. 111, no. 16, pp. 5866–5871, 2014.

[18] Culotta, V. C.; Klomp, L. W.; Strain, J.; Casareno, R. L.; Krems, B.; Gitlin, J. D., “The Copper Chaperone for Superoxide Dismutase,” *Journal of Biological Chemistry*, vol. 272, no. 38, pp. 23469–23472, 1997.

[19] Wang, M.; Zhao, Q.; Liu, W., “The Versatile Low-molecular Weight Thiols: Beyond Cell Protection,” *Bioessays*, vol. 37, no. 12, pp. 1262–1267, 2015.

[20] Priora, R.; Coppo, L.; Salzano, S.; Di Simplicio, P.; Ghezzi, P., “Measurement of Mixed Disulfides Including Glutathionylated Proteins,” *Methods in Enzymology*, vol. 473, pp. 149–159, 2010.

[21] Antelmann, H. and Helmann, J. D., “Thiol-based Redox Switches and Gene Regulation,” *Antioxidants and Redox Signalling*, vol. 14, no. 6, pp. 1049–1063, 2011.

[22] Fang, Z. and Dos Santos, P. C., “Protective Role of Bacillithiol in Superoxide Stress and Fe-S Metabolism in *Bacillus Subtilis*,” *Microbiology Open*, vol. 4, no. 4, pp. 616–631, 2015.

[23] Ma, Z.; Chandrangsu, P.; Helmann, T. C.; Romsang, A.; Gaballa, A.; Helmann, J. D., “Bacillithiol is a Major Buffer of the Labile Zinc Pool in *Bacillus Subtilis*,” *Molecular and Microbiology*, vol. 94, no. 4, pp. 756–770, 2014.

[24] Hatori, Y. and Lutsenko, S., “An Expanding Range of Functions for the Copper Chaperone/antioxidant Protein Atox1,” *Antioxidants and Redox Signalling*, vol. 19, no. 9, pp. 945–957, 2013.

[25] Jozefczak, M.; Remans, T.; Vangronsveld, J.; Cuypers, A., “Glutathione is a Key Player in Metal-induced Oxidative Stress Defenses,” *International Journal of Molecular Sciences*, vol. 13, no. 3, pp. 3145–3175, 2012.

[26] Jothivasan, V. K.; Hamilton, C. J., “Mycothiol: Synthesis, Biosynthesis and Biological Functions of the Major Low Molecular Weight Thiol in Actinomycetes,” *Natural Product Reports*, vol. 25, no. 6, pp. 1091–1117, 2008.

[27] Newton, G. L.; Rawat, M.; La Clair, J. J.; Jothivasan, V. K.; Budiarto, T.; Hamilton, C. J.; Claiborne, A.; Helmann, J. D.; Fahey, R. C., “Bacillithiol is an Antioxidant Thiol Produced in Bacilli,” *Nature Chemical Biology*, vol. 5, no. 9, pp. 625–627, 2009.

[28] Banci, L.; Bertini, I.; Cantini, F.; Ciofi-Baffoni, S., “Cellular Copper Distribution: a Mechanistic Systems Biology Approach,” *Cellular and Molecular Life Sciences*, vol. 67, no. 15, pp. 2563–2589, 2010.

[29] Chillappagari, S.; Miethke, M.; Trip, H.; Kuipers, O. P.; Marahiel, M. A., "Copper Acquisition is Mediated by YcnJ and Regulated by YcnK and CsoR in *Bacillus Subtilis*," *Journal of Bacteriology*, vol. 191, no. 7, pp. 2362–2370, 2009.

[30] Lewinson, O.; Lee, A. T.; Rees, D. C., "A P-type ATPase Importer That Discriminates Between Essential and Toxic Transition Metals," *Proceedings of the National Academy of Sciences*, vol. 106, no. 12, pp. 4677–4682, 2009.

[31] Banci, L.; Bertini, I.; McGreevy, K. S.; Rosato, A., "Molecular Recognition in Copper Trafficking," *Natural Product Reports*, vol. 27, no. 5, pp. 695–710, 2010.

[32] Balasubramanian, R.; Rosenzweig, A. C., "Copper Methanobactin: a Molecule Whose Time Has Come," *Current Opinion in Chemical Biology*, vol. 12, no. 2, pp. 245–249, 2008.

[33] Boal, A. K.; Rosenzweig, A. C., "Structural Biology of Copper Trafficking," *Chemical Reviews*, vol. 109, no. 10, pp. 4760–4779, 2009.

[34] Pufahl, R. A.; Singer, C. P.; Peariso, K. L.; Lin, S. J.; Schmidt, P. J.; Fahrni, C. J.; Culotta, V. C.; Penner-Hahn, J. E.; O'Halloran, T. V., "Metal Ion Chaperone Function of the Soluble Cu(I) Receptor Atx1," *Science*, vol. 278, no. 5339, pp. 853–856, 1997.

[35] Radford, D. S.; Kihlken, M. A.; Borrelly, G. P.; Harwood, C. R.; Le Brun, N. E.; Cavet, J. S., "CopZ from *Bacillus Subtilis* Interacts in vivo with a Copper Exporting CPx-type ATPase CopA," *FEMS Microbiology Letters*, vol. 220, no. 1, pp. 105–112, 2003.

[36] Ohrvik, H.; Wittung-Stafshede, P., "Identification of New Potential Interaction Partners for Human Cytoplasmic Copper Chaperone Atox1: Roles in Gene Regulation?," *International Journal of Molecular Sciences*, vol. 16, no. 8, pp. 16728–16739, 2015.

[37] Arnesano, F.; Banci, L.; Bertini, I.; Cantini, F.; Ciofi-Baffoni, S.; Huffman, D. L.; O'Halloran, T. V., "Characterization of the Binding Interface Between the Copper Chaperone Atx1 and the First Cytosolic Domain of Ccc2 ATPase," *Journal of Biological Chemistry*, vol. 276, no. 44, pp. 41365–41376, 2001.

[38] Banci, L.; Bertini, I.; Del Conte, R.; Mangani, S.; Meyer-Klaucke, W., "X-ray Absorption and NMR Spectroscopic Studies of CopZ, a Copper Chaperone in *Bacillus subtilis*: the Coordination Properties of the Copper Ion," *Biochemistry*, vol. 42, no. 8, pp. 2467–2474, 2003.

[39] Pitts, A. L.; Hall, M. B., "Investigating the Electronic Structure of the Atox1 Copper(I) Transfer Mechanism with Density Functional Theory," *Inorganic Chemistry*, vol. 52, no. 18, pp. 10387–10393, 2013.

[40] Banci, L.; Bertini, I.; Del Conte, R.; Markey, J.; Ruiz-Duenas, F. J., "Copper Trafficking: the Solution Structure of *Bacillus Subtilis* CopZ," *Biochemistry*, vol. 40, no. 51, pp. 15660–15668, 2001.

[41] Arnesano, F.; Banci, L.; Bertini, I.; Huffman, D. L.; O'Halloran, T. V., "Solution Structure of the Cu(I) and apo Forms of the Yeast Metallochaperone, Atx1," *Biochemistry*, vol. 40, no. 6, pp. 1528–1539, 2001.

[42] Blindauer, C. A., "Bacterial Metallothioneins: Past, Present, and Questions for the Future," *Journal of Biological Inorganic Chemistry*, vol. 16, no. 7, pp. 1011–1024, 2011.

[43] Gold, B.; Deng, H.; Bryk, R.; Vargas, D.; Eliezer, D.; Roberts, J.; Jiang, X.; Nathan, C., "Identification of a Copper-binding Metallothionein in Pathogenic Mycobacteria," *Nature Chemical Biology*, vol. 4, no. 10, pp. 609–616, 2008.

[44] Sutherland, D. E. K.; Stillman, M. J., "The "Magic Numbers" of Metallothionein," *Metallomics*, vol. 3, no. 5, pp. 444–463, 2011.

[45] Ruttkay-Nedecky, B.; Nejdl, L.; Gumulec, J.; Zitka, O.; Masarik, M.; Eckschlager, T.; Stiborova, M.; Adam, V.; Kizek, R., "The Role of Metallothionein in Oxidative Stress," *International Journal of Molecular Sciences*, vol. 14, no. 3, pp. 6044–6066, 2013.

[46] Gourdon, P.; Liu, X. Y.; Skjorringe, T.; Morth, J. P.; Moller, L. B.; Pedersen, B. P.; Nissen, P., "Crystal Structure of a Copper-Transporting PIB-Type ATPase," *Nature*, vol. 475, no. 7354, pp. 59–64, 2011.

[47] Rosenzweig, A. C.; Arguello, J. M., "Toward a Molecular Understanding of Metal Transport by P(1B)-Type ATPases," *Current Topics in Membranes*, vol. 69, pp. 113–136, 2012.

[48] Gonzalez-Guerrero, M.; Arguello, J. M., "Mechanism of Cu+-Transporting ATPases: Soluble Cu+ Chaperones Directly Transfer Cu+ to Transmembrane Transport Sites," *Proceedings of the National Academy of Science USA*, vol. 105, no. 16, pp. 5992–5997, 2008.

[49] Walker, J. M.; Huster, D.; Ralle, M.; Morgan, C. T.; Blackburn, N. J.; Lutsenko, S., "The N-terminal Metal-binding Site 2 of the Wilson's Disease Protein Plays a Key Role in the Transfer of Copper from Atox1," *The Journal of Biological Chemistry*, vol. 279, no. 15, pp. 15376–15384, 2004.

[50] Achila D; Banci L; Bertini I; Bunce J; Ciofi-Baffoni S; Huffman DL., "Structure of Human Wilson Protein Domains 5 and 6 and Their Interplay with Domain 4 and the Copper Chaperone HAH1 in Copper Uptake," *Proceedings of the National Academy of Sciences*, vol. 103, no. 15, pp. 5729–5734, 2006.

[51] Banci, L.; Bertini, I.; Ciofi-Baffoni, S.; Kandias, N. G.; Robinson, N. J.; Spyroulias, G. A.; Su, X. C.; Tottey, S.; Vanarotti, M., "The Delivery of Copper for Thylakoid Import Observed by NMR," *Proceedings of the National Academy of Sciences*, vol. 103, no. 22, pp. 8320–8325, 2006.

[52] Singleton, C.; Le Brun, N. E., "Atx1-like Chaperones and Their Cognate P-type ATPases: Copper-Binding and Transfer," *Biometals*, vol. 20, no. 3-4, pp. 275–289, 2007.

[53] De Feo, C. J.; Aller, S. G.; Siluvai, G. S.; Blackburn, N. J.; Unger, V. M., "Three-dimensional Structure of the Human Copper Transporter hCTR1," *Proceedings of the National Academy of Science USA*, vol. 106, no. 11, pp. 4237–4242, 2009.

[54] Ohrvik, H.; Thiele, D. J., "How Copper Traverses Cellular Membranes Through the Mammalian Copper Transporter 1, Ctr1," *Annals of the New York Academy of Sciences*, vol. 1314, pp. 32–41, 2014.

[55] Matson Dzebo, M.; Arioz, C.; Wittung-Stafshede, P., "Extended Functional Repertoire for Human Copper Chaperones," *Biomolecular Concepts*, 2016.

[56] Levy, A. R.; Yarmiayev, V.; Moskovitz, Y.; Ruthstein, S., "Probing the Structural Flexibility of the Human Copper Metallochaperone Atox1 Dimer and its Interaction with the CTR1 C-terminal Domain," *Journal of Physical Chemistry*, vol. 118, no. 22, pp. 5832–5842, 2014.

[57] Wernimont, A. K.; Huffman, D. L.; Lamb, A. L.; O'Halloran, T. V.; Rosenzweig, A. C., "Structural basis for Copper Transfer by the Metallochaperone for the Menkes/Wilson Disease Proteins," *Nature Structural Biology*, vol. 7, no. 9, pp. 766–771, 2000.

[58] Palm-Espling, M. E.; Niemiec, M. S.; Wittung-Stafshede, P., "Role of Metal in Folding and Stability of Copper Proteins in vitro," *Biochimica et Biophysica Acta*, vol. 1823, no. 9, pp. 1594–1603, 2012.

[59] Wittung-Stafshede, P., "Unresolved Questions in Human Copper Pump Mechanisms," *Quarterly Review of Biophysics*, vol. 48, no. 4, pp. 471–478, 2015.

[60] Menkes, J. H.; Alter, M.; Steigleder, G. K.; Weakley, D. R.; Sung, J. H., "A Sex-linked Recessive Disorder with Retardation of Growth, Peculiar Hair, and Focal Cerebral and Cerebellar Degeneration," *Pediatrics*, vol. 29, pp. 764–779, 1962.

[61] Wilson, S. A. K., "Progressive Lenticular Degeneration: A Familial Nervous Disease Associated with Cirrhosis of the Liver," *The Lancet*, vol. 179, no. 4626, pp. 1115–1119, 1912.

[62] Wu, X.; Sinani, D.; Kim, H.; Lee, J., "Copper Transport Activity of Yeast Ctr1 is Down-regulated via its C terminus in Response to Excess Copper," *The Journal of Biological Chemistry*, vol. 284, no. 7, pp. 4112–4122, 2009.

[63] Cobine, P. A.; Ojeda, L. D.; Rigby, K. M.; Winge, D. R., "Yeast Contain a Non-proteinaceous Pool of Copper in the Mitochondrial Matrix," *Journal of Biological Chemistry*, vol. 279, no. 14, pp. 14447–14455, 2004.

[64] Xiao, Z.; Wedd, A. G., "A C-terminal Domain of the Membrane Copper Pump Ctr1 Exchanges Copper(I) with the Copper Chaperone Atx1," *Chemical Communications*, no. 6, pp. 588–589, 2002.

[65] Jensen, L. T.; Howard, W. R.; Strain, J. J.; Winge, D. R.; Culotta, V. C., "Enhanced Effectiveness of Copper Ion Buffering by CUP1 Metallothionein Compared with CRS5 Metallothionein in Saccharomyces Cerevisiae," *Journal of Biological Chemistry*, vol. 271, no. 31, pp. 18514–18519, 1996.

[66] Huffman, D. L.; O'Halloran, T. V., "Energetics of Copper trafficking Between the Atx1 Metallochaperone and the Intracellular Copper Transporter, Ccc2," *Journal of Biological Chemistry*, vol. 275, no. 25, pp. 18611–18614, 2000.

[67] Banci, L.; Bertini, I.; Cantini, F.; Felli, I. C.; Gonnelli, L.; Hadjiliadis, N.; Pierattelli, R.; Rosato, A.; Voulgaris, P., "The Atx1-Ccc2 complex is a Metal-Mediated Protein-Protein Interaction," *Nature Chemical Biology*, vol. 2, no. 7, pp. 367–368, 2006.

[68] Banci, L.; Bertini, I.; Chasapis, C. T.; Rosato, A.; Tenori, L., "Interaction of the Two Soluble Metal-binding Domains of Yeast Ccc2 with Copper(I)-Atx1," *Biochemical and Biophysical Research Communications*, vol. 364, no. 3, pp. 645–649, 2007.

[69] Franke, S.; Grass, G.; Rensing, C.; Nies, D. H., "Molecular Analysis of the Copper-Transporting Efflux System CusCFBA of *Escherichia coli*," *Journal of Bacteriology*, vol. 185, no. 13, pp. 3804–3812, 2003.

[70] Mealman, T. D.; Bagai, I.; Singh, P.; Goodlett, D. R.; Rensing, C.; Zhou, H.; Wysocki, V. H.; McEvoy, M. M., "Interactions Between CusF and CusB Identified by NMR Spectroscopy and Chemical Cross-linking Coupled to Mass Spectrometry," *Biochemistry*, vol. 50, no. 13, pp. 2559–2566, 2011.

[71] Worrall, J. A.; Vijgenboom, E., "Copper Mining in Streptomyces: Enzymes, Natural Products and Development," *Natural Product Reports*, vol. 27, no. 5, pp. 742–756, 2010.

[72] Keijser, B. J.; van Wezel, G. P.; Canters, G. W.; Kieser, T.; Vijgenboom, E., "The Ram-dependence of *Streptomyces lividans* Differentiation is Bypassed by Copper," *Journal of Molecular Microbiology and Biotechnology*, vol. 2, no. 4, pp. 565–574, 2000.

[73] Cruz-Morales, P.; Vijgenboom, E.; Iruegas-Bocardo, F.; Girard, G.; Yanez-Guerra, L. A.; Ramos-Aboites, H. E.; Pernodet, J. L.; Anne, J.; van Wezel, G. P.; Barona-Gomez, F., "The Genome Sequence of *Streptomyces lividans* 66 Reveals a Novel tRNA-dependent Peptide Biosynthetic System Within a Metal-Related Genomic Island," *Genome Biology and Evolution*, vol. 5, no. 6, pp. 1165–1175, 2013.

[74] Chaplin, A. K.; Tan, B. G.; Vijgenboom, E.; Worrall, J. A., "Copper Trafficking in the CsoR Regulon of *Streptomyces lividans*," *Metallomics*, vol. 7, no. 1, pp. 145–155, 2015.

[75] Kunst, F.; et.al. , "The Complete Genome Sequence of the Gram-positive Bacterium *Bacillus Subtilis*," *Nature*, vol. 390, no. 6657, pp. 249–256, 1997.

[76] Zweers, J. C.; Barak, I.; Becher, D.; Driessen, A. J.; Hecker, M.; Kontinen, V. P.; Saller, M. J.; Vavrova, L.; van Dijl, J. M., "Towards the Development of *Bacillus Subtilis* as a Cell Factory for Membrane Proteins and Protein Complexes," *Microbial Cell Factories*, vol. 7, p. 10, 2008.

[77] Hirooka, K.; Edahiro, T.; Kimura, K.; Fujita, Y., "Direct and Indirect Regulation of the ycnKJI Operon Involved in Copper Uptake Through Two Transcriptional Repressors, YcnK and CsoR, in *Bacillus Subtilis*," *Journal of Bacteriology*, vol. 194, no. 20, pp. 5675–5687, 2012.

[78] Gaballa, A.; Helmann, J. D., "*Bacillus Subtilis* CPx-type ATPases: Characterization of Cd, Zn, Co and Cu Efflux Systems," *Biometals*, vol. 16, no. 4, pp. 497–505, 2003.

[79] Smaldone, G. T.; Helmann, J. D., "CsoR Regulates the Copper Efflux Operon CopZA in *Bacillus Subtilis*," *Microbiology*, vol. 153, no. Pt 12, pp. 4123–4128, 2007.

[80] Singleton, C.; Banci, L.; Ciofi-Baffoni, S.; Tenori, L.; Kihlken, M. A.; Boetzel, R. and Le Brun, N. E., "Structure and Cu(I)-Binding Properties of the N-terminal Soluble Domains of *Bacillus Subtilis* CopA," *Biochemical Journal*, vol. 411, no. 3, pp. 571–579, 2008.

[81] Hearnshaw, S.; West, C.; Singleton, C.; Zhou, L.; Kihlken, M. A.; Strange, R. W.; Le Brun, N. E.; Hemmings, A. M., "A Tetranuclear Cu(I) Cluster in the Metallochaperone Protein CopZ," *Biochemistry*, vol. 48, no. 40, pp. 9324–9326, 2009.

[82] Zhou, L.; Singleton, C. and Le Brun, N. E., "CopAb, the Second N-terminal Soluble Domain of *Bacillus Subtilis* CopA, Dominates the Cu(I)-binding Properties of CopAab," *Dalton Transactions*, vol. 41, no. 19, pp. 5939–5948, 2012.

[83] Zhou, L.; Singleton, C.; Hecht, O.; Moore, G. R.; Le Brun, N. E., "Cu(I)- and Proton-binding Properties of the First N-terminal Soluble Domain of *Bacillus Subtilis* CopA," *FEBS Journal*, vol. 279, no. 2, pp. 285–298, 2012.

[84] Zhou, L.; Singleton, C.; Le Brun, N. E., "High Cu(I) and Low Proton Affinities of the CXXC motif of *Bacillus Subtilis* CopZ," *Biochemical Journal*, vol. 413, no. 3, pp. 459–465, 2008.

[85] Bertani, G., "Studies on Lysogenesis. The Mode of Phage Liberation by Lysogenic *Escherichia Coli*," *Journal of Bacteriology*, vol. 62, no. 3, pp. 293–300, 1951.

[86] Birnboim, H. C. and Doly, J., "A Rapid Alkaline Extraction Procedure for Screening Recombinant Plasmid DNA," *Nucleic Acids Research*, vol. 7, no. 6, pp. 1513–1523, 1979.

[87] Hanahan, D., *DNA Cloning: A Practical Approach*. Oxford, UK: IRL Press, 1985.

[88] Inoue, H.; Nojima, H.; Okayama, H., "High Efficiency Transformation of *Escherichia Coli* with Plasmids," *Gene*, vol. 96, no. 1, pp. 23–28, 1990.

[89] Kihlken, M. A.; Leech, A. P. and Le Brun, N. E., "Copper-Mediated Dimerization of CopZ, a Predicted Copper Chaperone from *Bacillus Subtilis*," *Biochemical Journal*, vol. 368, no. Pt 3, pp. 729–739, 2002.

[90] Porath, J.; Carlsson, J.; Olsson, I. and Belfrage, G., "Metal Chelate Affinity Chromatography, a New Approach to Protein Fractionation," *Nature*, vol. 258, no. 5536, pp. 598–599, 1975.

[91] Hochuli, E.; Dobeli, H.; Schacher, A., "New Metal Chelate Adsorbent Selective for Proteins and Peptides Containing Neighbouring Histidine Residues," *Journal of Chromatography*, vol. 411, pp. 177–184, 1987.

[92] Stellwagen, E., "Gel filtration," *Methods in Enzymology*, vol. 463, pp. 373–385, 2009.

[93] O'Fagain, C.; Cummins, P. M.; O'Connor, B. F., "Gel Filtration Chromatography," *Methods in Molecular Biology*, vol. 681, pp. 25–33, 2011.

[94] Burgess, R. R., "Protein Precipitation Techniques," *Methods in Enzymology*, vol. 463, pp. 331–342, 2009.

[95] Schmid, F., *Biological Macromolecules: UV-visible Spectrophotometry*. John Wiley and Sons, Ltd, 2001.

[96] Nilapwar, S. M.; Nardelli, M.; Westerhoff, H. V.; Verma, M., "Absorption Spectroscopy," *Methods in Enzymology*, vol. 500, pp. 59–75, 2011.

[97] Pace, C. N.; Vajdos, F.; Fee, L.; Grimsley, G.; Gray, T., "How to Measure and Predict the Molar Absorption Coefficient of a Protein," *Protein Science*, vol. 4, no. 11, pp. 2411–2423, 1995.

[98] Sreerama, N.; Woody, R. W., "Computation and Analysis of Protein Circular Dichroism Spectra," *Methods in Enzymology*, vol. 383, pp. 318–351, 2004.

[99] Martin, S. R.; Schilstra, M. J., "Circular Dichroism and Its Application to the Study of Biomolecules," *Methods in Cellular Biology*, vol. 84, pp. 263–293, 2008.

[100] Bruker, "MicrOTOF-QII User Manual," Bremen, Germany, 2008.

[101] Banerjee, S.; Mazumdar, S., "Electrospray Ionization Mass Spectrometry: a Technique to Access the Information Beyond the Molecular Weight of the Analyte," *International Journal of Analytical Chemistry*, vol. 2012, p. 282574, 2012.

[102] Wilm, M., "Principles of Electrospray Ionization," *Molecular and Cellular Proteomics*, vol. 10, no. 7, p. M111.009407, 2011.

[103] Baldwin, M. A., "Mass Spectrometers for the Analysis of Biomolecules," *Methods in Enzymology*, vol. 402, pp. 3–48, 2005.

[104] Dole, M.; Mack, L. L.; Hines, R. L.; Mobley, R. C.; Ferguson, L. D.; Alice, M. B., "Molecular Beams of Macroions," *The Journal of Chemical Physics*, vol. 49, no. 5, pp. 2240–2249, 1968.

[105] Iribarne, J. V.; Thomson, B. A., "On the Evaporation of Small Ions from Charged Droplets," *The Journal of Chemical Physics*, vol. 64, no. 6, pp. 2287–2294, 1976.

[106] Carlton, D. D.; Schug, K.A., "A Review on the Interrogation of Peptide-Metal Interactions Using Electrospray Ionization-Mass Spectrometry," *Analytica Chimica Acta*, vol. 686, no. 1-2, pp. 19–39, 2011.

[107] Kelly, R. T.; Tolmachev, A. V.; Page, J. S.; Tang, K.; Smith, R. D., "The Ion Funnel: Theory, Implementations, and Applications," *Mass Spectrometry Reviews*, vol. 29, no. 2, pp. 294–312, 2010.

[108] Herbert, C.G. and Johnstone, R., *Mass Spectrometry Basics*. CRC Press, 2003.

[109] Mathieu, E., "The Vibratory Movement of an Elliptical Membrane," *Journal de Mathematiques Pures et Appliquees*, vol. 13, pp. 137–203, 1868.

[110] De Hoffmann, E.; Stroobant, V., *Mass Spectrometry*. Wiley, London, 2007.

[111] Fenn, J. B.; Mann, M.; Meng, C. K.; Wong, S. F.; Whitehouse, C. M., "Electrospray Ionization for Mass Spectrometry of Large Biomolecules," *Science*, vol. 246, no. 4926, pp. 64–71, 1989.

[112] Loo, J. A., "Studying Noncovalent Protein Complexes by Electrospray Ionization Mass Spectrometry," *Mass Spectrometry Reviews*, vol. 16, no. 1, pp. 1–23, 1997.

[113] Hopper, J. T.; Robinson, C. V., "Mass Spectrometry Quantifies Protein Interactions - From Molecular Chaperones to Membrane Porins," *Angewandte Chemie-International Edition in English*, vol. 53, no. 51, pp. 14002–14015, 2014.

[114] Kebarle, P.; Tang, L., "From Ions in Solution to Ions in the Gas Phase - the Mechanism of Electrospray Mass-Spectrometry," *Analytical Chemistry*, vol. 65, no. 22, pp. A972–A986, 1993.

[115] Warnke, S.; von Helden, G.; Pagel, K., "Protein Structure in the Gas Phase: The Influence of Side-Chain Microsolvation," *Journal of the American Chemical Society*, vol. 135, no. 4, pp. 1177–1180, 2013.

[116] Rajabi, K.; Ashcroft, A. E.; Radford, S. E., "Mass Spectrometric Methods to Analyze the Structural Organization of Macromolecular Complexes," *Methods*, vol. 89, pp. 13–21, 2015.

[117] Pan, J.; Xu, K.; Yang, X.; Choy, W. Y.; Konermann, L., "Solution-Phase Chelators for Suppressing Nonspecific Protein-Metal Interactions in Electrospray Mass Spectrometry," *Analytical Chemistry*, vol. 81, no. 12, pp. 5008–5015, 2009.

[118] Xu, A. S.; Peng, L. L.; Havel, J. A.; Petersen, M. E.; Fiene, J. A.; Hulse, J. D., "Determination of Nicotine and Cotinine in Human Plasma by Liquid Chromatography-Tandem Mass Spectrometry with Atmospheric-Pressure Chemical Ionization interface," *Journal of Chromatography B: Biomedical Sciences and Applications*, vol. 682, no. 2, pp. 249–257, 1996.

[119] Breuker, K.; McLafferty, F. W., "Stepwise Evolution of Protein Native Structure with Electrospray into the Gas Phase," *Proceedings of the National Academy of Science USA*, vol. 105, no. 47, pp. 18145–18152, 2008.

[120] Peschke, M.; Verkerk, U. H.; Kebarle, P., "Features of the ESI Mechanism That Affect the Observation of Multiply Charged Noncovalent Protein Complexes and the Determination of the Association constant by the titration method," *Journal of the American Society of Mass Spectrometry*, vol. 15, no. 10, pp. 1424–1434, 2004.

[121] Benesch, J. L.; Ayoub, M.; Robinson, C. V.; Aquilina, J. A., "Small Heat Shock Protein Activity is Regulated by Variable Oligomeric Substructure," *Journal of Biological Chemistry*, vol. 283, no. 42, pp. 28513–28517, 2008.

[122] Benesch, J. L.; Ruotolo, B. T., "Mass Spectrometry: Come of Age for Structural and Dynamical Biology," *Current Opinion in Structural Biology*, vol. 21, no. 5, pp. 641–649, 2011.

[123] Seo, J.; Hoffmann, W.; Warnke, S.; Bowers, M. T.; Pagel, K.; von Helden, G., "Retention of Native Protein Structures in the Absence of Solvent: A Coupled Ion Mobility and Spectroscopic Study," *Angewandte Chemie International Edition*, vol. 55, no. 45, pp. 14173–14176, 2016.

[124] Heck, A., "Native Mass Spectrometry: a Bridge Between Interactomics and Structural Biology," *Nature Methods*, vol. 5, no. 11, pp. 927–933, 2008.

[125] Potier, N.; Rogniaux, H.; Chevreux, G.; Van Dorsselaer, A., "Ligand-Metal Ion Binding to Proteins: Investigation by ESI Mass Spectrometry," *Methods in Enzymology*, vol. 402, pp. 361–389, 2005.

[126] Gross, J. H., *Mass Spectrometry: a Textbook*. Springer Science and Business Media, 2006.

[127] Reinhold, B. B.; Reinhold, V. N., "Electrospray Ionization Mass Spectrometry - Deconvolution by an Entropy-Based Algorithm ," *Journal of the American Society of Mass Spectrometry*, vol. 3, no. 3, pp. 207–215, 1992.

[128] Ferrige, A. G.; Seddon, M. J.; Jarvis, S., "Maximum Entropy Deconvolution in Electrospray Mass Spectrometry," *Rapid Communications in Mass Spectrometry*, vol. 5, no. 8, pp. 374–377, 1991.

[129] Blindauer, C. A., "Lessons on the Critical Interplay Between Zinc Binding and Protein Structure and Dynamics," *Journal of Inorganic Biochemistry*, vol. 121, pp. 145–155, 2013.

[130] Merrifield, M. E.; Huang, Z.; Kille, P.; Stillman, M. J., "Copper Speciation in the Alpha and Beta Domains of Recombinant Human Metallothionein by Electrospray Ionization Mass Spectrometry," *Journal of Inorganic Biochemistry*, vol. 88, no. 2, pp. 153–172, 2002.

[131] Kaltashov, I.A.; Abzalimov, R. R., "Do Ionic Charges in ESI MS Provide Useful Information on Macromolecular Structure?," *Journal of the American Society of Mass Spectrometry*, vol. 19, no. 9, pp. 1239–1246, 2008.

[132] Heck, A. J. R.; van den Heuvel, R. H. H., "Investigation of Intact Protein Complexes by Mass Spectrometry," *Mass Spectrometry Reviews*, vol. 23, no. 5, pp. 368–389, 2004.

[133] Hilton, G. R.; Benesch, J. L. P., "Two Decades of Studying Non-covalent Biomolecular Assemblies by Means of Electrospray Ionization Mass Spectrometry," *Journal of the Royal Society Interface*, vol. 9, no. 70, pp. 801–816, 2012.

[134] Kaluarachchi, H.; Siebel, J. F.; Kaluarachchi-Duffy, S.; Krecisz, S.; Sutherland, D. E.; Stillman, M. J.; Zamble, D. B., "Metal Selectivity of the *Escherichia coli* Nickel Metallochaperone, SlyD," *Biochemistry*, vol. 50, no. 49, pp. 10666–10677, 2011.

[135] Lu, S. C., "Regulation of Hepatic Glutathione Synthesis: Current Concepts and Controversies," *The FASEB Journal*, vol. 13, no. 10, pp. 1169–1183, 1999.

[136] Spies, H. S.; Steenkamp, D. J., "Thiols of Intracellular Pathogens. Identification of Ovothiol A in Leishmania Donovani and Structural Analysis of a Novel Thiol from Mycobacterium Bovis," *European Journal of Biochemistry*, vol. 224, no. 1, pp. 203–213, 1994.

[137] Fahey, R. C., "Glutathione Analogs in Prokaryotes," *Biochimica et Biophysica Acta*, vol. 1830, no. 5, pp. 3182–3198, 2013.

[138] Xiao, Z.; Brose, J.; Schimo, S.; Ackland, S. M.; La Fontaine, S.; Wedd, A. G., "Unification of the Copper(I) Binding Affinities of the Metallochaperones Atx1, Atox1, and Related Proteins: Detection Probes and Affinity Standards," *Journal of Biological Chemistry*, vol. 286, no. 13, pp. 11047–11055, 2011.

[139] Badarau, A.; Firbank, S. J.; McCarthy, A. A.; Banfield, M. J.; Dennison, C., "Visualizing the Metal-binding Versatility of Copper Trafficking Sites," *Biochemistry*, vol. 49, no. 36, pp. 7798–7810, 2010.

[140] Leszczyszyn, O. I.; Blindauer, C. A., "Zinc Transfer from the Embryo-Specific Metallothionein E(C) From Wheat: a Case Study," *Physical Chemistry Chemical Physics*, vol. 12, no. 41, pp. 13408–13418, 2010.

[141] Urvoas, A.; Amekraz, B.; Moulin, C.; Le Clainche, L.; Stocklin, R.; Moutiez, M., "Analysis of the Metal-binding Selectivity of the Metallochaperone CopZ from Enterococcus Hirae by Electrospray ionization Mass Spectrometry," *Rapid Communications in Mass Spectrometry*, vol. 17, no. 16, pp. 1889–1896, 2003.

[142] Palumaa, P.; Kangur, L.; Voronova, A.; Sillard, R., "Metal-binding Mechanism of Cox17, a Copper Chaperone for Cytochrome c Oxidase," *Biochemical Journal*, vol. 382, no. Pt 1, pp. 307–314, 2004.

[143] Sharma, S. V.; Jothivasan, V. K.; Newton, G. L.; Upton, H.; Wakabayashi, J. I.; Kane, M. G.; Roberts, A. A.; Rawat, M.; La Clair, J. J.; Hamilton, C. J., "Chemical and Chemoenzymatic Syntheses of Bacillithiol: a Unique Low-Molecular-Weight Thiol Amongst low G + C Gram-positive Bacteria," *Angewandte Chemie-International Edition in English*, vol. 50, no. 31, pp. 7101–7104, 2011.

[144] Xiao, Z.; Loughlin, F.; George, G. N.; Howlett, G. J.; Wedd, A. G., "C-terminal Domain of the Membrane Copper Transporter Ctr1 From Saccharomyces Cerevisiae Binds Four Cu(I) Ions as a Cuprous-Thiolate Polynuclear Cluster: Sub-femtomolar Cu(I) Affinity of Three Proteins Involved in Copper trafficking," *Journal of the American Chemical Society*, vol. 126, no. 10, pp. 3081–3090, 2004.

[145] Kamau, P.; Jordan, R. B., "Complex Formation Constants for the Aqueous Copper(I)-acetonitrile System by a Simple General Method," *Inorganic Chemistry*, vol. 40, no. 16, pp. 3879–3883, 2001.

[146] Dobo, A.; Kaltashov, I. A., "Detection of Multiple Protein Conformational Ensembles in Solution Via Deconvolution of Charge-State Distributions in ESI MS," *Analytical Chemistry*, vol. 73, no. 20, pp. 4763–4773, 2001.

[147] Singleton, C.; Le Brun, N. E., "The N-terminal Soluble Domains of *Bacillus Subtilis* CopA Exhibit a High Affinity and Capacity for Cu(I) Ions," *Dalton Transactions*, no. 4, pp. 688–696, 2009.

[148] Xiao, Z.; Wedd, A. G., "The Challenges of Determining Metal-protein Affinities," *Natural Product Reports*, vol. 27, no. 5, pp. 768–789, 2010.

[149] Hasler, D. W.; Faller, P.; Vasak, M., "Metal-thiolate Clusters in the C-terminal Domain of Human Neuronal Growth Inhibitory Factor (GIF)," *Biochemistry*, vol. 37, no. 42, pp. 14966–14973, 1998.

[150] Pountney, D. L.; Schauwecker, I.; Zarn, J.; Vasak, M., "Formation of Mammalian Cu8-Metallothionein in vitro: Evidence for the Existence of Two Cu(I)4-thiolate Clusters," *Biochemistry*, vol. 33, no. 32, pp. 9699–9705, 1994.

[151] Hussain, F.; Wittung-Stafshede, P., "Impact of Cofactor on Stability of Bacterial (CopZ) and Human (Atox1) Copper Chaperones," *Biochimica et Biophysica Acta*, vol. 1774, no. 10, pp. 1316–1322, 2007.

[152] Felitsyn, N.; Peschke, M.; Kebarle, P., "Origin and Number of Charges Observed on Multiply-Protonated Native Proteins Produced by ESI," *International Journal of Mass Spectrometry*, vol. 219, no. 1, pp. 39–62, 2002.

[153] Lee, J. W.; Soonsanga, S.; Helmann, J. D., "A Complex Thiolate Switch Regulates the *Bacillus Subtilis* Organic Peroxide Sensor OhrR," *Proceedings of the National Academy of Science USA*, vol. 104, no. 21, pp. 8743–8748, 2007.

[154] Chi, B. K.; Gronau, K.; Mader, U.; Hessling, B.; Becher, D.; Antelmann, H., "S-bacillithiolation Protects Against Hypochlorite Stress in *Bacillus Subtilis* as Revealed by Transcriptomics and Redox Proteomics," *Molecular and Cellular Proteomics*, vol. 10, no. 11, p. M111.009506, 2011.

[155] Arguello, J. M., "Identification of Ion-selectivity Determinants in Heavy-Metal Transport P1B-type ATPases," *Journal of Membrane Biology*, vol. 195, no. 2, pp. 93–108, 2003.

[156] Arnesano, F.; Banci, L.; Bertini, I.; Bonvin, A. M., "A Docking Approach to the Study of Copper Trafficking Proteins; Interaction Between Metallochaperones and Soluble Domains of Copper ATPases," *Structure*, vol. 12, no. 4, pp. 669–676, 2004.

[157] Niemiec, M. S.; Dingeldein, A. P.; Wittung-Stafshede, P., "T versus D in the MTCXXC motif of Copper Transport Proteins Plays a Role in Directional Metal Transport," *Journal of Biological Inorganic Chemistry*, vol. 19, no. 6, pp. 1037–1047, 2014.

[158] Forbes, J. R.; Hsi, G.; Cox, D. W., "Role of the Copper-binding Domain in the Copper Transport Function of ATP7B, the P-type ATPase Defective in Wilson Disease," *Journal of Biological Chemistry*, vol. 274, no. 18, pp. 12408–12413, 1999.

[159] Morin, I.; Gudin, S.; Mintz, E.; Cuillel, M., "Dissecting the Role of the N-terminal Metal-binding Domains in Activating the Yeast Copper ATPase in vivo," *FEBS Journal*, vol. 276, no. 16, pp. 4483–4495, 2009.

[160] Wu, C. C.; Rice, W. J.; Stokes, D. L., "Structure of a Copper Pump Suggests a Regulatory Role for its Metal-binding Domain," *Structure*, vol. 16, no. 6, pp. 976–985, 2008.

[161] Tsivkovskii, R.; MacArthur, B. C.; Lutsenko, S., "The Lys1010-Lys1325 Fragment of the Wilson's Disease Protein Binds Nucleotides and Interacts with the N-terminal Domain of this Protein in a Copper-Dependent Manner," *Journal of Biological Chemistry*, vol. 276, no. 3, pp. 2234–2242, 2001.

[162] Inesi, G.; Pilankatta, R.; Tadini-Buoninsegni, F., "Biochemical Characterization of P-type Copper ATPases," *Biochemical Journal*, vol. 463, no. 2, pp. 167–176, 2014.

[163] Singleton, C.; Hearnshaw, S.; Zhou, L.; Le Brun, N. E.; Hemmings, A. M., "Mechanistic Insights Into Cu(I) Cluster Transfer Between the Chaperone CopZ and its Cognate Cu(I)-Transporting P-type ATPase, CopA," *Biochemical Journal*, vol. 424, no. 3, pp. 347–356, 2009.

[164] Banci, L.; Bertini, I.; Ciofi-Baffoni, S.; Gonnelli, L.; Su, X. C., "Structural Basis for the Function of the N-terminal Domain of the ATPase CopA from *Bacillus Subtilis*," *Journal of Biological Chemistry*, vol. 278, no. 50, pp. 50506–50513, 2003.

[165] Maryon, E. B.; Molloy, S. A.; Kaplan, J. H., "Cellular Glutathione plays a Key Role in Copper Uptake Mediated by Human Copper Transporter 1," *The American Journal of Physiololgy - Cell Physiology*, vol. 304, no. 8, pp. C768–779, 2013.

[166] Fan, B.; Grass, G.; Rensing, C.; Rosen, B. P., "*Escherichia coli* CopA N-terminal Cys(X)(2)Cys Motifs are not Required for Copper Resistance or Transport," *Biochemical and Biophysical Research Communications*, vol. 286, no. 2, pp. 414–418, 2001.

[167] Hatori, Y.; Hirata, A.; Toyoshima, C.; Lewis, D.; Pilankatta, R.; Inesi, G., "Intermediate Phosphorylation Reactions in the Mechanism of ATP Utilization by the Copper ATPase (CopA) of Thermotoga maritima," *Journal of Biological Chemistry*, vol. 283, no. 33, pp. 22541–22549, 2008.

[168] Yatsunyk, L. A.; Rosenzweig, A. C., "Cu(I) binding and transfer by the N terminus of the Wilson disease protein," *Journal of Biological Chemistry*, vol. 282, no. 12, pp. 8622–8631, 2007.

[169] Changela, A.; Chen, K.; Xue, Y.; Holschen, J.; Outten, C. E.; O'Halloran, T. V.; Mondragon, A., "Molecular basis of metal-ion selectivity and zeptomolar sensitivity by CueR," *Science*, vol. 301, no. 5638, pp. 1383–1387, 2003.

[170] Ansbacher, T.; Chourasia, M.; Shurki, A., "Copper-chaperones with Dicoordinated Cu(I)–Unique Protection Mechanism," *Proteins*, vol. 81, no. 8, pp. 1411–1419, 2013.

[171] Allen, S.; Badarau, A.; Dennison, C., "The Influence of Protein Folding on the Copper Affinities of Trafficking and Target Sites," *Dalton Transactions*, vol. 42, no. 9, pp. 3233–3239, 2013.

[172] Banci, L.; Bertini, I.; Cantini, F.; Rosenzweig, A. C.; Yatsunyk, L. A., "Metal binding Domains 3 and 4 of the Wilson Disease Protein: Solution Structure and Interaction with the Copper(I) Chaperone HAH1," *Biochemistry*, vol. 47, no. 28, pp. 7423–7429, 2008.

[173] Niemiec, M. S.; Weise, C. F.; Wittung-Stafshede, P., "In Vitro Thermodynamic Dissection of Human Copper Transfer from Chaperone to Target Protein," *PLoS One*, vol. 7, no. 5, p. e36102, 2012.

[174] Niemiec, M. S.; Dingeldein, A. P.; Wittung-Stafshede, P., "Enthalpy-entropy Compensation at Play in Human Copper Ion Transfer," *Scientific Reports*, vol. 5, p. 10518, 2015.

[175] Wernimont, A. K.; Yatsunyk, L. A.; Rosenzweig, A. C., "Binding of copper(I) by the Wilson Disease Protein and its Copper Chaperone," *The Journal of Biological Chemistry*, vol. 279, no. 13, pp. 12269–12276, 2004.

[176] Banci, L.; Bertini, I.; Ciofi-Baffoni, S.; Del Conte, R.; Gonnelli, L., "Understanding Copper Trafficking in Bacteria: Interaction Between the Copper Transport Protein CopZ and the N-terminal Domain of the Copper ATPase CopA from *Bacillus Subtilis*," *Biochemistry*, vol. 42, no. 7, pp. 1939–1949, 2003.

[177] Zhou, L., *Studies of Cu(I) Trafficking Proteins from Bacillus subtilis.* PhD Thesis, 2009.

[178] Huffman, D. L.; O'Halloran, T. V., "Function, Structure, and Mechanism of Intracellular Copper Trafficking Proteins," *Annual Review of Biochemistry*, vol. 70, pp. 677–701, 2001.

[179] Singleton, C., *Studies of Cu(I) Trafficking Proteins from Bacillus subtilis.* PhD Thesis, 2008.

[180] Rae, T. D.; Schmidt, P. J.; Pufahl, R. A.; Culotta, V. C.; O'Halloran, T. V., "Undetectable Intracellular Free Copper: the Requirement of a Copper Chaperone for Superoxide Dismutase," *Science*, vol. 284, no. 5415, pp. 805–808, 1999.

[181] Shoshan, M. S.; Tshuva, E. Y., "The MXCXXC Class of Metallochaperone Proteins: Model Studies," *Chemical Society Reviews*, vol. 40, no. 11, pp. 5282–5292, 2011.

[182] Banci, L.; Bertini, I.; Ciofi-Baffoni, S.; Su, X. C.; Borrelly, G. P.; Robinson, N. J., "Solution Structures of a Cyanobacterial Metallochaperone: Insight into an Atypical Copper-binding Motif," *Journal of Biological Chemistry*, vol. 279, no. 26, pp. 27502–27510, 2004.

[183] Arnesano, F.; Banci, L.; Bertini, I.; Ciofi-Baffoni, S.; Molteni, E.; Huffman, D. L.; O'Halloran, T. V., "Metallochaperones and Metal-transporting ATPases: a Comparative Analysis of Sequences and Structures," *Genome Research*, vol. 12, no. 2, pp. 255–271, 2002.

[184] Hussain, F.; Rodriguez-Granillo, A.; Wittung-Stafshede, P., "Lysine-60 in Copper Chaperone Atox1 Plays an Essential Role in Adduct Formation with a Target Wilson Disease Domain," *Journal of the American Chemical Society*, vol. 131, no. 45, pp. 16371–16373, 2009.

[185] Dalosto, S. D., "Computer Simulation of the Interaction of Cu(I) with Cys Residues at the Binding Site of the Yeast Metallochaperone Cu(I)-Atx1," *Journal of Physical Chemistry*, vol. 111, no. 11, pp. 2932–2940, 2007.

[186] Tanchou, V.; Gas, F.; Urvoas, A.; Cougouluegne, F.; Ruat, S.; Averseng, O.; Quemeneur, E., "Copper-mediated Homo-dimerisation for the HAH1 Metallochaperone," *Biochemistry Biophysics Research Communications*, vol. 325, no. 2, pp. 388–394, 2004.

[187] Miras, R.; Morin, I.; Jacquin, O.; Cuillel, M.; Guillain, F.; Mintz, E., "Interplay between glutathione, Atx1 and copper. 1. Copper(I) glutathionate induced dimerization of Atx1," *Journal of Biological Inorganic Chemistry*, vol. 13, no. 2, pp. 195–205, 2008.

[188] Wimmer, R.; Herrmann, T.; Solioz, M.; Wuthrich, K., "NMR structure and metal interactions of the CopZ copper chaperone," *Journal of Biological Chemistry*, vol. 274, no. 32, pp. 22597–22603, 1999.

[189] Petzoldt, S.; Kahra, D.; Kovermann, M.; Dingeldein, A. P.; Niemiec, M. S.; Aden, J.; Wittung-Stafshede, P., "Human Cytoplasmic Copper Chaperones Atox1 and CCS Exchange Copper Ions in vitro," *Biometals*, vol. 28, no. 3, pp. 577–585, 2015.

[190] Poger, D.; Fillaux, C.; Miras, R.; Crouzy, S.; Delangle, P.; Mintz, E.; Den Auwer, C.; Ferrand, M., "Interplay Between Glutathione, Atx1 and Copper: X-ray Absorption Spectroscopy Determination of Cu(I) Environment in an Atx1 Dimer," *Journal of Biological Inorganic Chemistry*, vol. 13, no. 8, pp. 1239–1248, 2008.

[191] Alvarez, H. M.; Xue, Y.; Robinson, C. D.; Canalizo-Hernandez, M. A.; Marvin, R. G.; Kelly, R. A.; Mondragon, A.; Penner-Hahn, J. E.; O'Halloran, T. V., "Tetrathiomolybdate Inhibits Copper Trafficking Proteins Through Metal Cluster Formation," *Science*, vol. 327, no. 5963, pp. 331–334, 2010.

[192] Chaplin, A.K. , *Metalloenzymes Required for Glycan Processing and Morphological Development in Streptomyces lividans.* PhD Thesis, 2016.

[193] Williams, P. A.; Blackburn, N. J.; Sanders, D.; Bellamy, H.; Stura, E. A.; Fee, J. A.; McRee, D. E., "The CuA Domain of Thermus thermophilus ba3-type Cytochrome c Oxidase at 1.6 A Resolution," *Nature Structural Biology*, vol. 6, no. 6, pp. 509–516, 1999.

[194] Badarau, A.; Dennison, C., "Copper Trafficking Mechanism of CXXC-Containing Domains: Insight from the pH-Dependence of Their Cu(I) Affinities," *Journal of the American Chemical Society*, vol. 133, no. 9, pp. 2983–2988, 2011.

[195] Gonzalez-Guerrero, M.; Eren, E.; Rawat, S.; Stemmler, T. L.; Arguello, J. M., "Structure of the Two Transmembrane Cu+ Transport Sites of the Cu+ -ATPases," *Journal of Biological Chemistry*, vol. 283, no. 44, pp. 29753–29759, 2008.

[196] Hasan, N. M.; Gupta, A.; Polishchuk, E.; Yu, C. H.; Polishchuk, R.; Dmitriev, O. Y.; Lutsenko, S., "Molecular Events Initiating Exit of a Copper-transporting ATPase ATP7B From the Trans-Golgi Network," *Journal of Biological Chemistry*, vol. 287, no. 43, pp. 36041–36050, 2012.

[197] Lin, S. H.; Guidotti, G., "Purification of Membrane Proteins," *Methods in Enzymology*, vol. 463, pp. 619–629, 2009.

[198] Linke, D., "Detergents: an Overview," *Methods in Enzymology*, vol. 463, pp. 603–617, 2009.

[199] Prive, G. G., "Detergents for the Stabilization and Crystallization of Membrane Proteins," *Methods*, vol. 41, no. 4, pp. 388–397, 2007.

[200] Baginski, E. S.; Foa, P. P.; Zak, B., "Microdetermination of Inorganic Phosphate, Phospholipids, and Total Phosphate in Biologic Materials," *Clinical Chemistry*, vol. 13, no. 4, pp. 326–332, 1967.

[201] Cariani, L.; Thomas, L.; Brito, J.; del Castillo, J. R., "Bismuth Citrate in the Quantification of Inorganic Phosphate and its Utility in the Determination of Membrane-Bound Phosphatases," *Analytical Biochemistry*, vol. 324, no. 1, pp. 79–83, 2004.

[202] Tiehm, A., "Degradation of Polycyclic Aromatic Hydrocarbons in the Presence of Synthetic Surfactants," *Applied and Environmental Microbiology*, vol. 60, no. 1, pp. 258–263, 1994.

[203] Chae, P. S.; Rasmussen, S. G.; Rana, R. R.; Gotfryd, K.; Chandra, R.; Goren, M. A.; Kruse, A. C.; Nurva, S.; Loland, C. J.; Pierre, Y.; Drew, D.; Popot, J. L.; Picot, D.; Fox, B. G.; Guan, L.; Gether, U.; Byrne, B.; Kobilka, B.; Gellman, S. H., "Maltose-Neopentyl Glycol (MNG) Amphiphiles for Solubilization, Stabilization and Crystallization of Membrane Proteins," *Nature Methods*, vol. 7, no. 12, pp. 1003–1008, 2010.

[204] Chintalapati, S.; Al Kurdi, R.; van Scheltinga, A. C.; Kuhlbrandt, W., "Membrane structure of CtrA3, a Copper-Transporting P-type-ATPase from Aquifex Aeolicus," *Journal of Molecular Biology*, vol. 378, no. 3, pp. 581–595, 2008.

[205] Hung, Y. H.; Layton, M. J.; Voskoboinik, I.; Mercer, J. F.; Camakaris, J., "Purification and Membrane Reconstitution of Catalytically Active Menkes Copper-Transporting P-type ATPase (MNK; ATP7A)," *The Biochemical Journal*, vol. 401, no. 2, pp. 569–579, 2007.

[206] Torres, C.; Galian, C.; Freiberg, C.; Fantino, J. R.; Jault, J. M., "The YheI/YheH Heterodimer from *Bacillus Subtilis* is a Multidrug ABC Transporter," *Biochimica et Biophysica Acta*, vol. 1788, no. 3, pp. 615–622, 2009.

[207] Mandal, A. K.; Cheung, W. D.; Arguello, J. M., "Characterization of a Thermophilic P-type Ag+/Cu+-ATPase from the Extremophile Archaeoglobus fulgidus," *Journal of Biological Chemistry*, vol. 277, no. 9, pp. 7201–7208, 2002.

[208] Geertsma, E. R.; Nik Mahmood, N. A.; Schuurman-Wolters, G. K.; Poolman, B., "Membrane Reconstitution of ABC Transporters and Assays of Translocator Function," *Nature Protocols*, vol. 3, no. 2, pp. 256–266, 2008.

[209] Schurig-Briccio, L. A.; Gennis, R. B., "Characterization of the PIB-Type ATPases Present in Thermus thermophilus," *Journal of Bacteriology*, vol. 194, no. 15, pp. 4107–4113, 2012.

[210] Gutmann, D. A.; Mizohata, E.; Newstead, S.; Ferrandon, S.; Postis, V.; Xia, X.; Henderson, P. J.; van Veen, H. W.; Byrne, B., "A high-throughput Method for Membrane Protein Solubility Screening: the Ultracentrifugation Dispersity Sedimentation Assay," *Protein Science*, vol. 16, no. 7, pp. 1422–1428, 2007.

[211] Newton, G. L.; Buchmeier, N.; Fahey, R. C., "Biosynthesis and Functions of Mycothiol, the Unique Protective Thiol of Actinobacteria," *Microbiology and Molecular Biology Reviews*, vol. 72, no. 3, pp. 471–494, 2008.

[212] Banci, L.; Bertini, I.; Ciofi-Baffoni, S.; D'Onofrio, M.; Gonnelli, L.; Marhuenda-Egea, F. C.; Ruiz-Duenas, F. J., "Solution Structure of the N-terminal Domain of a Potential Copper-Translocating P-type ATPase from *Bacillus subtilis* in the apo and Cu(I) Loaded States," *Journal of Molecular Biology*, vol. 317, no. 3, pp. 415–429, 2002.

[213] Rodriguez-Granillo, A.; Crespo, A.; Estrin, D. A.; Wittung-Stafshede, P., "Copper-transfer Mechanism from the Human Chaperone Atox1 to a Metal-binding Domain of Wilson Disease Protein," *Journal of Physical Chemistry*, vol. 114, no. 10, pp. 3698–3706, 2010.

[214] Sutherland, D.E.; Summers, K.L.; Stillman, M.J., "Modeling the Zn(2+) and Cd(2+) Metalation Mechanism in Mammalian Metallothionein 1a," *Biochemical and Biophysical Research Communications*, vol. 426, no. 4, pp. 601–607, 2012.

Appendix: Summary of ESI-MS

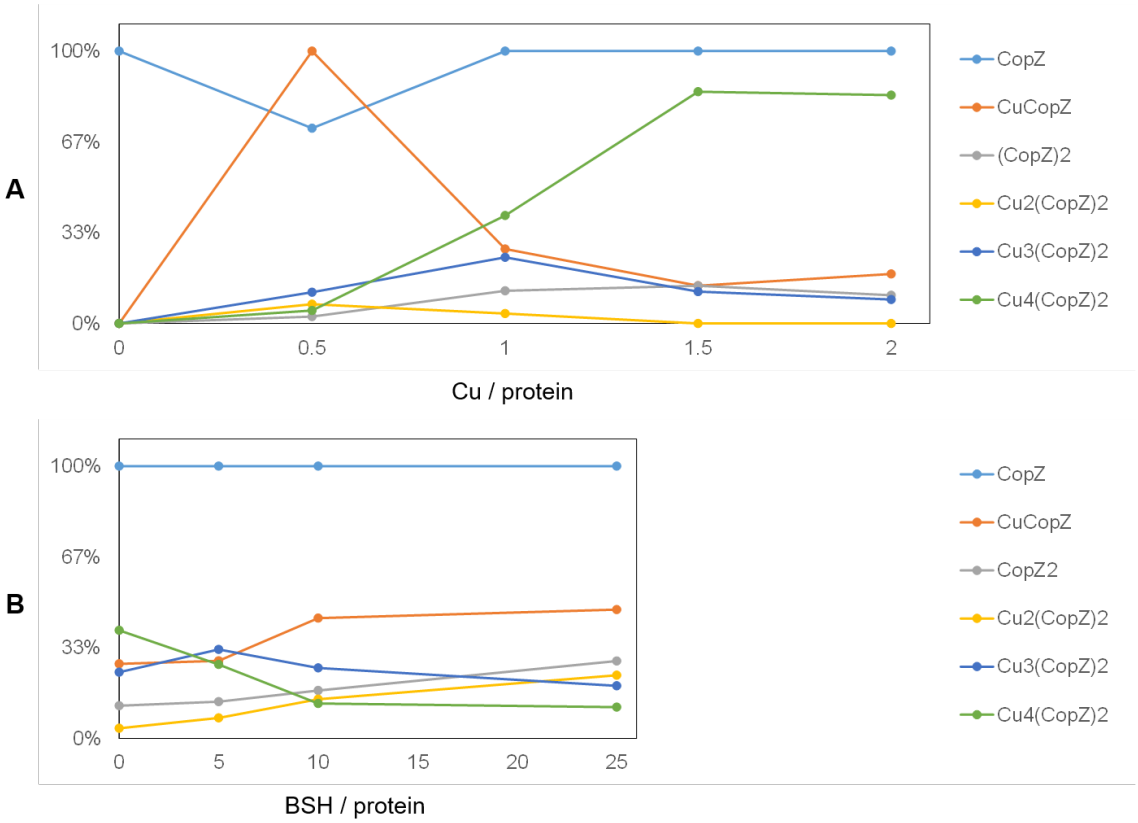

CopZ species observed via ESI-MS The major species observed via ESI-MS under conditions tested in experimental Chapter 4. These plots illustrate changes in relative intensities with increasing: **A)** copper-to-protein ratio or **B)** thiol-to-protein ratio for a sample prepared at 1 Cu / protein. At a level of 0 thiol / protein in (B), the data points are the same as plotted in (A). Plots include the major species only, additional protein complexes may have been observed via ESI-MS (see Chapter 4). The filled circles represent data points, with connecting lines included for ease of interpretation only.

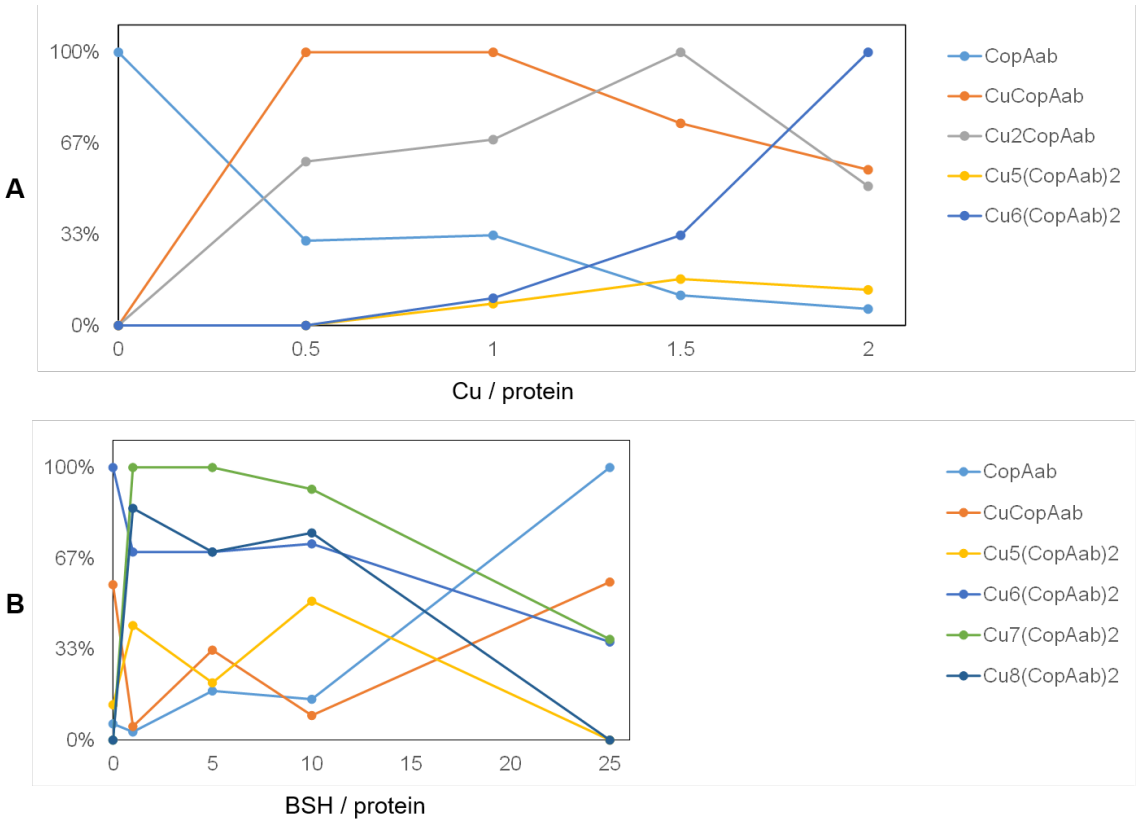

CopAab species observed via ESI-MS The major species observed via ESI-MS under conditions tested in experimental Chapter 5. These plots illustrate changes in relative intensities with increasing: **A)** copper-to-protein ratio or **B)** thiol-to-protein ratio for a sample prepared at 2 Cu / protein. At a level of 0 thiol / protein in (B), the data points are the same as plotted in (A). Plots include the major species only, additional protein complexes may have been observed via ESI-MS (see Chapter 5). The filled circles represent data points, with connecting lines included for ease of interpretation only.

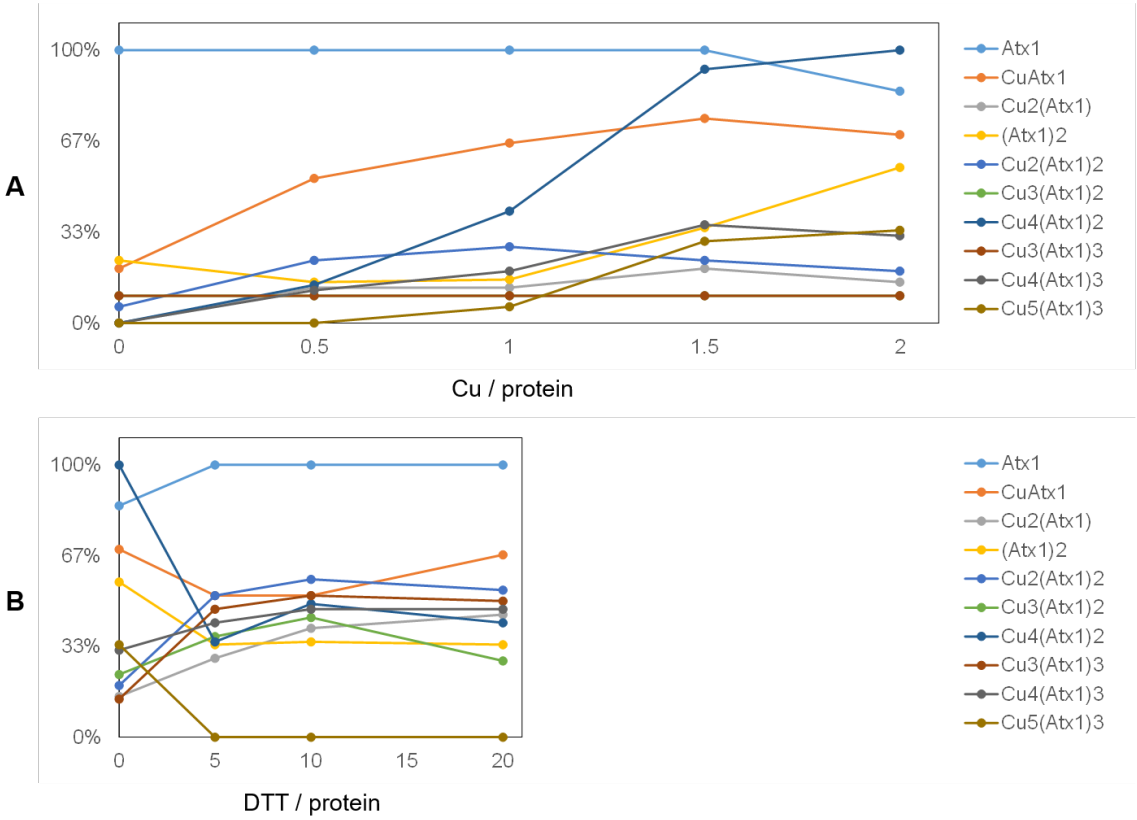

Atx1 species observed via ESI-MS The major species observed via ESI-MS under conditions tested in experimental Chapter 7. These plots illustrate changes in relative intensities with increasing: **A)** copper-to-protein ratio or **B)** thiol-to-protein ratio for a sample prepared at 2 Cu / protein. At a level of 0 thiol / protein in (B), the data points are the same as plotted in (A). Plots include the major species only, additional protein complexes may have been observed via ESI-MS (see Chapter 7). The filled circles represent data points, with connecting lines included for ease of interpretation only.

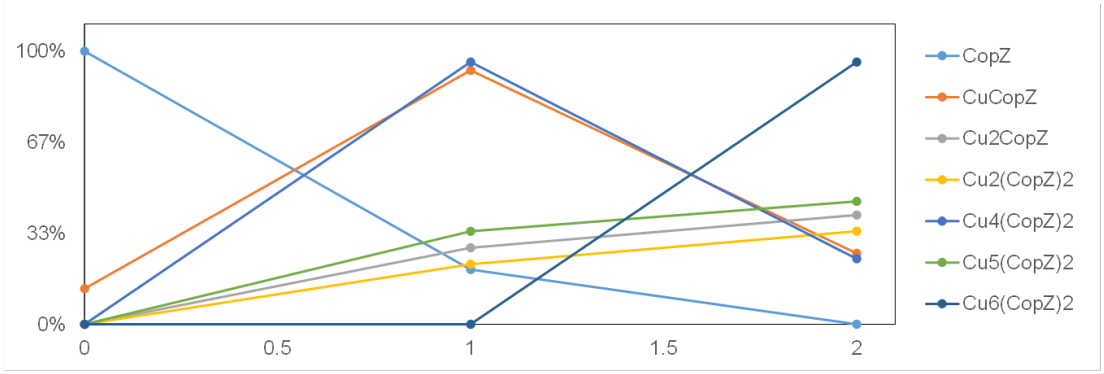

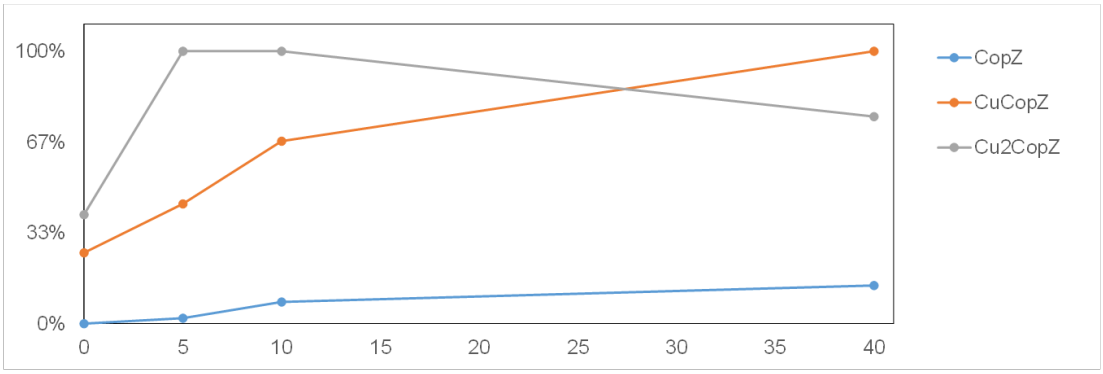

CopZ-3079 species observed via ESI-MS The major species observed via ESI-MS under conditions tested in experimental Chapter 7. These plots illustrate changes in relative intensities with increasing: **A)** copper-to-protein ratio or **B)** thiol-to-protein ratio for a sample prepared at 2 Cu / protein. At a level of 0 thiol / protein in (B), the data points are the same as plotted in (A). Plots include the major species only, additional protein complexes may have been observed via ESI-MS (see Chapter 7). The filled circles represent data points, with connecting lines included for ease of interpretation only.

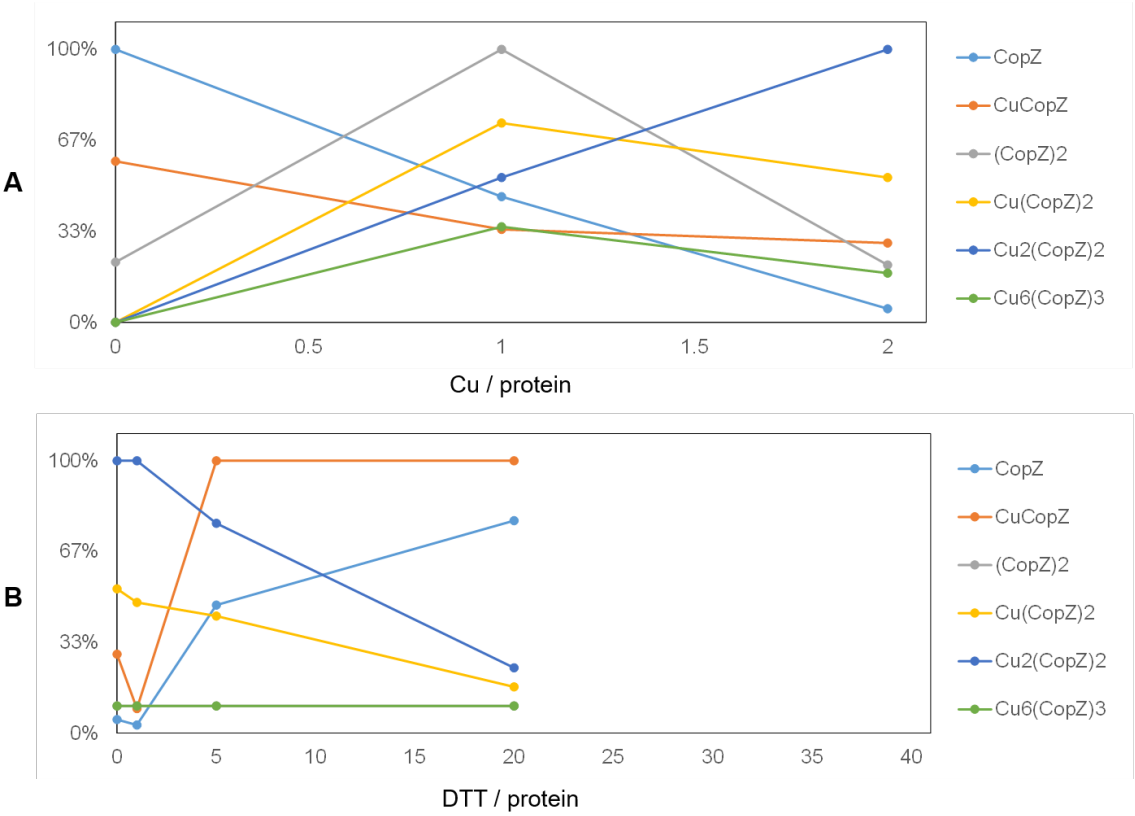

CopZ-1317 species observed via ESI-MS The major species observed via ESI-MS under conditions tested in experimental Chapter 7. These plots illustrate changes in relative intensities with increasing: **A)** copper-to-protein ratio or **B)** thiol-to-protein ratio for a sample prepared at 2 Cu / protein. At a level of 0 thiol / protein in (B), the data points are the same as plotted in (A). Plots include the major species only, additional protein complexes may have been observed via ESI-MS (see Chapter 7). The filled circles represent data points, with connecting lines included for ease of interpretation only.